Role of Genetic Haploinsufficiency in the Biology and Targeted Therapy of Del(5q) Myelodysplastic Syndrome

Rebekka Katharina Marita Schneider-Kramann

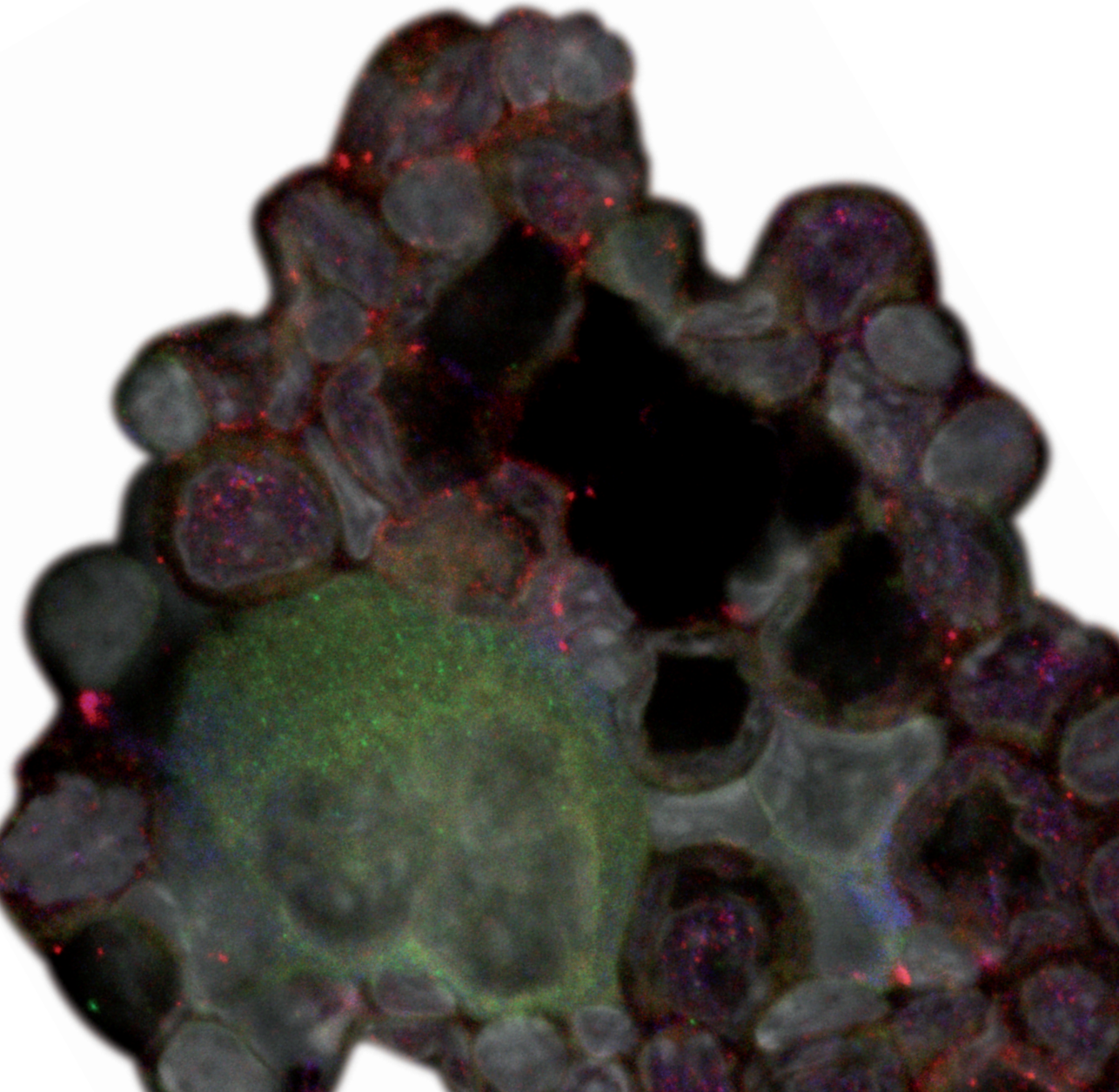

Role of Genetic Haploinsufficiency in the Biology and Targeted Therapy of Del(5q) Myelodysplastic Syndrome

Rol van genetische haploinsufficiëntie in de biologie en gerichte therapie van del (5q) myelodysplastisch syndroom

Rebekka Katharina Marita Schneider-Kramann

Erasmus MC
University Medical Center Rotterdam

ISBN: 978-94-92683-03-8
Layout: E.C.M.M. Simons
Cover: E.C.M.M. Simons
Printing: Optima Grafische Communicatie (www.ogc.nl)

The work presented in this thesis was financially supported by the German Research Foundation (DFG). Printing of this thesis was financially supported by Erasmus University Rotterdam.

Role of Genetic Haploinsufficiency in the Biology and Targeted Therapy of Del(5q) Myelodysplastic Syndrome

Rol van genetische haploinsufficiëntie in de biologie en gerichte therapie van del (5q) myelodysplastisch syndroom

Thesis

to obtain the degree of Doctor from the
Erasmus University Rotterdam
by command of the
rector magnificus

Prof.dr. H.A.P. Pols

and in accordance with the decision of the Doctorate Board.

The public defence shall be held on

Tuesday, 18 April 2017 at 15.30 hrs

by

Rebekka Katharina Marita Schneider-Kramann

born in Bonn-Beuel, Germany

Erasmus University Rotterdam

PHD COMMITTEE

Promotors: Prof.dr. H.R. Delwel
Prof.dr. I.P. Touw

Other members: Dr. T. Cupedo
Prof.dr. S. Sleijfer
Prof.dr. G. de Haan

To Rafael and my parents

CONTENTS

1

GENERAL INTRODUCTION

disease	abbreviation	Peripheral blood	Bone marrow
Refractory anemia with unlineage dysplasia Refractory anemia Refractory neutropenia Refractory thrombocytopenia	RCUD RA RN RT	Uni- or bicytopenia, blasts <1%	Unilineage dysplasia (≥10% of cells in one myeloid lineage), blasts <5%, ring sideroblasts comprising <15% of erythroid precursors
Refractory anemia with ring sideroblasts	RARS	Anemia, no blasts	Ring sideroblasts ≥15% of erythroid precursors, dysplasia limited to erythroid lineage, blasts <5%
Refractory cytopenia with multilineage dysplasia	RCMD	Cytopenia(s), blasts <1%, no Auer rods, monocytes <1x10^9/liter	Dysplasia in more than one lineage, blasts <5%, no Auer rods
Refractory anemia with excess blasts-1	RAEB-1	Cytopenia(s), blasts <5%, no Auer rods, monocytes <1x10^9/liter	Dysplasia in more than one lineage, blasts 5-9%, no Auer rods
Refractory anemia with excess blasts-2	RAEB-2	Cytopenia(s), blasts 5-19%, absence or presence of Auer rods, monocytes <1x10^9/liter	Dysplasia in more than one lineage, blasts 10-19%, presence or absence of Auer rods
Myelodysplastic syndrome, unclassifiable	MDS-U	Cytopenias, blasts<1%	Unequivocal morphologic dysplasia in <10% of cells of at least one lineage when accompanied by a clonal cytogenetic abnormality, blasts<5%
MDS with isolated del(5q)	-	Anemia, increased or normal platelet count, blasts<1%	Normal or increased megakaryocytes with hypolobated nuclei, blasts <5%, isolated del(5q) cytogenetic abnormality, no Auer rods
Chronic myelomonocytic leukemia	CMML	Persistent monocytosis, monocytes >1x10^9/liter	Dysplasia in one or more myeloid lineage; if dysplasia is absent, diagnosis can be made when (1) acquired clonal cytogenetic or molecular genetic lesion is present, (2) monocytosis persists for more than 3 months and other causes are excluded< no Philadelphia chromosome or BCR-ABL fusion gene; no rearrangement of PDGFRA or PDGFRB; blasts<20%
Myelodysplastic/myeloproliferative neoplasm, unclassifiable	MDS/MPN	(1) Clinical, laboratory, morphological features of MDS and <20% bone marrow blasts; (2) prominent myeloproliferative features, including either platelets>450x109/liter with associated megakaryocyte proliferation or white blood cells ≥13x109/liter without splenomegaly; (3) no prior MDS or MPN, no BCR-ABL1 fusion gene, no rearrangement of PDGFRA or PDGFRB, no isolated del(5q) or (3q), no recent exposure to cytotoxic therapy or hematopoietic growth factors. Alternatively, de novo disease with mixed MDS/MPN features that cannot be assigned to another category of MDS, MPN, or MDS/MPN.	
RARS associated with marked thrombocytosis	RARS-T		

Figure 1: The 2008 World Health Organization (WHO) classification of myelodysplastic syndromes and myelodysplastic/myeloproliferative neoplasms. **Introduction**

I. MYELODYSPLASTIC SYNDROME (MDS)

Myelodysplastic syndromes (MDS) are a heterogeneous group of clonal hematopoietic disorders that are characterized by ineffective hematopoiesis, peripheral blood cytopenias, and a propensity to transform into acute leukemia. Morphologic dysplasia, identified by examination of the bone marrow, is a defining feature of MDS and is an important criterion for disease classification.

The World Health Organization (WHO) currently discriminates seven distinct pathologic subtypes of MDS that are based on these morphologic features, the percentage of bone marrow cells that are blasts, and the number of affected hematatopoietic lineages (Tefferi and Vardiman 2009; Vardiman et al. 2009).

One distinctive feature of this malignancy is the presence of increased apoptosis in the bone marrow, which is, in contrast, generally hypercellular although it can also be normal or even hypocellular. Although significant efforts to understand the pathophysiology of MDS over the last years have led to the identification of key genetic and epigenetic alterations in patients, the definite pathogenetic mechanisms of MDS are not fully understood. Except for a small subset of patients that is eligible for stem cell transplantation, most MDS patients have a poor prognosis because frontline pharmacological therapies are not curative owing to the lack of well-defined molecular targets. Thus, there is an urgent need to characterize the molecular mechanisms involved in the pathogenesis of MDS to allow the establishment of good diagnostic protocols and specific, effective targeted therapies.

1.1 Myelodysplastic syndrome with isolated del(5q)

Interstitial deletion of chromosome 5q is the most common chromosomal abnormalities in MDS, identified in 10% to 15% of patients (Haase et al. 2007; Bejar et al. 2011). Deletions of chromosome 5q in MDS are somatically acquired, heterozygous and encompass many genes (Ebert 2009).

While the vast majority of patients with del(5q) MDS have large deletions, rare patients have smaller chromosomal deletions that have enabled geneticists to define common deleted regions (CDR) that are minimally necessary for a clinical phenotype. Two CDRs have been reported (Boultwood et al. 1994; Boultwood et al. 2002): (1) The CDR located more distally on chromosome 5q is minimally sufficient for the 5q-syndrome and is located at 5q52-33. (2) The CDR located more proximal to the centromere is located on 5q31. Most patients have deletions which encompass both loci, but the CDR provides a starting place for the search for critical genes.

Heterozygous deletions in cancer often highlight the locus of a tumor-suppressor gene, which undergoes homozygous inactivation, but in other cases, the disease is caused directly by mono-allelic deletions due to haploinsufficiency for one or more genes. Although 5q deletions are uniformly hemizygous, sequencing and CGH analysis failed to identify point

mutations or microdeletions of the retained 5q alleles (Graubert et al. 2009), nor has copy-neutral loss of heterozygosity been demonstrated at 5q (Gondek et al. 2008; Heinrichs et al. 2009). The absence of homozygous genetic inactivation of genes within the 5q common deleted region (CDR) indicates that the pathogenesis of del(5q) MDS is caused by haploinsufficiency or by silencing of classical tumor suppressors (e.g. by epigenetic mechanisms).

Patients with del(5q) MDS are clinically heterogeneous and can be classified into two broad categories on the basis of clinicopathologic features, prognosis, and response to specific therapy. Some patients with del(5q) display an aggressive disease course with increased risk of transformation to acute leukemia and a short overall survival (Kantarjian et al. 2009). This MDS subtype is often in the context of prior therapy with alkylating agents and/or radiation and is far more often accompanied by complex cytogenetic abnormalities and *TP53* mutation (Christiansen et al. 2001). Patients with del(5q) and additional multiple other karyotype abnormalities show a significant lower likelihood of complete response to lenalidomide compared with patients who have isolated del(5q) (Mollgard et al. 2011). Further, factors associated with adverse prognosis include deletion of the telomeric and centromeric regions of 5q as well as heterozygous mutations in *NPM1* or *MAML1 (on* 5q35 genes) *(Sportoletti et al. 2008; Jerez et al. 2012). NPM1 seems to* function as a haploinsufficient tumor suppressor in the development of multilineage hematopoietic neoplasms in a murine model, thereby contributing to MDS pathogenesis (Sportoletti, Grisendi et al. 2008).

MDS patients with del(5q) as the sole karyotypic abnormality have a relatively favorable prognosis, including patients with the 5q− syndrome (Greenberg et al. 2012). The 5q-syndrome has a very distinct genotype-phenotype relationship, which was first described by Van den Berghe in 1974 (Van den Berghe et al. 1974). The original manuscript described five patients with a macrocytic anemia, dyserythropoiesis with erythroid hypoplasia, normal to elevated platelet counts, hypolobulated megakaryocytes and an interstitial deletion involving the long arm of chromosome 5. The 5q-syndrome is now classified by the World Health Organization (WHO 2008) as a clonal hematopoietic disorder characterized by macrocytic anemia, normal to elevated platelet count in the peripheral blood, normal to increased hypolobated (micro)megakaryocytes, and an isolated del(5q) on initial diagnostic evaluation. Bona fide 5q− syndrome typically has a low bone marrow blast percentage (<5%; Auer rodsa are not present), a female-to-male ratio of 2:1, and a low risk of transformation to acute myeloid leukemia (AML), in particular in comparison with other MDS subtypes (5–16% versus 30–45%) (Vardiman, Thiele et al. 2009). Given the stability of the disease, with low rates of progression to AML, iron overload from chronic transfusions is a significant cause of morbidity and mortality.

A region that spans 1.5 Mb and contains 40 genes at 5q32-q33 was defined as the CDR for the 5q− syndrome (Boultwood, Fidler et al. 2002). A number of genes within this region are expressed at true haploinsufficient levels in $CD34^+$ cells of patients with del(5q) MDS

(Boultwood et al. 2007). Conditional deletion of this entire region recapitulates the severe macrocytic anemia in a murine model (Barlow et al. 2010).

Systematic functional screening of the complete list of candidate genes within the 5q33 common deleted region provided the first evidence for the importance of haploinsufficient gene expression in the del(5q) MDS pathogenesis (Ebert et al. 2008; Ebert 2011).

1.1.1 Pathogenesis of anemia in del(5q) MDS

The ribosomal protein S14 (*RPS14*) gene was identified as a critical gene for the erythroid phenotype of the 5q-syndrome using an RNA interference screen (Ebert, Pretz et al. 2008). Each of 40 genes in the 5q32-33 region was targeted by short hairpin (sh) RNAs, enabling a systematic evaluation of the effects of decreased expression of each gene. The shRNAs were introduced into primary human hematopoietic stem and progenitor cells (CD34+) using lentiviral vectors in order to examine the effect on erythroid differentiation. Only shRNA targeting RPS14 caused a severe block in erythroid differentiation without affection of megakaryopoiesis. Forced expression of *RPS14* in hematopoietic stem and progenitor cells purified from patients with the 5q− syndrome rescued the erythropoietic defect. Expression in del(5q) MDS is approximately 50% of expression in non del(5q) MDS and the non-deleted allele is not deleted showing that RPS14 is a haploinsufficiency disease gene.

RPS14 encodes a ribosomal protein that is of central importance for 18S precursor ribosomal RNA (pre-rRNA) processing and 40S ribosomal subunit formation. Inherited heterozygous loss-of-function mutations in at least 10 different ribosomal protein genes, including *RPS19* and *RPS24*, cause Diamond–Blackfan anemia (DBA), a rare congenital syndrome characterized by hypoplastic anemia and macrocytosis (Narla and Ebert 2010; Narla and Ebert 2011). The mutations are universally heterozygous, and functional studies indicate that homozygous inactivation of most if not all ribosomal genes would not be tolerated in a mammalian cell. In aggregate, the genetic data strongly indicate haploinsufficiency for ribosomal genes in the pathogenesis of macrocytic anemia in both DBA and the 5q-syndrome.

In both DBA and del(5q) MDS, haploinsufficiency of ribosomal genes is involved in the impairment of pre- rRNA processing and ribosome biogenesis and activates the p53 pathway (McGowan et al. 2008; Dutt et al. 2011). Decreased expression of RPS14 and RPS19 causes a dramatic increase in total p53 levels, expression of p53 target genes including p21 and cell cycle arrest.

Activation of p53 is mediated in large part through the actions of the human homolog of the mouse double minute 2 (MDM2) gene product (Raiser et al. 2014). MDM2 is an E3-ubiquitin ligase and key negative regulator of p53. MDM2 directly binds to the DNA binding domain of p53 where it interferes with transcriptional activation and ubiquitinates p53, thereby targeting it for proteasomal degradation. Disruption of ribosome assembly results in the liberation of free RPs that interact with MDM2 preventing its negative regulation of

p53 (Momand et al. 1992). Several ribosomal proteins including L5, L11, L23 and S7 bind to the zinc finger domain of MDM2 and inhibit p53 ubiquitination and degradation while triggering auto-ubiquitination of MDM2 (Narla and Ebert 2010). The resulting stabilization of p53 appears responsible for cell cycle arrest and apoptosis of erythroid precursors in the 5q- syndrome, manifest clinically as hypoplastic anemia.

Pharmacologic or genetic inactivation of p53 was shown to rescue the progenitor defect in mouse models of the 5q− syndrome, demonstrating the central mechanistic importance of p53 induction in the context of ribosomal protein haploinsufficiency (Barlow, Drynan et al. 2010). Taken together, these data indicate that the RP-MDM2-P53 axis is critical in the molecular pathogenesis of the 5q- syndrome.

It remains an open question how ribosomal haploinsufficiency causes a distinct erythroid-specific phenotype. p53 is a central mechanism in the erythroid differentiation defect in ribosomopathies. The mechanisms leading to induction of p53 are partly understood and have been mainly linked to the MDM2-p53 axis. The effect of ribosomal haploinsufficiency on protein synthesis are not completely understood. Central questions in del(5q) MDS specifically and in ribosomopathies are:

1. Does ribosomal haploinsufficiency impact protein synthesis in hematopoietic cells and in particular in the affected erythroid lineage?
2. Which proteins are differentially expressed in ribosomopathies and what is their impact on erythroid differentiation and p53 induction

In **chapter 2**, we describe the phenotype of a novel, conditional *Rps14* knockout mouse model that we have generated and address these questions. We describe a so far unexpected link between ribosomal haploinsufficiency and the p53-dependent erythroid differentiation defect.

1.1.2 Pathogenesis of megakaryocyte abnormalities in del(5q) MDS

While thrombocytopenia is common in MDS in general, some patients with del(5q) MDS even have an elevated platelet count and the bone marrow commonly displays pathognomonic, hypolobulated micromegakaryocytes (Giagounidis and Aul 2008). Patients with DBA do not have thrombocytosis, indicating that haploinsufficiency for a ribosomal gene does not generally cause elevated platelet counts or the hypolobulated and distinctive megakaryocyte morphology (Narla and Ebert 2010).

An analysis of of noncoding RNA in bone marrow from MDS patients identified several microRNAs (miRNAs) with dysregulated expression. MiR-145 and miR-146a, were shown to be abundantly expressed in normal hematopoietic progenitor cell populations and were specifically reduced in del(5q) MDS, and are indeed localized to 5q CDR (Starczynowski et al. 2010; Kumar et al. 2011).

Depletion of both miR-145 and miR-146a in murine HSPCs results in the clinically relevant thrombocytosis and megakaryocyte dysplasia, mediated in part by upregulation

of the miR-145 and miR-146a target genes *TIRAP* and *TRAF6* and consequently increased IL-6 secretion. It was suggested in these studies that miR-145 normally acts via repression of the transcription factor FLI1 to regulate megakaryocyte and erythroid maturation and differentiation. Cell culture models using patient samples demonstrated that the coordinate loss of miR-145 and *RPS14* in $CD34^+$ progenitors causes megakaryocyte differentiation, reduced erythroid colony formation, and reduced HSPC expansion, thereby recapitulating clinical key features of del(5q) MDS, and more specifically the 5q-syndrome. In line with this mechanism is the finding that patients with 5q- syndrome and decreased miR-145 levels demonstrate reciprocally increased expression of FLI1 (Kumar, Narla et al. 2011). The forced expression of miR-145 in CD34+ HSPCs purified from MDS patients mediates normalization of the megakaryocyte/erythroid colony ratio in patients with hemizygous del(5q), but not in patients with 5q diploidy.

1.1.3 Cell of origin and clonal selection

The del(5q) deletion is present in the hematopoietic stem cell compartment and can be found in all lineages (Nilsson et al. 2000; Nilsson et al. 2002). Cells harboring del(5q) gain a clonal advantage in the bone marrow and outcompete normal hematopoiesis over time.

Recent elegant sequencing studies in defined hematopoietic stem and progenitor cell populations in patients with isolated del(5q) MDS showed that the 5q-deletion is the initiating and potentially the only required genetic lesion for the development of del(5q) MDS and that the 5q deletion precedes acquisition of recurrent driver mutations in the progression of isolated del(5q) MDS (Woll et al. 2014). A total of 34 somatic lesions, including del(5q) and driver mutations, were identified in bulk bone marrow cells of 15 patients with lower-risk MDS and all these lesions could be tracked back to the stem cell compartment. In MDS cases with del(5q) and additional driver mutations, acquisition of del(5q) preceded recurrent gene mutations, with the exception of four MDS cases with sideroblastic anemia in which the del(5q) was preceded by *SF3B1* gene mutations. In all cases with isolated del(5q) or RAEB1/RCMD, the del(5q) was predicted to be the first (or only) genetic lesion.

It is still not completely understood how genetic haploinsufficiency confers a clonal advantage to HSC. A systematic dissection of all genes on 5q for genes that contribute to the clonal advantage of the del(5q) clone has not yet been reported.

However, murine models have provided the first functional evidence for the role of individual genes in the hematopoietic stem cell function and leukemia progression.

The early growth response 1 (EGR1) gene encodes a transcription factor that is a direct transcriptional regulator of many known tumor suppressor genes, including TP53, CDKN1A (p21) and PTEN (Min et al. 2008). Further, EGR1 has been shown to play a role in maintaining hematopoietic stem cell (HSC) quiescence and retention in the bone marrow. EGR1 is also located in the 5q31 CDR, was shown to be deleted in >95% of patients and is expressed at haploinsufficient levels (Joslin et al. 2007). In a murine model with heterozygous inactivation

of EGR1, HSC have increased mobilization from the bone marrow. In addition, mice with heterozygous loss of EGR1 develop leukemia with increased frequency and decreased latency in mice treated with the dealkylating agent, N-ethyl-nitrosourea (ENU) to induce secondary mutations comparable to therapy-related myeloid neoplasms (t-MN) (Joslin, Fernald et al. 2007).

Quite a few patients, however, have deletions of substantially larger regions of 5q CDR. As such, other genes localized to 5q outside the CDRs probably contribute to the phenotypic heterogeneity and clinical presentation of patients with del(5q) MDS. *APC*, located on 5q23, is deleted in the vast majority (95%) of del(5q) MDS and encodes a negative regulator of β-catenin/Wnt signaling. Inactivating mutations in APC are pathogenic in colon cancer. Mouse models demonstrate that haploinsufficiency of *Apc* causes expansion of the long-term HSC population but also exhaustion of the HSC function in secondary transplants (Wang et al. 2010). Similarly, mice lacking the APC(min) allele – resulting in heterozygous loss of function for APC- have increased repopulation ability only in primary transplants but decreased repopulation potential in secondary transplants (Lane et al. 2010).

Given the role of b-Catenin in the regulation of hematopoietic stem cell renewal and malignancies, APC haploinsufficiency might contribute to the pathogenesis of del(5q) MDS through increased Wnt signaling and intranuclear b-Catenin accumulation.

Current evidence suggests that the clinical phenotype of the 5q− syndrome represents the compound effects of haploinsufficiency of multiple genes within the 5q33 CDR. Recent studies showed that combined heterozygous loss of *Egr1* and *Apc* in mice promotes the pathogenesis of MDS/AML, in particular in co-operation with knockdown of *Trp53* and/or alkylating agent therapy (Stoddart et al. 2013; Stoddart et al. 2014).

Multiple other genes have been implicated in the pathogenesis of del(5q) MDS but the precise role of these genes in the phenotype of patients with del(5q) MDS has not been well-established. The SPARC gene is located on the CDR and homozygous deletion has been shown to cause thrombocytopenia in mice as well as decreased erythroid colony formation. SPARC has haploinsufficient expression in del(5q) MDS and treatment with lenalidomide increased the expression of the gene (Lehmann et al. 2007).

It remains an open question in the field how haploinsufficiency confers a clonal advantage to hematopoietic cells. Studies so far suggested that Wnt signaling might play a central role in this process.

Central questions in the clonal advantage of the HSC in del(5q) MDS are:

1. Can haploinsufficiency for one gene confer a clonal advantage to the HSC?
2. How does Wnt-signaling contribute to the clonal advantage in del(5q) MDS?
3. Can the identified mechanisms be targeted for eradication of the del(5q) MDS HSC?

In **chapter 3**, we study the role of the casein kinase 1A1 gene (*CSNK1A1). CSNK1A1* is a putative tumor suppressor gene located in the common deleted region for del(5q) myelodysplastic syndrome (MDS) and a part of the b-Catenin destruction complex. We generated a murine

model with conditional inactivation of *Csnk1a1* and study the hematopoietic stem cell expansion and the role of b-Catenin on the regulation of the hematopoietic stem cell. We demonstrate a mechanism in the clonal advantage of the HSC which sensitizes del(5q) MDS cells to therapy (**Chapter 3 and Chapter 4**).

1.1.4 Treatment options

Lenalidomide has been approved by the US Food and Drug Administration for the treatment of low-risk MDS with del(5q). In this patient cohort, lenalidomide induces a complete cytogenetic response in 50% to 60%, while 55% to 70% achieve transfusion independence (List et al. 2006; Fenaux et al. 2011). Nevertheless, in patients with complete cytogenetic remission, the del(5q) clone persists in $CD34^{+}CD38{-}CD90+$ hematopoietic stem cell fraction. Further, the presence of small disease subclones with *TP53* mutations in biopsies before treatment is associated with relative resistance to lenalidomide and might also predict a reduced a reduced treatment response (Jadersten et al. 2009). Lenalidomide has been shown to inhibit the growth of MDS del(5q) erythroblasts but did not affect normal cells in culture (Pellagatti et al. 2007).

The mode of action of lenalidomide has been investigated in several studies. Lenalidomide has been shown to upregulate several genes, including the tumor suppressor gene *SPARC* and the TGF-β family member activin A, in hematopoietic progenitor cells from patients with del(5q) MDS and normal individuals (Pellagatti, Jadersten et al. 2007; Venner et al. 2013). SPARC, located at 5q32-q33 within the CDR of the 5q- syndrome, has anti-proliferative, anti-adhesive, and anti-angiogenic properties, all known effects of immunomodulatory drugs (Komrokji and List 2011). Wei et al demonstrated that lenalidomide inhibits two phosphatases, Cdc25C and PP2Acα. The genes for these phosphatases are located on 5q and are deleted in most patients with del(5q) MDS (Wei et al. 2009). Cdc25C and PP2Acα are co-regulators of the G2-M checkpoint in the cell cycle and thus their inhibition by lenalidomide leads to G2 arrest and apoptosis. These data suggest that haploinsufficiency of Cdc25C and PP2Acα in del(5q) MDS causes an enhanced sensitivity to lenalidomide.

Lenalidomide has been shown to promote degradation of p53 by inhibiting auto-ubiquitination of MDM2 in del(5q) MDS (Wei et al. 2013). In this study, it has been suggested that lenalidomide restores MDM2 functionality in the 5q-syndrome to overcome p53 activation in response to ribosomal stress.

Lenalidomide is clearly an effective treatment for lower-risk, transfusion-dependent MDS patients with del(5q), however not all patients respond to lenalidomide and approximately half of MDS patients with del(5q) acquire resistance to the drug within two to three years (List, Dewald et al. 2006).

There is thus a clinical need for novel treatments for MDS patients with del(5q). It is crucial to understand targets of lenalidomide to find a more specific therapy leading to the complete elimination of the del(5q) MDS. It would be optimal to directly target

haploinsufficiency of the del(5q) MDS clone to eliminate the 5q- clone but not normal hematopoiesis.

In **chapter 4**, we demonstrate that lenalidomide induces the ubiquitination and consequent degradation of *CSNK1A1* by the CRBN-CRL4 E3 ubiquitin ligase. Knockdown of *CSNK1A1* sensitized primary CD34+ cells to lenalidomide, suggesting that haploinsufficiency of *CSNK1A1* might increase lenalidomide sensitivity in del(5q) hematopoietic cells.

MODEL SYSTEMS FOR DISSECTING HEMATOPOIESIS IN EXTRAMEDULLARY SITES

Hematopoietic stem and progenitor cells reside in a complex microenvironment containing mesenchymal progenitor cells, adipocytes, osteoblasts, endothelial cells and multiple components of the extracellular matrix (Scadden 2007). Collectively, these cellular elements and the extracellular matrix constitute the hematopoietic niche that regulates the size of the hematopoietic stem and progenitor cell pool and their fate.

It was shown that mesenchymal stromal cells play a critical role in the function and self-renewal of hematopoietic stem and progenitor cells (Crisan et al. 2008; Mendez-Ferrer et al. 2010; Scadden 2012; Medyouf et al. 2014). Mesenchymal stromal cells as precursors of mesenchymal cell types in the bone marrow niche as adipocytes, osteoblasts and fibroblasts represent important, defining cell types of the niche.

A number of studies have been conducted to understand the components of the hematopoietic niche where the stem cell resides and proliferates.

Three major components have been defined which distinguish the bone marrow niche from other types of mesenchymal tissues: 1) mesenchymal stromal cells, 2) extracellular matrix, mainly collagen I and 3) cells with osteogenic potential that ensure the mineral content of the bone (Leisten et al. 2012). In vivo, primitive hematopoietic stem and progenitor cells reside in close association with the endosteal niche, that means in close proximity to the collagen I bone matrix, mesenchymal stromal cells and osteoblasts and their precursors, have high proliferative potential and repopulating abilities.

The bone marrow has further emerged as an attractive therapeutic target for cellular and molecular therapies that aim to modulate the host's blood and immune system but also for the treatment of MDS (Raaijmakers and Scadden 2008; Raaijmakers et al. 2010). A deeper understanding of the mechanism that governs HSPC trafficking and engraftment is essential to improve the clinical effectiveness of hematopoietic transplantation, the development of new oncotherapies, and the targeting of bone marrow therapeutics.

A major challenge in probing the bone marrow microenvironment is that the experimental platforms to do so are non-physiological and/or low-throughput in nature. *In vitro* models using transwell chambers have been explored to understand HSPC migration,

but these experiments do not account for the complexity of this tissue and its components (Jorda et al. 2002).

Comparable to the components which have been described to distinguish the bone from other mesenchymal tissues, necessary components for the regulation of hematopoietic stem and progenitor cells have been described (Wright et al. 2001; Lapidot et al. 2005; Wilson and Trumpp 2006; Kiel and Morrison 2008). These components include (1) a specialized sinusoidal vasculature, (2) non-hematopoietic cells that support retention and engraftment by direct cell–cell interactions and by the secretion of soluble and insoluble factors, and (3) a sponge-like geometry that concentrates hematopoietic cells and molecules within the cavity. *In vivo* experiments using adoptive transfer or parabiotic mouse models retain these components and are the gold standard for studying hematopoietic cell trafficking in a physiological setting. Although these methods provide valuable insight into migration and functional engraftment of HSPCs, in situ analysis of the dynamics of cells in the bone marrow remain elusive because of the anatomical inaccessibility and opacity of bone. Intravital imaging of calvarial bone marrow has been developed to capture an unprecedented level of HSPC dynamics in the bone marrow and has contributed significantly to our understanding of hematopoietic niches (Sipkins et al. 2005; Lo Celso et al. 2009). Aside from the likelihood that calvarial bone may not represent other classical marrow cavities, a key limitation with this approach and other in vivo studies is that the bone marrow microenvironment is determined by the host's genetics with little opportunity for manipulating cell populations in a controlled fashion. These limitations also restrict the modeling of human-specific environmental interactions.

It was thus the goal of the study described in **chapter 5** to to build a reproducible and accessible structure that can be used to create localized microenvironments with controlled and defined variables for experimentation. Ectopic implants that recreate key features of a tissue are an intermediate approach that can offer a tremendous advantage to the study and manipulation of a microenvironment for basic and applied research (Krebsbach et al. 1997; Chen et al. 2011). Investigators, including ourselves, have attempted to make tissue-engineered structures that resemble bone (Sacchetti et al. 2007; Schneider et al. 2010; Schneider et al. 2010; Song et al. 2010), but considerable improvements are needed to allow adoption of these constructs in hematopoietic cell biology.

In the current study it was our goal to focus on important design criteria including (1) the opportunity for reproducible and user-defined properties such as the choice of substrate, extracellular matrix, cell types, and degradability; (2) the ability to induce vascularisation; (3) accessibility and suitability for complementary histological/cytological analysis; and, most importantly, (4) the functional ability to capture and retrieve endogenous hematopoietic cells efficiently.

REFERENCES

Barlow, J. L., L. F. Drynan, et al. (2010). „A p53-dependent mechanism underlies macrocytic anemia in a mouse model of human 5q- syndrome." Nat Med **16**(1): 59-66.

Bejar, R., R. Levine, et al. (2011). „Unraveling the molecular pathophysiology of myelodysplastic syndromes." J Clin Oncol **29**(5): 504-515.

Boultwood, J., C. Fidler, et al. (1994). „Molecular mapping of uncharacteristically small 5q deletions in two patients with the 5q- syndrome: delineation of the critical region on 5q and identification of a 5q- breakpoint." Genomics **19**(3): 425-432.

Boultwood, J., C. Fidler, et al. (2002). „Narrowing and genomic annotation of the commonly deleted region of the 5q- syndrome." Blood **99**(12): 4638-4641.

Boultwood, J., A. Pellagatti, et al. (2007). „Gene expression profiling of CD34+ cells in patients with the 5q- syndrome." Br J Haematol **139**(4): 578-589.

Chen, A. A., D. K. Thomas, et al. (2011). „Humanized mice with ectopic artificial liver tissues." Proc Natl Acad Sci U S A **108**(29): 11842-11847.

Christiansen, D. H., M. K. Andersen, et al. (2001). „Mutations with loss of heterozygosity of p53 are common in therapy-related myelodysplasia and acute myeloid leukemia after exposure to alkylating agents and significantly associated with deletion or loss of 5q, a complex karyotype, and a poor prognosis." J Clin Oncol **19**(5): 1405-1413.

Crisan, M., S. Yap, et al. (2008). „A perivascular origin for mesenchymal stem cells in multiple human organs." Cell Stem Cell **3**(3): 301-313.

Dutt, S., A. Narla, et al. (2011). „Haploinsufficiency for ribosomal protein genes causes selective activation of p53 in human erythroid progenitor cells." Blood **117**(9): 2567-2576.

Ebert, B. L. (2009). „Deletion 5q in myelodysplastic syndrome: a paradigm for the study of hemizygous deletions in cancer." Leukemia **23**(7): 1252-1256.

Ebert, B. L. (2011). „Molecular dissection of the 5q deletion in myelodysplastic syndrome." Semin Oncol **38**(5): 621-626.

Ebert, B. L., J. Pretz, et al. (2008). „Identification of RPS14 as a 5q- syndrome gene by RNA interference screen." Nature **451**(7176): 335-339.

Fenaux, P., A. Giagounidis, et al. (2011). „A randomized phase 3 study of lenalidomide versus placebo in RBC transfusion-dependent patients with Low-/Intermediate-1-risk myelodysplastic syndromes with del5q." Blood **118**(14): 3765-3776.

Giagounidis, A. A. and C. Aul (2008). „The 5q- syndrome." Cancer Treat Res **142**: 133-148.

Gondek, L. P., R. Tiu, et al. (2008). „Chromosomal lesions and uniparental disomy detected by SNP arrays in MDS, MDS/MPD, and MDS-derived AML." Blood **111**(3): 1534-1542.

Graubert, T. A., M. A. Payton, et al. (2009). „Integrated genomic analysis implicates haploinsufficiency of multiple chromosome 5q31.2 genes in de novo myelodysplastic syndromes pathogenesis." PLoS One **4**(2): e4583.

Greenberg, P. L., H. Tuechler, et al. (2012). „Revised international prognostic scoring system for myelodysplastic syndromes." Blood **120**(12): 2454-2465.

Haase, D., U. Germing, et al. (2007). „New insights into the prognostic impact of the karyotype in MDS and correlation with subtypes: evidence from a core dataset of 2124 patients." Blood **110**(13): 4385-4395.

Heinrichs, S., R. V. Kulkarni, et al. (2009). „Accurate detection of uniparental disomy and microdeletions by SNP array analysis in myelodysplastic syndromes with normal cytogenetics." Leukemia **23**(9): 1605-1613.

Jadersten, M., L. Saft, et al. (2009). „Clonal heterogeneity in the 5q- syndrome: p53 expressing progenitors prevail during lenalidomide treatment and expand at disease progression." Haematologica **94**(12): 1762-1766.

Jerez, A., L. P. Gondek, et al. (2012). „Topography, clinical, and genomic correlates of 5q myeloid malignancies revisited." J Clin Oncol **30**(12): 1343-1349.

Jorda, M. A., S. E. Verbakel, et al. (2002). „Hematopoietic cells expressing the peripheral cannabinoid receptor migrate in response to the endocannabinoid 2-arachidonoylglycerol." Blood **99**(8): 2786-2793.

Joslin, J. M., A. A. Fernald, et al. (2007). „Haploinsufficiency of EGR1, a candidate gene in the del(5q), leads to the development of myeloid disorders." Blood **110**(2): 719-726.

Kantarjian, H., S. O'Brien, et al. (2009). „The heterogeneous prognosis of patients with myelodysplastic syndrome and chromosome 5 abnormalities: how does it relate to the original lenalidomide experience in MDS?" Cancer **115**(22): 5202-5209.

Kiel, M. J. and S. J. Morrison (2008). „Uncertainty in the niches that maintain haematopoietic stem cells." Nat Rev Immunol **8**(4): 290-301.

Komrokji, R. S. and A. F. List (2011). „Role of lenalidomide in the treatment of myelodysplastic syndromes." Semin Oncol **38**(5): 648-657.

Krebsbach, P. H., S. A. Kuznetsov, et al. (1997). „Bone formation in vivo: comparison of osteogenesis by transplanted mouse and human marrow stromal fibroblasts." Transplantation **63**(8): 1059-1069.

Kumar, M. S., A. Narla, et al. (2011). „Coordinate loss of a microRNA and protein-coding gene cooperate in the pathogenesis of 5q- syndrome." Blood **118**(17): 4666-4673.

Lane, S. W., S. M. Sykes, et al. (2010). „The Apc(min) mouse has altered hematopoietic stem cell function and provides a model for MPD/MDS." Blood **115**(17): 3489-3497.

Lapidot, T., A. Dar, et al. (2005). „How do stem cells find their way home?" Blood **106**(6): 1901-1910.

Lehmann, S., J. O'Kelly, et al. (2007). „Common deleted genes in the 5q- syndrome: thrombocytopenia and reduced erythroid colony formation in SPARC null mice." Leukemia **21**(9): 1931-1936.

Leisten, I., R. Kramann, et al. (2012). „3D co-culture of hematopoietic stem and progenitor cells and mesenchymal stem cells in collagen scaffolds as a model of the hematopoietic niche." Biomaterials **33**(6): 1736-1747.

List, A., G. Dewald, et al. (2006). „Lenalidomide in the myelodysplastic syndrome with chromosome 5q deletion." N Engl J Med **355**(14): 1456-1465.

Lo Celso, C., H. E. Fleming, et al. (2009). „Live-animal tracking of individual haematopoietic stem/progenitor cells in their niche." Nature **457**(7225): 92-96.

McGowan, K. A., J. Z. Li, et al. (2008). „Ribosomal mutations cause p53-mediated dark skin and pleiotropic effects." Nat Genet **40**(8): 963-970.

Medyouf, H., M. Mossner, et al. (2014). „Myelodysplastic cells in patients reprogram mesenchymal stromal cells to establish a transplantable stem cell niche disease unit." Cell Stem Cell **14**(6): 824-837.

Mendez-Ferrer, S., T. V. Michurina, et al. (2010). „Mesenchymal and haematopoietic stem cells form a unique bone marrow niche." Nature **466**(7308): 829-834.

Min, I. M., G. Pietramaggiori, et al. (2008). „The transcription factor EGR1 controls both the proliferation and localization of hematopoietic stem cells." Cell Stem Cell **2**(4): 380-391.

Mollgard, L., L. Saft, et al. (2011). „Clinical effect of increasing doses of lenalidomide in high-risk myelodysplastic syndrome and acute myeloid leukemia with chromosome 5 abnormalities." Haematologica **96**(7): 963-971.

Momand, J., G. P. Zambetti, et al. (1992). „The mdm-2 oncogene product forms a complex with the p53 protein and inhibits p53-mediated transactivation." Cell **69**(7): 1237-1245.

Narla, A. and B. L. Ebert (2010). „Ribosomopathies: human disorders of ribosome dysfunction." Blood **115**(16): 3196-3205.

Narla, A. and B. L. Ebert (2011). „Translational medicine: ribosomopathies." Blood **118**(16): 4300-4301.

Nilsson, L., I. Astrand-Grundstrom, et al. (2002). „Involvement and functional impairment of the CD34(+)CD38(-) Thy-1(+) hematopoietic stem cell pool in myelodysplastic syndromes with trisomy 8." Blood **100**(1): 259-267.

Nilsson, L., I. Astrand-Grundstrom, et al. (2000). „Isolation and characterization of hematopoietic progenitor/stem cells in 5q-deleted myelodysplastic syndromes: evidence for involvement at the hematopoietic stem cell level." Blood **96**(6): 2012-2021.

Pellagatti, A., M. Jadersten, et al. (2007). „Lenalidomide inhibits the malignant clone and up-regulates the SPARC gene mapping to the commonly deleted region in 5q- syndrome patients." Proc Natl Acad Sci U S A **104**(27): 11406-11411.

Raaijmakers, M. H., S. Mukherjee, et al. (2010). „Bone progenitor dysfunction induces myelodysplasia and secondary leukaemia." Nature **464**(7290): 852-857.

Raaijmakers, M. H. and D. T. Scadden (2008). „Evolving concepts on the microenvironmental niche for hematopoietic stem cells." Curr Opin Hematol **15**(4): 301-306.

Raiser, D. M., A. Narla, et al. (2014). „The emerging importance of ribosomal dysfunction in the pathogenesis of hematologic disorders." Leuk Lymphoma **55**(3): 491-500.

Sacchetti, B., A. Funari, et al. (2007). „Self-renewing osteoprogenitors in bone marrow sinusoids can organize a hematopoietic microenvironment." Cell **131**(2): 324-336.

Scadden, D. T. (2007). „The stem cell niche in health and leukemic disease." Best Pract Res Clin Haematol **20**(1): 19-27.

Scadden, D. T. (2012). „Rethinking stroma: lessons from the blood." Cell Stem Cell **10**(6): 648-649.

Schneider, R. K., S. Neuss, et al. (2010). „[Mesenchymal stem cells for bone tissue engineering]." Pathologe **31 Suppl 2**: 138-146.

Schneider, R. K., A. Puellen, et al. (2010). „The osteogenic differentiation of adult bone marrow and perinatal umbilical mesenchymal stem cells and matrix remodelling in three-dimensional collagen scaffolds." Biomaterials **31**(3): 467-480.

Sipkins, D. A., X. Wei, et al. (2005). „In vivo imaging of specialized bone marrow endothelial microdomains for tumour engraftment." Nature **435**(7044): 969-973.

Song, J., M. J. Kiel, et al. (2010). „An in vivo model to study and manipulate the hematopoietic stem cell niche." Blood **115**(13): 2592-2600.

Sportoletti, P., S. Grisendi, et al. (2008). „Npm1 is a haploinsufficient suppressor of myeloid and lymphoid malignancies in the mouse." Blood **111**(7): 3859-3862.

Starczynowski, D. T., F. Kuchenbauer, et al. (2010). „Identification of miR-145 and miR-146a as mediators of the 5q- syndrome phenotype." Nat Med **16**(1): 49-58.

Stoddart, A., A. A. Fernald, et al. (2013). „Haploinsufficiency of del(5q) genes, Egr1 and Apc, cooperate with Tp53 loss to induce acute myeloid leukemia in mice." Blood.

Stoddart, A., J. Wang, et al. (2014). „Cell intrinsic and extrinsic factors synergize in mice with haploinsufficiency for Tp53, and two human del(5q) genes, Egr1 and Apc." Blood **123**(2): 228-238.

Tefferi, A. and J. W. Vardiman (2009). „Myelodysplastic syndromes." N Engl J Med **361**(19): 1872-1885.

Van den Berghe, H., J. J. Cassiman, et al. (1974). „Distinct haematological disorder with deletion of long arm of no. 5 chromosome." Nature **251**(5474): 437-438.

Vardiman, J. W., J. Thiele, et al. (2009). „The 2008 revision of the World Health Organization (WHO) classification of myeloid neoplasms and acute leukemia: rationale and important changes." Blood **114**(5): 937-951.

Venner, C. P., J. W. Woltosz, et al. (2013). „Correlation of clinical response and response duration with miR-145 induction by lenalidomide in CD34(+) cells from patients with del(5q) myelodysplastic syndrome." Haematologica **98**(3): 409-413.

Wang, J., A. A. Fernald, et al. (2010). „Haploinsufficiency of Apc leads to ineffective hematopoiesis." Blood **115**(17): 3481-3488.

Wei, S., X. Chen, et al. (2013). „Lenalidomide promotes p53 degradation by inhibiting MDM2 auto-ubiquitination in myelodysplastic syndrome with chromosome 5q deletion." Oncogene **32**(9): 1110-1120.

Wei, S., X. Chen, et al. (2009). „A critical role for phosphatase haplodeficiency in the selective suppression of deletion 5q MDS by lenalidomide." Proc Natl Acad Sci U S A **106**(31): 12974-12979.

Wilson, A. and A. Trumpp (2006). „Bone-marrow haematopoietic-stem-cell niches." Nat Rev Immunol **6**(2): 93-106.

Woll, P. S., U. Kjallquist, et al. (2014). „Myelodysplastic Syndromes Are Propagated by Rare and Distinct Human Cancer Stem Cells In Vivo." Cancer Cell.

Wright, D. E., A. J. Wagers, et al. (2001). „Physiological migration of hematopoietic stem and progenitor cells." Science **294**(5548): 1933-1936.

2

RPS14 HAPLOINSUFFICIENCY CAUSES A BLOCK IN ERYTHROID DIFFERENTIATION MEDIATED BY S100A8/S100A9

Rebekka K. Schneider[1,2], Monica Schenone[3], Monica Ventura Ferreira[2], Rafael Kramann[4], Cailin E. Joyce[5], Christina Hartigan[3], Fabian Beier[2], Tim H. Brümmendorf[2], Ulrich Gehrming[6], Uwe Platzbecker[7], Guntram Büsche[8], Ruth Knüchel[9], Michelle C. Chen[1], Christopher S. Waters[1], Edwin Chen[1], Lisa P. Chu[1], Carl D. Novina[5], R. Coleman Lindsley[1, 5], Steven A. Carr[2], Benjamin L. Ebert[1,3]

[1]Division of Hematology, Department of Medicine, Brigham and Women's Hospital, Harvard Medical School, Boston, MA 02115, USA.
[2]Department of Hematology, Hemostaseology, Oncology and Stem Cell Transplantation, University Hospital RWTH Aachen, 52074 Aachen, Germany
[3]Broad Institute of Harvard University and the Massachusetts Institute of Technology, Cambridge, MA 02142, USA
[4]Renal Division, Brigham and Women's Hospital, Boston, MA 02115, USA.
[5]Dana-Farber Cancer Institute, Boston, MA, 02215
[6]Department of Hematology, Oncology and Clinical Immunology, Heinrich-Heine-University, 40225 Düsseldorf, Germany
[7]Department of Medicine I, University Hospital Carl Gustav Carus, University of Technology 01307 Dresden, Germany
[8]Institute of Pathology, Hannover Medical School, 30625 Hannover, Germany
[9]Institute of Pathology, University Hospital RWTH Aachen, 52074 Aachen, Germany

Nature Medicine 2016 March; 22(3):288-97.

ABSTRACT

Heterozygous deletion of *RPS14* occurs in del(5q) MDS and has been linked to impaired erythropoiesis, characteristic of this disease subtype. We generated a murine model with conditional inactivation of *Rps14* and demonstrated a p53-dependent erythroid differentiation defect with apoptosis at the transition from polychromatic to orthochromatic erythroblasts resulting in age-dependent progressive anemia, megakaryocyte dysplasia, and loss of hematopoietic stem cell (HSC) quiescence. Using quantitative proteomics, we identified significantly increased expression of proteins involved in innate immune signaling, particularly the heterodimeric S100a8/S100a9 proteins in purified erythroblasts. S100a8 expression was significantly increased in erythroblasts, monocytes and macrophages and recombinant S100a8 was sufficient to induce an erythroid differentiation defect in wild-type cells. We rescued the erythroid differentiation defect in *Rps14* haploinsufficient HSCs by genetic inactivation of S100a8 expression. Our data link *Rps14* haploinsufficiency to activation of the innate immune system via induction of S100A8/A9 and the p53-dependant erythroid differentiation defect in del(5q) MDS.

INTRODUCTION

Isolated, interstitial deletion of Chromosome 5q in patients with myelodysplastic syndrome (MDS) is associated with a clinical phenotype termed the 5q- syndrome that is characterized by a severe macrocytic anemia, a normal or elevated platelet count with hypolobated micromegakaryocytes and a low rate of progression to acute myelogenous leukemia[1-3]. The severe macrocytic anemia in del(5q) MDS patients has been linked to haploinsufficiency of the ribosomal protein small subunit 14 (RPS14)[4]. In a screen of the 5q33 common deleted region associated with the 5q- syndrome, only shRNAs targeting the *RPS14* gene caused a severe block in erythroid differentiation, while forced overexpression of *RPS14* in cells from MDS patients with the 5q deletion rescued erythropoeisis[4].

Germline, heterozygous inactivating mutations or deletions of *RPS19* and other ribosomal protein genes cause Diamond-Blackfan anemia (DBA), a disorder that, like del(5q) MDS, is characterized by macrocytic anemia[5-9]. Decreased expression of individual ribosomal proteins, including RPS19 and RPS14, increases p53 levels and p53 target gene expression in cell lines, primary human hematopoietic progenitor cells, and patient samples[10-12]. Pharmacologic or genetic inactivation of p53 rescues the differentiation defect of progenitor cells in multiple model systems[7,8,10,13].

Several *in vivo* models of ribosome dysfunction have been described[14]. A murine model with hematopoietic-specific heterozygous deletion of *Rps6* recapitulated the erythroid phenotype of del(5q) MDS and DBA that is rescued by p53 inactivation, though *RPS6* inactivation has not been described in either DBA or MDS[7,8,15]. To model del(5q) MDS, a mouse was generated wherein a series of DNA segments syntenic to the commonly deleted region on human chromosome 5, including *Rps14*, was conditionally deleted from the hematopoietic stem cell compartment[13]. Heterozygous loss of this region resulted in a macrocytic anemia and dysplastic megakaryocytes, thereby recapitulating aspects of the 5q-syndrome. The smallest deleted segment tested that maintained the erythroid defect included *Rps14* and 7 other genes.

In order to investigate the hematologic phenotype and molecular consequences specific to *Rps14* haploinsufficiency *in vivo*, and to explore the role of this gene in del(5q) MDS, we generated a murine model with conditional *Rps14* inactivation.

RESULTS

Rps14 haploinsufficiency induces a p53-dependent erythroid differentiation defect in late-stage erythroblasts

We generated a conditional *Rps14* knockout model in which exons 2-4 are flanked by loxP sites (Suppl. Fig. 1a). Following crosses to *Mx1Cre+* transgenic mice, we induced *Rps14* excision in hematopoietic cells by poly(I:C) treatment and confirmed haploinsufficient expression of *Rps14* (Suppl. Fig. 1b, c). Mice with *Rps14* haploinsufficiency in hematopoietic cells developed a progressive anemia (Fig. 1a; Suppl. Fig. 1d, e). At approximately 550 days of age, the reticulocyte count of *Rps14* haploinsufficient mice decreased precipitously and was associated with death in a subset of mice (Fig. 1a, b).

We next determined whether *Rps14* haploinsufficiency causes a discrete, stage-specific defect in erythroid development. We characterized the stages of erythropoiesis by flow cytometry on the basis of Ter119 and CD71 expression (Supplementary Fig. 1d). *Rps14* haploinsufficient mice had impaired erythropoiesis at the transition from $CD71^{+}Ter119^{+}$ basophilic and early chromatophilic erythroblasts (RII) to $CD71^{intermediate/low}Ter119^{+}$ poly/orthochromatophilic erythroblasts and enucleated erythrocytes (RIII/RIV), (Fig. 1c). *Rps14* haploinsufficient mice had significant splenomegaly with repression of the white pulp due to an expansion of the early erythroid compartment (Fig. 1d; Suppl. Fig. 1i). Younger mice, 22 weeks after excision, also had impaired differentiation at the RIII/IV transition ($p<0.001$) with a decrease in quiescence of cells in the RI population ($p>0.001$,); (Suppl. Fig. 1f, g), together suggesting that younger *Rps14* haploinsufficient mice induce compensatory increase in erythropiesis causing a delay in development of severe anemia. To determine whether the anemia is driven by *Rps14* haploinsufficiency in hematopoietic cells but not in the bone marrow stroma, we generated mixed bone marrow chimeras (Suppl. Fig. 1h). Wild-type mice transplanted with *Rps14* haploinsufficient hematopoietic cells developed anemia with kinetics similar to untransplanted mice, confirming that the phenotype is caused by excision of *Rps14* in hematopoietic cells.

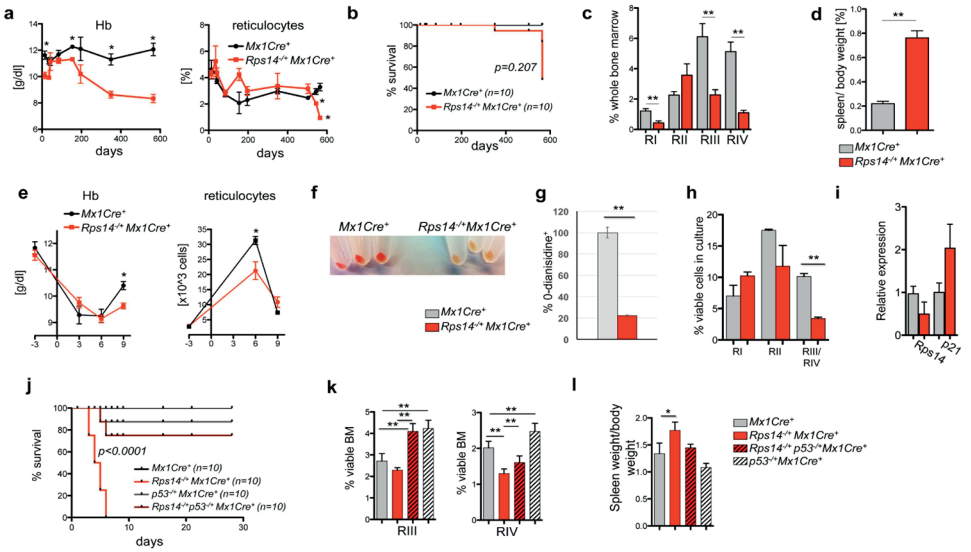

Figure 1: *Rps14* haploinsufficiency results in a p53-mediated erythroid differentiation defect. (a) Hemoglobin levels (Hb) and % of reticulocytes in the peripheral blood from *Rps14*$^{-/+}$*Mx1Cre*$^{+}$ mice in comparison to *Mx1Cre*$^{+}$ wild-type controls. (mean±SD, n=10; *p<0.05). (b) Kaplan-Meier survival curve of *Rps14*$^{-/+}$*Mx1Cre*$^{+}$ (n=10) and *Mx1Cre*$^{+}$ control mice (n=10). Time point 0 is the day of the first of three poly(I:C) inductions. (c) Frequency of RI-RIV erythroid progenitor populations (RI: CD71^{high}Ter119^{-}; RII: CD71^{high}Ter119^{+}; RIII: CD71^{intermediate}Ter119^{+}; RIV: CD71^{-}Ter119^{+}) among viable bone marrow cells in *Mx1Cre*$^{+}$ and *Rps14*$^{-/+}$*Mx1Cre*$^{+}$ mice 18 months after poly(I:C); (mean±SD, n=5; **p<0.001). (d) Relative spleen to body weight [%] of *Mx1Cre*$^{+}$ and *Rps14*$^{-/+}$*Mx1Cre*$^{+}$ mice 18 months after poly(I:C); (mean±SD, n=5; **p<0.001). (e) Hb level and reticulocyte counts in the peripheral time blood at serial time points before and after 25mg/kg Phenylhydrazine injection (mean±SD, n=8; *p<0.05). (f) Cell pellets of lineage-negative HSPCs subjected to erythroid differentiation *in vitro* for 5 days. (g) Quantification of different erythroid differentiation stages 5 days after induction of erythroid differentiation (mean±SD; n=3 biological replicates; **p<0.001). (h) Quantification of *p21* and *Rps14* transcript levels by quantitative real-time PCR in cells exposed for 5 days to erythroid differentiation. Data are normalized to expression in *Mx1Cre*$^{+}$ control cells (n=5 biological replicates; mean±SD). (i) Kaplan-Meier survival curve after treatment with 35mg/kg Phenylhydrazine on two consecutive days (day 0 and day 1) of *Rps14*$^{-/+}$*Mx1Cre*$^{+}$ (n=10), *p53*$^{-/+}$*Mx1Cre*$^{+}$ (n=10), *Rps14*$^{-/+}$*p53*$^{-/+}$*Mx1Cre*$^{+}$ (n=10) and *Mx1Cre*$^{+}$ control mice (n=10). (j) Frequency of RIII and RIV erythroid progenitor populations among viable bone marrow cells in 10-12 week old *Rps14*$^{-/+}$*Mx1Cre*$^{+}$ (n=14), *p53*$^{-/+}$*Mx1Cre*$^{+}$ (n=5), *Rps14*$^{-/+}$*p53*$^{-/+}$*Mx1Cre*$^{+}$ (n=5) and *Mx1Cre*$^{+}$ control mice (n=8) characterized by differential CD71 and Ter119 expression 9 days after the first treatment with 25mg/kg Phenylhydrazine (mean±SD; **p<0.001). Unpaired two-sided *t*-test (a-i) or multiple group comparison (i, j) using analysis of variance with posthoc Tukey correction were applied for statistical analysis.

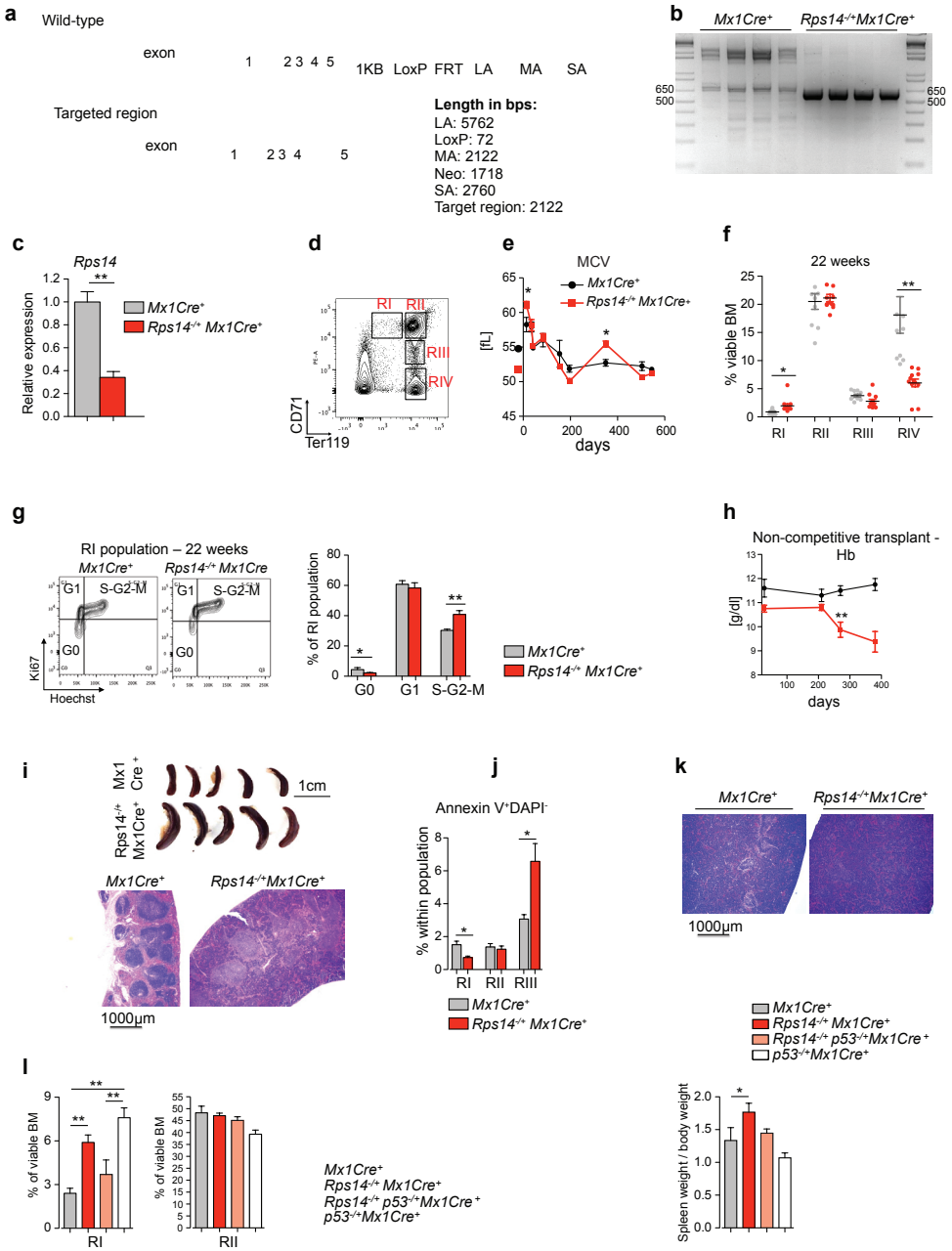
a
Wild-type
exon
1
2 3 4 5
1KB LoxP FRT LA MA SA
Targeted region
exon
1
2 3 4
5
Length in bps:
LA: 5762
LoxP: 72
MA: 2122
Neo: 1718
SA: 2760
Target region: 2122
b
Mx1Cre+
Rps14-/+Mx1Cre+
650
500
650
500
c
Rps14
Relative expression
Mx1Cre+
Rps14-/+ Mx1Cre+
d
RI
RII
RIII
RIV
CD71
Ter119
e
MCV
Mx1Cre+
Rps14-/+ Mx1Cre+
[fL]
days
f
22 weeks
% viable BM
RI
RII
RIII
RIV
g
RI population – 22 weeks
Mx1Cre+
Rps14-/+ Mx1Cre
G1
S-G2-M
G0
Ki67
Hoechst
% of RI population
G0
G1
S-G2-M
Mx1Cre+
Rps14-/+ Mx1Cre+
h
Non-competitive transplant - Hb
[g/dl]
days
i
Mx1 Cre+
Rps14-/+ Mx1Cre+
1cm
Mx1Cre+
Rps14-/+Mx1Cre+
1000µm
j
Annexin V+DAPI-
% within population
RI
RII
RIII
Mx1Cre+
Rps14-/+ Mx1Cre+
k
Mx1Cre+
Rps14-/+Mx1Cre+
1000µm
Mx1Cre+
Rps14-/+ Mx1Cre+
Rps14-/+ p53-/+Mx1Cre+
p53-/+Mx1Cre+
l
% of viable BM
RI
% of viable BM
RII
Mx1Cre+
Rps14-/+ Mx1Cre+
Rps14-/+ p53-/+Mx1Cre+
p53-/+Mx1Cre+
Spleen weight / body weight

Supplementary figure 1: **Targeting construct and consequences of *Rps14* haploinsufficiency on the erythroid phenotype.** (a) Schematic of the targeting construct. The *Rps14* target region is 2.12 Kb and includes exon 2-4. The region was designed such that the 5' homology arm extends about 5.76 Kb 5' to the single LoxP. The 3' homology arm ends 3' to the loxP/FRT flanked Neo cassette and is 2.76 Kb long. The loxP/FRT flanked Neo cassette was inserted 255 bp downstream of exon 4. The single loxP site was inserted 379 bp upstream of exon 2. The total size of the targeting construct (including vector backbone and Neo cassette) was 14.74 Kb. (b) Excision PCR confirming the removal of the targeted region 10 days after poly(I:C) injection in Rps14$^{-/+}$Mx1Cre^{+} but not *Mx1Cre*$^{+}$ control cells. (c) Quantification of *Rps14* transcript levels by quantitative real-time PCR in lineage-negative bone marrow cells 10 days after poly(I:C) injection. Data are normalized to expression in *Mx1Cre*$^{+}$ control cells (n=8; mean±SD, **p<0.001). (d) Representative flow blot for the gating strategies of the RI-RIV erythroid progenitor populations by CD71 and Ter119 staining. Region I (CD71^{high}Ter119^{intermediate}) reflects proerythroblasts, region II are basophilic erythroblasts (CD71^{high}Ter119^{+}), region III represents late basophilic and chromatophilic erythroblasts (CD71^{intermediate}Ter119^{+}) and region IV orthochromatophilic erythroblasts (CD71^{-}Ter119^{+}) (according to Socolovsky et al. 2001). (e) Mean corpuscular volume (MCV) of red blood cells in the peripheral blood from *Rps14*$^{-/+}$*Mx1Cre*$^{+}$ mice in comparison to *Mx1Cre*$^{+}$ wild-type controls. (mean±SD, n=10; *p<0.05). (f) Quantification of the frequencies of the RI-RIV population in *Mx1Cre*$^{+}$ and *Rps14*$^{-/+}$*Mx1Cre*$^{+}$ mice 22 weeks after poly(I:C); (mean±SD, n=10 for *Mx1Cre*$^{+}$; 12 for *Rps14*$^{-/+}$*Mx1Cre*$^{+}$; *p<0.05; **p<0.001). (g) Cell cycle analysis using combined Ki67 and Hoechst staining within cells stained with CD71 and Ter119. Representative flow plots and quantification of the frequencies of RI cells within the G0, G1 and S-G2-M phase in *Mx1Cre*$^{+}$ and *Rps14*$^{-/+}$*Mx1Cre*$^{+}$ mice 22 weeks after poly(I:C). (mean±SD, n=10 for *Mx1Cre*$^{+}$; 12 for *Rps14*$^{-/+}$*Mx1Cre*$^{+}$; *p<0.05; **p<0.001). (h) Hemoglobin kinetics in wild-type recipient mice (CD45.1) that were transplanted with *Mx1Cre*$^{+}$ and *Rps14*$^{-/+}$*Mx1Cre*$^{+}$ whole bone marrow cells 4 weeks after poly(I:C). (n=5; mean±SD, **p<0.001). (i) Representative macroscopical and histopathological images of spleens in *Mx1Cre*$^{+}$ and *Rps14*$^{-/+}$*Mx1Cre*$^{+}$ mice 18 months after poly(I:C); (mean±SD, n=5; **p<0.001). HE-staining, 4x magnification. (j) Annexin-positive/DAPI-negative, apoptotic cells within the RI-RIII population at day 9 after Phenylhydrazine treatment in *Rps14*$^{-/+}$*Mx1Cre*$^{+}$ (n=5) and *Mx1Cre*$^{+}$ control mice (n=5), (*p<0.05). (k) Representative spleen histopathology in *Rps14*$^{-/+}$*Mx1Cre*$^{+}$, *p53*$^{-/+}$*Mx1Cre*$^{+}$, *Rps14*$^{-/+}$*p53*$^{-/+}$*Mx1Cre*$^{+}$ and *Mx1Cre*$^{+}$ control mice. Relative spleen to body weight [%] of *Mx1Cre*$^{+}$ and *Rps14*$^{-/+}$*Mx1Cre*$^{+}$ mice 9 days after the first treatment with 25mg/kg Phenylhydrazine in *Rps14*$^{-/+}$*Mx1Cre*$^{+}$ (n=14), *p53*$^{-/+}$*Mx1Cre*$^{+}$ (n=5), *Rps14*$^{-/+}$*p53*$^{-/+}$*Mx1Cre*$^{+}$ (n=5) and *Mx1Cre*$^{+}$ control mice (n=8) (mean±SD; *p<0.05). (l) Frequency of RI and RII erythroid progenitor populations among viable bone marrow cells in *Rps14*$^{-/+}$*Mx1Cre*$^{+}$ (n=5), *p53*$^{-/+}$*Mx1Cre*$^{+}$ (n=5), *Rps14*$^{-/+}$*p53*$^{-/+}$*Mx1Cre*$^{+}$ (n=5) and *Mx1Cre*$^{+}$ control mice (n=8) characterized by differential CD71 and Ter119 expression (mean±SD; **p<0.001).

We next examined the effect of *Rps14* haploinsufficiency on stress erythropoiesis by inducing hemolysis with phenylhydrazine (PH) treatment *in vivo*. Following acute hemolytic stress, *Rps14* haploinsufficient mice developed more severe anemia and had a delayed reticulocyte response compared to *Mx1Cre* control mice (Fig. 1e). The RI population ($CD71^{+}Ter119^{-}$) was significantly increased in $Rps14^{-/+}Mx1Cre^{+}$ mice, while the RIV population ($CD71^{low}Ter119^{high}$) was significantly decreased, highlighting a terminal erythroid differentiation defect consistent with induction of apoptosis in the RIII ($CD71^{intermediate}Ter119^{+}$) population (Fig. 1h, Supp. Fig. 1j). $Rps14^{-/+}Mx1Cre^{+}$ mice were characterized by significant splenomegaly with effacement of the normal spleen architecture and expansion of the red pulp ($p<0.05$; Supp. Fig. 1k).

To analyze the effect of *Rps14* haploinsufficiency on erythroid differentiation in the absence of *in vivo* compensatory mechanisms, we analyzed erythroid differentiation of lineage-negative hematopoietic stem and progenitor cells (HSPC) *in vitro*. After 5 days, $Mx1Cre^{+}$ HSPCs differentiated into hemoglobinized $CD71^{-}Ter119^{+}$ cells while *Rps14* haploinsufficient cells did not terminally differentiate (Fig. 1f-g). This terminal differentiation defect was accompanied by a significant reduction in cell proliferation, decrease in cell viability, and induction of the p53 downstream target p21 (Fig. 1h).

The p53 pathway is activated by decreased expression of ribosomal protein genes and has been linked to the erythroid defect in other models of ribosome dysfunction[7,8,10,13]. We found that compound haploinsufficiency for *p53* and *Rps14* prevented mortality from high dose PH (35mg/kg, Fig 1i). Following treatment with lower PH dose (25mg/kg), compound haploinsufficiency for *p53* normalized the erythropoietic recovery and spleen size changes caused by *Rps14* haploinsufficiency (Fig. 1j; Suppl. Fig. 1k, l). In aggregate, these experiments demonstrate that *Rps14* haploinsufficiency causes a *p53*-dependent terminal erythroid differentiation defect.

Rps14 haploinsufficiency alters hematopoietic stem and progenitor cells

We next evaluated whether *Rps14* haploinsufficiency alters hematopoiesis more broadly. In a histopathological analysis of the bone marrow, we found that 18-month old *Rps14* haploinsufficient mice had a slightly decreased cellularity, diffuse hemosiderin deposition, and significantly increased numbers of hypolobulated micro-megakaryocytes, consistent with the pathognomonic morphology in del(5q) MDS patients (Fig. 2a; Suppl. Fig. 2a, b). *Rps14* haploinsufficient mice had a mild thrombocytosis and platelet dysplasia in peripheral blood smears (Suppl. Fig. 2c). The white blood cell counts (WBC) were normal (Suppl. Fig. 2d). While the HSPC compartment was not altered in young *Rps14* haploinsufficient mice (Suppl. Fig. 2e), long-term hematopoietic stem cells (LT-HSCs; $lineage^{low}ckit^{+}Sca1^{+}CD48^{-}CD150^{+}$) and multipotent progenitor cells (MPPs; $lineage^{low}ckit^{+}Sca1^{+}CD48^{+}CD150^{-}$) were significantly increased in the bone marrow at 18 months (Fig. 2c). To analyze whether the expansion of LT-HSCs might be due to exit from quiescence and enhanced LT-HSC cycling,

we performed cell cycle analysis on HSPCs. In comparison with *Mx1Cre*$^{+}$ controls, *Rps14* haploinsufficient LT-HSCs had a significantly lower percentage of cells in the G0 phase of cell cycle, and a significantly higher percentage of cells in the cycling G1 as well as S-G2-M fraction, consistent with exit from quiescence (Fig. 2c). As the telomere length reflects the replicative history of a cell, we measured telomere length in bone marrow cells from *Rps14* haploinsufficient and *Mx1Cre*$^{+}$ control mice. *Rps14* haploinsufficient bone marrows had significantly shorter telomeres than *Mx1Cre*$^{+}$ control mice (Suppl. Fig. 2i; $p<0.001$).

We next examined the capacity of HSPCs to reconstitute hematopoiesis following transplantation. We transplanted whole bone marrow cells from 18 month old *Rps14*$^{-/+}$*Mx1Cre*$^{+}$ and *Mx1Cre*$^{+}$ controls into 6-8 week old CD45.1 recipient mice. *Rps14*$^{-/+}$*Mx1Cre*$^{+}$ mice died 6-7 weeks after transplantation with reduced hemoglobin (Hb) levels and an erythroid differentiation block from RII to RIII/IV, comparable to the differentiation block observed in the primary mice (Fig. 2d). The *Rps14*$^{-/+}$*Mx1Cre*$^{+}$ mice had a significant decrease in both LT- and ST-HSCs and an increase in MPPs (Fig. 2e and Suppl. Fig. 2f), but no decrease in the chimerism in the bone marrow (Suppl. Fig. 2g).

Since *Rps14* haploinsufficiency leads to a significant increase in LT-HSCs in primary mice, we examined the functional capacity of *Rps14* haploinsufficient cells in a competitive repopulation assay. We transplanted *Rps14*$^{fl/+}$*Mx1Cre*$^{+}$ or *Mx1Cre*$^{+}$ bone marrow cells in competition with an equal number of age-matched CD45.1 competitor BM cells into lethally irradiated CD45.1 recipient mice (Fig. 2f). Four weeks after transplantation, mice were treated with poly(I:C) to induce hemizygous *Rps14* inactivation. *Rps14* haploinsufficient cells out-competed CD45.1 competitor cells in the primary transplant, while *Mx1Cre*$^{+}$ control cells had no competitive advantage (Fig. 2f). To determine the long-term repopulation potential, whole bone marrow cells from primary recipients were transplanted into secondary recipients. In the first transplant, the contribution of *Rps14* haploinsufficient bone marrow cells was stable and showed a significantly higher chimerism than *Mx1Cre*$^{+}$ controls. By 32 weeks in the secondary transplant, we observed a progressive decrease in the *Rps14* chimerism to levels comparable to *Mx1Cre*$^{+}$ control cells in the bone marrow.

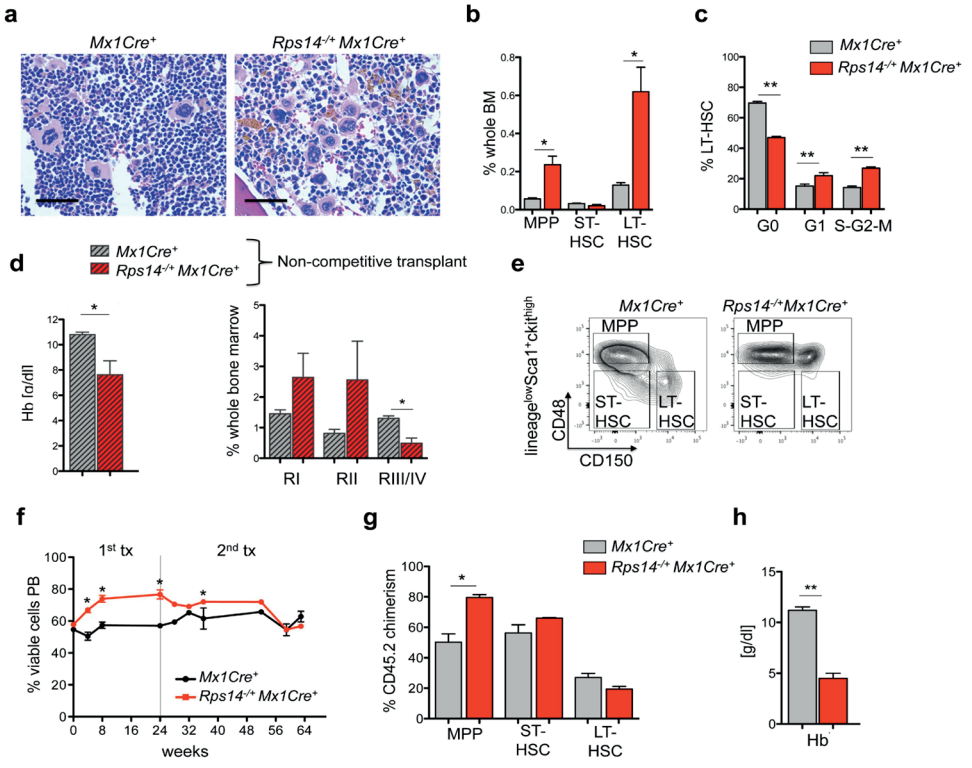

Figure 2: *Rps14* haploinsufficiency alters hematopoietic stem and progenitor cells

(a) Bone marrow histopathology in HE-stained bone marrow sections (40x magnification; scale bar 50μm) 18 months after the first poly(I:C) injection in *Rps14*$^{-/+}$*Mx1Cre*$^{+}$ (n=5) and *Mx1Cre*$^{+}$ mice (n=4), representative pictures are shown. (b) Frequency of MPPs (lineage^{low}ckit^{+}Sca1^{+}CD48^{+}CD150^{-}), ST-HSCs (lineage^{low}ckit^{+}Sca1^{+}CD48^{-}CD150^{-}) and LT-HSCs (lineage^{low}ckit^{+}Sca1^{+}CD48^{-}CD150^{+}) 18 months after the first poly(I:C) injection in *Rps14*$^{-/+}$*Mx1Cre*$^{+}$ (n=5) and *Mx1Cre*$^{+}$ mice (n=4); (mean±SD; *p<0.05). (c) Cell cycle was analyzed by combined proliferation (Ki67) and cell cycle (Hoechst33342) staining in permeabilized LT-HSCs from bone marrow (GO: Ki67^{-}Hoechst^{-}; G1: Ki67^{+}Hoechst^{-}; S-G2-M: Ki67^{+}Hoechst^{+}); (mean±SD; n=5; **p<0.001). (d) Whole bone marrow cells from primary 18 months old mice were transplanted in 6-8 week old SJL/CD45.1 recipient mice (n=5). Hemoglobin levels (Hb) in the peripheral blood from chimeric *Rps14*$^{-/+}$*Mx1Cre*$^{+}$ mice in comparison to *Mx1Cre*$^{+}$ wild-type controls 6 weeks after transplantation and frequency of the RI-RIV erythroid progenitor populations (RI: CD71^{high}Ter119^{-}; RII: CD71^{high}Ter119^{+}; RIII/IV: CD71$^{intermediate/low}$Ter119^{+}) in CD45.1 mice transplanted with aged *Mx1Cre*$^{+}$ and *Rps14*$^{-/+}$*Mx1Cre*$^{+}$ bone marrow cells 6 weeks after transplantation. (e) Representative flow plots of the HSC compartment of populations defined as MPPs, ST-HSCs and LT-HSCs in CD45.1 mice transplanted with old *Mx1Cre*$^{+}$ (n=4) and *Rps14*$^{-/+}$*Mx1Cre*$^{+}$ (n=5) bone marrow cells 6 weeks after transplantation. ((f) Identical numbers of *Rps14*$^{-/+}$Mx1Cre^{+} and *Mx1Cre*$^{+}$ controls were mixed in equal ratios (approximately 50:50) and transplanted in lethally irradiated CD45.1 recipients. Time point 0 reflects the first bleeding 4 weeks after transplantation (engraftment) before inducing the excision of *Rps14* by poly(I:C) injections. After 24 weeks, bone marrow was harvested and transplanted for secondary transplants. (mean±SD, n=5; *p<0.05). (g) Donor chimerism (CD45.2) of the HSC (MPP, ST-HSC, LT-HSC) compartment (mean±SD, n=5; *p<0.05). (h) Hemoglobin levels (Hb) in the peripheral blood from chimeric *Rps14*$^{-/+}$*Mx1Cre*$^{+}$ or *Mx1Cre*$^{+}$ mice 64 weeks after engraftment (40 weeks after secondary transplantation). (mean±SD, n=5; *p<0.05). Unpaired two-sided *t*-test was applied for statistical analysis.

Given the progressive decrease in *Rps14* chimerism, we evaluated HSC abundance. In multipotent progenitors cells, the frequency of *Rps14* haploinsufficient cells was significantly higher than WT counterparts, whereas no differences were observed in ST- and LT-HSCs (Fig. 2g). In differentiated lineages, we observed significant myeloid skewing of *Rps14* haploinsufficient cells, reflected by increased chimerism within the $Gr1^{+}CD11b^{+}$ population. In contrast, chimerism within lymphoid populations did not differ significantly from *Mx1Cre*$^{+}$ control chimerism; (Suppl. Fig. 2h). The chimerism of $Ter119^{+}$ erythroid cells was significantly decreased in mice transplanted with *Rps14* haploinsufficient bone marrow (Suppl. Fig. 2h), highlighting the distinct erythroid phenotype. Mice transplanted with equivalent numbers of *Rps14* haploinsufficient and wild type bone marrow cells succumbed to a severe anemia (Fig. 2h) in the setting of relatively preserved whole blood chimerism suggesting that *Rps14* haploinsufficiency might have cell-extrinsic effects that suppress erythropoiesis.

In aggregate, *Rps14* haploinsufficiency causes impaired terminal erythroid differentiation, an increase in hematopoietic stem cell frequency with myeloid skewing, and age-dependant loss of the HSC function. Overall, this hematopoietic phenotype resembles alterations during HSC aging and inflammation in the bone marrow[16-18].

Ribosomal haploinsufficiency leads to global reduction in protein synthesis

Having established a mouse model that faithfully recapitulates the cardinal features of del(5q) MDS, we sought to understand how heterozygous deletion of *Rps14*, a component of the 40S ribosomal subunit, alters ribosome assembly and protein synthesis.

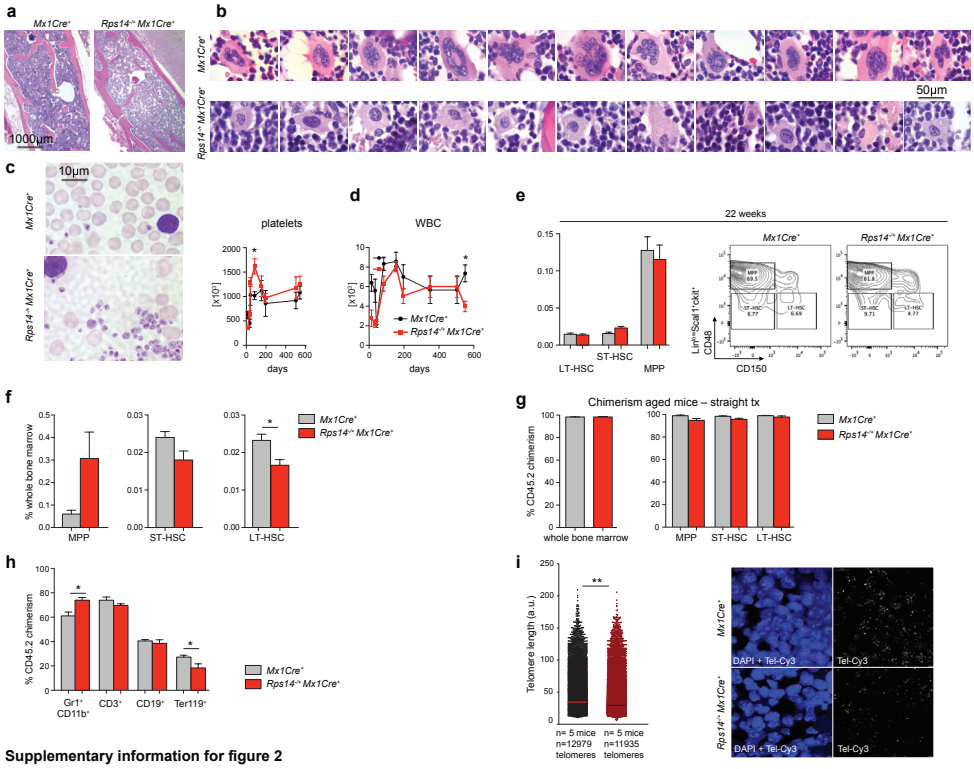

Supplementary information for figure 2

Supplementary figure 2: Hematological phenotype of *Rps14* haploinsufficient mice. (a) Histopathological overview of the spinal part of the bone marrow in *Rps14*$^{-/+}$*Mx1Cre*$^{+}$ (n=5) and *Mx1Cre*$^{+}$ mice (n=4) 18 months after the first poly(I:C) injection. HE-staining. 4x magnification. (b) Representative high-power magnification pictures (100x with oil) of HE-stained bone marrows from *Rps14*$^{-/+}$*Mx1Cre*$^{+}$ (n=5) and *Mx1Cre*$^{+}$ mice (n=4) 18 months after the first poly(I:C) injection. (c) Representative peripheral blood smear, May-Gruenwald-Giemsa staining and platelet counts in the peripheral blood from *Rps14*$^{-/+}$*Mx1Cre*$^{+}$ mice in comparison to *Mx1Cre*$^{+}$ wild-type controls. (mean±SD, n=10; *p<0.05). (d) White blood cell (WBC) count in the peripheral blood from *Rps14*$^{-/+}$*Mx1Cre*$^{+}$ mice in comparison to *Mx1Cre*$^{+}$ wild-type controls. (mean±SD, n=10; *p<0.05). (e) Representative flow plots and frequency of MPPs (lineage^{low}ckit^{+}Sca1^{+}CD48^{+}CD150^{-}), ST-HSCs (lineage^{low}ckit^{+}Sca1^{+}CD48^{-}CD150^{-}) and LT-HSCs (lineage^{low}ckit^{+}Sca1^{+}CD48^{-}CD150^{+}) in *Mx1Cre*$^{+}$ and *Rps14*$^{-/+}$*Mx1Cre*$^{+}$ mice 22 weeks after poly(I:C). (f) Whole bone marrow cells from primary 18 months old mice were injected in 6-8 week old SJL/CD45.1 recipient mice. Frequency of MPPs (lineage^{low}ckit^{+}Sca1^{+}CD48^{+}CD150^{-}), ST-HSCs (lineage^{low}ckit^{+}Sca1^{+}CD48^{-}CD150^{-}) and LT-HSCs (lineage^{low}ckit^{+}Sca1^{+}CD48^{-}CD150^{+}) 6 weeks after transplantation in *Rps14*$^{-/+}$*Mx1Cre*$^{+}$ (n=5) and *Mx1Cre*$^{+}$ mice (n=4); (mean±SD; *p<0.05). (g) Whole bone marrow donor chimerism (CD45.2) and donor chimerism in MPPs, ST-HSCs and LT-HSCs of 18 months old whole bone marrow cells from *Rps14*$^{-/+}$*Mx1Cre*$^{+}$ and *Mx1Cre*$^{+}$ mice 6 weeks after transplantation. (h) Lineage donor (CD45.2) chimerism of competitive transplants 64 weeks after engraftment (40 weeks after secondary transplantation). (mean±SD, n=5; *p<0.05). (i) Confocal Q-FISH to measure the telomere length in *Rps14*$^{-/+}$*Mx1Cre*$^{+}$ and *Mx1Cre*$^{+}$ bone marrows 18 months after poly(I:C). (n=5 mice; n=12979 telomeres measured for *Mx1Cre*$^{+}$ and n=11935 telomeres measured for *Rps14*$^{-/+}$*Mx1Cre*$^{+}$*; **p<0.001). Representative confocal images showing telomeres in nucleated, DAPI-positive cells

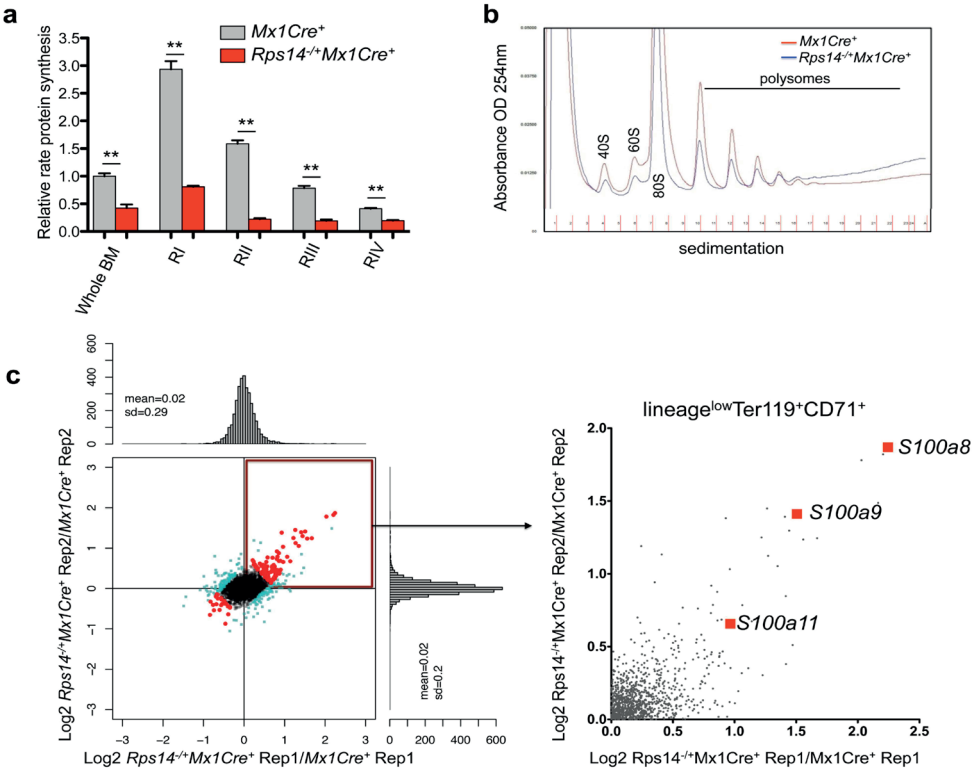

Figure 3: Reduced protein synthesis in *Rps14* haploinsufficient cells. (a) OP-Puro incorporation in bone marrow (BM) cells *in vivo* 1 h after administration in 20 week old *Mx1Cre*$^{+}$ control cells or *Rps14*$^{-/+}$*Mx1Cre*$^{+}$ cells [(16 weeks after the first injection of poly(I:C)]. Quantification of OP-Puro fluorescence reflecting protein synthesis rate in hematopoietic stem and progenitor cells relative to unfractionated bone marrow. Relative protein synthesis and quantification of OP-Puro fluorescence in erythroid RI-RIV progenitor populations relative to unfractionated bone marrow (mean±SD, n=5; **p<0.001; Unpaired two-sided *t*-test was applied for statistical analysis). (b) Polysome profiles from sort-purified lineage^{low}CD71^{high}Ter119^{+} erythroid progenitor cells in *Mx1Cre*$^{+}$ control cells or *Rps14*$^{-/+}$*Mx1Cre*$^{+}$ cells. The x-axis shows the distance along the gradient. The arbitrary Y-axis shows the relative absorbance. Data are representative of 3 independent experiments (each n=3 biological replicates). (c) Proteomic analysis of induced changes in protein expression of *Rps14* haploinsufficient sort-purified lineage^{low}CD71^{high}Ter119^{+} erythroid progenitor cells relative to *Mx1Cre*$^{+}$ cells (300µg protein for each technical replicate=4 biological replicates). Log2 ratios and scatter plot for individual proteins for replicate 1 and 2, where each dot represents a unique protein. The upper right quadrant represents proteins that are significantly up-regulated by *Rps14* haploinsufficiency in replicate 1 and 2 (Rep 1 and 2) relative to *Mx1Cre*$^{+}$ control cells. Detailed statistical methods for the proteomic analysis are described in the methods section.

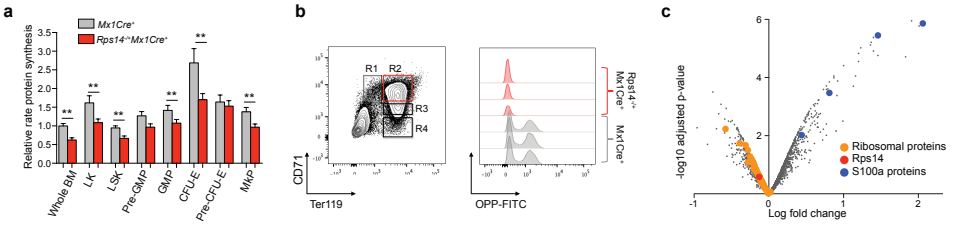

Supplementary figure 3: Reduced protein synthesis in *Rps14* haploinsufficient cells. (a) OP-Puro incorporation in bone marrow (BM) hematopoietic stem and progenitor cell populations in vivo 1 h after administration. Quantification of OP-Puro fluorescence reflecting protein synthesis rate in hematopoietic stem and progenitor cells relative to unfractionated bone marrow. Relative protein synthesis relative to unfractionated bone marrow (mean±SD, n=5; **p<0.001). (b) Representative flow blots showing the gating strategy for determination of OP-Puro incorporation in erythroid progenitor cell populations. (c) Volcano plot showing the log fold change of protein expression (X-Axis) to the –log10 adjusted p-value. Orange dots highlight all ribosome associated proteins, blue dots S100a proteins and the red dot Rps14.

We first analyzed whether *Rps14* haploinsufficiency induces quantitative changes in protein synthesis using a fluorogenic assay (O-propargyl-puromycin; OP-Puro) to visualize protein synthesis in vivo[19]. We administered a single intraperitoneal injection of OP-Puro (50 mg/kg) and measured OP-Puro incorporation as a reflection of total protein translation in a defined period of time. Overall, OP-Puro incorporation was significantly reduced in *Rps14*$^{-/+}$*Mx1Cre*$^{+}$ cells relative to wild-type cells. The reduction in protein synthesis was most striking in erythroid progenitor cells (Fig. 3a; Suppl. Fig. 3a-b), consistent with the erythroid differentiation block in these cells and the erythroid-specific requirement for high levels of ribosome biogenesis, ribosome activity, and protein translation[20].

To determine whether the *Rps14* haploinsufficiency specifically influences ribosomal subunit/polysome formation, we performed sucrose gradient analysis of intact polysomes from FACS-purified erythroid progenitor cells (lineage^{low}CD71$^{high\text{-}intermediate}$Ter119^{+}, RII-III). We observed intact formation of polysome subunits (Fig. 3b), as expected given the rather mild, age-dependent phenotype. These findings indicate that while protein synthesis is impaired, the ribosomes that are assembled function normally. Ribosomal subunits that fail to assemble into an intact 80S ribosome may be rapidly degraded, as has been described previously [21-23].

Gene symbol	Protein name	logFC	adj. p-value
S100a8	Protein S100-A8	2.057	0.0019735
Pglyrp1	Peptidoglycan recognition protein 1	2.013	0.00197349
Retnlg	Myeloid cysteine-rich protein	1.905	0.00197349
Mgp	Matrix Gla protein	1.826	0.005770276
S100a9	Protein S100-A9	1.4595	0.002959553
Ltf	Lactotransferrin	1.4575	0.005587191
Lcn2	Neutrophil gelatinase-associated lipocalin	1.4005	0.002959553
Chi3l1	Chitinase-3-like protein 1	1.397	0.004868785
Camp	Cathelin-related antimicrobial peptide	1.3705	0.003652307
Ngp	OS=Mus musculus GN=Ngp E=2 SV=1	1.3565	0.003848308
Apobr	Apolipoprotein B receptor	1.2345	0.004214127
Lrg1	Leucine-rich HEV glycoprotein	1.201	0.007654588
Padi4	Protein-arginine deiminase type-4	1.198	0.005221609
Hp	Haptoglobin	1.1555	0.01958689
Lyz2	Lysozyme C-2	1.1315	0.033817984
Anxa1	Annexin A1	0.997	0.009836916
Ear2	Eosinophil cationic protein 2	0.9915	0.170633883
Gys1	Glycogen [starch] synthase, muscle	0.924	0.025785806
Mmp9	Matrix metalloproteinase-9	0.907	0.05404763
Gda	Guanine deaminase	0.8985	0.025569514
Nfrkb	Nuclear factor related to kappa-B-binding protein	0.8675	0.01958689
Aldh3b1	Aldehyde dehydrogenase family 3 member B1	0.865	0.021200077
S100a11	Protein S100-A11	0.8115	0.04566109
Itgb2	Integrin beta-2	0.7905	0.037963425
Itgam	Integrin alpha-M	0.8055	0.026112389
Ncf2	Neutrophil cytosol factor 2	0.771	0.037963425

Supplementary Table 1: Differentially expressed proteins identified by iTRAQ-based mass spectrometry (adjusted p-value of <0.05)

Ribosomal haploinsufficiency induces increased levels of proteins involved in innate immune function

To determine whether specific proteins are differentially expressed in *Rps14* haploinsufficient erythroid progenitor cells and to elucidate a mechanism for the severe erythroid differentiation defect, we performed quantitative proteomics. We purified erythroid progenitor cells (lineage^{low}CD71$^{high\text{-}intermediate}$Ter119^{+}, RII-III) and used isobaric tags for relative and absolute quantification (iTRAQ)-based mass spectrometry (Fig. 3c). We detected 3,524 proteins with at least two unique peptides and ratios per replicate. Of these, 26 proteins were differentially expressed (adjusted p-value of <0.05; Supplementary table 1). Ribosome-associated proteins had decreased expression, consistent with global reduction in protein synthesis but intact polysome formation (Suppl. Fig. 3c). In *Rps14* haploinsufficient cells, proteins involved in innate immune system activation were most enriched, including S100a8 and S100a9. In MDS patients, S100A9/CD33 pathway and innate immune activation have been implicated in disease pathogenesis [24,25].

To validate that *Rps14* haploinsufficiency induces expression of innate immune response proteins, we examined S100a8 expression by immunohistochemistry in bone marrows of *Rps14* heterozygote knockout mice and *Mx1Cre*$^{+}$ controls (Fig. 4a; Suppl. Fig. 4d). S100a8 expression was significantly increased in *Rps14* haploinsufficient bone marrows and distinct clusters of S100A8 expressing cells were identified (Fig. 4a). We confirmed that S100a8 protein and mRNA expression were increased in lineage-negative bone marrow cells (Fig. 4b). We simultaneously analyzed surface marker staining and intracellular S100a8 staining to quantify S100a8 expression in defined cell populations. We found significantly increased S100a8 in the erythroid progenitor populations affected by the differentiation block (Gr1^{-}CD11b^{-}CD71^{high}Ter119^{high} and Gr1^{-}CD11b^{-}CD71^{low}Ter119^{high}; RIII-RIV population), and in monocytes and macrophages of *Rps14* haploinsufficient bone marrows (Fig. 4d-e; Suppl. Fig. 4a-b).

Figure 4: S100a8 is significantly up-regulated in *Rps14* haploinsufficient bone marrows, is regulated by *p53* induction, and is necessary for the erythroid differentiation defect. (a) Immunohistochemical staining of S100a8 in bone marrows from *Mx1Cre*$^{+}$ and *Rps14*$^{-/+}$*Mx1Cre*$^{+}$ mice 8 weeks after the induction of the *Rps14* excision with poly(I:C); representative pictures are shown (n=5). Scale bar 100μm. (b) Quantification of S100a8 in lineage-negative bone marrow cells by quantitative real-time PCR (mean±SD, n=5; *p<0.05). Data are normalized to expression in *Mx1Cre*$^{+}$ control cells 8 weeks post poly(I:C). Western blot on protein lysates from *Mx1Cre*$^{+}$ and *Rps14*$^{-/+}$*Mx1Cre*$^{+}$ lineage-negative bone marrow cells. Data are representative of 3 independent experiments. (c) Mean fluorescence intensity (MFI) in CD11b^{-}Gr1^{-} erythroid progenitor populations characterized by CD71 and Ter119 expression (RI-RIV). (mean±SD, n=5; *p<0.05). Mean fluorescence intensity (MFI) of S100a8 expression in Gr1^{+}CD11^{+} granulocytes, Gr1^{-}CD11b^{+} monocytes and F4/80^{+} macrophages (mean±SD, n=5; *p<0.05). (d) Co-immunofluorescent staining of F4/80 (green), p53 (dark blue) and S100a8 (red) on cytospins of *Rps14*$^{-/+}$*Mx1Cre*$^{+}$ and *Mx1Cre*$^{+}$ bone marrow cells 12 weeks after the induction of the *Rps14* excision with poly(I:C). Inserts highlight areas of magnification shown in the lower panel. Scale bar: 20μm. Data are representative of 3 independent experiments. (e) Percentage of p53 and S100a8 co-expressing cells in RI-III erythroid progenitor cells from *Rps14*$^{-/+}$*Mx1Cre*$^{+}$ and *Mx1Cre*$^{+}$ mice 12 weeks after the induction of the *Rps14* excision with poly(I:C), (mean±SD, n=5; *p<0.05). (f) Representative histograms showing S100a8 expression in the RIII erythroid progenitor cell population and mean fluorescence intensity (MFI) of S100a8 expression in F4/80^{+} macrophages and RIII erythroblasts in *Mx1Cre*$^{+}$*, p53*$^{-/-}$*, Rps14*$^{-/+}$*Mx1Cre*$^{+}$ and *Rps14*$^{-/+}$*p53*$^{-/-}$ *Mx1Cre*$^{+}$ mice 6 days after induction of hemolysis with Phenylhydrazine (mean±SD,

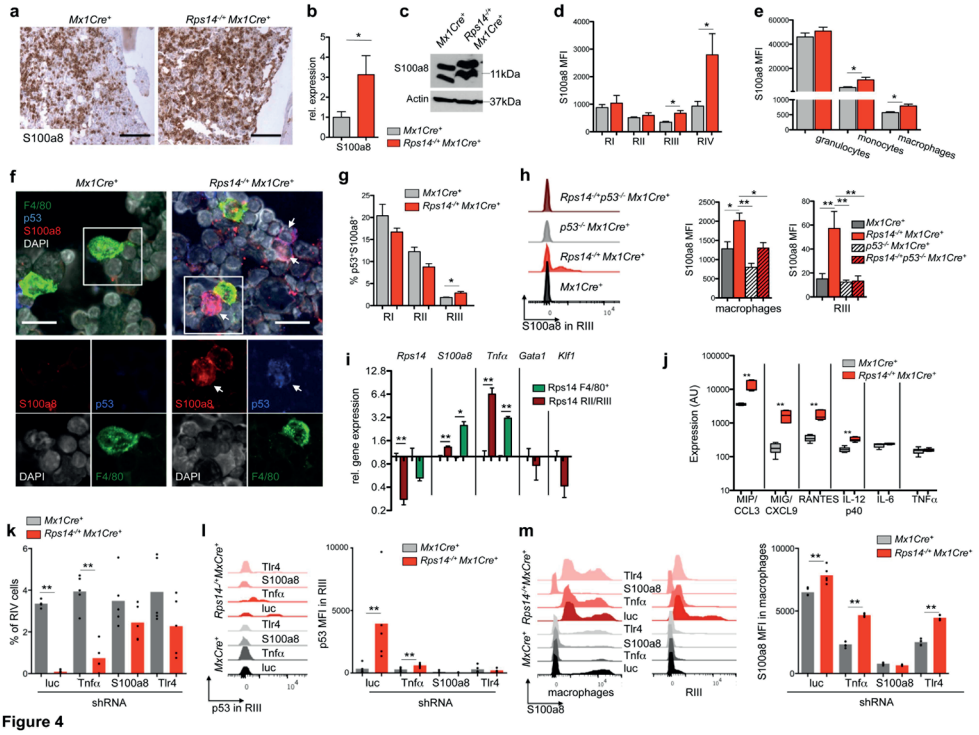

Figure 4

n=5; *p<0.05; *p*<0.001). (g) Fluorescence intensity normalized to background signals of inflammatory cytokines in bone marrows from *Mx1Cre*$^{+}$ and *Rps14*$^{-/+}$*Mx1Cre*$^{+}$ mice 12 weeks after the induction of the *Rps14* excision with poly(I:C). Log10 scale. (mean±SD, n=4; **p<0.001). (h) Ckit^{+} HSPCs were transduced with lentiviral shRNAs (n=5 each) targeting *Tnfa*, *S100a8* and *Tlr4* and a luc control. Transduced cells were selected with puromycin and induced to undergo erythroid differentiation for 5 days *in vitro.* The frequency of RIV erythroid progenitor populations in the culture is shown (mean±SD, **p<0.001). Circles represent the median of three replicates for each individual shRNA (n=5). The mean of all shRNAs targeting a given gene is shown with a grey bar or red bar. (i) Representative histogram presentation and mean fluorescence intensity (MFI) of p53 expression in the RIII population of HSPCs transduced with shRNA targeting *Tnfa, S100a8* and *Tlr4* and *luc* control after 5 days of erythroid differentiation *in vitro*. (mean±SD, **p<0.001, n=5). Circles represent the median of three replicates for each individual shRNA (n=5). The mean of all shRNAs targeting a given gene is shown with a grey bar or red bar. (j) Representative histograms in F4/80^{+} macrophages and in the RIII population and mean fluorescence intensity (MFI) of S100a8 expression in macrophages of HSPCs transduced with shRNA targeting *Tnfa*, *S100a8* and *Tlr4* and *luc* control after 5 days of erythroid differentiation *in vitro*. (mean±SD, **p<0.05, **p<0.001, n=5). Circles represent the median of three replicates for each individual shRNA (n=5). The mean of all shRNAs targeting a given gene is shown with a grey bar or red bar. Unpaired two-sided *t*-test (b, c, e; h-j) or multiple group comparison by analysis of variance with posthoc Tukey correction (f) were applied for statistical analysis.

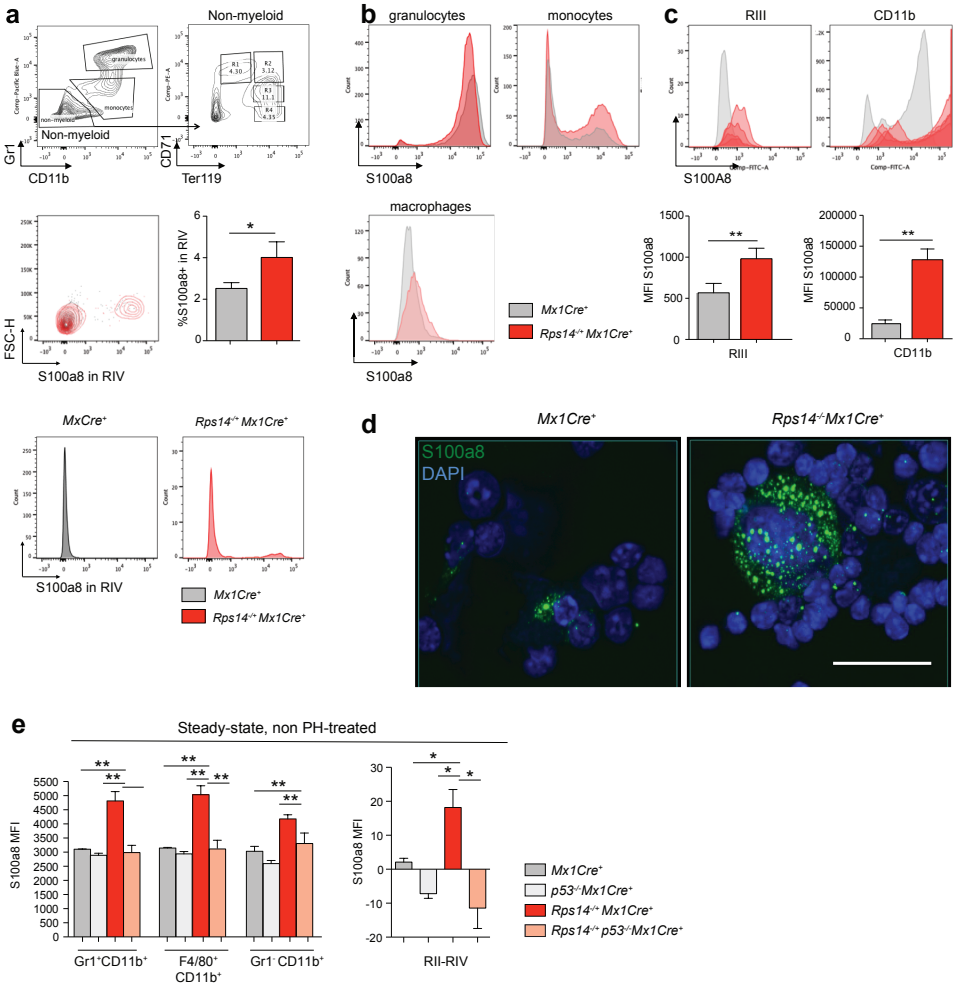

Supplementary figure 4: S100a8 is significantly up-regulated in *Rps14* haploinsufficient bone marrows, is regulated by *p53* induction, and is necessary for the erythroid differentiation defect. (a) Gating strategy for validating the up-regulation of S100a8 in erythroid progenitor populations (CD71/Ter119) and Gr1/CD11b-positive cells. Whole bone marrow was stained with Gr1, CD11b, Ter119 and CD71. Erythroid progenitors were gated from the non-myeloid cell population ($Gr1^-CD11b^-$). Representative flow blot showing S100a8 positive cells within the RIV population in *Rps14*$^{-/+}$*Mx1Cre*$^+$ and *Mx1Cre*$^+$mice (red: *Rps14*$^{-/+}$*Mx1Cre*$^+$ and grey). Quantification of the frequency of S100a8 expressing cells within the RIV population. (mean±SD, n=5; *p<0.05). Histogram showing S100A8 expression in the RIV population. (b) Histograms depicting S100a8 expression in granulocytes ($Gr1^{high}CD11b^+$), monocytes ($Gr1^{low}CD11b^+$) and macrophages ($CD11b^+F4/80^+$). (c) Histograms showing S100a8 expression in transplant experiments of 18 months old whole bone marrow cells in young recipients (compare Figure 2) 6 weeks after transplantation. Mean fluorescence intensity (MFI) of S100a8 in the RIII population and in monocytes in *Rps14*$^{-/+}$*Mx1Cre*$^+$ (n=5) and *Mx1Cre*$^+$ mice (n=4); (mean±SD; **p<0.001). (d) S100a8 (green) immunofluorescence on lineage-depleted whole bone marrows of *Rps14*$^{-/+}$*Mx1Cre*$^+$ (n=5) and *Mx1Cre*$^+$ mice (n=4). Nuclei are highlighted by DAPI staining. (e) Mean fluorescence intensity (MFI) of S100a8 expression in $Gr1^+CD11^+$ granulocytes, $Gr1^-CD11b^+$ monocytes, $F4/80^+$ macrophages and RII-RIV erythroblasts in *Mx1Cre*$^+$, *p53*$^{-/-}$, *Rps14*$^{-/+}$*Mx1Cre*$^+$ and *Rps14*$^{-/+}$*p53*$^{-/-}$ *Mx1Cre*$^+$ mice 12 weeks after poly(I:C) (mean±SD, n=3; *p<0.05; *p*<0.001).

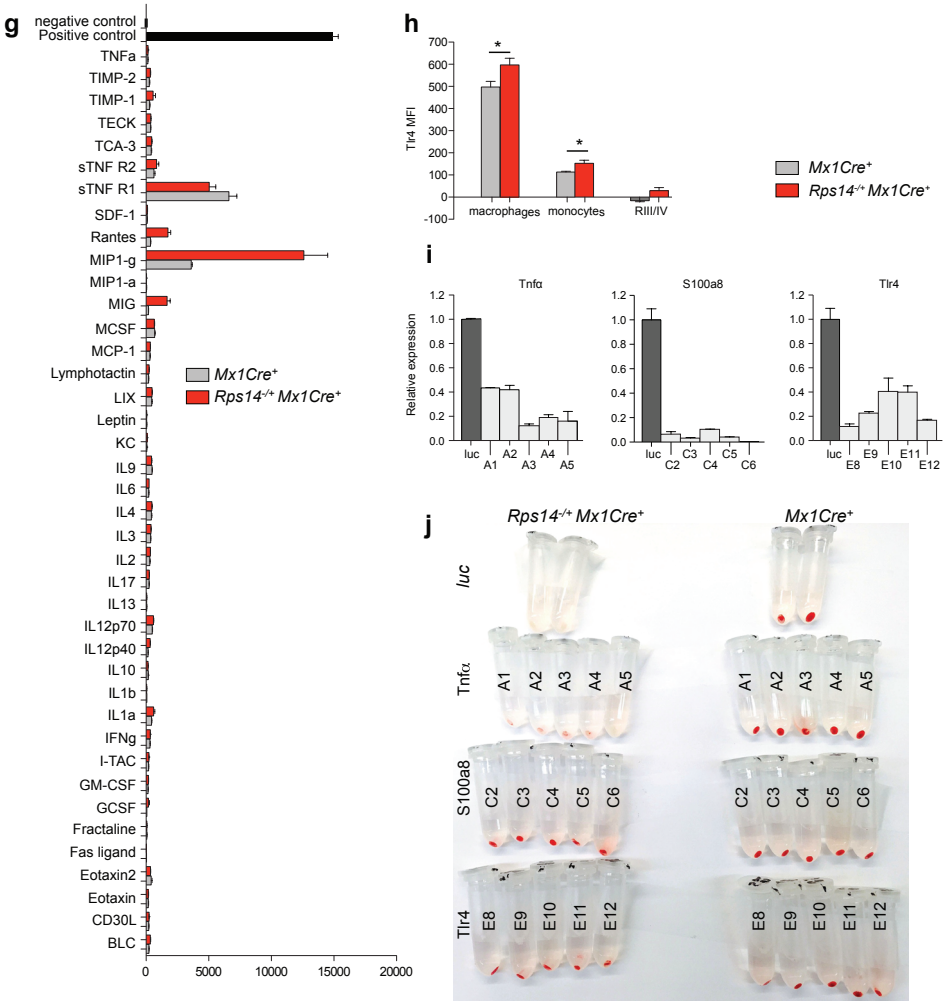

Quantification (qt-RT-PCR) of *Rps14*, *S100a8*, *Tnfa, Gata1* and *Klf1* expression in sort-purified RII/III erythroblasts (dark red) and F4/80$^+$ macrophages (green). The expression values are relative to *Mx1Cre*$^+$ control cells which were normalized to 1. (mean±SD, n=5; *p<0.05). (g) Intensity of expression of 40 cytokines detected by the cytokine expression array compared to negative and positive control. Fluorescence intensity normalized to background signals of inflammatory cytokines in bone marrows from *Mx1Cre*$^+$ and *Rps14*$^{-/+}$*Mx1Cre*$^+$ mice 12 weeks after the induction of the *Rps14* excision with poly(I:C). Log10 scale. (mean±SD, n=4). (h) Mean intensity fluorescence (MFI) of TLR4 on monocytes and macrophages [mean±SD, n=4 (MxCre), n=5 Rps14); *p<0.05)]. (i) Knockdown validation of shRNA targeting Tnfa, S100a8 and Tlr4 in ckit+ HSPC 6 days after transduction and selection with Puromycin compared to HSPC transduced with luc control shRNA. Efficient knockdown was confirmed for each of the 5 shRNA applied in the experiments. A1-5, C2-6 and E8-E12 highlights the different shRNA that were tested in the experiment (3 replicates per shRNA). (j) Cell pellets of ckit$^+$ HSPC derived from either *Mx1Cre*$^+$ and *Rps14*$^{-/+}$*Mx1Cre*$^+$ mice and transduced for 48 hours with shRNA and then subjected to erythroid differentiation in the presence of puromycin for additional 7 days *in vitro*. A1-5, C2-6 and E8-E12 highlights the different shRNA that were tested in the experiment (3 replicates per shRNA; representative pictures are shown).

As we observed a rapidly developing anemia in chimeric mice transplanted with aged *Rps14* haploinsufficient whole bone marrow cells (compare Fig. 2), we analyzed S100a8 expression in the bone marrow of these mice. Both monocytes and $Gr1^{-}CD11b^{-}CD71^{low}Ter119^{high}$ (RIV) erythroblasts in *Rps14* haploinsufficient mice had dramatically increased expression of S100a8, suggesting that additional stress in the bone marrow, like transplantation or aging, potentiates the expression of S100a8 with consequent effects on hematopoiesis (Suppl. Fig. 4c; $p<0.01$).

The functional unit of mammalian erythropoiesis, the erythroblastic island, consists of a central macrophage that extends cytoplasmic protrusions to a ring of surrounding erythroblasts. As we specifically found increased S100a8 expression in both erythroblasts and macrophages, we examined expression of S100a8 and p53 in the erythroblastic island. We performed confocal imaging on *Rps14* haploinsufficient bone marrow spins and $Mx1Cre^{+}$ control cells (Fig. 4d). F4/80-positive macrophages co-expressed S100a8. In close proximity to macrophages, we detected a significant increase in S100a8-expressing cells in *Rps14* haploinsufficient bone marrows, some of which had induction of p53.

To validate that p53 was induced in erythroid progenitor cells with S100a8 induction, we analyzed co-expression of p53 and S100a8 in erythroid progenitor cells by flow cytometry (Fig. 4e). In the RIII population, we identified a significant induction of p53 in S100a8-expressing cells. Since p53 is a known regulator of S100a8[26-29], we analyzed the expression of *S100a8* in *Rps14* haploinsufficiency in the presence and absence of p53, as well as during steady-state (Suppl. Fig. 4e) and stress erythropoiesis induced by PH treatment (Fig. 4f). We detected significantly decreased expression of S100a8 in $Rps14^{-/+}p53^{-/-}Mx1Cre^{+}$ macrophages and RIII erythroid progenitor cells, compared to p53 WT controls, indicating that the induction of p53 by ribosomal haploinsufficiency regulates the expression of S100a8 (Fig. 4f, Suppl. Fig. 4e).

Having shown that *Rps14* haploinsufficiency affects not only erythroblasts but also monocytes/macrophages, we measured *S100a8* mRNA expression in purified $lineage^{low}CD11b^{-}CD71^{high/intermediate}Ter119^{+}$ (RII/RIII) erythroblasts and $lineage^{low}F4/80^{+}$ macrophages. Both erythroblasts and macrophages from *Rps14* haploinsufficient cells had decreased *Rps14* and increased *S100a8* gene expression (Supplementary Fig. 4f; $p<0.05$ $F4/80^{+}$; $p>0.001$ RII/RIII). In addition, both erythroblasts and macrophages had elevated expression of the *Tnfa* gene, a down-stream target of the heterodimeric S100A8/A9 complex[26,30] and a powerful repressor of erythropoiesis[25,31]. Consistent with the impaired erythroid differentiation, expression of the erythroid transcription factors *Klf1* and *Gata1* was decreased.

T o investigate whether *Rps14* haploinsufficiency induces an inflammatory environment in the bone marrow that represses erythropoiesis and hematopoiesis by cell-extrinsic mechanisms, we profiled levels of 40 cytokines in bone marrow serum (Fig. 4j; Suppl. Fig. 4g). We found 4 cytokines to be significantly increased in *Rps14* heterozygous mice: macrophage-inflammatory protein (MIP/CCL3), CXCL9, RANTES, and IL12(p40). These cytokines are

predominantly expressed in activated macrophages/monocytes, have negative effects on erythropoiesis and hematopoiesis and are significantly elevated in patients with low-risk MDS[32-35]. Recent studies have demonstrated that S100A8 and S100A9 are endogenous activators of Toll-like receptor-4 (TLR4)[36]. We found that Tlr4 expression was activated on both macrophages and monocytes in the bone marrow of *Rps14* haploinsufficient mice but not on erythroblasts, suggesting that S100a8 activates macrophages and monocytes and drives an inflammatory environment (Suppl. Fig. 4h; $p<0.05$).

We examined the roles of S100a8, Trl4, and Tnfα in causing abnormal erythropoiesis in *Rps14* haploinsufficient mice using validated small hairpin RNAs (shRNAs) (Suppl. Fig 4i). We transduced ckit$^+$ HSPCs with test and control shRNAs, induced erythroid differentiation *in vitro*, and evaluated effects using flow cytometry and hemoglobinization (Fig. 4h; Suppl. Fig. 4j). Knockdown of *S100a8 and Tlr4* improved erythroid differentiation and reduced p53 induction (Fig. 4i), indicating that *S100a8/Tlr4* is central to the erythropoietic defect of *Rps14* haploinsufficiency. *Tnfa* knockdown had a similar, although less robust effect on erythropoiesis and had no effect on *S100a8 expression,* suggesting a pro-inflammatory role downstream of S100a8 (Fig. 4i-j).

S100a8 is necessary and sufficient for the erythroid differentiation defect due to *Rps14* haploinsufficiency

To explore a cell non-autonomous mechanism of the erythroid differentiation defect by S100a8, we induced erythroid differentiation of wild-type lineage-negative HSPCs in the presence of recombinant S100a8 protein (rS100a8). HSPCs cultured in the presence of rS100a8 had a differentiation block at the RIII/RIV transition (Fig. 5a, Suppl. Fig. 5a), consistent with the differentiation defect in *Rps14* haploinsufficient cells, with significantly increased p53-induction in the RII/III population (Fig. 5b).

We next used CRISPR/Cas9-mediated genetic inactivation *S100a8* to validate the requirement for *S100a8* expression in the erythroid differentiation defect of *Rps14* haploinsufficient cells. We transduced HSPCs with a lentiviral vector expressing the Cas9 nuclease and a small guide RNA (sgRNA) targeting *S100a8*, then analyzed *in vitro* erythroid differentiation as above. Compared to control non-targeting sgRNA (NTG-sgRNA:Cas9), CRISPR-mediated inactivation of S100a8 (S100a8-sgRNA:Cas9) in *Rps14* haploinsufficient cells rescued terminal differentiation of hemoglobinized RIV erythroid cells (Fig. 5c). We confirmed efficient introduction of frameshift insertion/deletion mutations and reduced protein-level expression of *S100a8* in myeloid and erythroid cells (Fig. 5d; Suppl. Fig. 5c).

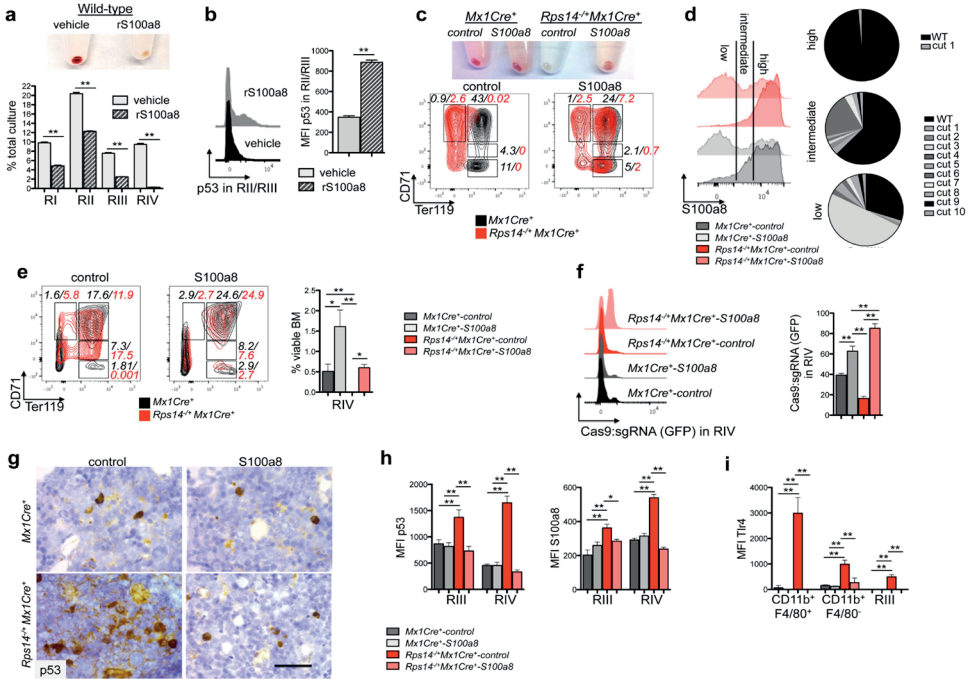

Figure 5

Figure 5: S100a8 is essential for the erythroid differentiation defect due to *Rps14* haploinsufficiency

Lineage negative wild-type HSPCs were subjected to erythroid differentiation for 5 days in the presence of vehicle or S100a8 recombinant protein (rS100a8). Cell pellets 5 days after induction of differentiation (representative picture of 5 biological replicates is shown) and frequency of RI-RIV erythroid progenitor populations in the culture. (mean±SD, n=5 biological replicates; **p<0.001). (b) Intracellular flow cytometry for p53 expression within the RII/RIII populations in erythroid differentiation culture *in vitro* in presence or absence of recombinant S100a8. Representative histograms of p53 expression and mean fluorescence intensity of p53 within this population (mean±SD, n=5 biological replicates; **p<0.001). (c) Cell pellets of ckit$^+$ HSPCs from *Rps14$^{-/+}$Mx1Cre$^+$* or *Mx1Cre$^+$* mice expressing S100a8 or control sgRNAs following erythroid differentiation *in vitro*. Representative flow plots of the erythroid progenitor populations characterized by CD71 and Ter119 expression (RI-RIV); (data representative from n=3 biological replicates are shown). (d) Representative histogram presentation of S100a8 expression in Gr1^{low}CD11b$^+$ monocytes in the erythroid differentiation culture *in vitro* after 5 days from *Rps14$^{-/+}$Mx1Cre$^+$* or *Mx1Cre$^+$* cells which were transduced with either S100a8 or control sgRNAs. The pie chart represents the mutations introduced by the S100a8 sgRNA:Cas9 transduced cells after sequencing of S100a8 high, intermediate, and low fractions. (e) ckit$^+$ HSPCs were transduced with a lentiviral vector expressing Cas9 and an sgRNA targeting S100a8 or control sgRNAs (non-targeting guide, NTG) and were transplanted 24 hours after infection into lethally irradiated wild-type recipients. 6 weeks after transplantation, recovered hematopoiesis in the transplanted mice was confirmed and PH was injected to induce hemolysis. 6 days after the first dose of PH, the bone marrow was harvested. Representative flow plots of the RI - RIV erythroid progenitor populations (mean±SD, n=5; **p<0.001; *p<0.05). (f) Representative histograms depicting GFP expression, representing cells transduced with control- or S100a8 sgRNA:Cas9 in the RIV population (mean±SD, n=5; **p<0.001). (g) p53 immunohistochemistry in bone marrows from *Rps14$^{-/+}$Mx1Cre$^+$* or *Mx1Cre$^+$* mice transduced with either control control or S100a8 sgRNA:Cas9. Scale bar: 50µm. (h) Quantification of the mean fluorescence intensity (MFI) of intracellular staining with p53 and S100a8 in erythroid progenitor populations (RIII and IV) in bone marrows from *Rps14$^{-/+}$Mx1Cre$^+$* or *Mx1Cre$^+$* mice transduced with either control or S100a8 sgRNA:Cas9. (mean±SD, n=5; *p<0.05; **p<0.001). (i) Quantification of the mean fluorescence intensity (MFI) of intracellular staining with Tlr4 in macrophages (CD11b$^+$F4/80$^+$), monocytes (CD11b$^+$F4/80$^-$) and in erythroid progenitor populations (RIII) in bone marrows from *Rps14$^{-/+}$Mx1Cre$^+$* or *Mx1Cre$^+$* mice transduced with either control or S100a8 sgRNA:Cas9. (mean±SD, n=5; *p<0.05; **p<0.001). Unpaired two-sided *t*-test (a-b) or multiple group comparison (e-i) using analysis of variance with posthoc Tukey correction were applied for statistical analysis.

We next determined whether *S100a8* is necessary for the erythroid differentiation defect in *Rps14* haploinsufficiency *in vivo* after PH-induced hemolysis (Fig. 5e-i). We transplanted HSPCs expressing either S100a8-sgRNA:Cas9 or control NTG-sgRNA:Cas9 into lethally irradiated wild-type recipients and treated with PH 6 weeks later. In contrast to controls, S100a8-sgRNA:Cas9 expression in *Rps14*$^{+/-}$*Mx1Cre*$^{+}$ hematopoietic cells rescued the ablation of the RIV population (Fig. 5e; Suppl. Fig. 5e-f), leading to a marked positive selection of Cas9:sgRNA-GFP^{+} RIV cells (Fig. 5f); reduced induction of p53 and S100a8 in erythroid cells (Fig. 5g, h; Suppl. Fig. 5g); decreased the frequency of Tlr4-expressing macrophages (Fig. 5i; Suppl. Fig. 5d, e, g); and reduced the induction of Tnfα (Suppl. Fig. 5h). These data demonstrate the role of S100a8 in the induction of a p53-dependent erythroid differentiation defect and the increase in Tlr4-expressing macrophages in *Rps14* haploinsufficiency.

To examine the cell-intrinsic effect of S100a8 in *Rps14* haploinsufficiency, we purified RII erythroblasts and measured the effect of S100a8 inactivation on terminal differentiation in the absence of myeloid cells (Suppl. Fig. 5i). Purified *Rps14* haploinsufficient RII progenitor cells expressing a control sgRNA did not terminally differentiate and underwent apoptosis, while those expressing S100a8-sgRNA:Cas9 differentiated into hemoglobinized, terminally differentiated erythroid cells, demonstrating that S100a8 directly affects erythroid progenitor cells by intrinsic mechanisms.

To examine whether S100a8 has cell-extrinsic effects, we analyzed S100a8 and p53 induction in wild-type competitor cells (CD45.1), as well as *Mx1Cre*$^{+}$ or *Rps14* (CD45.2) haploinsufficient cells, in competitive transplant studies (Suppl. Fig. 5j). Induction of S100a8 expression was restricted to CD45.2 *Rps14* haploinsufficient cells ($p<0.05$). In contrast, we observed p53 induction in both the CD45.1 competitor cells and CD45.2 *Rps14* haploinsufficient cells ($p<0.05$), indicating that increased S100a8 expression in *Rps14* haploinsufficient exerts a pro-apoptotic effect on wild-type cells that may drive progressive anemia in a cell-extrinsic fashion, even in the setting of preserved whole bone marrow chimerism. In summary, these data demonstrate that S100a8 exerts both cell-intrinsic cell-extrinsic effects on erythropoiesis.

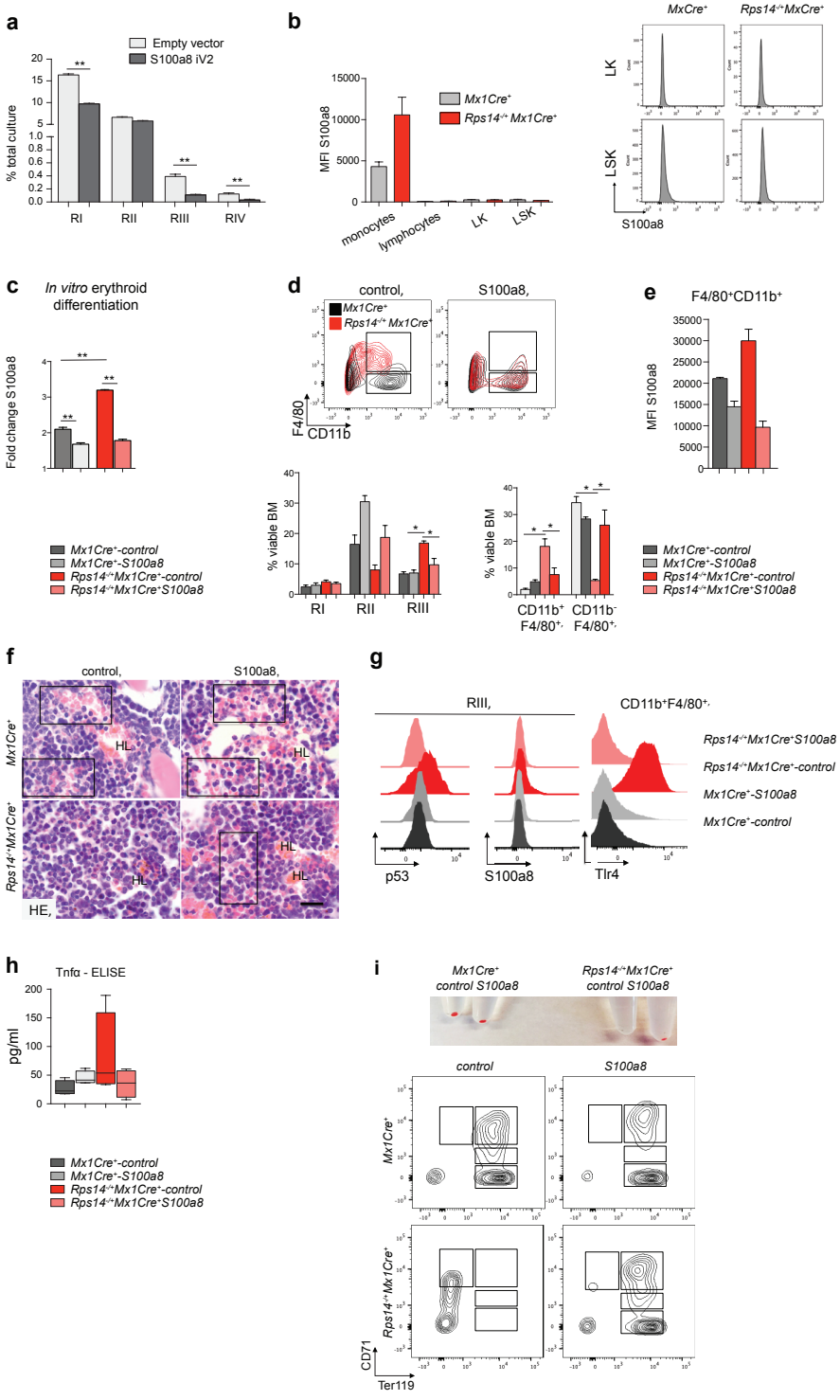
a
Empty vector
S100a8 iV2
% total culture
RI
RII
RIII
RIV
b
MFI S100a8
Mx1Cre+
Rps14-/+ Mx1Cre+
monocytes
lymphocytes
LK
LSK
MxCre+
Rps14-/+MxCre+
S100a8
c
In vitro erythroid differentiation
Fold change S100a8
Mx1Cre+-control
Mx1Cre+-S100a8
Rps14-/+Mx1Cre+-control
Rps14-/+Mx1Cre+S100a8
d
control,
S100a8,
F4/80
CD11b
% viable BM
RI
RII
RIII
CD11b+ F4/80+
CD11b- F4/80+
e
F4/80+CD11b+
MFI S100a8
f
control,
S100a8,
Mx1Cre+
Rps14-/+Mx1Cre+
HL
HE,
g
RIII,
CD11b+F4/80+
Rps14-/+Mx1Cre+S100a8
Rps14-/+Mx1Cre+-control
Mx1Cre+-S100a8
Mx1Cre+-control
p53
S100a8
Tlr4
h
Tnfα - ELISE
pg/ml
i
Mx1Cre+ control S100a8
Rps14-/+Mx1Cre+ control S100a8
control
S100a8
CD71
Ter119

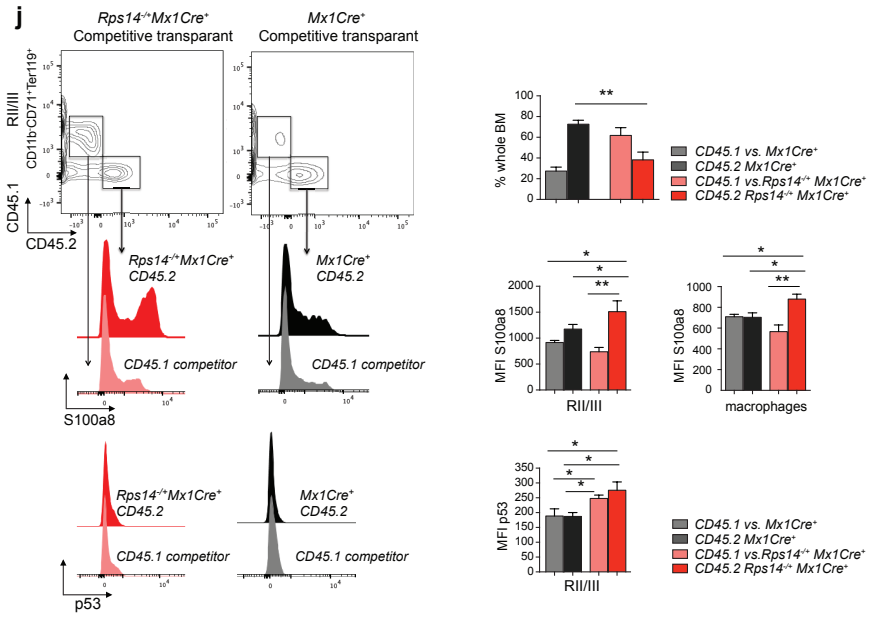

Supplementary figure 5: S100a8 is essential for the erythroid differentiation defect due to *Rps14* haploinsufficiency
(a) ckit$^+$ wild-type HSPCs were transduced with S100a8 overexpression vectors or empty vector. 48 hours after transduction, GFP$^+$ cells were sort-purified and subsequently subjected to erythroid differentiation for 5 days. Frequency of RI-RIV erythroid progenitor populations in the culture after 5 days. (mean±SD; **p<0.001). (b) Mean fluorescence intensity (MFI) of S100a8 in the monocytes, lymphocytes, LK and LSK in *Rps14*$^{-/+}$*Mx1Cre*$^+$ (n=5) and *Mx1Cre*$^+$ mice (n=4). (c) Quantification of mean fluorescence intensity of S100a8 relative to the negative control (=1) Gr1^{low}CD11b$^+$ monocytes and (mean±SD, n=3 biological replicates; **p<0.001) confirming the downregulation of S100a8 after transduction with S100a8 sgRNA/Cas9 or NTG. (d) ckit+ HSPCs were transduced with a lentiviral vector expressing Cas9 and an sgRNA targeting S100a8 or control (non-targeting guide) and were transplanted 24 hours after infection into lethally irradiated wild-type recipients. 6 weeks after transplantation, recovered hematopoiesis in the transplanted mice was confirmed and PH was injected to induce hemolysis. 6 days after the first dose of PH, the bone marrow was harvested. Representative flow plots of the macrophage (CD11b$^+$F4/80$^+$) and monocyte (CD11b$^+$F4/80$^-$) population in *Rps14*$^{-/+}$*Mx1Cre*$^+$ (n=5) and *Mx1Cre*$^+$ mice (n=5) transduced with either control:Cas9 or S100a8 sgRNA:Cas9 6 days after induction of hemolysis with PH. Quantification of the erythroid progenitor populations (RI-III; RIV is shown in main figure 5) and macrophage and monocyte population. mean±SD, n=5; *p<0.05. (e) Quantification of the MFI of S100a8 expression in macrophages. (mean±SD, n=5). (f) HE-staining of bone marrows from *Rps14*$^{-/+}$*Mx1Cre*$^+$ or *Mx1Cre*$^+$ mice transduced with either control:Cas9 or S100a8 sgRNA:Cas9. HL=hemolysis; inserts show enucleated red blood cells. Scale bar: 50µm. (g) Histograms showing representative expression of p53 and S100a8 in RIII erythroblasts and Tlr4 expression in macrophages. (h) Tnfa was determined in enzyme linked immunosorbent assay (ELISA) in the bone marrow serum in in *Rps14*$^{-/+}$*Mx1Cre*$^+$ (n=5) and *Mx1Cre*$^+$ mice (n=5) transduced with either control:Cas9 or S100a8 sgRNA:Cas9, 6 days after induction of hemolysis with PH. (i) Lineage-negative cells from *Rps14*$^{-/+}$*Mx1Cre*$^+$ (n=3) and *Mx1Cre*$^+$ mice (n=3) were purified using bead-separation and transduced with control:Cas9 or S100a8 sgRNA:Cas9. After 48 hours, positively transduced, GFP$^+$CD71$^+$Ter119$^{low-intermediate}$ RI/RII erythroid progenitor cells were sort-purified and subjected to erythroid differentiation *in vitro* for another 48 hours. Representative cell pellets harvested after 48 hours are shown as well as representative flow plots of CD71/Ter119 staining. (j) Aged *Rps14* or *Mx1Cre*$^+$ control whole bone marrow cells (18 months) were mixed in a 1:1 competition and the expression of S100a8 and p53 was analyzed after 4 months when the mice presented with progressive anemia. S100a8 and p53 expression was analyzed by intracellular flow cytometry in competitor cells (CD45.1) and *Rps14* haploinsufficient or *Mx1Cre*$^+$ cells (CD45.2), respectively, in the RII/III population or macrophages. The gating on the CD45.1 and CD45.2 within the RII/III population is shown representatively and representative histograms analyzing S100a8 or p53 expression are presented. The mean fluorescence intensity of S100a8 and p53 within these populations and in the CD45.1/CD45.2 fraction within the F4/80$^+$ macrophage compartment was quantified. (mean±SD; *p<0.05; **p<0.001).

Frequency of S100A8-positive cells in del(5q) MDS human bone marrows positively correlates with disease severity

To examine whether ribosomal haploinsufficiency leads to activation of S100A8 in patients with del(5q) MDS, we performed immunofluorescence for S100A8 and the erythroid marker glycophorin A (GlyA) on bone marrow biopsies from non-MDS controls (normal) and MDS patients with and without del(5q) (Fig. 6; Suppl. Table 2; Suppl. Fig. 6a, b). In non-MDS controls, rare S100A8 expressing cells were interspersed in the hematopoietic marrow. In del(5q) MDS, S100A8-positive were positioned in the marrow in groups of greater than 5 cells. The frequency of S100A8-expressing nucleated cells was significantly increased in del(5q) MDS bone marrow biopsies compared to non-MDS bone marrows (Suppl. Fig. 6b). GlyA-positive early erythroid progenitor cells occasionally co-expressed S100A8 (Fig. 6a, insert), just as seen in the *Rps14* haploinsufficient murine model. In aggregate, these data indicate that impaired erythropoiesis in the bone marrow of del(5q) MDS patients is associated with aberrant expression of S100A8.

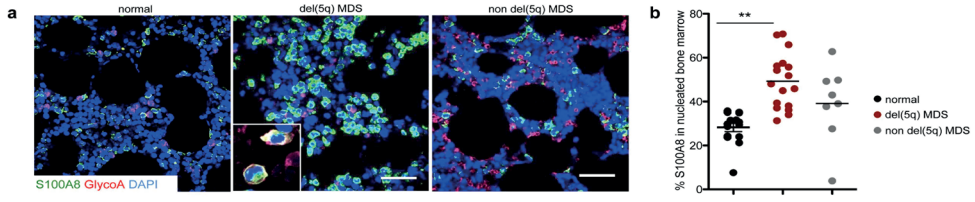

Figure 6

Figure 6: S100A8-frequency is significantly increased in del(5q) MDS human bone marrows compared to non-MDS controls. (a) Representative images of co-immunoflurescent staining of Glycophorin A (GlyA), S100A8 and DAPI as a nuclear staining in healthy (non-MDS; n=15), del(5q) MDS patients (n=21) and normal karyotype MDS (non del(5q), n=9). DAPI (blue), S100A8 (green), GlyA (magenta). Insert depicts S100A8 and GlyA expressing cells. Scale bars: 100µm. Immunofluorescence for all patients is shown in Supplementary Figure 6. (b) Quantification of $S100A8^{+}$ cells as a percentage of DAPI-positive nucleated bone marrow cells (S100A8 frequency in the nucleated marrow). (mean±SD, $p<0.001$). Unpaired two-sided *t*-test was applied for statistical analysis.

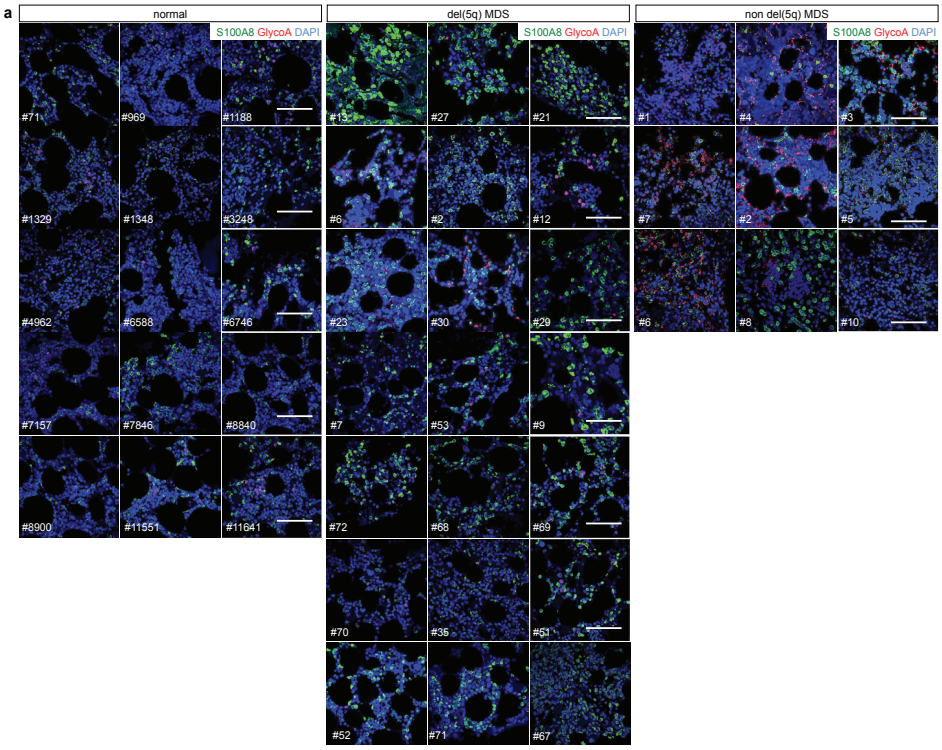

Supplementary figure 6: Images of co-immunoflurescent staining of Glycophorin A (GlyA), S100A8 and DAPI as a nuclear staining in normal bone marrows (n=15), del(5q) MDS (n=20) patients and normal karyotype MDS (non del(5q); n=9) and. DAPI (blue), S100A8 (green), GlyA (magenta). Scale bars: 100µm.

DISCUSSION

Anemia is the most common hematologic manifestation of MDS, particularly in patients with del(5q) MDS. In a novel conditional knockout mouse model of *Rps14*, we found that *Rps14* haploinsufficiency is sufficient to cause a p53-dependent erythroid differentiation defect with apoptosis resulting in age-dependent progressive anemia, megakaryocyte dysplasia, and loss of hematopoietic stem cell (HSC) quiescence. In an unbiased proteomic analysis, we identified a link between *Rps14* haploinsufficiency and induction of the danger associated molecular pattern (DAMP) heterodimer S100A8/S100A9 in monocytes, macrophages, and erythroblasts. Our studies link the p53-dependent erythroid differentiation defect to induction of S100A8 and an inflammatory environment produced by monocytes and macrophages, demonstrating that ribosomal haploinsufficiency exerts both cell intrinsic and extrinsic effects on erythroblasts and on hematopoiesis.

S100A8/S100A9 is induced during inflammatory processes including infection, autoimmunity, and cancer[26,36,37]. In addition to granuloyctes and macrophages, which produce these proteins under steady-state conditions, other cell types induce S100A8/S100A9 expression in response to stress[30]. We found significant induction of S100A8 in both $CD11b^+$ monocytes and $F4/80^+$ macrophages and concomitant increased expression of S100A8 in late-stage erythroblast, which was associated with p53 induction. Spatially, erythroid progenitor cells interact with a central macrophage in the erythroblastic island. Our data indicate that disruption of the regulatory mechanisms in the erythroblastic island contribute to the erythroid differentiation defects in *Rps14* haploinsufficient bone marrows. S100A9 activation has been described in MDS patient samples[24,38] and myeloid-derived suppressor cells (MDSC) driven by the S100A9/CD33 pathway perturb hematopoiesis[24]. Based on our data we posit that S100A8/S100A9 are induced as a stress response upon ribosomal haploinsufficiency in monocytes, macrophages, and erythroblasts and contribute to the MDS phenotype.

S100A8/A9 is an endogenous TLR4 ligand upstream of TNFa leading to NF-kB activation and secretion of pro-inflammatory cytokines[37]. Our data demonstrate that S100a8 acts upstream of Tlr4 and Tnfa in the Rps14 haploinsufficiency erythroid differentiation defect. Of note, RPS14 and miR-145 are universally co-deleted in the 5q- syndrome, and both converge on TLR4 signaling[25,40-44], highlighting the cooperating effects of genes on 5q.

S100 proteins participate in an autoregulatory feedback loop with p53, serving both as upstream drivers of p53 transcription and as direct downstream p53 transcriptional targets[26-29]. Consistent with these reports, our data demonstrate that p53 is required for induction of S100a8 expression in *Rps14* haploinsufficient cells, and that recombinant S100a8 is sufficient to induce p53 activity in erythroid progenitor cells, leading to a block in terminal erythroid differentiation.

Specific cytokines are elevated in the serum of MDS patients[33] and these inflammatory signals can alter proliferation and apoptosis of MDS HSPCs [45,46]. Indeed, chronic immune stimulation, coupled with senescence-dependent changes[48] in both HSPCs and the BM microenvironment[49] may be central to disease pathogenesis[25,41,50]. Our analysis of *Rps14* haploinsufficient HSCs suggests that inflammatory cues induced by *Rps14* haploinsufficiency impact HSC aging and quiescence[17,18,43,47]. In patients with chronic inflammation, cytokines in bone marrow have been associated with inhibition of erythropoiesis[51]. In particular, TNFa expression has been implicated in erythroid defects observed in patients with DBA[31] and is up-regulated in the bone marrow serum of MDS patients [52,53]. TNF-receptor associated factor 6 (TRAF6) activation, as a target of miRNA145 and miRNA146a, also induces myelodysplasia in a mouse model.

Deletion of the long arm of chromosome 5 leads to haploinsufficient expression of numerous genes. Based on our data we posit that the DAMP heterodimers S100A8/S100A9 are induced as a stress response upon ribosomal haploinsufficiency in monocytes, macrophages, and erythroblasts and contribute to the MDS phenotype. S100A8/A9 is an endogenous TLR4 ligand up-stream of TNFa leading to NF-kB activation and secretion of pro-inflammatory cytokines[1]. Our data demonstrate that S100a8 induced by Rps14 haploinsufficiency acts upstream of TLR4 in the erythroid differentiation defect. Of note, RPS14 and miR-145 are universally co-deleted in the 5q- syndrome and both converge on acting up- or downstream of TLR4 signaling[2-7], highlighting cooperating effects of genes on 5q.

Our data further demonstrate that p53 is required for induction of S100a8 expression in *Rps14* haploinsufficient cells, and that recombinant S100a8 is sufficient to induce p53 activity in differentiating erythroid progenitor cells leading to a block in terminal erythroid differentiation. It was shown in recent reports that S100 proteins can be intracellularly located and regulate cell growth, cell-cycle progression and apoptosis by interacting with the relevant intracellular signal-regulation pathways. S100 proteins can interact with p53 and affect p53 transcriptional activity, resulting in expression changes of p53 target genes[1].

Our data indicate an unexpected link between haploinsufficiency for a ribosomal gene, *Rps14*, activation of S100A8/S100A9 and other inflammatory molecules, and inhibition of erythropoiesis. Inhibition of this process, potentially through pharmacologic targeting of S100A8/S100A9, could improve red blood cell production in del(5q) MDS. These findings underscore a molecular link between the genetic abnormalities in MDS patients, activation of the innate immune system, and ineffective hematopoiesis that characterizes the disease.

Pat. Nr	IPSS-Score	WHO	blasts frequency %	hemoglobin g/dl	ANC /µl	platelets /nl (GPT/l)	ferritin ng/ml
5q-2	intermediate-1	MDS, isolated 5q	0	9	7936	634	1938
5q-6	low risk	RCMD, 5q-	0	9	n.a.	423	954.3
5q-12	low risk	MDS, isolated 5q	0	6.279	1290	146	1324.2
5q-13	low risk	MDS, isolated 5q	0	8.694	5860	136	1238.2
5q-21	low risk	MDS, isolated 5q	0	10.626	5930	546	2424.8
5q-23	low risk	RA, 5q-	0	8.3	4950	218	8867
5q-27	intermediate-1	MDS, isolated 5q	0	10.143	1480	102	1745.1
5q-29	intermediate-1	MDS, isolated 5q	0	7.728	1350	69	6471.4
5q-30	low risk	RA, 5q-	0	10.5	7700	674	691.9
5q-35	low risk	MDS, isolated 5q	1	8.7	1630	429	454.4
5q-51	intermediate-1	MDS, isolated 5q	<1	8.7	1240	70	515.3
5q-52	n.d.	RCMD	3	10.3	1600	287	1880.2
5q-53	intermediate-1	RCMD, isolated 5q	4	8.4	1000	467	274.8
5q-68	n.d.	MDS, isolated 5q	<5	11.3	2360	579	383.7
5q-69	low risk	MDS, isolated 5q	1	8.2	1870	384	168
5q-70	low risk	MDS, isolated 5q	3.5	8.9	2420	199	n.d.
5q-71	low risk	RAEB I, isolated 5q	2	8.4	980	360	275.5
5q-7	low risk	MDS, isolated 5q	0	8.6	1240	280	5880
5q-9	intermediate-1	MDS, isolated 5q	n.d.	6.7	1782	160	1758
5q-67	low risk	RCMD; 5q-	0	11.1	11200	640	316.5
5q-72	low risk	RCMD; 5q-	n.d.	n.d.	n.d.	n.d.	n.d.
Non5q-1	intermediate-1	RAEB I	0	8.3	2100	117	427.9
Non5q-2	low risk	RCMD	0	13.8	140	198	148.1
Non5q-3	intermediate-1	RARS	0	8.8	2390	42	2743.0
Non5q-4	intermediate-2	RAEB II	0	8.1	730	160	2645.0
Non5q-5	low risk	RCMD	0	11.6	5400	31	n.a.
Non5q-6	intermediate-1	RCMD	0	6.9	900	28	533.2
Non5q-7	low risk	RCMD	0	11.2	3900	282	182.0
Non5q-8	intermediate-2	RAEB I	0	6.8	770	95	379.3
Non5q-9	n.a.	RCMD	0	10	n.a.	172	n.a.
Non5q-10	intermediate-1	NA	0	8.7	2600	329	845.5
normal-7157	n.a.	n.a.	0	15.3	5100	227	n.d.
normal -3248	n.a.	n.a.	0	12.1	2700	249	n.d.
normal - 71	n.a.	n.a.		15.1	2400	184	n.d.
normal- 1348	n.a.	n.a.	0	15.3	3400	210	n.d.
normal -8840	n.a.	n.a.	0	16.2	6500	190	n.d.
normal - 6588	n.a.	n.a.	0	15.2	3800	200	n.d.
normal - 1329	n.a.	n.a.	0	13.1	3600	180	n.d.
normal- 11551	n.a.	n.a.	0	13.9	4000	212	n.d.
normal -11641	n.a.	n.a.	0	13.5	3100	247	n.d.
normal - 969	n.a.	n.a.	0	15.2	4900	244	n.d.
normal -6746	n.a.	n.a.	0	16.6	4600	166	n.d.
normal -4962	n.a.	n.a.	0	13.3	2300	140	n.d.
normal -1188	n.a.	n.a.	0	13.6	3100	205	n.d.
normal -8900	n.a.	n.a.	0	14.1	4400	167	n.d.
normal -7846	n.a.	n.a.	0	12.5	4000	247	n.d.

Supplementary table 2: Clinical data for bone marrow biopsies included in the study.

METHODS

Generation of *Rps14* conditional knockout mouse and mouse experiments

The Rps14 target region is 2.12 Kb and includes exon 2-4. Briefly, a 10.64 Kb region used to construct the targeting vector was first subcloned from a positively identified C57BL/6 BAC clone (RP23: 205B18). The region was designed such that the 5' homology arm extends about 5.76 Kb 5' to the single LoxP. The 3' homology arm ends 3' to the loxP/FRT flanked Neo cassette and is 2.76 Kb long. The loxP/FRT flanked Neo cassette was inserted 255 bp downstream of exon 4. The single loxP site, containing engineered ApaLI and Bcl I sites for southern blot analysis, was inserted 379 bp upstream of exon 2. The targeting vector was confirmed by restriction analysis after each modification step. P6 and T7 primers anneal to the backbone vector sequence and read into the 5' and 3' ends of the BAC sub-clone. N1 and N2 primers anneal to the 5' and 3' ends of the LoxP/FRT Neo cassette and sequence the SA and LA, respectively. The BAC was subcloned into a ~2.4kb backbone vector (pSP72, Promega) containing an ampicillin selection cassette for retransformation of the construct prior to electroporation. A pGK-gb2 loxP/FRT Neo cassette was inserted into the gene. The targeting construct was linearized using NotI prior to electroporation into ES cells. The total size of the targeting construct (including vector backbone and Neo cassette) is 14.74 Kb. Targeted iTL IC1 (C57BL/6N) embryonic stem cells were microinjected into Balb/c blastocysts. Resulting chimeras with a high percentage black coat color were mated to wild-type C57BL/6N mice to generate F1 heterozygous offspring. Tail DNA was analyzed from pups with black coat color. A PCR was performed to detect presence of the distal LoxP site using the 'LEVI 3' (5'- GTG ATC TCA ACG CAG GTG TGT AGC -3') and 'SDL2' (5'- TAA CAG CAT GGA AGT CGG GTC TCA -3') primers. This reaction amplifies a wild type product 474 bp in size. The presence of a second PCR product 73 bp greater than the wild type product indicates a positive LoxP PCR.

Chimeric mice were generated by standard methods. The Neo cassette was deleted by crossing with transgenic FLP1 recombinase mice purchased from Jackson Lab (Strain:B6. Cg-Tg(ACTFLPe)9205Dym/J). Rps14 littermate mice were genotyped by PCR with primers reverse (5'–GTG ATC TCA ACG CAG GTG TGT AGC-3') and forward (5'-TAA CAG CAT GGA AGT CGG GTC TCA-3') using the following parameters: 95ºC for 3 min, followed by 35 cycles of 95ºC for 30 sec, 60ºC for 1 min, and 72ºC for 1 min. Following confirmation of germline transmission, mice were crossed with the Mx1-cre mouse strain (Jackson: 002527). To excise *Rps14* exon 2-4, 6-8 week old *Rps14* conditional mice (and Mx1Cre^{+} mice as controls) were given three rounds of 200 μg of poly(I:C) (GE Healthcare Life Sciences) using intraperitoneal injections. Excision after Cre recombination was confirmed by PCR with primers to detect a floxed portion of the construct (Ndel 2: 5'-GTA TCT CCA ATG GTC AGC AAT CAC GG-3' and

LEVI: 5'- GTG ATC TCA ACG CAG GTG TGT AGC -3'). The knockout size is 511bp in size and a WT size of 623bp. For Qt-RT-PCR, I use the following Taqman probes were used: Rps14 mCG6028 Taqman expression Assay (Assay ID Mm00849906_g1; Life Technologies # 4331182). *Rps14* haploinsufficient mice were further bred to p53 null mice (Jackson stock number 00813). Animals were monitored two to three times a week for the presence of disease by general inspection and palpation. Peripheral blood was collected from the retro-orbital cavity using an EDTA- treated glass capillary and automated total and differential blood cell counts were determined using Hemavet 950 (Drew Scientific). Following sacrifice, mice were examined for the presence of abnormalities, and organs were collected for further cell and histopathological analysis. Due to the experimental design, the genotypes of the mice could not be blinded or randomized. The group size was chosen based on our experience with conditional murine knockout models of genes on 5q in order to detect a disease typical fold change as significant[54]. All groups of mice (controls and studied genotypes) were age- and sex-matched. Mouse experiments were performed according to an IACUC approved protocol at Children's Hospital Boston.

Flow cytometry and cell isolation

Bone marrow (BM) cells were isolated by flushing and crushing pelvis, hind leg bones and vertebrae with mortar and pestle in PBS (GIBCO) supplemented with 2% heat inactivated fetal bovine serum (FBS) and Penicillin/Streptomycin (GIBCO). Whole bone marrow was lysed on ice with red blood cell (RBC) lysis solution (Invitrogen/Life Technologies), and washed in PBS (GIBCO) with 2% FBS. Single-cell suspensions of spleen were prepared by pressing tissue through a 70µm cell strainer followed by red blood cell lysis. Cells were labeled with monoclonal antibodies in 2% FBS/PBS for 30 min on ice. For flow cytometric analysis and isolation of specific hematopoietic progenitors, cells were incubated with combinations of antibodies zo the following cell surface markers, conjugated to FITC, Pe, APC, PercP-Cy5.5, APC-Cy7 (APC-efluor780), Pe-Cy7, Alexa Fluor 700, Pacific blue (efluor450) or biotin: CD3 (17A2), CD5 (53-7.3), CD11b (M1/70), Gr1 (RB6-8C5), B220 (RA3-6B2), Ter119 (TER119), CD71 (C2), ckit (2B8), Sca1 (D7), CD34 (RSM34), CD16/32 (93), CD150 (TC15-12F12.2), CD48 (HM48-1), CD45.1 (A20), CD45.2 (104). For sorting of lineage-negative cells, lineage markers included CD3, CD5, CD11b, Gr1 and Ter119. For sorting of erythroid progenitor cells, the lineage cocktail did not include Ter119. All reagents were acquired from BD Biosciences, eBiosciences, or BioLegend. To increase the sorting efficiency, whole bone marrow samples were either lineage-depleted or ckit enriched using paramagnetic microbeads and an autoMACS magnetic separator (Miltenyi Biotec). Cell Sorting was performed on a FACSAria flow cytometer (BD Biosciences), data acquisition was performed on an LSR II or Canto II (BD Biosciences). Data were analyzed by FlowJo (Tree Star) software.

Long-term Competitive repopulation assays

In competitive bone marrow transplantation studies, $2x10^6$ freshly isolated bone marrow cells were transplanted in competition with $2x10^6$ freshly isolated CD45.1$^+$ bone marrow cells via tail vein injection into female lethally irradiated 6-8 week old (10.5 Gy) CD45.1$^+$ recipient mice. The donor cell chimerism was determined in the peripheral blood four weeks after transplantation before the excision of Rps14 was induced by poly(I:C) injection (week 0) as well as every four to eight weeks. Red blood cells were lysed (Invitrogen/Life Technologies) and the remaining cells were stained with antibodies against CD45.2, CD45.1, Gr1, CD11b, CD3, CD19 (eBio1D3) to assess the donor cell engraftment. For secondary transplants, $5x10^6$ bone marrow cells collected from primary recipients were transplanted into lethally irradiated CD45.1 recipient mice.

***In vivo* measurement of protein synthesis**

One hundred microliter of a 20mM solution of O-Propargyl-Puromycin (OP-Puro; life technologies) were injected intraperitoneally and mice injected with PBS were used as controls. Bone marrow and spleen were harvested after one hour and then kept on ice. $3x10^6$ cells were stained with antibodies against cell surface markers, fixed in 1% paraformaldehyde, and permeabilized in PBS with 3% fetal bovine serum and 0.1% saponin. The azide-alkyne cyclo-addition was performed using the Click-iT Cell Reaction Buffer Kit (Life Technologies) and azide conjugated to Alexa Fluor 488 (Life Technologies) at 5μM final concentration for 30 minutes. Cells were washed twice again and then analyzed by flow cytometry. 'Relative rates of protein synthesis' were calculated by normalizing OP-Puro signals to whole bone marrow after subtracting autofluorescence background as described by Singer et al[19].

Methylcellulose Assays

48 hours after viral transduction, 15,000 ckit$^+$ cells were sorted and plated in semi-solid methylcellulose culture medium (M3434, StemCell Technologies) and incubated at 37°C in a humidified atmosphere. Colony formation was assessed 7 days after plating.

shRNA and sgRNA:CRISPR Cas9 vector construction, virus production and transduction

Lentivirally expressed shRNAs in the pLKO.1 backbone vector (puromycin resitance) were obtained from the RNAi Consortium at the Broad Institute. S100A8 guide RNA (gRNA; forward 5'-CAC CGA ATT GTG GTA GAC ATC AAT G-3'; reverse 5'-AAA CCA TTG ATG TCT ACC ACA ATT C-3') were cloned into pL-CRISPR.EFS.GFP (http://www.addgene.org/57827) using BsmBI restriction digestion. Lentiviral particles were produced by transient transfection of 293T cells with lentivirus plasmid together with pSPAX and VSVG packaging plasmids using TransIT-LT (Mirus). Lentiviral particles were concentrated using ultracentrifugation. Ckit$^+$ or lineage-negative cells were cultured in StemSpan SFEM (StemCell Technologies) supplemented with 50 ng/ml murine Thpo and 50 ng murine Scf (both Peprotech) for 24 h

and then transduced with concentrated lentiviral supernatant in presence of 2 μg/ml Polybrene using spin-infection for 90 minutes at 2,200rpm at 37C.

Sequencing analysis of CRISPR variants

To assess the proportion and diversity of CRISPR variants, we performed PCR amplicon deep sequencing of bulk genomic DNA at the S100a8 sgRNA target site (chr3:90669574-90669596; mm9 genome build) using the primers S100a8-g1-F: GGACACTCAGTAGTGACCATTT and S100a8-g1-R: GAGTAACTGCAGCTCCCATC. After addition of sample indexes and sequencing adaptors, the product was subjected to 150 nucleotide paired-end sequencing on an Illumina MiSeq, producing approximately 100,000 reads per sample. Reads were then aligned to the genomic reference and grouped according to specific insertion and deletion sequences.

***In vitro* erythroid differentiation**

Total bone marrow cells were labeled with biotin-conjugated a-lineage antibodies, consisting of α-CD3e, α-CD11b, α-CD45R/B220, α-Ly6G/Ly6C and α-TER-119 (BD Pharmingen, San Diego, CA) and purified using anti-biotin beads and negative selection on the AutoMACS (Miltenyi). Purified cells were then seeded in fibronectin-coated (2μg/cm^2) tissue-culture treated polystyrene wells (BD Discovery Labware, Bedford, MA) at a cell density of 10^5 per ml. Erythroid differentiation was carried out according to modified, published protocols[55]. The erythropoietic medium consisted of IMDM supplemented with Epo at 10 units/ml, 10ng/ml SCF (Peprotech), 10μM dexamethasone (Sigma), 15% FBS, 1% detoxified BSA, 200μg/ml holotransferrin (Sigma, St. Louis, MO), 10μg/ml recombinant human insulin (Sigma), 2mM L-glutamine, 10^{-4} ß-mercaptoethanol and penicillin/streptomycin. After 48 hours the medium was replaced by maintenance medium consisting of IMDM with 20% FBS, 2mM L-glutamine and 10^{-4} b-mercaptoethanol. Recombinant S100a8 (mouse, Abnova P4345) protein was used where indicated in concentrations of 1μg/ml.

Phenylhydrazine treatment

Phenylhydrazine (PH) was purchased from Sigma and injected subcutaneously at two consecutive days (day 0 and 1) at the dose of 35 or 25 mg/kg as previously described[56]. Peripheral blood was collected 4 days before the start of treatment and at day 3, 6 and 9. PH treatment experiments were carried out in 8-12 week old mice.

Polysome profiling

For polysome profiling of primary erythroid progenitor cells, whole bone marrow was lineage-depleted (CD3, CD5, B220, Gr1, CD11b) using microbeads and the autoMACS as described above and stained for Ter119 and CD71. Erythroid progenitor cells (lineage^{negative}CD71^{high}Ter119$^{intermediate/high}$) were sort-purified in pure FCS, cultured for 1 hours in IMDM with 20% FCS and 2mM L-glutamine at 37°C at humidified conditions. Cells (ca.

$3x10^6$) were then harvested, spun down and incubated with 100µg/ml of cycloheximide for 10 minutes at 37°C, washed with ice-cold PBS containing 100µg/ml of cycloheximide and lysed in 300ul 5mM Tris (pH7.4), 2.5mM MgCl2, 1.5mM KCl. Gradients were poured using a Biocomp Gradient Station. Polysomes were separated on a 10-50% linear sucrose gradient containing 20mM HEPES-KOH (pH 7.4). 5mM $MgCl_2$, 100mM KCL, 2mM DTT and 100µh/ml cycloheximide and centrifuged at 36,000 rpm for 2 hours in a Beckman Coulter L8-M centrifuge with SW40Ti rotor. Gradients were fractionated using a Gilson FC-203B fractionator. Absorbance at 254nm was used to visualize the gradients using a BioRad EM-1 Econo UV monitor.

iTRAQ labeling of peptides and basic reversed phase (brp) fractionation

20 million RII/RIII erythroblasts (4 biological replicates per 1 technical/process replicate) were sort-purified and resuspended in 500µl lysis buffer (8M Urea, 50 mM Tris HCl, 1 mM EDTA, 75 mM NaCl, aprotinin, leupeptin, PMSF, NaF, PIC2, and PIC3; all Sigma), vortexed on ice and spun at 20,000xg for 10 min at 4 °C. 300ug protein of each sample were reduced (2 uL 500 mM DTT, 30 minutes, RT), alkylated (4 uL 500 mM IAA, 45 minutes, dark) and digested using 2ug of sequencing grade trypsin overnight with shaking at room temperature (Suppl. Table 3). The samples were then quenched with 20 uL 10% FA and desalted on10 mg SepPak columns. Desalted peptides were labeled with iTRAQ reagents according to the manufacturer's instructions (AB Sciex, Foster City, CA). Peptides were dissolved in 30 µl of 0.5 M TEAB pH 8.5 solution and labelling reagent was added in 70 ul of ethanol. After 1 h incubation the reaction was stopped with 50 mM Tris/HCl pH 7.5. Differentially labelled peptides were mixed and subsequently desalted on a 30 mg SepPak column.Basic Reversed Phase fractionation and subsequent concatenation of the differentially labelled and combined peptides was performed as described by Mertins et al.[57] with the following amendments: the Zorbax 300 Å Extended-C18 column used was 2.1x150mm with a 3.5µm bead size (Agilent).

Mass Spectrometry Analysis

Reconstituted peptides were separated on an online nanoflow EASY-nLC 1000 UHPLC system (Thermo Fisher Scientific) and analyzed on a benchtop Orbitrap Q Exactive mass spectrometer (Thermo Fisher Scientific). The peptide samples were injected onto a capillary column (Picofrit with 10 µm tip opening / 75 µm diameter, New Objective, PF360-75-10-N-5) packed in-house with 20 cm C18 silica material (1.9 µm ReproSil-Pur C18-AQ medium, Dr. Maisch GmbH, r119.aq). The UHPLC setup was connected with a custom-fit microadapting tee (360 µm, IDEX Health & Science, UH-753), and capillary columns were heated to 50 °C in column heater sleeves (Phoenix-ST) to reduce backpressure during UHPLC separation. Injected peptides were separated at a flow rate of 200 nL/min with a linear 80 min gradient from 100% solvent A (3% acetonitrile, 0.1% formic acid) to 30% solvent B (90% acetonitrile,

0.1% formic acid), followed by a linear 6 min gradient from 30% solvent B to 90% solvent B. Each sample was run for 120 min, including sample loading and column equilibration times. The Q Exactive instrument was operated in the data-dependent mode acquiring HCD MS/MS scans (R=17,500) after each MS1 scan (R=70,000) on the 12 top most abundant ions using an MS1 ion target of 3x 10^6 ions and an MS2 target of 5x10^4 ions. The maximum ion time utilized for the MS/MS scans was 120 ms; the HCD-normalized collision energy was set to 27; the dynamic exclusion time was set to 20s, and the peptide match and isotope exclusion functions were enabled.

Quantification and identification of peptides and proteins

All mass spectra were processed using the Spectrum Mill software package v4.2 pre-release (Agilent Technologies) which includes modules developed by us for iTRAQ -based quantification. Precursor ion quantification was done using extracted ion chromatograms (XIC's) for each precursor ion. The peak area for the XIC of each precursor ion subjected to MS/MS was calculated automatically by the Spectrum Mill software in the intervening high-resolution MS1 scans of the LC-MS/MS runs using narrow windows around each individual member of the isotope cluster. Peak widths in both the time and *m/z* domains were dynamically determined based on MS scan resolution, precursor charge and *m/z,* subject to quality metrics on the relative distribution of the peaks in the isotope cluster vs. theoretical. Similar MS/MS spectra acquired on the same precursor m/z in the same dissociation mode within +/- 60 sec were merged. MS/MS spectra with precursor charge >7 and poor quality MS/MS spectra, which failed the quality filter by not having a sequence tag length > 1 (i.e., minimum of 3 masses separated by the in-chain mass of an amino acid) were excluded from searching. For peptide identification MS/MS spectra were searched against mouse Uniprot database to which a set of common laboratory contaminant proteins was appended. Search parameters included: ESI-QEXACTIVE-HCD scoring parameters, trypsin enzyme specificity with a maximum of two missed cleavages, 40% minimum matched peak intensity, +/- 20 ppm precursor mass tolerance, +/- 20 ppm product mass tolerance, and carbamidomethylation of cysteines and iTRAQ labeling of lysines and peptide n-termini as fixed modifications. Allowed variable modifications were oxidation of methionine, N-terminal acetylation, Pyroglutamic acid (N-termQ), deamidated (N), Pyro Carbamidomethyl Cys (N-termC), with a precursor MH+ shift range of -18 to 64 Da. Identities interpreted for individual spectra were automatically designated as valid by optimizing score and delta rank1-rank2 score thresholds separately for each precursor charge state in each LC-MS/MS while allowing a maximum target-decoy-based false-discovery rate (FDR) of 1.0% at the spectrum level. In calculating scores at the protein level and reporting the identified proteins, redundancy is addressed in the following manner: the protein score is the sum of the scores of distinct peptides. A distinct peptide is the single highest scoring instance of a peptide detected through an MS/MS spectrum. MS/MS spectra for a particular peptide

may have been recorded multiple times, (i.e. as different precursor charge states, isolated from adjacent brp fractions, modified by oxidation of Met) but are still counted as a single distinct peptide. When a peptide sequence >8 residues long is contained in multiple protein entries in the sequence database, the proteins are grouped together and the highest scoring one and its accession number are reported. In some cases when the protein sequences are grouped in this manner there are distinct peptides which uniquely represent a lower scoring member of the group (isoforms or family members). Each of these instances spawns a subgroup and multiple subgroups are reported and counted towards the total number of proteins. iTRAQ ratios were obtained from the protein-comparisons export table in Spectrum Mill. To obtain iTRAQ protein ratios the median was calculated over all distinct peptides assigned to a protein subgroup in each replicate[58]. To assign differential expressed proteins we used the Limma package in the R environment to calculate moderated *t*-test *p*, as described previously. We also added Blandt-Altman testing to filter out proteins for which the CI for reproducibility was below 95%. Normalized iTRAQ ratios for the 2 biological replicates were filtered to retain only those deemed reproducible. Reproducible replicates were then subjected to a moderated t-test to assess statistical significance. This statistic is similar to the ordinary t-statistic, with the exception that the standard errors are calculated using an empirical Bayes method utilizing information across all proteins, thereby making inference about each individual protein more robust. The nominal p-values arising from the moderated t-statistic are corrected for multiple testing by controlling the false discovery rate (FDR), as proposed by Benjamini and Hochberg. Proteins with an FDR adjusted p-value of less than 0.01 were deemed to be reproducibly regulated. Statistical significance was assessed using only reproducible data points.

Cytokine Array

To detect inflammatory cytokines in the bone marrow serum, we applied the mouse Inflammation Array G1 (CODE: AAM-INF-G1, 8 sample size) according to manusfacturer's instructions. For detection of TNFα in the bone marrow serum, we used the TNF-alpha quantikine ELISA assay (R&D systems). The long bones of mice were kept on ice and flushed with a total of 200µl pure PBS. Cell-serum suspensions were spun down twice at 4°C at 2,200rpm and the supernatant was harvested and then spun at 13,000rpm for 10min. The protein content was determined using the Pierce protein content BCA assay kit and 100µg protein in 100µl were used per sample.

Western blots

Western blots were performed according to standard protocols. In brief, cell lysis was performed in RIPA buffer with protease/phosphatase inhibitors. After protein quantification, lysates were resuspended in Laemmli Sample Buffer, and loaded to gradient gels (Criterion Tris-HCl Gel, 8-16%). Proteins were transferred onto Immobilon polyvinyl difluoride (PVDF)

membranes. As primary antibodies S100A8 (Abcam ab92331), Rps14 (Abcam ab199273), Actin (EPR8484) were used. Blots were incubated with HRP-conjugated secondary antibody and developed using SuperSignal West Pico Chemiluminescent Substrate (Pierce).

Histopathology, immunohistochemistry and immunofluorescence

For histological and immunohistochemical analyses, organs and bones were fixed in 3.7% formaldehyde overnight, dehydrated and prepared for paraffin embedding. Hematoxylin-Eosin (H&E) staining was done according to routine protocols. For immunohistochemical stainings, the Avidin-Biotin Complex (ABC)/HRP (Dako Cytomation, K5001) was applied for color development using an Autostainer platform (Dako Cytomation, Glostrup, Denmark). Peripheral blood smears were stained with May-Grünwald-Giemsa (Sigma-Aldrich). For immunofluorescence studies, sternum sections were fixed in 4% paraformaldehyde on ice for 1 hour, then incubated in 30% sucrose in PBS at 4°C overnight. Cytospins were air-dried first and then fixed in 4% paraformaldehyde for 10 minutes at room temperature. OCT-embedded (Sakura Finetek) tissues were cryosectioned into 7 µm sections and mounted on Superfrost slides (Fisher Scientific). For immunofluorescence stainings, sections were washed in 1X PBS, blocked in 10% normal goat serum (Vector Labs) and incubated with primary antibodies specific for S100A8 (Abcam ab92331) or p53 (Cell Signaling, 1C12) or CD68 (DAKO, clone PGM1). Secondary antibodies were FITC-, Cy3, or Cy5- conjugated (Jackson ImmunoResearch). Nuclei were then stained with DAPI (4´,6´-´diamidino-2-phenylindole) and mounted in Prolong Gold (Life Technologies). Images were obtained on a Nikon Eclipse E400 microscope (Nikon, Tokyo, Japan) equipped with a SPOT RT color digital camera model 2.1.1 (Diagnostic Instruments) or obtained on a confocal microscope (Nikon C1 eclipse, Nikon, Melville, NY).

Confocal Q-FISH

Deparaffinization and antigen retrieval paraffin-embedded bone marrow specimens was carried out using standard protocols. Telomere Q-FISH staining was performed as described previously[59,60]. Briefly, Telomeres were stained with Cy3-(C3TA2) PNA (Panagene, South Corea) followed by six further washing steps and DNA staining was done using DAPI solution (Sigma, US). All images of BM sections were captured within 48h after sample processing and stored at 4°C. Telomere length analysis was performed using the LSM710 (Zeiss, Jena, Germany) confocal microscope. Images were captured using 63x optical magnification with additional 1.2x digital zoom and multi-tracking mode on 0.5 µm steps was used to acquire images of DAPI and Cy3 staining. Maximum projection of 5 single consecutive steps was done and acquired images were used for further digital image analysis. 5 representative images of randomly chosen areas were captured of each bone marrow. Telomere length detection was carried out using Definiens software (Definiens, Germany). Nuclei and telomeres were detected based on the respective DAPI and Cy3 intensity. Mean nuclear background of the

Cy3 staining nuclei was calculated and subtracted of each detected telomere within the respective nucleus. Median value of all detected telomeres was used for analysis.

Primary human samples and confocal microscopy

Patient samples originated from different study centers in Germany and this study was approved by according institutional review boards (University of Technology Dresden, Heinrich-Heine-University Düsseldorf, University Hospital RWTH Aachen, all Germany). Samples were deidentified at the time of inclusion. All patients provided informed consent and the data collection was performed in accordance with the Declaration of Helsinki. Criteria for inclusion of del(5q) MDS patients were: cytogenetic isolated del(5q), blast counts <5% in the bone marrow and International Prognostic Scoring System (IPSS) of low risk or intermediate-1. Patient data are summarized in supplementary table 1. Bone marrow biopsies were fixed for 24 hours using the Hannover Solution (12% buffered formaldehyde plus 64% methanol), decalcified (EDTA), dehydrated and embedded in paraffin. For immunofluorescence, samples were deparaffinized, hydrated using decreasing ethanol series and subject to heat-induced antigen retrieval using citrate buffer pH 6.0 before proceeding to the immunofluorescence co-stainings. Sections were first blocked with 1x Roti®-block (Carl Roth, Karlsruhe, Germany) for 1h at RT, washed with PBS-Tween and then incubated at 4°C overnight with a primary rabbit monoclonal anti-S100A8 antibody (Abcam, ab92331, 1:250). After washing steps, section were incubated for 30 minutes at RT with a goat anti-rabbit secondary antibody Alexa Fluor®488 conjugate (Life Technologies, Darmstadt, A-11034). Sections were then incubated at 4°C overnight with a primary mouse monoclonal anti-Glycophorin A antibody (Dako, M0819, 1:50) or anti-MPO (DAKO, A0398, 1:300) followed by incubation for 30 minutes at RT with a donkey anti-mouse secondary antibody Alexa Fluor®633 or Alexa Fluor®555 conjugate (Life Technologies, Darmstadt). Nuclei were stained with DAPI and mounted with Vectashield® mounting media (Vector Labs, CA, USA). All antibodies were diluted in 0.1x Roti®-block. Fluorescence was acquired with a confocal laser-scanning microscope (LSM 710, Zeiss, Germany) running Zen 2012 software (Zeiss). A 405 nm diode laser (DAPI) and a 488 nm/ 633 nm argon laser (Alexa Fluor®488/ Alexa Fluor®633) were used for fluorescence excitation. Maximal intensity projections of 3 z-stacks of 1µm each were acquired. Quantification of S100A8 in nucleated cells was done using Image J open source software.

Statistical analysis

Data are presented as mean±SEM. Comparison of two groups was performed using unpaired t-test. For multiple group comparison, analysis of variance with posthoc Tukey correction was applied. Statistical analyses were performed using GraphPad Prism 5.0c (GraphPad Software Inc., San Diego, CA). A p value of less than 0.05 was considered significant.

REFERENCES

1 Ebert, B. L. Deletion 5q in myelodysplastic syndrome: a paradigm for the study of hemizygous deletions in cancer. *Leukemia* **23**, 1252-1256, doi:10.1038/leu.2009.53 (2009).

2 Ebert, B. L. Molecular dissection of the 5q deletion in myelodysplastic syndrome. *Seminars in oncology* **38**, 621-626, doi:10.1053/j.seminoncol.2011.04.010 (2011).

3 Komrokji, R. S., Padron, E., Ebert, B. L. & List, A. F. Deletion 5q MDS: molecular and therapeutic implications. *Best practice & research. Clinical haematology* **26**, 365-375, doi:10.1016/j.beha.2013.10.013 (2013).

4 Ebert, B. L. *et al.* Identification of RPS14 as a 5q- syndrome gene by RNA interference screen. *Nature* **451**, 335-339, doi:10.1038/nature06494 (2008).

5 Choesmel, V. *et al.* Impaired ribosome biogenesis in Diamond-Blackfan anemia. *Blood* **109**, 1275-1283, doi:10.1182/blood-2006-07-038372 (2007).

6 Ruggero, D. & Shimamura, A. Marrow failure: a window into ribosome biology. *Blood* **124**, 2784-2792, doi:10.1182/blood-2014-04-526301 (2014).

7 McGowan, K. A. *et al.* Ribosomal mutations cause p53-mediated dark skin and pleiotropic effects. *Nature genetics* **40**, 963-970, doi:10.1038/ng.188 (2008).

8 McGowan, K. A. *et al.* Reduced ribosomal protein gene dosage and p53 activation in low-risk myelodysplastic syndrome. *Blood* **118**, 3622-3633, doi:10.1182/blood-2010-11-318584 (2011).

9 Matsson, H. *et al.* Erythropoiesis in the Rps19 disrupted mouse: Analysis of erythropoietin response and biochemical markers for Diamond-Blackfan anemia. *Blood cells, molecules & diseases* **36**, 259-264, doi:10.1016/j.bcmd.2005.12.002 (2006).

10 Dutt, S. *et al.* Haploinsufficiency for ribosomal protein genes causes selective activation of p53 in human erythroid progenitor cells. *Blood* **117**, 2567-2576, doi:10.1182/blood-2010-07-295238 (2011).

11 Pellagatti, A. *et al.* Induction of p53 and up-regulation of the p53 pathway in the human 5q- syndrome. *Blood* **115**, 2721-2723, doi:10.1182/blood-2009-12-259705 (2010).

12 Zhou, X., Hao, Q., Liao, J., Zhang, Q. & Lu, H. Ribosomal protein S14 unties the MDM2-p53 loop upon ribosomal stress. *Oncogene* **32**, 388-396, doi:10.1038/onc.2012.63 (2013).

13 Barlow, J. L. *et al.* A p53-dependent mechanism underlies macrocytic anemia in a mouse model of human 5q- syndrome. *Nature medicine* **16**, 59-66, doi:10.1038/nm.2063 (2010).

14 Raiser, D. M., Narla, A. & Ebert, B. L. The emerging importance of ribosomal dysfunction in the pathogenesis of hematologic disorders. *Leukemia & lymphoma* **55**, 491-500, doi:10.3109/10428194.2013.812786 (2014).

15 Volarevic, S. *et al.* Proliferation, but not growth, blocked by conditional deletion of 40S ribosomal protein S6. *Science* **288**, 2045-2047 (2000).

16 Morrison, S. J., Wandycz, A. M., Akashi, K., Globerson, A. & Weissman, I. L. The aging of hematopoietic stem cells. *Nature medicine* **2**, 1011-1016 (1996).

17 Pang, W. W. *et al.* Human bone marrow hematopoietic stem cells are increased in frequency and myeloid-biased with age. *Proceedings of the National Academy of Sciences of the United States of America* **108**, 20012-20017, doi:10.1073/pnas.1116110108 (2011).

18 Du, W. *et al.* Inflammation-mediated notch signaling skews fanconi anemia hematopoietic stem cell differentiation. *J Immunol* **191**, 2806-2817, doi:10.4049/jimmunol.1203474 (2013).

19 Signer, R. A., Magee, J. A., Salic, A. & Morrison, S. J. Haematopoietic stem cells require a highly regulated protein synthesis rate. *Nature* **509**, 49-54, doi:10.1038/nature13035 (2014).

20 Lajtha, L. G. & Oliver, R. A kinetic model of the erythron. *Proceedings of the Royal Society of Medicine* **54**, 369-371 (1961).

21 Karbstein, K. Inside the 40S ribosome assembly machinery. *Current opinion in chemical biology* **15**, 657-663, doi:10.1016/j.cbpa.2011.07.023 (2011).

22 Strunk, B. S. & Karbstein, K. Powering through ribosome assembly. *RNA* **15**, 2083-2104, doi:10.1261/rna.1792109 (2009).

23 Strunk, B. S. *et al.* Ribosome assembly factors prevent premature translation initiation by 40S assembly intermediates. *Science* **333**, 1449-1453, doi:10.1126/science.1208245 (2011).

24 Chen, X. *et al.* Induction of myelodysplasia by myeloid-derived suppressor cells. *The Journal of clinical investigation* **123**, 4595-4611, doi:10.1172/JCI67580 (2013).

25 Starczynowski, D. T. *et al.* Identification of miR-145 and miR-146a as mediators of the 5q- syndrome phenotype. *Nature medicine* **16**, 49-58, doi:10.1038/nm.2054 (2010).

26 Bresnick, A. R., Weber, D. J. & Zimmer, D. B. S100 proteins in cancer. *Nature reviews. Cancer* **15**, 96-109, doi:10.1038/nrc3893 (2015).

27 Li, C. *et al.* A novel p53 target gene, S100A9, induces p53-dependent cellular apoptosis and mediates the p53 apoptosis pathway. *The Biochemical journal* **422**, 363-372, doi:10.1042/BJ20090465 (2009).

28 Tan, M., Heizmann, C. W., Guan, K., Schafer, B. W. & Sun, Y. Transcriptional activation of the human S100A2 promoter by wild-type p53. *FEBS letters* **445**, 265-268 (1999).

29 Mueller, A. *et al.* The calcium-binding protein S100A2 interacts with p53 and modulates its transcriptional activity. *The Journal of biological chemistry* **280**, 29186-29193, doi:10.1074/jbc.M505000200 (2005).

30 Hiratsuka, S., Watanabe, A., Aburatani, H. & Maru, Y. Tumour-mediated upregulation of chemoattractants and recruitment of myeloid cells predetermines lung metastasis. *Nature cell biology* **8**, 1369-1375, doi:10.1038/ncb1507 (2006).

31 Bibikova, E. *et al.* TNF-mediated inflammation represses GATA1 and activates p38 MAP kinase in RPS19-deficient hematopoietic progenitors. *Blood* **124**, 3791-3798, doi:10.1182/blood-2014-06-584656 (2014).

32 Schepers, K. *et al.* Myeloproliferative Neoplasia Remodels the Endosteal Bone Marrow Niche into a Self-Reinforcing Leukemic Niche. *Cell stem cell*, doi:10.1016/j.stem.2013.06.009 (2013).

33 Kordasti, S. Y. *et al.* IL-17-producing CD4(+) T cells, pro-inflammatory cytokines and apoptosis are increased in low risk myelodysplastic syndrome. *British journal of haematology* **145**, 64-72, doi:10.1111/j.1365-2141.2009.07593.x (2009).

34 Su, S. *et al.* Inhibition of immature erythroid progenitor cell proliferation by macrophage inflammatory protein-1alpha by interacting mainly with a C-C chemokine receptor, CCR1. *Blood* **90**, 605-611 (1997).

35 Frisch, B. J. *et al.* Functional inhibition of osteoblastic cells in an in vivo mouse model of myeloid leukemia. *Blood* **119**, 540-550, doi:10.1182/blood-2011-04-348151 (2012).

36 Vogl, T. *et al.* Mrp8 and Mrp14 are endogenous activators of Toll-like receptor 4, promoting lethal, endotoxin-induced shock. *Nature medicine* **13**, 1042-1049, doi:10.1038/nm1638 (2007).

37 Ehrchen, J. M., Sunderkotter, C., Foell, D., Vogl, T. & Roth, J. The endogenous Toll-like receptor 4 agonist S100A8/S100A9 (calprotectin) as innate amplifier of infection, autoimmunity, and cancer. *Journal of leukocyte biology* **86**, 557-566, doi:10.1189/jlb.1008647 (2009).

38 Wei, Y. *et al.* Global H3K4me3 genome mapping reveals alterations of innate immunity signaling and overexpression of JMJD3 in human myelodysplastic syndrome CD34+ cells. *Leukemia* **27**, 2177-2186, doi:10.1038/leu.2013.91 (2013).

39 Sahin, E. *et al.* Telomere dysfunction induces metabolic and mitochondrial compromise. *Nature* **470**, 359-365, doi:10.1038/nature09787 (2011).

40 Chang, K. H. *et al.* p62 is required for stem cell/progenitor retention through inhibition of IKK/NF-kappaB/Ccl4 signaling at the bone marrow macrophage-osteoblast niche. *Cell reports* **9**, 2084-2097, doi:10.1016/j.celrep.2014.11.031 (2014).

41 Starczynowski, D. T. & Karsan, A. Deregulation of innate immune signaling in myelodysplastic syndromes is associated with deletion of chromosome arm 5q. *Cell Cycle* **9**, 855-856 (2010).

42 Starczynowski, D. T. *et al.* TRAF6 is an amplified oncogene bridging the RAS and NF-kappaB pathways in human lung cancer. *The Journal of clinical investigation* **121**, 4095-4105, doi:10.1172/JCI58818 (2011).

43 Reynaud, D. *et al.* IL-6 controls leukemic multipotent progenitor cell fate and contributes to chronic myelogenous leukemia development. *Cancer Cell* **20**, 661-673, doi:10.1016/j.ccr.2011.10.012 (2011).

44 Rhyasen, G. W. *et al.* Targeting IRAK1 as a therapeutic approach for myelodysplastic syndrome. *Cancer Cell* **24**, 90-104, doi:10.1016/j.ccr.2013.05.006 (2013).

45 Kristinsson, S. Y. *et al.* Chronic immune stimulation might act as a trigger for the development of acute myeloid leukemia or myelodysplastic syndromes. *Journal of clinical oncology : official journal of the American Society of Clinical Oncology* **29**, 2897-2903, doi:10.1200/JCO.2011.34.8540 (2011).

46 Takizawa, H., Boettcher, S. & Manz, M. G. Demand-adapted regulation of early hematopoiesis in infection and inflammation. *Blood* **119**, 2991-3002, doi:10.1182/blood-2011-12-380113 (2012).

47 Rossi, D. J. *et al.* Deficiencies in DNA damage repair limit the function of haematopoietic stem cells with age. *Nature* **447**, 725-729, doi:10.1038/nature05862 (2007).

48 Verschoor, C. P. *et al.* Blood CD33(+)HLA-DR(-) myeloid-derived suppressor cells are increased with age and a history of cancer. *Journal of leukocyte biology* **93**, 633-637, doi:10.1189/jlb.0912461 (2013).

49 Raaijmakers, M. H. *et al.* Bone progenitor dysfunction induces myelodysplasia and secondary leukaemia. *Nature* **464**, 852-857, doi:10.1038/nature08851 (2010).

50 Fang, J. *et al.* Cytotoxic effects of bortezomib in myelodysplastic syndrome/acute myeloid leukemia depend on autophagy-mediated lysosomal degradation of TRAF6 and repression of PSMA1. *Blood* **120**, 858-867, doi:10.1182/blood-2012-02-407999 (2012).

51 Means, R. T., Jr. Pathogenesis of the anemia of chronic disease: a cytokine-mediated anemia. *Stem Cells* **13**, 32-37, doi:10.1002/stem.5530130105 (1995).

52 Sawanobori, M. *et al.* Expression of TNF receptors and related signaling molecules in the bone marrow from patients with myelodysplastic syndromes. *Leukemia research* **27**, 583-591 (2003).

53 Jacobs-Helber, S. M. *et al.* Tumor necrosis factor-alpha expressed constitutively in erythroid cells or induced by erythropoietin has negative and stimulatory roles in normal erythropoiesis and erythroleukemia. *Blood* **101**, 524-531, doi:10.1182/blood-2001-11-0084 (2003).

54 Schneider, R. K. *et al.* Role of casein kinase 1A1 in the biology and targeted therapy of del(5q) MDS. *Cancer Cell* **26**, 509-520, doi:10.1016/j.ccr.2014.08.001 (2014).

55 Shuga, J., Zhang, J., Samson, L. D., Lodish, H. F. & Griffith, L. G. In vitro erythropoiesis from bone marrow-derived progenitors provides a physiological assay for toxic and mutagenic compounds. *Proceedings of the National Academy of Sciences of the United States of America* **104**, 8737-8742, doi:10.1073/pnas.0701829104 (2007).

56 Gritsman, K. *et al.* Hematopoiesis and RAS-driven myeloid leukemia differentially require PI3K isoform p110alpha. *The Journal of clinical investigation* **124**, 1794-1809, doi:10.1172/JCI69927 (2014).

57 Mertins, P. *et al.* Integrated proteomic analysis of post-translational modifications by serial enrichment. *Nature methods* **10**, 634-637, doi:10.1038/nmeth.2518 (2013).

58 Rappsilber, J. & Mann, M. Analysis of the topology of protein complexes using cross-linking and mass spectrometry. *CSH protocols* **2007**, pdb prot4594, doi:10.1101/pdb.prot4594 (2007).

59 Beier, F. *et al.* Telomere length analysis in monocytes and lymphocytes from patients with systemic lupus erythematosus using multi-color flow-FISH. *Lupus* **16**, 955-962, doi:10.1177/0961203307084299 (2007).

60 Beier, F. *et al.* Accelerated telomere shortening in glycosylphosphatidylinositol (GPI)-negative compared with GPI-positive granulocytes from patients with paroxysmal nocturnal hemoglobinuria (PNH) detected by proaerolysin flow-FISH. *Blood* **106**, 531-533, doi:10.1182/blood-2004-10-3996 (2005).

3

ROLE OF CASEIN KINASE 1A1 IN THE BIOLOGY AND TARGETED THERAPY OF DEL(5Q) MDS

Rebekka K. Schneider[1], Vera Ademà[2,3,4], Dirk Heckl[1], Marcus Järås[1], Mar Mallo[2,3], Allegra M. Lord, Lisa P. Chu[1], Marie E. McConkey[1], Rafael Kramann[5], Ann Mullally[1], Rafael Bejar[6], Francesc Solé[2,3], Benjamin L. Ebert[1,7]

[1]Division of Hematology, Department of Medicine, Brigham and Women's Hospital, Harvard Medical School, Boston, MA 02115, USA.
[2]Josep Carreras Leukaemia Research Institute (IJC), ICO-Hospital Germans Trias i Pujol, Universitat Autònoma de Barcelona (UAB), 08916 Badalona, Spain.
[3]Laboratori de Citogenètica Molecular, Servei de Patologia, Hospital del Mar, GRETNHE, IMIM (Hospital del Mar Research Institute), 08003 Barcelona, Spain.
[4]Departament de Biologia Cellular, Fisiologia i Immunologia, Facultat de Biociències, Universitat Autonoma de Barcelona (UAB), 08193 Barcelona, Spain.
[5]Renal Division, Brigham and Women's Hospital, Boston, MA 02115, USA.
[6]Division of Hematology and Oncology, UCSD Moores Cancer Center, La Jolla, CA, USA.
[7]Broad Institute of Harvard University and the Massachusetts Institute of Technology, Cambridge, MA 02142, USA

Corresponding author:
Benjamin L. Ebert, MD PhD

Division of Hematology, Department of Medicine, Brigham and Women's Hospital, Harvard Medical School, Boston, MA 02115, USA. Broad Institute of Harvard University and the Massachusetts Institute of Technology, Cambridge, MA 02142, USA
bebert@partners.org

Running Title
Casein kinase 1A1 in del(5q) MDS

Cancer Cell. 2014 Oct 13;26(4):509-20

SUMMARY

The Casein kinase 1A1 gene (*CSNK1A1)* is a putative tumor suppressor gene located in the common deleted region for del(5q) myelodysplastic syndrome (MDS). We generated a murine model with conditional inactivation of *Csnk1a1* and found that *Csnk1a1* haploinsufficiency induces hematopoietic stem cell expansion and a competitive repopulation advantage whereas homozygous deletion induces hematopoietic stem cell failure. Based on this finding, we found that heterozygous inactivation of *Csnk1a1* sensitizes cells to a *CSNK1* inhibitor relative to cells with two intact alleles. In addition, we identified recurrent somatic mutations in *CSNK1A1* on the non-deleted allele of patients with del(5q) MDS. These studies demonstrate that *CSNK1A1* plays a central role in the biology of del(5q) MDS and is a promising therapeutic target.

SIGNIFICANCE

Our studies provide functional and genetic evidence indicating that *CSNK1A1* plays a central role in the pathogenesis of del(5q) MDS. We found that heterozygous inactivation of *Csnk1a1* causes hematopoietic stem cell expansion and β-catenin activation. In addition, we found that *Csnk1a1* haploinsufficiency sensitizes cells to casein kinase inhibition, demonstrating an approach for the targeting of heterozygous deletions in cancer. While no recurrently mutated genes have been previously identified in genes within the common deleted regions of chromosome 5q, we found recurrent mutations in *CSNK1A1* in a subset of del(5q) MDS patients. In aggregate, these findings indicate that *CSNK1A1* is a promising therapeutic treatment for the treatment of del(5q) MDS.

INTRODUCTION

Deletions of chromosome 5q are the most common cytogenetic abnormalities in MDS, and patients with isolated del(5q) have a distinct clinical phenotype (Ebert, 2011; Haase et al., 2007; Hasserjian, 2008). To date, no genes within the common deleted regions (CDR) have been found to undergo homozygous inactivation, copy-neutral loss of heterozygosity, or recurrent mutation (Gondek et al., 2008; Graubert et al., 2009; Heinrichs et al., 2009; Jerez et al., 2012; Mallo et al., 2013). Functional studies have revealed individual genes that contribute cooperatively to the clinical phenotype through genetic haploinsufficiency (Boultwood et al., 2010; Chen et al., 2011; Ebert, 2011; Kumar et al., 2011; Lane et al., 2010; Starczynowski et al., 2010). Heterozygous loss of the *RPS14* gene, for example, has been linked to impaired erythropoiesis via p53 activation (Dutt et al., 2011; Ebert et al., 2008). While several 5q genes have been reported to alter hematopoietic stem cell function, the mechanism of clonal dominance of del(5q) cells remains a critical unsolved question (Joslin et al., 2007; Lane et al., 2010; Min et al., 2008; Wang et al., 2010a).

CSNK1A1 encodes casein kinase 1α (CK1α), a serine/threonine kinase, and is located in the distal common deleted region (5q32) in del(5q) MDS. In a careful study of gene expression in $CD34^+$ cells from a large cohort of del(5q) and other MDS cases, *CSNK1A1* was one of the few genes in the del(5q) common deleted region that has approximately 50% normal expression (Boultwood et al., 2007). Recent studies demonstrated that *CSNK1A1* is a tumor suppressor gene in colon cancer and melanoma controlling proliferation by its function as a central regulator of β-catenin activity (Elyada et al., 2011; Sinnberg et al., 2010). In hematopoiesis, stem and progenitor cells respond in a graded fashion to canonical Wnt/β-catenin signaling (Luis et al., 2011). Constitutive activation of β-catenin has been reported to increase HSC numbers followed by apoptosis, HSC depletion, and bone marrow failure (Kirstetter et al., 2006; Scheller et al., 2006). In contrast, less profound activation is associated with HSC expansion with enhanced repopulation potential (Trowbridge et al., 2006). APC, like CK1α, is a member of the β-catenin destruction complex, and is inactivated in approximately 95% of cases with del(5q) MDS. Mice with heterozygous deletion of *Apc* (Wang et al., 2010a) or heterozygous for the Apc^{Min} allele (Lane et al., 2010) have increased repopulation potential in primary bone marrow transplants, but decreased repopulation potential of secondary transplants due to loss of HSC quiescence.

We sought to explore whether haploinsufficiency or mutation of *Csnk1a1* contributes to the biology of del(5q) MDS. In addition, given evidence that *Csnk1a1* is selectively essential for murine MLL-AF9 leukemia cells relative to normal hematopoietic cells (Jaras et al., 2014), we investigated whether CK1α is a therapeutic target in del(5q) MDS.

RESULTS

Csnk1a1 is required for adult murine hematopoiesis

To explore the role of *Csnk1a1* on hematopoietic stem cell (HSC) function, we generated a mouse model in which *Csnk1a1* exon 3, essential for CK1α kinase function (Bidere et al., 2009), is flanked by loxP sites. Following crosses to *Mx1Cre* transgenic mice, we induced *Csnk1a1* excision in hematopoietic cells by poly(I:C), and confirmed decreased mRNA and protein expression (Figure 1A and S1A).

We first examined whether *Csnk1a1* plays a critical role in hematopoiesis. Homozygous deletion of *Csnk1a1* in the hematopoietic system (*Csnk1a1*$^{-/-}$*Mx1Cre*$^{+}$) resulted in rapid lethality 5-17 days after gene excision, accompanied by a significant decrease in all peripheral blood counts and histologic evidence of fulminant bone marrow failure with evidence of ischemia in multiple organs (Figures 1B, C, D, E and S1B).

We next examined whether the observed hematologic abnormalities were associated with changes in hematopoietic stem and progenitor cells. Ten days after *Csnk1a1* excision, *Csnk1a1*$^{-/-}$*Mx1Cre*$^{+}$ mice had a highly significant reduction of HSC (LSK, lin^{low}Sca1^{+}ckit^{+}) including long-term (LT, lin^{low}Sca1^{+}ckit^{+}CD150^{+}CD48^{-}), short-term (ST, lin^{low}Sca1^{+}ckit^{+}CD150^{-}CD48^{-}) HSC and multipotent progenitor cells (MPP, lin^{low}Sca1^{+}ckit^{+}CD150^{-}CD48^{+}) indicating that *Csnk1a1* is essential for HSC survival (Figure 1F and S1C).

CK1α is a major regulator of p53 activity, so we investigated whether *Csnk1a1* ablation activates p53 in the bone marrow (Elyada et al., 2011; Wu et al., 2012). Homozygous, but not heterozygous *Csnk1a1* deletion caused accumulation of p53 as well as p21, a p53 target, demonstrating that p53 is both present and active (Figure 1G). Consistent with this finding, we found that only complete ablation of *Csnk1a1* led to significant induction of early and late apoptosis (Figure 1H and S1D). *Csnk1a1*-ablated HSC exited quiescence and entered the cell cycle, with a marked decrease in the number of *Csnk1a1*$^{-/-}$*Mx1Cre*$^{+}$ HSC (LSK) in G0 and a significant increase in S/G2/M compared to *Mx1Cre*$^{+}$ controls (Figure 1I and S1E-F).

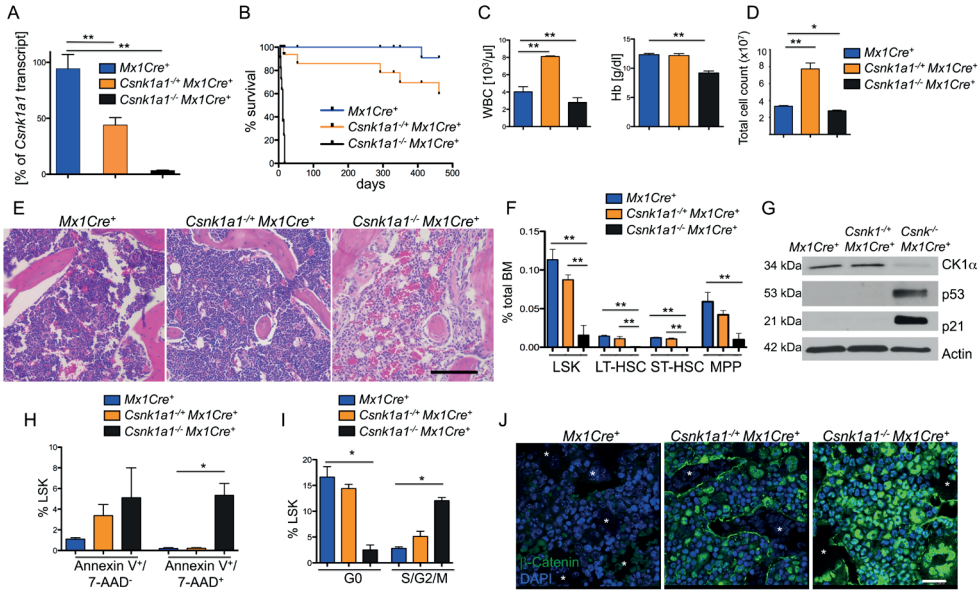

Figure 1: Conditional homozygous inactivation of *Csnk1a1* results in hematopoietic stem and progenitor cell ablation. (A) Deletion of *Csnk1a1* in whole bone marrow cells was determined 7 days after poly(I:C) induction by quantification of *Csnk1a1* transcript levels by qt-RT-PCR. Data is presented as remaining *Csnk1a1* transcript expression in percent relative to *Mx1Cre*$^+$-control mice (mean±SD, n=3). (B) Kaplan-Meier survival curve of *Csnk1a1*$^{-/+}$*Mx1Cre*$^+$ (n=10), *Csnk1a1*$^{-/-}$*Mx1Cre*$^+$ (n=10) and *Mx1Cre*$^+$ (n=10) control mice. Time point 0 is the day of the first of 3 poly(I:C) inductions. (C) Absolute numbers of white blood cells (WBC) and hemoglobin (Hb) levels in peripheral blood from *Csnk1a1*$^{-/+}$*Mx1Cre*$^+$, *Csnk1a1*$^{-/-}$*Mx1Cre*$^+$ and *Mx1Cre*$^+$ controls 10 days after poly(I:C) induction (mean±SD, n=3, *p<0.05, **p<0.001). (D) Numbers of whole bone marrow cells collected from tibias, femurs and pelvis of *Csnk1a1*$^{-/+}$*MxCre*$^+$, *Csnk1a1*$^{-/-}$*MxCre*$^+$ 10 days after poly(I:C) induction (mean ±SD; n=3, *p<0.001). (E) Histological analysis of HE-stained spine from *Csnk1a1*$^{-/+}$*Mx1Cre*$^+$, *Csnk1a1*$^{-/-}$*Mx1Cre*$^+$ and *Mx1Cre*$^+$ controls 10 days after poly(I:C). Scale bar: 200 µm. (F) Analysis of the HSC compartment, defined as Lin^{low}Sca1$^+$ckit$^+$ (LSK), long-term (LT; lin^{low}Sca1$^+$ckit$^+$CD48$^-$CD150$^+$), short-term (ST; lin^{low}Sca1$^+$ckit$^+$CD48$^-$CD150$^-$) HSC and multipotent progenitor cells (MPP, lin^{low}Sca1$^+$ckit$^+$CD48$^+$CD150$^-$) in the bone marrow from *Csnk1a1*$^{-/+}$*Mx1Cre*$^+$, *Csnk1a1*$^{-/-}$*Mx1Cre*$^+$ and *Mx1Cre*$^+$ controls 10 days after poly(I:C), (mean±SD, n=5, *p<0.05, **p<0.001). (G) Western blot of whole bone marrow lysate 8 days after induction of poly(I:C). (H) Apoptosis was assessed in the LSK fraction from BM by Annexin V and 7-AAD staining (early apoptosis: Annexin V$^+$/7-AAD$^-$; late apoptosis: Annexin V$^+$/7-AAD$^+$, (mean±SD, n=3, *p<0.05, **p<0.001). (I) Cell cycle was analyzed by combined proliferation (Ki67) and cell cycle (Hoechst 33342) staining in permeabilized LSK from bone marrow (G0: Ki67$^-$/Hoechst$^-$; S/G2/M: Ki67$^+$/Hoechst$^+$), (mean±SD, n=5, *p<0.05). (J) Immunofluorescence staining of paraffin-embedded bone marrow with an antibody against β-catenin (DAPI counterstaining). Asterisks highlight erythrocyte filled sinusoids. Scale bar: 20 µm. See also Figure S1.

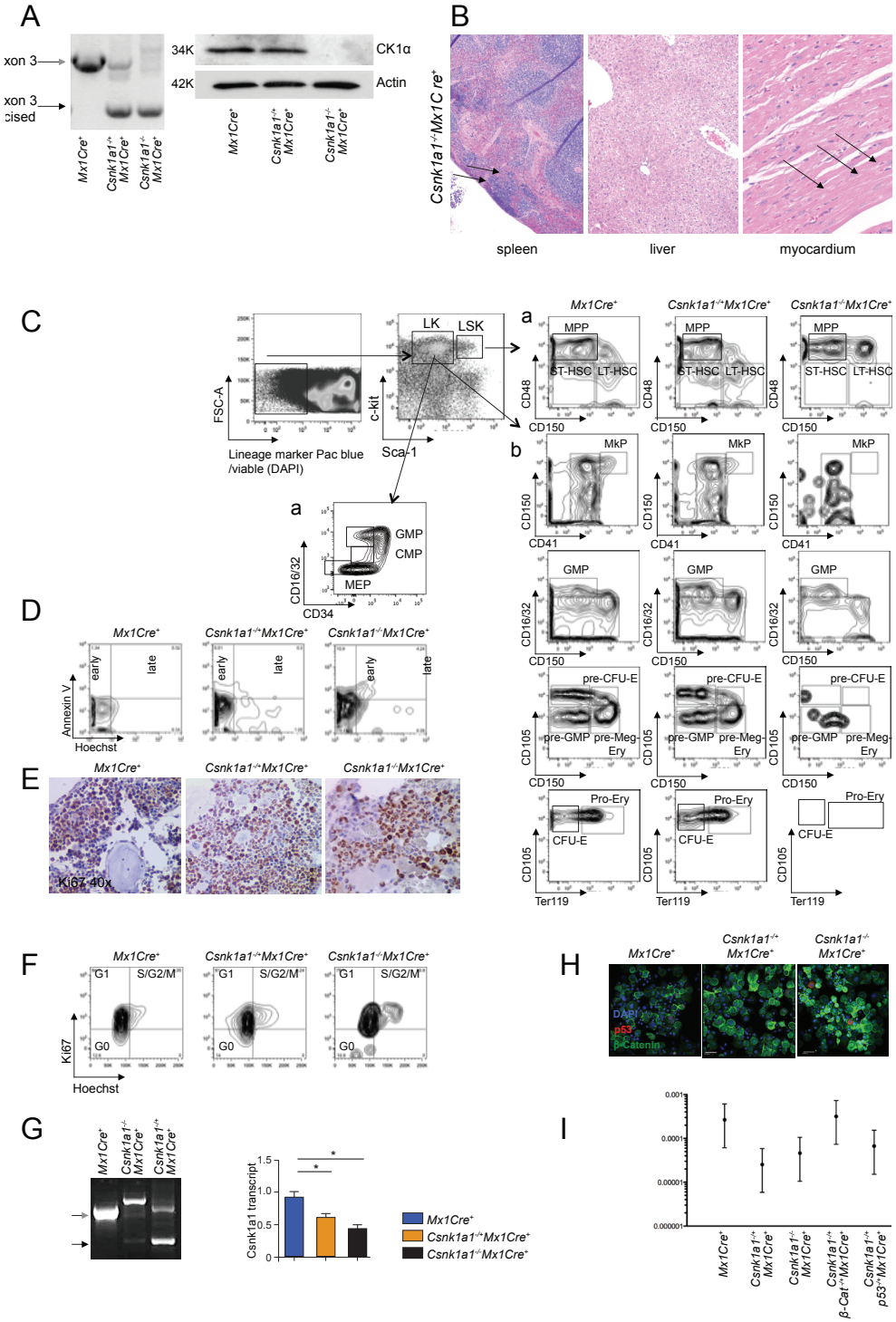
A
xon 3
xon 3
cised
34K
CK1α
42K
Actin
Mx1Cre+
Csnk1a1+/+ Mx1Cre+
Csnk1a1-/- Mx1Cre+
B
Csnk1a1-/-Mx1C re+
spleen
liver
myocardium
C
FSC-A
Lineage marker Pac blue /viable (DAPI)
LK
LSK
c-kit
Sca-1
a
GMP
CMP
MEP
CD16/32
CD34
Mx1Cre+
Csnk1a1-/+Mx1Cre+
Csnk1a1-/-Mx1Cre+
MPP
ST-HSC
LT-HSC
CD48
CD150
b
MkP
CD41
GMP
pre-CFU-E
pre-GMP
pre-Meg-Ery
CD105
Pro-Ery
CFU-E
Ter119
D
Annexin V
Hoechst
early
late
E
Ki67 40x
F
G1
S/G2/M
G0
Ki67
Hoechst
G
Csnk1a1 transcript
Mx1Cre+
Csnk1a1-/+Mx1Cre+
Csnk1a1-/-Mx1Cre+
H
DAPI
p53
β-Catenin
I
Csnk1a1+/+ Mx1Cre+
Csnk1a1-/- Mx1Cre+
Csnk1a1+/+ β-Cat+/+Mx1Cre+
Csnk1a1+/+ p53-/-Mx1Cre+

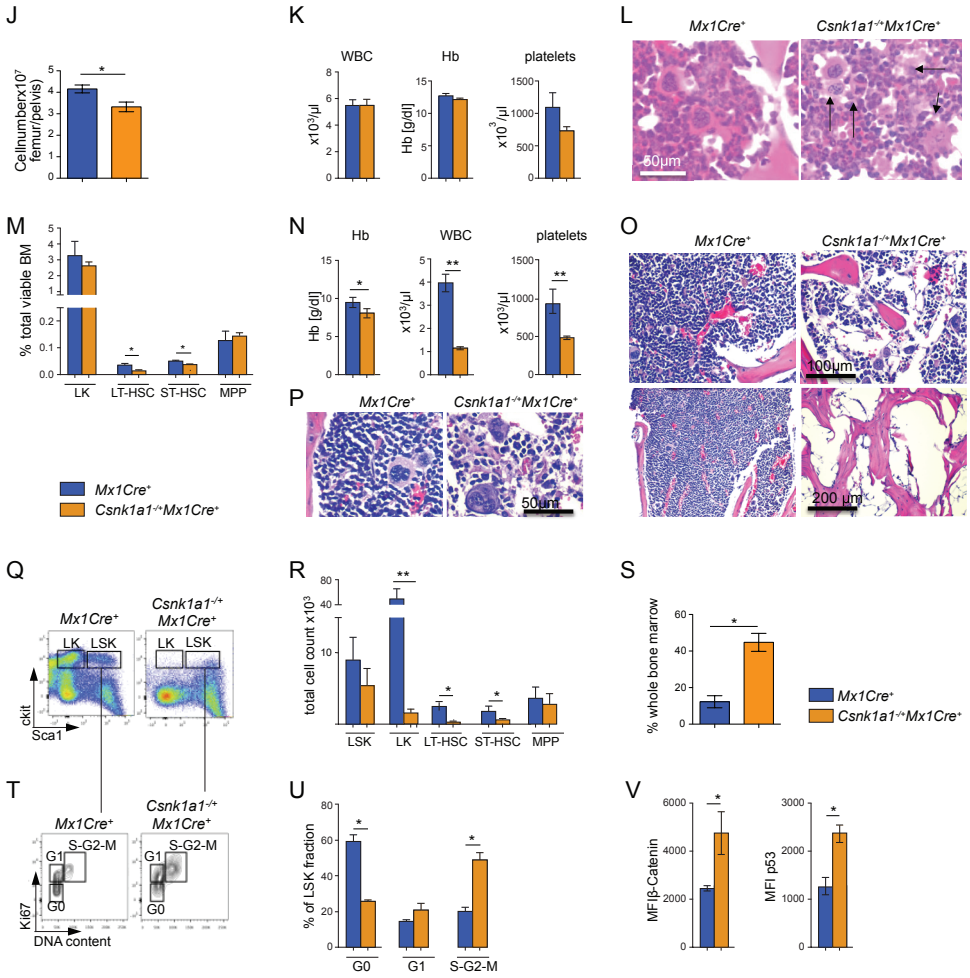

Figure S1: Characterization of primary *Mx1Cre*⁺ mice. (A) Validation of *Csnk1a1* excision after poly(I:C) by PCR (left) and by Western Blot (right). (B) Autopsies including histopathological examinations in *Csnk1a1*$^{-/-}$*Mx1Cre*⁺ mice revealed pale parenchymal organs and rarefication of the red pulp in the spleen with extramedullar erythropoiesis (arrows), prominently in subcapsular localization. Liver and the myocardium showed signs of ischemia. In the liver cytoplasmatic vacuolization and pyknotic nuclei were observed. Defined areas of the myocardium showed wavy fibers with loss of transversal striations, partially with loss of the cell nucleus (arrows). HE-staining. Scale bar each as indicated. (C) Hematopoietic stem and progenitor cells were analyzed by staining murine whole bone marrow cells with a lineage cocktail (CD3, B220, Gr1, CD11b, Ter119) and viability staining (DAPI) and either (a) classical stem and myeloid progenitor cell markers to dissect the LSK compartment in MPP (LSK CD48⁺), LT-HSC and ST-HSC (CD48 and CD150/Slamf1) and the LK compartment in GMP, CMP, MEP [FcgRII/III (CD16/32) and CD34] or (b) 6 myelo-erythroid progenitor cell fractions of the LK compartment [CD41 (Itga2b), Endoglin (CD105), CD150 (Slamf1), FcgRII/III (CD16/32), Ter119]. Representative contour blots of *Mx1Cre*⁺ control, *Csnk1a1*$^{-/+}$ Mx1Cre⁺, *Csnk1a1*$^{-/-}$ *Mx1Cre*⁺ stem and progenitor cells, only live cells are displayed. (D) Representative flow blots of Annexin V and Hoechst stained LSK cells. (E) Ki67 immunohistochemistry on paraffin-embedded bone marrow sections. Scale bar as indicated. (F) Representative contour flow blots of combined Ki67 (proliferation) and Hoechst 3342 (cell cycle) staining gating on LSK cells. (G) Mesenchymal stromal cells (MSC) were negative for CD31 and CD45 but positive for CD29, Sca1, CD44 and CD105. The *Csnk1a1* excision was confirmed by PCR (n=4, mean±SD, *p<0.05). (H) β-catenin and p53 immunofluorescence in MSC isolated from *Mx1Cre*⁺ control, *Csnk1a1*$^{-/+}$ Mx1Cre⁺, *Csnk1a1*$^{-/-}$ *Mx1Cre*⁺ bone

marrows (DAPI counterstain: blue, β-catenin: green, p53: red. Scale bar as indicated). (I) Limiting-dilution analysis of long-term culture-initiating cells (LT-CIC) was applied as a quantitative method of estimating hematopoietic stem cell-supporting activity of MSC isolated from *Mx1Cre+* controls and *Csnk1a1*$^{-/+}$*Mx1Cre*$^{+}$, *Csnk1a1*$^{-/-}$*Mx1Cre*$^{+}$, *Csnk1a1*$^{-/+}$*β-catenin*$^{-/+}$*Mx1Cre*$^{+}$ and *Csnk1a1*$^{-/+}$*p53*$^{-/+}$*Mx1Cre*$^{+}$MSC (n=10, mean±SD, *p<0.05). (J, K) *Csnk1a1* haploinsufficient mice were analyzed eight weeks after poly(I:C) i.p. injections. *Csnk1a1* haploinsufficient mice had a rather hypocellular bone marrow, but normal blood counts (n=5, mean±SD, *p<0.05). (L) Histopathological evaluation revealed hypolobulated micro-megakaryocytes (arrows) but normal trilineage maturation of hematopoiesis. (M) Analysis of the stem cell compartment after eight weeks (n=4, mean±SD, *p<0.05). (N) Blood counts of aged *Csnk1a1* haploinsufficient mice were analyzed 15 months after induction of poly(I:C), (n=4, mean±SD, *p<0.05*; **p<0.001). The peripheral blood revealed a pan-cytopenia consistent with (O) a hypocellular partially empty bone marrow in HE-staining. Scale bar as indicated. (P) Detailed histopathological analysis demonstrated a significant reduction of the myeloid and erythroid lineage, but quite intact lymphoid maturation. The stroma, in particular surrounding sinusoids, was prominent and significant dysplasia of small megakaryocytes with signs of emperipolesis and apoptosis was noted. No malignant transformation; the blast count in BM smears was <5%. HE staining, Scale bar as indicated. (Q) Representative lin^{-}Sca1^{-}ckit^{+} flow plots and (R) composite data of hematopoietic stem cell analysis by flow cytometry (lin^{-}Sca1^{+}ckit^{+}, LSK cells), including long-term (lin^{-}Sca1^{+}ckit^{+}CD48^{-} CD150^{+}, LT-HSC) and short-term (lin^{-}Sca1^{+}ckit^{+}CD48^{-}CD150^{+}, ST-HSC) hematopoietic stem cells (n=4, mean±SD, *p<0.05; **p<0.001). (S) Composite data of flow cytometry analysis of lin^{-}Sca1^{+}ckit^{-} cells reflecting the stromal compartment (n=4, mean±SD, *p<0.05). (T, U) Cell cycle analysis of the LSK fraction by flow cytometry (n=4, mean±SD, *p<0.05). (V) Intracellular expression of β-catenin as well as p53 in HSC (LSK), (n=4, mean±SD, *p<0.05).

Csnk1a1 loss induces increased β-catenin levels in both hematopoietic and stromal cells

CK1α is a critical regulator of β-catenin (Cheong and Virshup, 2011). In our murine model, heterozygous and homozygous knockout of *Csnk1a1* induced strong nuclear accumulation of β-catenin (Figure 1J). In the heterozygous knockout bone marrow, positive staining was predominantly in hematopoietic cells proximal to endothelial and endosteal cells, while in the homozygous knockout bone marrow, β-catenin nuclear accumulation was observed in nearly all cell types, highlighting a graded β-catenin activation by *Csnk1a1* gene dosage.

In addition, we observed a striking accumulation of β-catenin in the bone marrow stroma cells of heterozygous and homozygous *Csnk1a1* knockout mice, consistent with the expression of *Mx1Cre* in bone marrow stroma (Walkley et al., 2007). We validated this finding in mesenchymal stroma cells (MSC) isolated from endosteal bone (Zhu et al., 2010) and confirmed *Csnk1a1* excision in the stroma (Figure S1G). We found strong β-catenin expression in MSC from heterozygous *Csnk1a1* knockout mice, and even more pronounced expression in homozygous knockout mice (Figure S1H). In in vitro long-term culture initiating cell assays, both *Csnk1a1*$^{-/+}$*Mx1Cre*$^{+}$ and *Csnk1a1*$^{-/-}$*Mx1Cre*$^{+}$ MSC had significantly impaired hematopoiesis-supporting capacity. Inactivation of β-catenin rescued the effect of *Csnk1a1* loss in stromal cells (Figure S1I). The hematopoietic effects of *Csnk1a1* haploinsufficiency that we found in vitro were also observed in vivo. Eight weeks after pIpC treatment, we observed a significant reduction in bone marrow cellularity and in the percentage of LT- and ST-HSC in *Csnk1a1*$^{-/+}$*Mx1Cre*$^{+}$ mice compared to *Mx1Cre*$^{+}$ controls (Figure S1J-M). Consistent with this finding, the survival of *Csnk1a1*$^{-/+}$*Mx1Cre*$^{+}$ primary mice was significantly impaired (Figure 1B). After 15 months *Csnk1a1*$^{-/+}$*Mx1Cre*$^{+}$ mice developed pancytopenia, a significant decrease in the LT-HSC and ST-HSC, and a near complete loss of myeloid progenitor cells

(Figure S1N-V). These results are comparable to the recently described consequences of constitutively active β-catenin in osteoblasts (Kode et al., 2014), though we did not observe any evidence of malignant transformation in *Csnk1a1*$^{-/+}$*Mx1Cre*$^{+}$ mice at 15 months.

Cell intrinsic *Csnk1a1* ablation leads to bone marrow failure

Having observed that *Csnk1a1* excision in primary *Mx1Cre*$^{+}$ mice has striking effects on hematopoiesis, and given the cell-extrinsic effects of stromal β-catenin activation on hematopoietic cells (Kode et al., 2014; Lane et al., 2010; Stoddart et al., 2013; Wang et al., 2010a), we examined the cell-intrinsic effects of *Csnk1a1* inactivation in hematopoietic cells using bone marrow transplantation into wild-type recipient mice. We transplanted whole bone marrow cells from *Csnk1a1*$^{-/-}$*Mx1Cre*$^{+}$ or *Mx1Cre*$^{+}$ mice (CD45.2^{+}) into lethally irradiated WT recipient mice (CD45.1^{+}). Prior to induction of *Csnk1a1* excision, 4 weeks after transplantation, more than 90% of peripheral blood cells in recipient mice were reconstituted with donor-derived CD45.2^{+} cells. All recipient chimeric mice reconstituted with *Csnk1a1*$^{-/-}$*Mx1Cre*$^{+}$ cells became moribund with bone marrow failure 8–14 days after *Csnk1a1* excision (Figure 2A and S2A-C). Flow cytometric analysis revealed a complete loss of hematopoietic stem and progenitor cells in recipient mice. These studies confirm that a cell intrinsic function of *Csnk1a1* is essential for hematopoiesis.

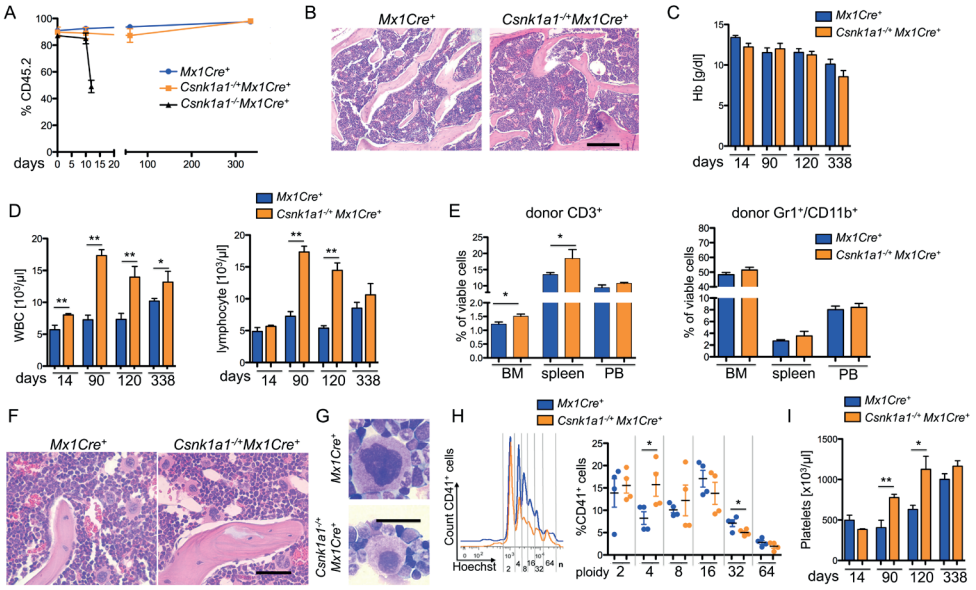

Figure 2: Homozygous *Csnk1a1* inactivation causes cell intrinsic hematopoietic stem cell ablation, while *Csnk1a1* heterozygous inactivation causes cell-intrinsic lineage expansion. (A) Donor chimerism (CD45.2) of *Csnk1a1*$^{-/+}$*Mx1Cre*$^{+}$, *Csnk1a1*$^{-/-}$*Mx1Cre*$^{+}$ and *Mx1Cre*$^{+}$ derived hematopoietic cells was monitored over time (mean±SD, n=7, **p<0.001). (B) Histomorphological analysis of transplanted *Csnk1a1*$^{-/+}$*Mx1Cre*$^{+}$ and *Mx1Cre*$^{+}$ cells 8 weeks after poly(I:C) induction. Scale bar: 200 µm. (C) Hemoglobin (Hb) levels were followed over time (mean±SD, n=7, non-significant). (D) White blood cell and lymphocyte count were monitored over time (mean±SD, n=7, *p<0.05, **p<0.001). (E) Distribution of donor derived (CD45.2^{+}) myeloid (Gr1^{+}/CD11b^{+}) and T-cells (CD3^{+}) was analyzed by flow cytometry in bone marrow, spleen and peripheral blood (mean±SD, n=5, *p<0.05). (F) Histomorphological analysis of megakaryocyte dysplasia in transplanted *Mx1Cre*$^{+}$ and *Csnk1a1*$^{-/+}$*Mx1Cre*$^{+}$ 8 weeks after poly(I:C) induction. Scale bar: 100 µm. (G) Detailed megakaryocyte morphology on cytospin preparations (May-Gruenwald-Giemsa staining, Oil immersion, Scale bar: 20 µm). (H) Representative ploidy analysis and quantification on CD45.2^{+}, CD41^{+} megakaryocytes using Hoechst33342 staining on fixed and permeabilized cells. (mean±SD, n=4, *p<0.05). (I) Platelet counts were taken over time (mean±SD, n=7, *p<0.05). See also Figure S2.

In striking contrast to mice transplanted with *Csnk1a1*$^{-/-}$*Mx1Cre*$^{+}$ cells, mice transplanted with *Csnk1a1*$^{-/+}$*Mx1Cre*$^{+}$ had no change in survival compared to *Mx1Cre*$^{+}$ control mice (Figure S2A). Transplanted *Csnk1a1* haploinsufficient hematopoietic cells fully reconstituted the bone marrow, resulting in a normal to hypercellular marrow, a normal hemoglobin, and significantly elevated white blood cell counts with lymphocytosis (Figures 2B-D). The lymphocytosis was caused by an increase in T-cells, consistent with reports demonstrating that moderate Wnt-activation promotes T-cell differentiation (Luis et al., 2012; Luis et al., 2011). The percentage of Gr1^{+}CD11b^{+} myeloid cells (Figure 2E) and CD19^{+} B-cells (Figure S2D) was not affected.

Pathological evaluation of the *Csnk1a1* haploinsufficient bone marrow revealed increased and mildly dysplastic hypolobulated (micro)megakaryocytes in atypical locations, reminiscent of the megakaryocyte morphology in del(5q) MDS (Figure 2F and S2E-F).

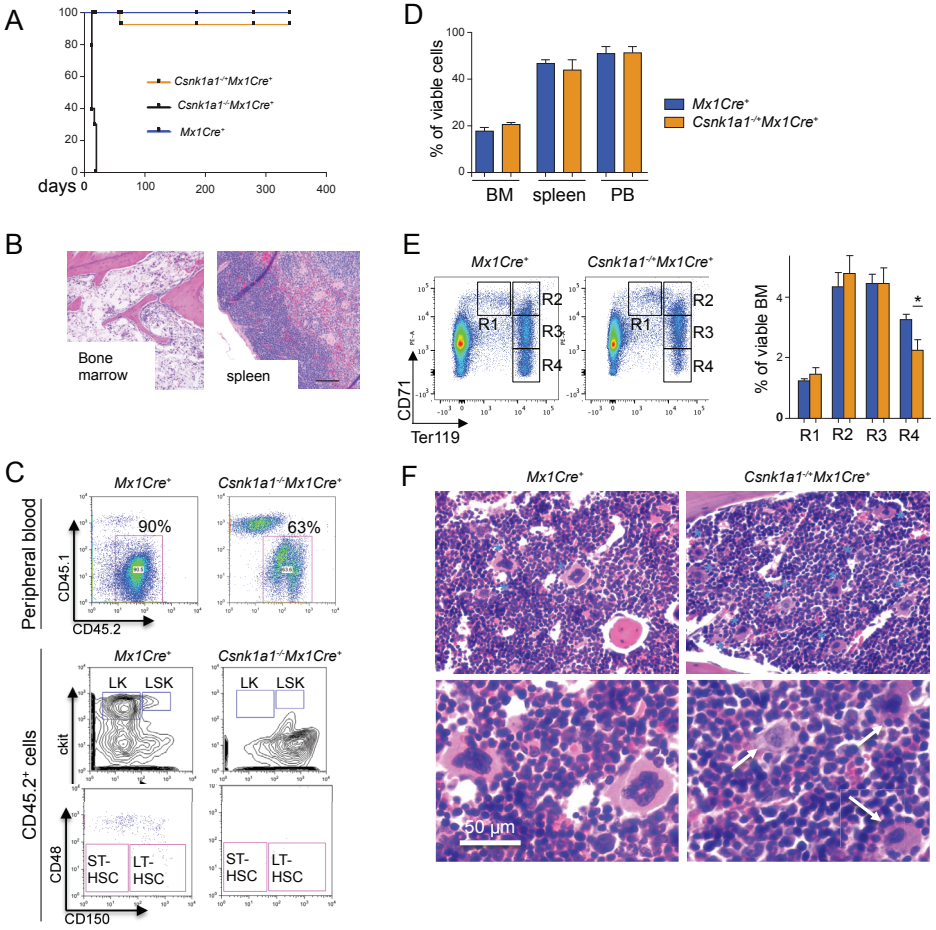

Figure S2: Related to figure 2. Rapid bone marrow failure after *Csnk1a1* ablation is an intrinsic effect. (A) Kaplan Meier survival curves over a time frame of 351 days [(day 0=first dose of poly(I:C)]. (B) Representative histomorphological analysis of bone marrow and spleen showing an empty bone marrow and extramedullar hematopoiesis, respectively, in *Csnk1a1*$^{-/-}$ *Mx1Cre*$^{+}$ mice 10 days after poly(I:C) treatment. Scale bar: 200 µm. (C) Representative flow plots of the CD45.1 and CD45.2 chimerism as well as the HSC compartment. (D) CD19^{+} B-cells in bone marrow (BM), spleen or peripheral blood (PB) (composite data, mean±SD, n=5, no significant differences). (E) CD71/Ter119 analysis of the bone marrow showing a terminal differentiation defect from the polychromatophilic erythroblast stage (R3) to the orthochromatophilic erythroblast/reticulocyte stage (R4), (n=5, mean±SD, *p<0.05). (F) The bone appeared normo- to hypercellular in mice transplanted with *Csnk1a1*$^{-/-}$*Mx1Cre*$^{+}$ in the long-term transplant setting. Micro-megakaryocytes were increased in their number (as highlighted by blue asterisks), hypolobulated and presented with spherical nuclei. Scale bar as indicated.

the presence of 10 ng/ml murine thrombopoietin. Nuclear ploidy analysis of the CD41^{+} megakaryocytes revealed a shift towards hypoploidy, consistent with hypolobation apparent in cytospins of the cultures (Figure 2G, H). Over time, the mice developed a significantly elevated platelet count (Figure 2I).

Haploinsufficiency of *Csnk1a1* leads to β-catenin activation and cell-intrinsic expansion of hematopoietic stem cells

CSNK1A1 has been reported to be a tumor suppressor gene in solid tumors due to activation of β-catenin (Elyada et al., 2011; Sinnberg et al., 2010). We first examined whether *Csnk1a* haploinsufficiency causes a cell-intrinsic effect on the number and function of HSC in a non-competitive transplantation assay. We found an increase in the percentage of the HSC-enriched LSK compartment, in contrast to the decrease in LSK and LK cells observed in the setting of an abnormal microenvironment in primary *Mx1Cre*$^{+}$ animals (Figure 1F and S1M, R). In particular, the proportion of LT-HSC was significantly elevated (Figure 3A).

To analyze whether HSC expansion might be due to exit from quiescence and enhanced HSC proliferation, we performed cell cycle analysis on hematopoietic stem and progenitor cells. In comparison to CD45.2^{+} *Mx1Cre*$^{+}$ control baseline hematopoiesis, CD45.2^{+} LSK cells and LT-HSC from *Csnk1a1*$^{-/-}$*Mx1Cre*$^{+}$ cells had a significantly lower percentage of cells in the quiescent G0 fraction (in LT-HSC not LSK) and a significantly higher percentage of cells in the cycling G1 fraction (Figure 3B) and in the S-phase as seen by BrdU incorporation (Figure S3A), consistent with exit from quiescence.

We next examined whether *Csnk1a1* heterozygous hematopoietic stem cells have altered β-catenin or cyclin D1 activity, as these pathways could contribute to decreased quiescence. *Csnk1a1*$^{-/+}$*Mx1Cre*$^{+}$ hematopoietic cells, transplanted into WT mice, had increased nuclear β-catenin accumulation by immunohistochemistry (Figure S3B) and by intracellular flow cytometry (Figure 3C-E). We found increased β-catenin in the stem cell enriched LSK fraction. β-catenin accumulation in HSC was accompanied by significantly increased expression of cyclin D1, a major regulator of cell cycle progression, corroborating the G1-phase progression in the cell cycle of *Csnk1a1* haploinsufficient cells. In the lineage-positive fraction, the differences in β-catenin were not apparent. These experiments demonstrate that heterozygous *Csnk1a1* inactivation is associated with increased levels of β-catenin in the hematopoietic stem cell.

As heterozygous deletion of *APC* occurs in approximately 95% of MDS cases and APC and CK1*α* are both negative regulators of β-catenin, we analyzed the combinatorial effect of *Csnk1a1* and *Apc* on β-catenin levels and hematopoietic stem cell expansion (Figure S3F). Compound heterozygous (*Csnk1a1*$^{-/+}$*Apc*$^{-/+}$*Mx1Cre*$^{+}$) hematopoietic cells were transplanted into lethally irradiated mice and analyzed over a period of 52 weeks. Compound heterozygous inactivation of *Csnk1a1* and *Apc* resulted in significantly increased LT-HSCs, increased β-catenin levels, and increased activation of the cell cycle in hematopoietic stem cells in long-term transplants (Figure S3G-J). In aggregate, our data highlight a central role for β-catenin in the pathophysiology of del(5q) MDS.

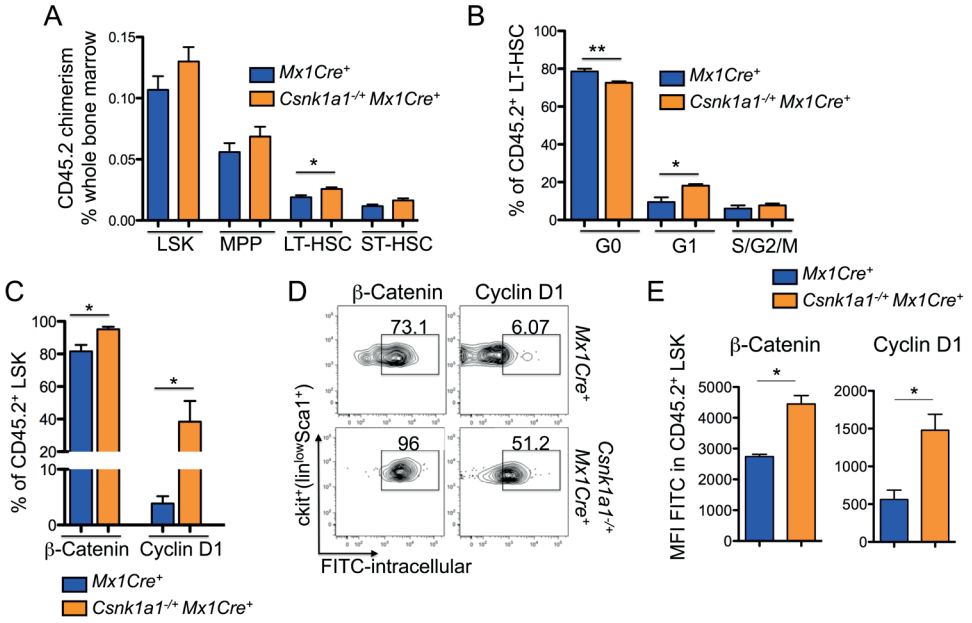

Figure 3: Haploinsufficiency of *Csnk1a1* leads to cell-intrinsic expansion of transplanted hematopoietic stem cells. (A) HSC chimerism (CD45.2) was analyzed in CD45.1 mice re-populated with *Csnk1a1*$^{-/+}$*Mx1Cre*$^{+}$ and *Mx1Cre*$^{+}$ cells 8 weeks after induction with poly(I:C) in the LSK, MPP, LT-HSC, and ST-HSC (mean±SD, n=5, *p<0.05). (B) Cell cycle was analyzed by combined proliferation (Ki67) and cell cycle (Hoechst 33342) staining in permeabilized LSK and LT-HSC from bone marrow (G0: Ki67^{-}/Hoechst^{-}; S/G2/M: Ki67^{+}/Hoechst^{+}), (mean±SD, n=5, *p<0.05). (C) Intracellular flow cytometry for β-catenin and cyclin D1 (FITC-labeled secondary antibody each) on the CD45.2^{+} viable LSK population (mean±SD, n=3, *p<0.05). (D) Corresponding representative flow blots to the quantitative analysis of intracellular β-catenin and cyclin D1, accumulation. (E) Mean fluorescence intensity (MFI) of intracellular β-catenin and cyclin D1 in LSK (mean±SD, n=3, *p<0.05). See also Figure S3.

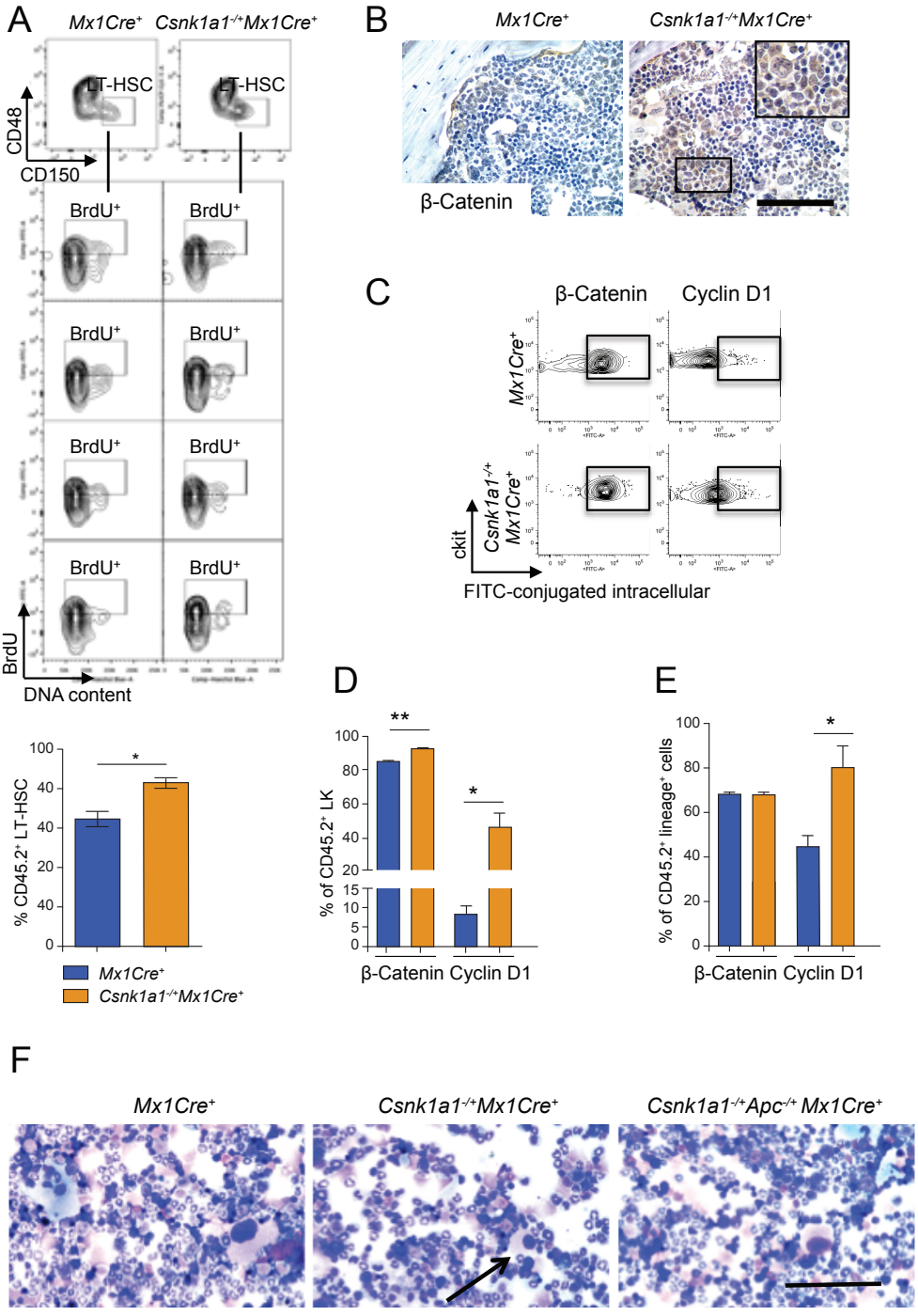
A
Mx1Cre+
Csnk1a1-/+Mx1Cre+
LT-HSC
LT-HSC
CD48
CD150
BrdU+
BrdU
DNA content
B
Mx1Cre+
Csnk1a1-/+Mx1Cre+
β-Catenin
C
β-Catenin
Cyclin D1
Mx1Cre+
Csnk1a1-/+ Mx1Cre+
ckit
FITC-conjugated intracellular
% CD45.2+ LT-HSC
Mx1Cre+
Csnk1a1-/+Mx1Cre+
D
% of CD45.2+ LK
β-Catenin Cyclin D1
E
% of CD45.2+ lineage+ cells
β-Catenin Cyclin D1
F
Mx1Cre+
Csnk1a1-/+Mx1Cre+
Csnk1a1-/+Apc-/+ Mx1Cre+

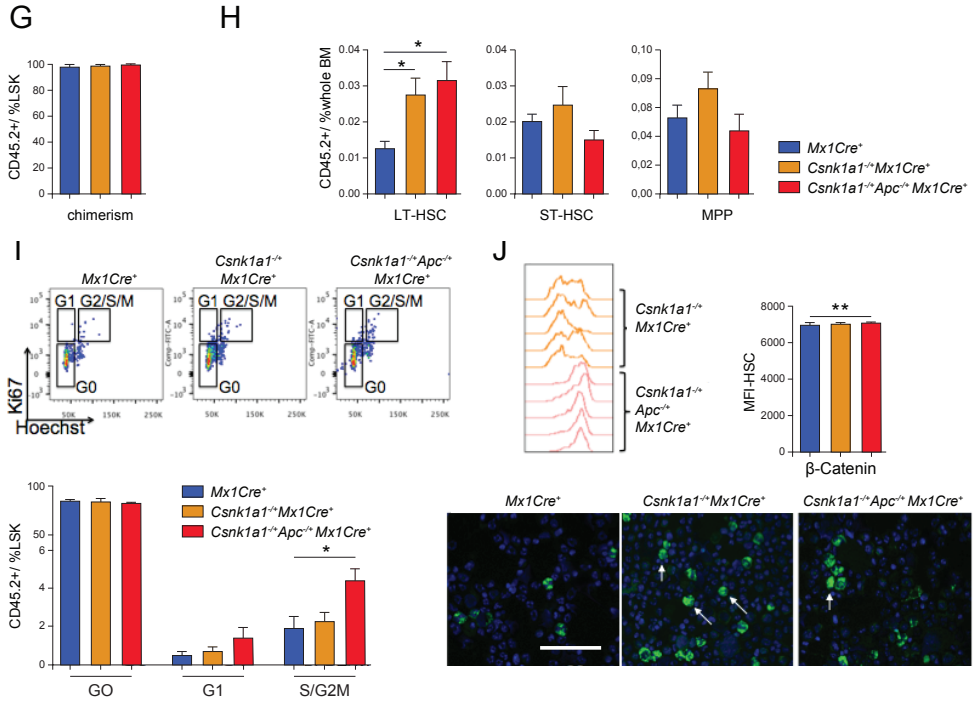

Figure S3: related to figure 3: Expanded HSC and increased β-catenin levels in *Csnk1a1*$^{-/+}$*Mx1Cre*$^{+}$ and *Csnk1a1*$^{-/+}$*Apc*$^{-/+}$*Mx1Cre*$^{+}$ mice.

(A) To further analyze proliferation changes in the expanded LT-HSC compartment in transplanted *Csnk1a1* haploinsufficient cells, we performed bromodeoxyuridine (BrdU) incorporation analysis. Mice received an initial intraperitoneal injection of BrdU (1 mg/6 g bodyweight) 18 hours prior to sacrifice. BrdU incorporation (S-phase) was analyzed in CD45.2^{+}lin^{-}Sca1^{+}ckit^{+}CD150^{+}CD48^{-} cells (LT-HSC). Quantification and composite data of cycling BrdU^{+} LT-HSC in transplanted *Csnk1a1* haploinsufficient cells versus *Mx1Cre*$^{+}$ cells (mean±SD, *p<0.05, n=4). (B) β-catenin immunohistochemistry on bone marrow chimeras of *Mx1Cre*$^{+}$ and *Csnk1a1*$^{-/+}$*Mx1Cre*$^{+}$ transplants. Scale bar: 200 µm. (C) Representative contour blots of β-catenin and cyclin D1 expression in CD45.2 LK (lin^{-}Sca1^{-}ckit^{+}) cells. (D) Composite data depicting CD45.2^{+} LK cells expression of β-catenin and cyclin D1 in progenitor cells of *Csnk1a1*$^{-/+}$Mx1Cre^{+}-derived LK cells compared to *Mx1Cre*$^{+}$ LK cells (n=5, mean±SD, *p<0.05, **p<0.001). (E) Composite data of intracellular β-catenin and cyclin D1 flow cytometry on lineage^{+} cells (mean±SD, *p<0.05). (F) Lethally irradiated CD45.1^{+} recipient mice were transplanted with *Csnk1a1*$^{-/+}$Mx1Cre^{+}, *Csnk1a1*$^{-/+}$*Apc*$^{-/+}$*Mx1Cre*$^{+}$ or *Mx1Cre*$^{+}$ whole bone marrow cells. Four weeks after transplantation, the gene excision was induced with poly(I:C). Morphological analysis of whole bone marrow cytospin preparations of mice transplanted with *Csnk1a1*$^{-/+}$Mx1Cre^{+}, *Csnk1a1*$^{-/+}$*Apc*$^{-/+}$*Mx1Cre*$^{+}$ or *Mx1Cre*$^{+}$ show trilineage differentiation without evidence for leukemic transformation and blast counts <5%. MGG staining, Scale bar 100 µm. (G) CD45.2^{+} chimerism of the hematopoietic stem cell enriched bone marrow fraction (mean±SD, n=5, ns). (H) HSC chimerism (CD45.2) in the whole bone marrow 336 days after induction with poly(I:C) including LT-HSC, ST-HSC and MPP (mean±SD, n=5, *p<0.05). (I) Representative flow blot and composite data of cell cycle analysis in HSC (lin^{-}Sca1^{+}ckit^{+}) using Ki67 and Hoechst 3342 staining (mean±SD, n=5, *p<0.05). (J) Histogram analysis of intracellular β-catenin expression analysis in permeabilized LSK, quantified mean fluorescence intensity (MFI) of β-catenin in LSK (mean±SD, n=5, *p<0.05) and β-catenin immunofluorescence on bone marrow cytospins. (arrows, blue: DAPI counterstaining, green: β-catenin; scale bar: 80 µm).

Csnk1a1 haploinsufficient HSCs have increased self-renewal ability in vivo

As *Csnk1a1* haploinsufficiency leads to a significant increase in cycling LT-HSCs, we examined the functional capacity of *Csnk1a1* haploinsufficient cells in a competitive repopulation assay. Four weeks after transplantation, mice were treated with poly(I:C) to induce *Csnk1a1* deletion. *Csnk1a1* haploinsufficient cells out-competed WT cells, while *Mx1Cre*$^{+}$ control cells were stable over time, and cells with homozygous *Csnk1a1* inactivation were rapidly depleted (Figure 4A).

To determine the long-term repopulating potential of *Csnk1a1* haploinsufficient bone marrow, whole bone marrow cells from the primary recipients were injected into lethally irradiated secondary and tertiary recipients. *Csnk1a1* haploinsufficient bone marrow cells had a significantly impaired response to the stress of transplantation, resulting in significantly lower numbers of CD45.2^{+} donors cells in the peripheral blood compared to *Mx1Cre*$^{+}$ controls each 4 weeks after secondary and tertiary transplantation. However, 16 weeks after each round of transplantation, *Csnk1a1* haploinsufficient cells recovered and again out-competed the control cells (Figure 4A).

Having observed a competitive advantage for *Csnk1a1* haploinsufficient bone marrow evaluated in the peripheral blood, we next evaluated hematopoietic stem and progenitor cells in the setting of competitive repopulation (Figure 4B-E). At both 16 weeks following the primary transplant and 16 weeks following the secondary transplant, *Csnk1a1* haploinsufficient cells were significantly more abundant than their wild type counterparts in the percentage of LSK cells and downstream myeloid progenitor cells, Gr1^{+}CD11b^{+} myeloid cells, and CD3^{+} T-cells in the bone marrow.

Csnk1a1 haploinsufficiency sensitizes cells to casein kinase 1 inhibition

Having demonstrated a selective advantage for cells with heterozygous *Csnk1a1* inactivation, and a severe disadvantage for cells with homozygous *Csnk1a1* inactivation, we postulated that *Csnk1a1* haploinsufficiency might sensitize cells to CK1α inhibition. Partial inhibition of CK1α would be expected to cause wild-type cells to have a phenotype similar to haploinsufficient cells, while CK1α inhibition in cells that already have one allele inactivated would approach closer to complete ablation of CK1α activity, thereby establishing a therapeutic window for CK1α inhibition in del(5q) MDS cells. We tested this hypothesis using D4476, a selective small molecule inhibitor of CK1 (Rena et al., 2004). Since D4476 has a short half-life in vivo, we treated purified myeloid progenitors from *Csnk1a1* haploinsufficient cells and *Mx1Cre*$^{+}$ controls with D4476 in vitro. D4476 significantly decreased viability and increased apoptosis in *Csnk1a1* haploinsufficient cells relative to *Mx1Cre*$^{+}$ controls at a range of concentrations, consistent with a therapeutic window for targeting *Csnk1a1* haploinsufficient cells (Figure 5A).

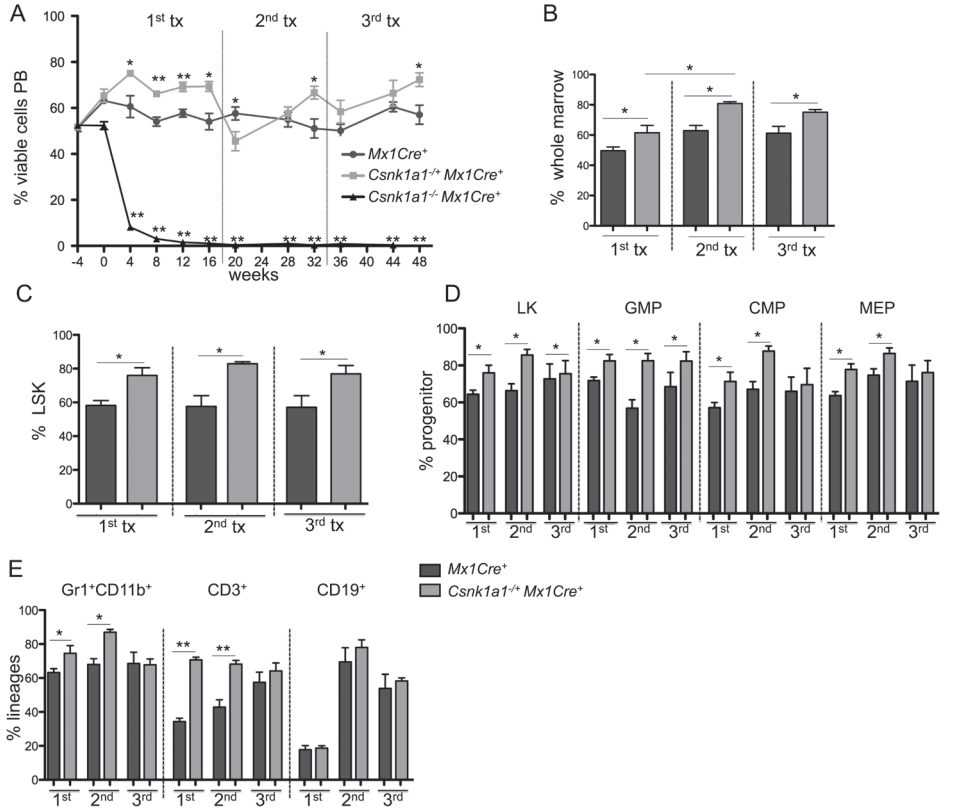

Figure 4: *Csnk1a1* haploinsufficient hematopoietic stem cells show increased repopulating ability consistent with increased self-renewal. (A) Identical numbers of *Csnk1a1*$^{-/+}$*Mx1Cre*$^{+}$ or *Csnk1a1*$^{-/-}$*Mx1Cre*$^{+}$ or *Mx1Cre*$^{+}$ controls were each mixed in equal ratios (approximately 50:50; time point -4 weeks) and transplanted in lethally irradiated CD45.1 recipients. Percentage of CD45.2 donor cell chimerism in the whole peripheral blood from peripheral blood of lethally irradiated recipient animals is shown. Time (weeks) denotes the time relative to termination of the poly(I:C) injections (poly(I:C)=timepoint 0). After 16 weeks, bone marrow was harvested and transplanted for secondary transplants, and 16 weeks later for tertiary transplants in lethally irradiated mice (mean±SD, n=5, *p<0.05; **p<0.001). (B) Donor chimerism of total bone marrow cells performed at 16 (first competitive transplant), 32 (secondary competitive transplant, 16 weeks after transplantation) or 48 (tertiary competitive transplant) weeks after poly(I:C) induction (mean±SD, n=5, *p<0.05). (C) Donor chimerism of the hematopoietic stem (LSK) and (D) progenitor cell compartment [lin^{low}Sca1^{-}ckit^{+}, LK; common-myeloid progenitors (CMP): LK CD34^{+}CD16/32^{-}; granulocyte-macrophage progenitors (GMP): LK CD34^{+}CD16/32^{+}; myeloerythroid progenitors (MEP): LK CD34^{-} CD16/32^{-}] performed at 16 (first competitive transplant) or 32 (secondary competitive transplant) or 48 (tertiary competitive transplant) weeks after poly(I:C) induction (mean±SD, n=5, *p<0.05). (E) Chimerism of hematopoietic lineages in the bone marrow each 16 weeks after the first, second and third competitive transplant. Composite data of donor (CD45.2^{+}) granulocytes (Gr1^{+}CD11b^{+}), B-cells (CD19^{+}) or T-cells (CD3^{+}) are shown (mean±SD, n=5, *p<0.05).

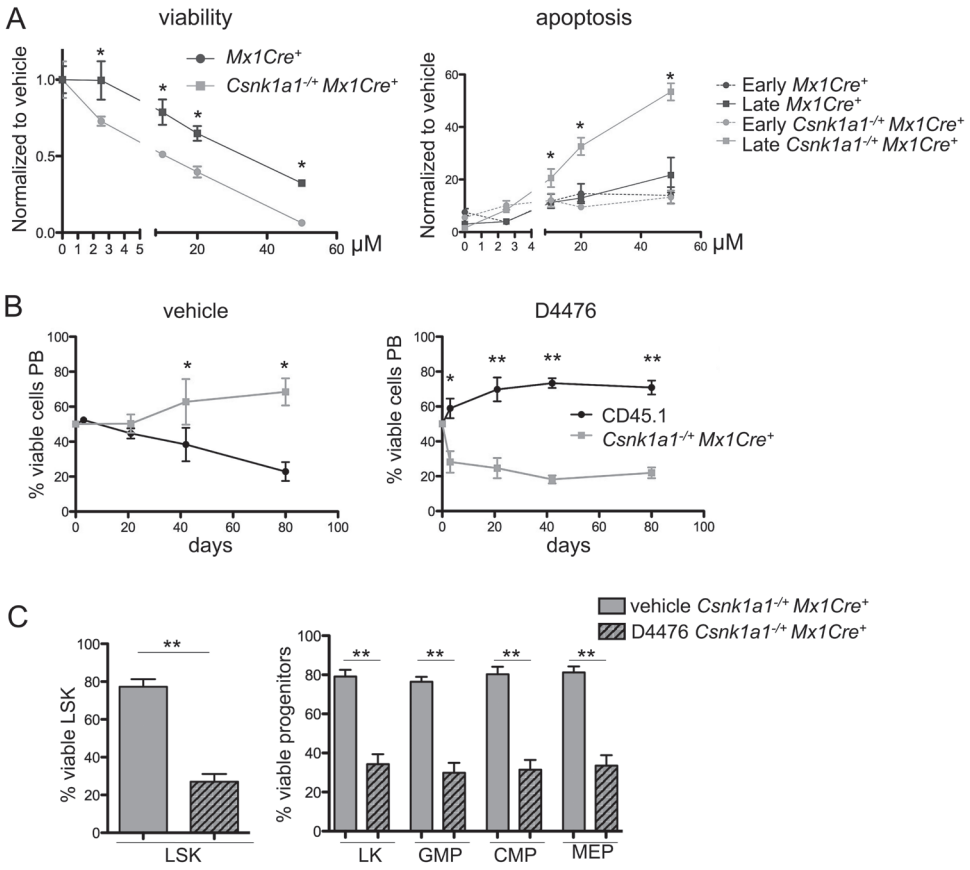

Figure 5: *Csnk1a1* haploinsufficiency provides a therapeutical window for the specific treatment of disease-propagating hematopoietic stem cells. (A) Sorted hematopoietic progenitor cells (LK) were pre-stimulated for 24 hours after the sort and treated for 72 hours with varying concentrations of D4476. Viability of cells was analyzed after 72 hours with the CellTitre glo assay, apoptosis by combined Annexin V and 7AAD staining discriminating early (Annexin V^+7AAD^-) and late apoptosis ($AnnexinV^+7AAD^+$) using flow cytometry. (B) 21 days after poly(I:C) treatment, *Csnk1a1*$^{-/+}$*Mx1Cre*$^+$ or CD45.1 bone marrow was harvested and LSK cells were sort-purified. Equal ratios of *Csnk1a1*$^{-/+}$*Mx1Cre*$^+$ and CD45.1$^+$ LSK were mixed and treated for 72 hours ex vivo with either D4476 or DMSO, followed by transplantation into lethally irradiated CD45.1 mice. The chimerism was followed over time in the peripheral blood (mean±SD, n=6, *p<0.05; **p<0.001). (C) The chimerism of *Csnk1a1*$^{-/+}$*Mx1Cre*$^+$ in the bone marrow was analyzed in the LSK and progenitor fractions after 12 weeks under DMSO or D4476 treatment conditions (mean±SD, n=6, **p<0.001). See also Figure S4.

To assess the relative effect of D4476 treatment on HSC and progenitor cell function in vivo, we performed a competitive repopulation experiment following ex vivo exposure to D4476. Purified LSK cells from *Csnk1a1*$^{-/+}$*Mx1Cre*$^{+}$ (CD45.2) and WT CD45.1 mice were mixed in a 1:1 ratio and treated ex vivo with either D4476 or DMSO control for 48 hours, followed by injection of the cells into lethally irradiated mice. Following DMSO treatment, *Csnk1a1* haploinsufficient cells out-competed the wild-type controls, as assessed by peripheral blood chimerism. In contrast, following treatment with D4476, *Csnk1a1* haploinsufficient cells were selectively depleted. Similarly, D4476 caused a selective depletion of *Csnk1a1* haploinsufficient stem and progenitor cells in the bone marrow (Figure 5B-C) and reduced *Csnk1a1* haploinsufficient hematopoietic stem and progenitor cells in colony-forming unit assays (Figure S4A).

To examine if partial, systemic inhibition of CK1α would be tolerated in a therapeutic approach targeting haploinsufficiency, we analyzed the effects of global heterozygous *Csnk1a1* inactivation. *Csnk1a1*$^{-/+}$*EIIaCre*$^{+}$ mice, in which heterozygous deletion of *Csnk1a1* is induced in all tissues, were born in normal Mendelian ratios without apparent malformations. Histopathological analysis at 6 and 10 months of age revealed structural integrity of organs, and blood counts were normal and stable over this period of time (Figure S4B-D). In aggregate, these data indicate that *Csnk1a1* inhibition is an attractive therapeutic approach for the selective targeting of *Csnk1a1* haploinsufficient cells, such as MDS cells with del(5q).

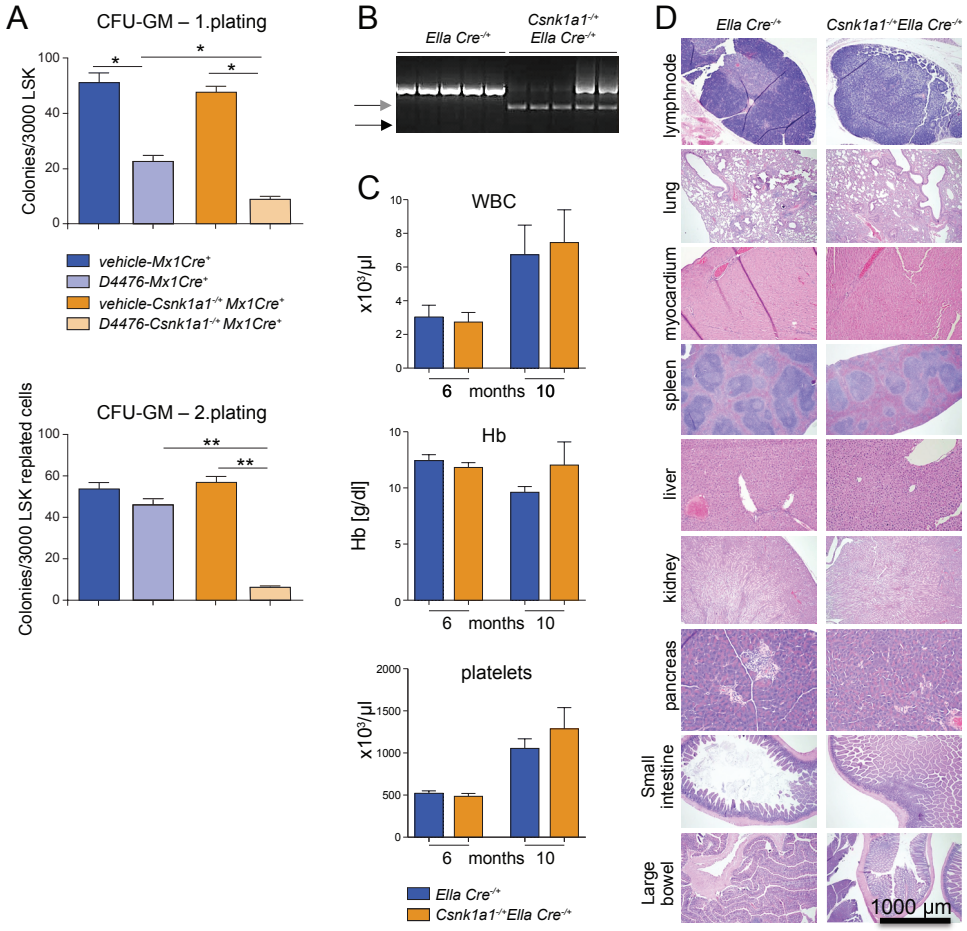

Figure S4: related to figure 5: *Csnk1a1* germline haploinsufficiency does not affect structural integrity of abdominal or thoracical organs

(A) Hematopoietic stem cells (LSK) were sorted from *Csnk1a1*$^{-/+}$*Mx1Cre*$^{+}$ and *Mx1Cre*$^{+}$ mice and subjected to 10 µM D4476 or vehicle. After 48 hours cells were harvested and methylcellulose assays were started with 3000 LSK each. After 8 days, cells were recovered from methylcellulose and re-plated on fresh methylcellulose. n=3 biological donors and 3 technical replicates. (mean±SD, n=9, *p<0.05). (B) Genomic DNA was isolated and the excision of the targeted exon 3 was validated by PCR in *Csnk1a1*$^{-/+}$*EIIaCre*$^{+}$ and *EIIaCre*$^{+}$ cells. (C) 6 and 10 months old *Csnk1a1*$^{-/+}$*EIIaCre*$^{+}$ mice do not differ in their peripheral blood counts from *EIIaCre*$^{+}$ mice (mean±SD, n=4, ns). (D) Histopathological comparison of lymph node, lung, myocardium, spleen, liver, kidney, pancreas, small intestine and large intestine in *Csnk1a1*$^{-/+}$*EIIaCre*$^{+}$ or *EIIaCre*$^{+}$ mice does not show any structural abnormalities or differences between the two groups. Scale bar as indicated.

Identification of recurrent somatic *CSNK1A1* mutations in patients with del(5q) MDS

In parallel with our functional studies, we performed whole-exome sequencing on MDS samples to identify genetic drivers of del(5q) MDS: genes that are selectively mutated in del(5q) MDS, or genes within the del(5q) CDRs that are recurrently somatically mutated in MDS cases without del(5q). We performed whole-exome sequencing on paired samples (MDS-derived bone marrow sample and matched normal $CD3^+$ cells) of 21 cases: 19 del(5q) and 2 with normal karyotypes. We identified two cases with somatic mutations in *CSNK1A1*, both in untreated cases with del(5q) with wild-type *TP53* (Table 1).

	#1	#2	#3
Age at diagnosis	85	82	65
Gender	M	F	F
FAB	RA	RA	RA
Karyotype	46,XY,del(5)(q13q31)[17]/46,XY[3]	46,XX,del(5)(q13q33)[14]/46,XX[6]	46,XX,del(5)(q13q33)[4]/46,XX[2]
IPSS-R	2, low risk	1, very low risk	1, very low risk
TP53	wild type	wild type	wild type
Hemoglobin [g/dL]	10.6	11.8	9.5
Absolute neutrophil count [10^9/l]	49.6	0.951	5.01
Platelets [cells/µl]	140,000	118,000	72,000

Table 1: Clinical data of patients with the identified somatic *CSNK1A1* mutations

Both mutations caused the same amino acid change, E98K (Figure 6A). The mutations were confirmed to be present and somatic by Sanger sequencing (Figure 6A).

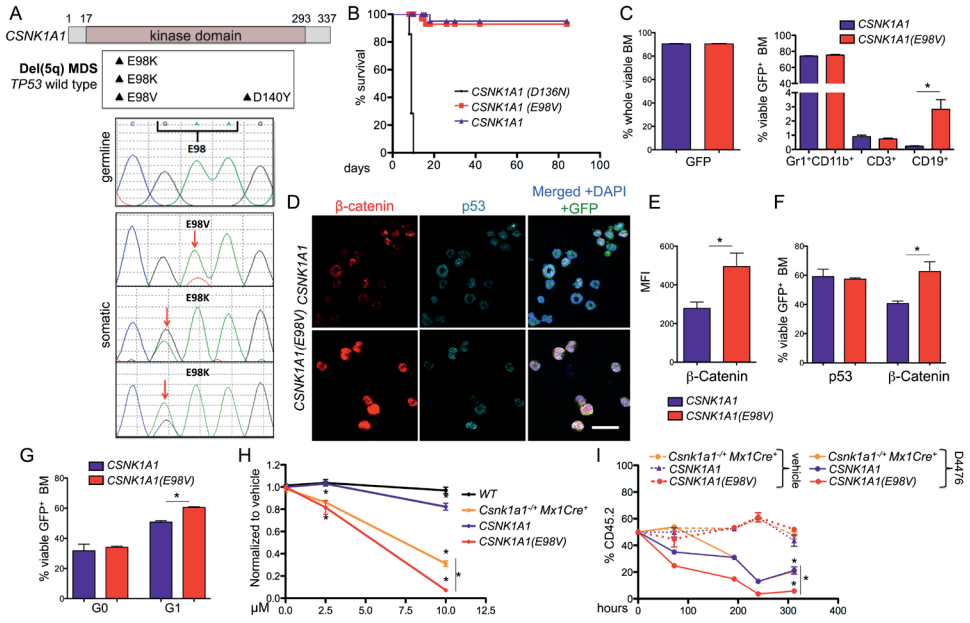

Figure 6: Identification and functional characterization of *CSNK1A1* mutations in del(5q) MDS patients

(A) Summary of *CSNK1A1* mutations identified in del(5q)MDS patients (upper panel). Sanger sequencing of the identified mutations on codon 98 (tumor/somatic) in comparison to germline controls (lower panel). (B) Kaplan-Meier survival analysis of chimeric mice transplanted with *Csnk1a1*$^{-/-}$*Mx1Cre*$^{+}$ hematopoietic stem and progenitor cells expressing *Csnk1a1* cDNA, *Csnk1a1* D136 cDNA or *Csnk1a1* E98V cDNA. Timepoint 0 is the first day of poly(I:C) induction (n=5). (C) GFP expression in whole BM (left) and distribution of the different lineages (Gr1^{+}CD11b^{+} neutrophils, CD3^{+} T-cells, CD19^{+} B-cells) in GFP^{+} BM cells (right). (mean±SD, n=3, *p<0.05). (D) Co-immunofluorescent staining of β-catenin and p53 in cytospin preparations of red blood cell lysed whole bone marrow cells (red: β-catenin, turquoise: p53, green: GFP MIG vector, blue: DAPI). Scale bar 20 μm. (E) Quantification of β-catenin intensity using the mean fluorescence intensity (MFI), (mean±SD, n=3, *p<0.05). (F) Intracellular flow cytometry measurement of β-catenin and p53 in permeabilized whole bone marrow cells. (mean±SD, n=3, *p<0.05). (G) Cell cycle was analyzed by combined Ki67 and Hoechst33342 staining in permeabilized whole bone marrow cells. (mean±SD, n=3, *p<0.05). (H) GFP^{+} LSK from mice transplanted with either *CSNK1A1* or *CSNK1A1* E98V-expressing *Csnk1a1*$^{-/-}$*Mx1Cre*$^{+}$ cells as well as *Csnk1a1* haploinsufficient LSK and WT LSK were sort purified and exposed to vehicle, 2.5 or 10 μM D4476 for 72 hours and viability of cells was analyzed after 72 hours with the CellTitre glo assay (mean±SD, n=5, *p<0.05). (I) LSK (all CD45.2) isolated as in (H) were treated in competition to CD45.1 wild type cells in one culture well to analyze selective ablation of cells under the same culture condition. (mean±SD, n=5, *p<0.05). See also Figure S5 and Table S1.

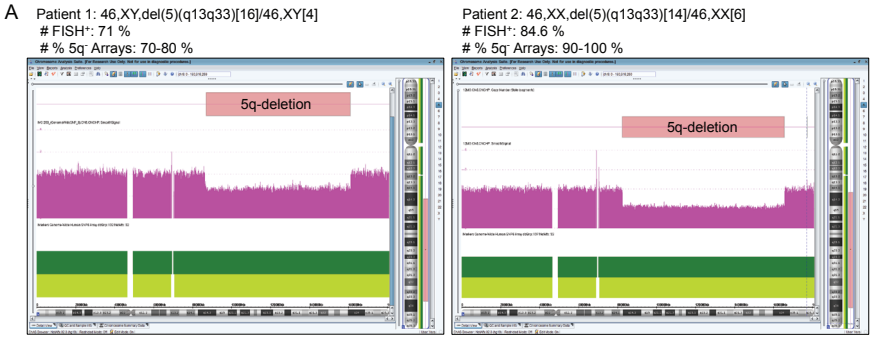

B

Position	Mutation (CDS)	Mutation (Amino Acid)	Mutation ID (COSM)	Count		reference	tissue
98	c.292G>A	p.E98K	COSM1241049	1	Substitution - Missense	Dulak	esophagus adenocarcinoma
98	c.293A>G	p.E98G	COSM1161523	1	Substitution - Missense		lymphoid neoplasm
140	c.418G>C	p.D140H	COSM1661311	1	Substitution - Missense	Sato et al., 2013	kidney
140	c.419A>C	p.D140A	COSM211577	1	Substitution - Missense	Graubert et al., 2012	MDS
136	c.406G>T	p.D136Y	COSM1064177	1	Substitution - Missense		endometrium

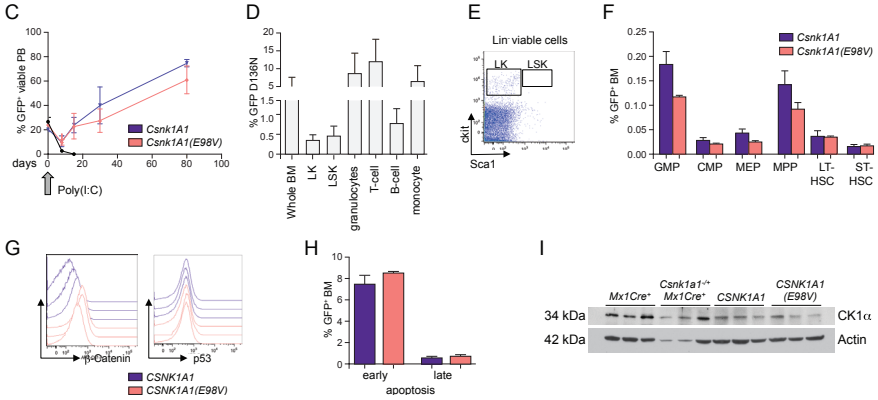

Figure S5: related to figure 6: The identified *CSNK1A1* mutation in del(5q) MDS patients occurs on the remaining allele of chromosome 5q and is not a loss of function mutation.

(A Single nucleotide polymorphism arrays (SNP-A) were performed with Genome-Wide Human SNP Array 6.0. The percentage of the 5q-deletion was 70-80 % in patient 1 and 90-100 % in patient 2. (B) Mutations of *CSNK1A1* in the same codon as in del(5q) MDS in other malignancies/tissues according to the catalogue of somatic mutations in cancer [*COSMIC, http://cancer.sanger.ac.uk; (Dulak et al., 2013; Graubert et al., 2012; Sato et al., 2013)]. Somatic missense mutations in *CSNK1A1* were identified in an adenocarcinoma of the esophagus (E98K), a Burkitt lymphoma (E98 V) and a renal clear cell carcinoma (D140H). (C) GFP expression in the peripheral blood over a period of 80 days [day 0= day of first poly(I:C) injection; mean±SD, n=5]. (D) Analysis of the *CSNK1A1*(D136N) (GFP) distribution in the bone marrow. (mean±SD, n=5). (E) Representative flow blot of the HSC compartment in mice transplanted with *Csnk1a1*$^{-/-}$*Mx1Cre*$^{+}$ hematopoietic cells overexpressing *CSNK1A1*(D136N). (F) The bone marrow of mice transplanted with *Csnk1a1*$^{-/-}$*Mx1Cre*$^{+}$ ckit^{+} hematopoietic stem and progenitor cells transduced with *CSNK1A1* cDNA or *CSNK1A1(*E98V) cDNA was analyzed 12 weeks after induction of the *Csnk1a1* excision by poly(I:C). Compound data show the distribution of the hematopoietic stem and progenitor cells in the GFP^{+} transduced bone marrow fraction (mean±SD, n=3, ns). (G) Histogram showing β-catenin and p53 expression in RBC lysed, GFP^{+} whole bone marrow cells. (H) Composite data of apoptosis detected by Annexin in GFP^{+} whole bone marrow cells (mean±SD, n=3, ns). (I) Western blots showing CK1α protein expression (Santa Cruz, Casein kinase 1a, C19) in *Mx1Cre*$^{+}$, *Csnk1a1*$^{-/+}$*Mx1Cre*$^{+}$ as well as transduced, transplanted and sorted *CSNK1A1* or *CSNK1A1(E98V)* expressing bone marrow cells in a *Csnk1a1*$^{-/-}$*Mx1Cre*$^{+}$ background [2 weeks after induction of poly(I:C); n=3 biological replicates].

Only a fraction (75% in patient 1 and 42% in patient 2) of the non-deleted *CSNK1A1* allele were mutated. By SNP array analysis (Figure S5A), the percentage of the del(5q) MDS clone was 70-80% in patient 1 and 90-100% in patient 2. These data indicate that deletion of chromosome 5q occurred first, and that the *CSNK1A1* mutation occurred on the remaining allele of chromosome 5q. The mutation was identified in only less than 5% of the matched control samples from T cells. We analyzed an additional set of 22 MDS samples with isolated del(5q) and found one additional mutation, also altering the same codon (E98V). We examined published MDS genome-sequencing data and found one *CSNK1A1* mutation, D140A, in a case with MDS and a normal karyotype (Graubert et al., 2012) and *CSNK1A1* D140Y in a patient with del(5q) MDS (Woll et al., 2014). Additional *CSNK1A1* mutations were identified in the literature in other malignancies (Dulak et al., 2013; Sato et al., 2013), two of which are also missense mutations of codon 98, and one of codon 140 (Figure S5B). *CSNK1A1* is therefore a gene with recurrent somatic mutations within a del(5q) CDR in MDS.

We tested the function of the *CSNK1A1 E98V* mutation by retroviral expression of the mutant cDNA in *Csnk1a1*$^{-/-}$*Mx1Cre*$^{+}$ hematopoietic cells, reflecting the finding of mutations in del(5q) cells without a wild-type allele. Ckit^{+} hematopoietic cells were transduced with retroviruses expressing a wild type *CSNK1A1* cDNA, the *CSNK1A1 E98V* mutation, or the *CSNK1A1 D136N* cDNA with mutational inactivation of the CK1α kinase activity (Bidere et al., 2009; Davidson et al., 2005; Peters et al., 1999). Four weeks after transplantation of transduced cells into lethally irradiated recipients, we induced excision of both endogenous *Csnk1a1* alleles. Mice transplanted with cells expressing the kinase-dead *CSNK1A1* D136N cDNA died rapidly as expected, as the mutant cDNA was unable to rescue the effect of the *Csnk1a1* ablation (Figure S5C-E). In contrast, cDNA overexpressing *CSNK1A1* and *CSNK1A1* E98V cDNA rescued the HSC ablation in *Csnk1a1*$^{-/-}$*Mx1Cre*$^{+}$ cells (Figure 6B and S5C). After 12 weeks, the bone marrow of the recipient mice was fully reconstituted by cells transduced with either *CSNK1A1* cDNA or *CSNK1A1 E98V* cDNA (Figure 6C). Cells expressing *CSNK1A1* or *CSNK1A1 E98V* reconstituted lineages, as well as stem and progenitor cells (Figures 6C and S5F).

We next examined the cellular consequences of the *CSNK1A1 E98V* mutation. *Csnk1a1*$^{-/-}$*Mx1Cre*$^{+}$ cells transduced with *CSNK1A1 E98V* cDNA, compared to cells expressing the wild-type cDNA, had increased nuclear β-catenin accumulation by immunofluorescence, and higher β-catenin accumulation by intracellular flow cytometry (Figure 6D-F and S5G). While expression of the kinase-dead *CSNK1A1 D136N* cDNA caused increased apoptosis and HSC ablation, the *CSNK1A1 E98V* cDNA did not induce p53 or apoptosis (Figure 6,D, F and S5G, H). Furthermore, bone marrow cells expressing *CSNK1A1 E98V* cDNA had an increased frequency of cells in the G1 phase of the cell cycle, with no change in cells in G0 (Figure 6G). In aggregate, these findings indicate that the codon 98 mutations are not loss-of-function, and do not cause increased p53 activation, but do increase β-catenin activity, providing a potential selective advantage to del(5q) MDS cells.

Having demonstrated that *Csnk1a1* haploinsufficient cells are sensitized to CK1 inhibition, we tested whether *CSNK1A1* E98V-expressing cells in a *Csnk1a1* null background are more sensitive to treatment with a CK1 inhibitor than wild-type or *Csnk1a1* haploinsufficient cells. GFP$^+$ *CSNK1A1* E98V and *CSNK1A1* expressing LSK cells and *Csnk1a1* haploinsufficient and wild-type LSK cells were sorted and treated with D4476 (Figure 6H). Treatment of *Csnk1a1*$^{-/-}$*Mx1Cre*$^+$ cells transduced with *CSNK1A1 E98V* cDNA were significantly more sensitive to the compound than *Csnk1a1* haploinsufficient cells. Similar results were obtained from a co-culture competition assay in the presence of D4476 (Figure 6I and S5I).

DISCUSSION

Our studies converged on a critical role for CK1α in the pathogenesis of del(5q) MDS. Activation of β-catenin downstream of *Csnk1a1* haploinsufficiency in a murine model, and downstream of *CSNK1A1* mutations in MDS patient samples, provides a potential mechanism of clonal selection. In contrast, homozygous inactivation of *Csnk1a1* is not tolerated due to activation of p53. The sensitivity of hematopoietic cells to *Csnk1a1* gene dosage provides a therapeutic window for targeting CK1α in haploinsufficient cells.

In a previous study, we found *Csnk1a1* to be a therapeutic target in AML, and that D4476 selectively kills leukemic stem cells relative to normal hematopoietic stem and progenitor cells (Jaras et al., 2014). Both the knockdown of *Csnk1a1* using shRNA and the genetically engineered mouse model show that reduction of *Csnk1a1* expression by more than 50% has a negative effect on hematopoietic stem cell expansion and survival. Haploinsufficiency, in contrast, increases the number and function of hematopoietic stem cells.

β-catenin is a major driver of stem cell self-renewal and neoplasia in multiple cellular lineages (Baba et al., 2005; Elyada et al., 2011; Willert et al., 2003; Yeung et al., 2010). Hematopoietic stem cells have a graded response to β-catenin, with modest levels leading to increased stem cell self-renewal (Baba et al., 2005), and more marked induction leading to stem cell exhaustion (Albuquerque et al., 2002; Kirstetter et al., 2006; Lane et al., 2010; Luis et al., 2011). Forced expression of β-catenin, in combination with HOXA9 and MEIS1, induces leukemia in progenitor cells (Wang et al., 2010b), and β-catenin is essential for leukemia cells driven by the MLL-AF9 oncogene (Miller et al., 2013). Histopathological studies have found nuclear, non-phosphorylated β-catenin expression in bone marrow specimen from de novo AML and MDS patients to be a predictor for clinical outcome, and these studies suggested an association between nuclear β-catenin expression and del(5q) MDS, though the number of samples studied was too small to be conclusive (Xu et al., 2008). CK1α is a member of the β-catenin destruction complex and is therefore a known, central regulator of β-catenin activity (Cheong and Virshup, 2011). In our studies, *Csnk1a1* haploinsufficiency conferred to increased intrinsic self-renewal of HSC, with associated nuclear β-catenin accumulation, cyclin D1 induction, and exit from quiescence in LT-HSCs.

Increased LT-HSC proliferation and expansion was a cell-intrinsic effect in our study. Inactivation of *Csnk1a1* in stromal cells in our model caused stromal β-catenin levels to increase, with consequent effects on hematopoiesis, including pancytopenia and hematopoietic stem and progenitor cell depletion. This observation is consistent with recent studies demonstrating that β-catenin accumulation in the stroma negatively regulates HSC maintenance and might also contribute to leukaemogenesis (Kode et al., 2014; Lane et al., 2010).

APC, another member of the β-catenin destruction complex, is also deleted in the vast majority of del(5q) MDS cases. Hematopoietic cells with *Apc* haploinsufficiency have

been shown to have enhanced repopulation potential, indicating a cell intrinsic gain of function in the LT-HSC population. However, in contrast to *Csnk1a1* haploinsufficiency, *Apc* haploinsufficient bone marrow was unable to repopulate secondary recipients due to loss of the quiescent HSC population (Lane et al., 2010; Wang et al., 2010a). Different levels of Wnt activation may explain these findings. Similarly, deletions of *Csnk1a1* and of *Apc* in the gut have significantly different effects. While *Csnk1a1* deletion led to robust activation of Wnt target genes and proliferation without invasion, *Apc* deletion induced immediate dysplastic transformation and rapid death (Elyada et al., 2011). CK1α has many phosphorylation targets that could alter stem cell function (Bidere et al., 2009; Elyada et al., 2011; Wu et al., 2012). As has been postulated previously, it is possible that CK1α inactivation restrains hyperactive Wnt signaling through mechanisms yet to be defined.

Our sequencing studies revealed recurrent mutations in a gene located in an MDS common deleted region on chromosome 5q. SNP array studies have not identified any genes on 5q that undergo homozygous deletion in del(5q) MDS (Gondek et al., 2008; Graubert et al., 2009; Heinrichs et al., 2009). Indeed, our studies would indicate that homozygous inactivation of *CSNK1A1* would be highly deleterious to a hematopoietic cell. Although *CSNK1A1* mutations in MDS are rare, they provide powerful evidence that these lesions are genetic drivers of clonal dominance. In functional studies, expression of the identified *CSNK1A1* E98V allele, in the setting of inactivation of both wild-type alleles to mimic the genetic context of the mutations observed in patients, caused an induction of nuclear β-catenin and a significant HSC cell cycle progression compared to expression of the wild-type *CSNK1A1*. Future experiments using a conditional knock-in mouse strain will be helpful to study the long-term hematopoietic effects of the mutant allele expressed at physiological levels.

Our results indicate that *CSNK1A1* is a CYCLOPS (copy number alteration yielding cancer liabilities owing to partial loss) gene (Nijhawan et al., 2012). Heterozygous inactivation of *Csnk1a1* sensitized cells to CK1 inhibition with D4476. The ablation of hematopoiesis in *Csnka1a1* null cells, and the normal to enhanced hematopoiesis in *Csnk1a1* haploinsufficient cells, provides a mechanistic basis for this therapeutic window. We demonstrated that systemic *Csnk1a1* haploinsufficiency in our murine model does not have significant effects on other organs, indicating that partial pharmacologic inhibition of CK1 would likely be well tolerated. While D4476 does not have pharmacokinetic properties for in vivo use, and lacks specificity for CK1α , a more selective compound has the potential for therapeutic utility in the treatment of patients with myeloid malignancies associated with del(5q).

EXPERIMENTAL PROCEDURES

Generation of a *Csnk1a1* conditional knockout mouse

Mouse embryonic stem (ES) cells with *Csnk1a1* exon 3 targeted in a C57BL/6N genetic background were generated by the KOMP consortium (project ID: CSD45494). The neomycin / lacZ cassette was flipped out in vitro by transfection of a plasmid expressing the flippase recombinase (FRT). Successful FRT recombination was validated by PCR (forward primer: 5'-TCGCACTTGAGCTATTGGGGAGT-3'; reverse primer: 5'-AGGCATGGTAGCTCACACCTGA-3'). Following confirmation of germline transmission, mice were crossed with the *Mx1-Cre* mouse strain (Jackson: 002527). To excise *Csnk1a1* exon 3, *Csnk1a1* conditional mice were given three rounds of 200 µg of poly(I:C) (GE Healthcare Life Sciences) using intraperitoneal injections. Successful excision of *Csnk1a1* exon 3 was validated using forward primer above and reverse 5´AGCTGGGCTACCAAGAGGCAA-3' primer. All experiments and procedures were conducted in the Children's Hospital Boston animal facility and were approved by the Children's Hospital Institutional Animal Care and Use Committee.

Flow cytometry

Bone marrow (BM) cells were isolated by flushing and crushing pelvis and hind leg bones with PBS (GIBCO) + 2% FBS + Penicillin/Streptomycin (GIBCO). Whole bone marrow was lysed on ice with red blood cell (RBC) lysis solution (Invitrogen/Life Technologies), and washed in PBS (GIBCO) + 2% FBS. Single-cell suspensions of spleen were prepared by pressing tissue through a cell strainer followed by red blood cell lysis. Cells were labeled with monoclonal antibodies in 2% FBS/PBS for 30 min on ice (see Supplemental Experimental Procedures for the information on antibodies used) and analyzed using an LSRII (BD biosciences). Apoptosis (Annexin V apoptosis detection kit, ebioscience) and cell cycle (Ki67 cell cycle and proliferation kit, BD biosciences) assays were performed according to the manufacturer's instructions.

Bone marrow transplantation assays

In transplantation assays of *Csnk1a1* cells into CD45.1 wild-type mice, $5x10^6$ freshly isolated whole bone marrow cells were harvested before poly(I:C) treatment, and injected into the tail-vein of lethally irradiated (1050 Rads) CD45.1-positive B6.SJL (Jackson) recipient mice without support cells. In competitive bone marrow transplantation studies, $2x10^6$ freshly isolated bone marrow cells were harvested and transplanted via tail vein into lethally irradiated $CD45.1^+$ recipient mice together with $2x10^6$ freshly isolated $CD45.1^+$ bone marrow competitor cells in an equal ratio. Four weeks after transplantation, blood samples were taken and donor cell chimerism was determined by flow cytometric analysis. Shortly thereafter, mice were given three rounds of poly(I:C) treatment and donor blood cell chimerism was determined every four weeks.

Western blots

Western blots were performed according to standard protocols. In brief, cell lysis was performed in RIPA buffer with protease/phosphatase inhibitors. After protein quantification, lysates were resuspended in Laemmli Sample Buffer, and loaded to gradient gels (Criterion Tris-HCl Gel, 8-16%). Proteins were transferred onto Immobilon polyvinyl difluoride (PVDF) membranes. As primary antibodies β-catenin (rabbit polyclonal, 9562, 1:500, Cell Signaling), p53 (mouse monoclonal, DO-1, 1:500, Santa Cruz), p21 (rabbit polyclonal, 1:200, C-19, Santa Cruz), Cycli n D1 (rabbit monoclonal, 1:200, SP4, Thermo Scientific) and GAPDH (rabbit polyclonal, 1:4000, Bethyl laboratories Inc) were applied.

Histopathology

For histological and immunohistochemical analyses, murine organs were fixed in 3.7% formaldehyde overnight, dehydrated and prepared for paraffin embedding. Hematoxylin-Eosin (H&E) staining was done according to routine protocols. For immunohistochemical stainings, the Avidin-Biotin Complex (ABC) was applied. Peripheral blood smears were stained with May-Grünwald-Giemsa (Sigma-Aldrich). Images were obtained on a Nikon Eclipse E400 microscope (Nikon, Tokyo, Japan) equipped with a SPOT RT color digital camera model 2.1.1 (Diagnostic Instruments).

Viral vector cloning

MIG-CSNK1A1, MIG-CSNK1A1(E98V) and MIG-CSNK1A1(D136N) were flanked by Not1 and Xho1 sites for convenient cloning into the MIG vector backbone.

Patient samples and Sequencing

Patients included in the whole exome sequencing were diagnosed between 2008 and 2013 at different Spanish hospitals affiliated to the MDS Spanish Group (*Grupo Español de SMD, GESMD*). Patients were diagnosed with MDS according to the French-American-British and 2008 World Health Organization classification. Samples were deidentified at the time of inclusion. This study was approved by institutional review boards (Clinical Research Ethics Committee Institut Català de la Salut/Germans Trias i Pujol Hospital and Clinical and Ethics Committee Parc de Salut MAR) and performed in accordance with the declaration of Helsinki. All patients gave their informed written consent. Whole-exome sequencing was performed using paired-end reads generated from DNA libraries prepared from MDS samples (whole bone marrow) with matched normal samples ($CD3^+$ lymphocytes isolated from peripheral blood). Whole-exome hybrid capture was carried out on 3 µg of genomic DNA, using the SureSelect Human Exome Kit version 3 (Agilent Technologies, Inc., Santa Clara, CA, USA). The captured exome library was sequenced with 100bp paired-end reads on an Illumina

HiSeq2000 platform (Illumina, San Diego, CA, USA). Whole-exome sequencing data were analyzed using an in-house bioinformatics pipeline as previously reported (BWA; GATK's; VarScan2; SAMTools; SnpEff: (Koboldt et al., 2012; McKenna et al., 2010). Somatic mutations identified as alterations present in tumor but not in the matched $CD3^+$ sample were validated by Sanger sequencing. Sanger sequencing was performed on genomic DNA isolated from whole bone marrow cells and $CD3^+$ cells using GentraPuregene Cell kit (Qiagen, Valencia, CA, USA). Exon 3 from *CSNK1A1* gene was amplified by polymerase chain reaction (PCR) using the following primers: forward primer: 5'-TCCTTTTGTTTCGTTAGGTGGT-3' and reverse primer 5'-AAGGTTAAATAGTGATGCACAGGA-3'; amplification size: 251 bp). Single nucleotide polymorphism array (SNP-A) were performed with Genome-Wide Human SNP Array 6.0 from Affymetrix. Assays were performed according to Affymetrix protocols.

Accession number

The Gene Expression Omnibus accession number for the SNP-arrays of patient 1 and 2 (with somatic mutations in *CSNK1A1*) is GSE59244.

Acknowledgements

We gratefully acknowledge the HSCI/Children's Hospital Boston (Mahnaz Paktinat and Ronald Mathieu) and Dana Farber Cancer Institute Flow Cytometry Core Facility (Suzan Lazo-Kallanian). We warm ly thank all members of the Ebert laboratory, in particular Damien Wilpitz, Brenton G. Mar and Jan Krönke, as well as Steven Lane (Queensland Institute of Medical Research, Brisbane, Australia), Dagmar Walter and Michael Milsom (HI-STEM, Heidelberg, Germany) for their insights, scientific discussion and collegiality. This work was supported by the NIH (R01HL082945), the Claudia Adams Barr Program, a Gabrielle's Angel Award, and a Leukemia and Lymphoma Society Scholar Award to B.L.E. R.K.S was supported by the German Research Foundation (DFG1188/3-1) and the Edward P. Evans Foundation. D.H. was supported by the German Cancer Aid. Whole-exome sequencing was supported in part by Instituto de Salud Carlos III, Ministerio de Sanidad y Consumo, Spain (PI 11/02010), by Red de Investigación Cooperativa en Cancer (RTICC, FEDER; RD12/0036/0044), 2014 SGR 225 GRE (Generalitat de Catalunya) and Celgene Spain. We sincerely acknowledge Lourdes Florensa, Leonor Arenillas, Maria Consuelo del Cañizo, Maria Diez-Campelo, Lurdes Zamora and Laura Palomo, for their implication on the project and selection of the patients and CNAG (Centro Nacional de Analisis Genomicos) for whole-exome sequencing studies.

Authorship Contributions: R.K.S, D.H., M.J. and B.L.E. designed experiments. R.K.S, D.H., A.M.L, L.P.C., M.E.M., A.M. and R.K. performed experiments and analyzed data. V.A., M.M., R.B. and F.S. collected patient samples and clinical information, performed whole exome sequencing, validation by Sanger sequencing and analyzed these data. R.K.S and B.L.E. wrote the manuscript. All authors provided critical review of the manuscript.

REFERENCES

Albuquerque, C., Breukel, C., van der Luijt, R., Fidalgo, P., Lage, P., Slors, F. J., Leitao, C. N., Fodde, R., and Smits, R. (2002). The ‚just-right' signaling model: APC somatic mutations are selected based on a specific level of activation of the beta-catenin signaling cascade. Human molecular genetics *11*, 1549-1560.

Baba, Y., Garrett, K. P., and Kincade, P. W. (2005). Constitutively active beta-catenin confers multilineage differentiation potential on lymphoid and myeloid progenitors. Immunity *23*, 599-609.

Bidere, N., Ngo, V. N., Lee, J., Collins, C., Zheng, L., Wan, F., Davis, R. E., Lenz, G., Anderson, D. E., Arnoult, D.*, et al.* (2009). Casein kinase 1alpha governs antigen-receptor-induced NF-kappaB activation and human lymphoma cell survival. Nature *458*, 92-96.

Boultwood, J., Pellagatti, A., Cattan, H., Lawrie, C. H., Giagounidis, A., Malcovati, L., Della Porta, M. G., Jadersten, M., Killick, S., Fidler, C.*, et al.* (2007). Gene expression profiling of CD34+ cells in patients with the 5q- syndrome. British journal of haematology *139*, 578-589.

Boultwood, J., Pellagatti, A., McKenzie, A. N., and Wainscoat, J. S. (2010). Advances in the 5q- syndrome. Blood *116*, 5803-5811.

Chen, T. H., Kambal, A., Krysiak, K., Walshauser, M. A., Raju, G., Tibbitts, J. F., and Walter, M. J. (2011). Knockdown of Hspa9, a del(5q31.2) gene, results in a decrease in hematopoietic progenitors in mice. Blood *117*, 1530-1539.

Cheong, J. K., and Virshup, D. M. (2011). Casein kinase 1: Complexity in the family. The international journal of biochemistry & cell biology *43*, 465-469.

Davidson, G., Wu, W., Shen, J., Bilic, J., Fenger, U., Stannek, P., Glinka, A., and Niehrs, C. (2005). Casein kinase 1 gamma couples Wnt receptor activation to cytoplasmic signal transduction. Nature *438*, 867-872.

Dulak, A. M., Stojanov, P., Peng, S., Lawrence, M. S., Fox, C., Stewart, C., Bandla, S., Imamura, Y., Schumacher, S. E., Shefler, E.*, et al.* (2013). Exome and whole-genome sequencing of esophageal adenocarcinoma identifies recurrent driver events and mutational complexity. Nature genetics *45*, 478-486.

Dutt, S., Narla, A., Lin, K., Mullally, A., Abayasekara, N., Megerdichian, C., Wilson, F. H., Currie, T., Khanna-Gupta, A., Berliner, N.*, et al.* (2011). Haploinsufficiency for ribosomal protein genes causes selective activation of p53 in human erythroid progenitor cells. Blood *117*, 2567-2576.

Ebert, B. L. (2011). Molecular dissection of the 5q deletion in myelodysplastic syndrome. Seminars in oncology *38*, 621-626.

Ebert, B. L., Pretz, J., Bosco, J., Chang, C. Y., Tamayo, P., Galili, N., Raza, A., Root, D. E., Attar, E., Ellis, S. R., and Golub, T. R. (2008). Identification of RPS14 as a 5q- syndrome gene by RNA interference screen. Nature *451*, 335-339.

Elyada, E., Pribluda, A., Goldstein, R. E., Morgenstern, Y., Brachya, G., Cojocaru, G., Snir-Alkalay, I., Burstain, I., Haffner-Krausz, R., Jung, S.*, et al.* (2011). CKIalpha ablation highlights a critical role for p53 in invasiveness control. Nature *470*, 409-413.

Gondek, L. P., Tiu, R., O'Keefe, C. L., Sekeres, M. A., Theil, K. S., and Maciejewski, J. P. (2008). Chromosomal lesions and uniparental disomy detected by SNP arrays in MDS, MDS/MPD, and MDS-derived AML. Blood *111*, 1534-1542.

Graubert, T. A., Payton, M. A., Shao, J., Walgren, R. A., Monahan, R. S., Frater, J. L., Walshauser, M. A., Martin, M. G., Kasai, Y., and Walter, M. J. (2009). Integrated genomic analysis implicates haploinsufficiency of multiple chromosome 5q31.2 genes in de novo myelodysplastic syndromes pathogenesis. PloS one *4*, e4583.

Graubert, T. A., Shen, D., Ding, L., Okeyo-Owuor, T., Lunn, C. L., Shao, J., Krysiak, K., Harris, C. C., Koboldt, D. C., Larson, D. E.*, et al.* (2012). Recurrent mutations in the U2AF1 splicing factor in myelodysplastic syndromes. Nature genetics *44*, 53-57.

Haase, D., Germing, U., Schanz, J., Pfeilstocker, M., Nosslinger, T., Hildebrandt, B., Kundgen, A., Lubbert, M., Kunzmann, R., Giagounidis, A. A*., et al.* (2007). New insights into the prognostic impact of the karyotype in MDS and correlation with subtypes: evidence from a core dataset of 2124 patients. Blood *110*, 4385-4395.

Hasserjian, R. P., LeBeau M.M.; List A.F.; Bennett J.M.; Thiele J (2008). Myelodysplastic syndrome with isolated del(5q). In WHO Classification of Tumours of Haematopoietic and Lymphoid Tissues, (World Health Organization Press: International Agency for Research on Cancer), p. 102.

Heinrichs, S., Kulkarni, R. V., Bueso-Ramos, C. E., Levine, R. L., Loh, M. L., Li, C., Neuberg, D., Kornblau, S. M., Issa, J. P., Gilliland, D. G*., et al.* (2009). Accurate detection of uniparental disomy and microdeletions by SNP array analysis in myelodysplastic syndromes with normal cytogenetics. Leukemia *23*, 1605-1613.

Jaras, M., Miller, P. G., Chu, L. P., Puram, R. V., Fink, E. C., Schneider, R. K., Al-Shahrour, F., Pena, P., Breyfogle, L. J., Hartwell, K. A*., et al.* (2014). Csnk1a1 inhibition has p53-dependent therapeutic efficacy in acute myeloid leukemia. The Journal of experimental medicine *211*, 605-612.

Jerez, A., Gondek, L. P., Jankowska, A. M., Makishima, H., Przychodzen, B., Tiu, R. V., O'Keefe, C. L., Mohamedali, A. M., Batista, D., Sekeres, M. A*., et al.* (2012). Topography, clinical, and genomic correlates of 5q myeloid malignancies revisited. Journal of clinical oncology : official journal of the American Society of Clinical Oncology *30*, 1343-1349.

Joslin, J. M., Fernald, A. A., Tennant, T. R., Davis, E. M., Kogan, S. C., Anastasi, J., Crispino, J. D., and Le Beau, M. M. (2007). Haploinsufficiency of EGR1, a candidate gene in the del(5q), leads to the development of myeloid disorders. Blood *110*, 719-726.

Kirstetter, P., Anderson, K., Porse, B. T., Jacobsen, S. E., and Nerlov, C. (2006). Activation of the canonical Wnt pathway leads to loss of hematopoietic stem cell repopulation and multilineage differentiation block. Nature immunology *7*, 1048-1056.

Koboldt, D. C., Zhang, Q., Larson, D. E., Shen, D., McLellan, M. D., Lin, L., Miller, C. A., Mardis, E. R., Ding, L., and Wilson, R. K. (2012). VarScan 2: somatic mutation and copy number alteration discovery in cancer by exome sequencing. Genome research *22*, 568-576.

Kode, A., Manavalan, J. S., Mosialou, I., Bhagat, G., Rathinam, C. V., Luo, N., Khiabanian, H., Lee, A., Murty, V. V., Friedman, R*., et al.* (2014). Leukaemogenesis induced by an activating beta-catenin mutation in osteoblasts. Nature *506*, 240-244.

Kumar, M. S., Narla, A., Nonami, A., Mullally, A., Dimitrova, N., Ball, B., McAuley, J. R., Poveromo, L., Kutok, J. L., Galili, N*., et al.* (2011). Coordinate loss of a microRNA and protein-coding gene cooperate in the pathogenesis of 5q- syndrome. Blood *118*, 4666-4673.

Lane, S. W., Sykes, S. M., Al-Shahrour, F., Shterental, S., Paktinat, M., Lo Celso, C., Jesneck, J. L., Ebert, B. L., Williams, D. A., and Gilliland, D. G. (2010). The Apc(min) mouse has altered hematopoietic stem cell function and provides a model for MPD/MDS. Blood *115*, 3489-3497.

Luis, T. C., Ichii, M., Brugman, M. H., Kincade, P., and Staal, F. J. (2012). Wnt signaling strength regulates normal hematopoiesis and its deregulation is involved in leukemia development. Leukemia *26*, 414-421.

Luis, T. C., Naber, B. A., Roozen, P. P., Brugman, M. H., de Haas, E. F., Ghazvini, M., Fibbe, W. E., van Dongen, J. J., Fodde, R., and Staal, F. J. (2011). Canonical wnt signaling regulates hematopoiesis in a dosage-dependent fashion. Cell stem cell *9*, 345-356.

Mallo, M., Del Rey, M., Ibanez, M., Calasanz, M. J., Arenillas, L., Larrayoz, M. J., Pedro, C., Jerez, A., Maciejewski, J., Costa, D*., et al.* (2013). Response to lenalidomide in myelodysplastic syndromes with del(5q): influence of cytogenetics and mutations. British journal of haematology *162*, 74-86.

McKenna, A., Hanna, M., Banks, E., Sivachenko, A., Cibulskis, K., Kernytsky, A., Garimella, K., Altshuler, D., Gabriel, S., Daly, M., and DePristo, M. A. (2010). The Genome Analysis Toolkit: a MapReduce framework for analyzing next-generation DNA sequencing data. Genome research *20*, 1297-1303.

Miller, P. G., Al-Shahrour, F., Hartwell, K. A., Chu, L. P., Jaras, M., Puram, R. V., Puissant, A., Callahan, K. P., Ashton, J., McConkey, M. E., *et al.* (2013). In Vivo RNAi screening identifies a leukemia-specific dependence on integrin beta 3 signaling. Cancer cell *24*, 45-58.

Min, I. M., Pietramaggiori, G., Kim, F. S., Passegue, E., Stevenson, K. E., and Wagers, A. J. (2008). The transcription factor EGR1 controls both the proliferation and localization of hematopoietic stem cells. Cell stem cell *2*, 380-391.

Nijhawan, D., Zack, T. I., Ren, Y., Strickland, M. R., Lamothe, R., Schumacher, S. E., Tsherniak, A., Besche, H. C., Rosenbluh, J., Shehata, S., *et al.* (2012). Cancer vulnerabilities unveiled by genomic loss. Cell *150*, 842-854.

Peters, J. M., McKay, R. M., McKay, J. P., and Graff, J. M. (1999). Casein kinase I transduces Wnt signals. Nature *401*, 345-350.

Rena, G., Bain, J., Elliott, M., and Cohen, P. (2004). D4476, a cell-permeant inhibitor of CK1, suppresses the site-specific phosphorylation and nuclear exclusion of FOXO1a. EMBO reports *5*, 60-65.

Sato, Y., Yoshizato, T., Shiraishi, Y., Maekawa, S., Okuno, Y., Kamura, T., Shimamura, T., Sato-Otsubo, A., Nagae, G., Suzuki, H., *et al.* (2013). Integrated molecular analysis of clear-cell renal cell carcinoma. Nature genetics *45*, 860-867.

Scheller, M., Huelsken, J., Rosenbauer, F., Taketo, M. M., Birchmeier, W., Tenen, D. G., and Leutz, A. (2006). Hematopoietic stem cell and multilineage defects generated by constitutive beta-catenin activation. Nature immunology *7*, 1037-1047.

Sinnberg, T., Menzel, M., Kaesler, S., Biedermann, T., Sauer, B., Nahnsen, S., Schwarz, M., Garbe, C., and Schittek, B. (2010). Suppression of casein kinase 1alpha in melanoma cells induces a switch in beta-catenin signaling to promote metastasis. Cancer research *70*, 6999-7009.

Starczynowski, D. T., Kuchenbauer, F., Argiropoulos, B., Sung, S., Morin, R., Muranyi, A., Hirst, M., Hogge, D., Marra, M., Wells, R. A., *et al.* (2010). Identification of miR-145 and miR-146a as mediators of the 5q- syndrome phenotype. Nature medicine *16*, 49-58.

Stoddart, A., Fernald, A. A., Wang, J., Davis, E. M., Karrison, T., Anastasi, J., and Le Beau, M. M. (2013). Haploinsufficiency of del(5q) genes, Egr1 and Apc, cooperate with Tp53 loss to induce acute myeloid leukemia in mice. Blood.

Trowbridge, J. J., Xenocostas, A., Moon, R. T., and Bhatia, M. (2006). Glycogen synthase kinase-3 is an in vivo regulator of hematopoietic stem cell repopulation. Nature medicine *12*, 89-98.

Walkley, C. R., Olsen, G. H., Dworkin, S., Fabb, S. A., Swann, J., McArthur, G. A., Westmoreland, S. V., Chambon, P., Scadden, D. T., and Purton, L. E. (2007). A microenvironment-induced myeloproliferative syndrome caused by retinoic acid receptor gamma deficiency. Cell *129*, 1097-1110.

Wang, J., Fernald, A. A., Anastasi, J., Le Beau, M. M., and Qian, Z. (2010a). Haploinsufficiency of Apc leads to ineffective hematopoiesis. Blood *115*, 3481-3488.

Wang, Y., Krivtsov, A. V., Sinha, A. U., North, T. E., Goessling, W., Feng, Z., Zon, L. I., and Armstrong, S. A. (2010b). The Wnt/beta-catenin pathway is required for the development of leukemia stem cells in AML. Science *327*, 1650-1653.

Willert, K., Brown, J. D., Danenberg, E., Duncan, A. W., Weissman, I. L., Reya, T., Yates, J. R., 3rd, and Nusse, R. (2003). Wnt proteins are lipid-modified and can act as stem cell growth factors. Nature *423*, 448-452.

Woll, P. S., Kjallquist, U., Chowdhury, O., Doolittle, H., Wedge, D. C., Thongjuea, S., Erlandsson, R., Ngara, M., Anderson, K., Deng, Q., *et al.* (2014). Myelodysplastic Syndromes Are Propagated by Rare and Distinct Human Cancer Stem Cells In Vivo. Cancer cell.

Wu, S., Chen, L., Becker, A., Schonbrunn, E., and Chen, J. (2012). Casein kinase 1alpha regulates an MDMX intramolecular interaction to stimulate p53 binding. Molecular and cellular biology *32*, 4821-4832.

Xu, J., Suzuki, M., Niwa, Y., Hiraga, J., Nagasaka, T., Ito, M., Nakamura, S., Tomita, A., Abe, A., Kiyoi, H*., et al.* (2008). Clinical significance of nuclear non-phosphorylated beta-catenin in acute myeloid leukaemia and myelodysplastic syndrome. British journal of haematology *140*, 394-401.

Yeung, J., Esposito, M. T., Gandillet, A., Zeisig, B. B., Griessinger, E., Bonnet, D., and So, C. W. (2010). beta-Catenin mediates the establishment and drug resistance of MLL leukemic stem cells. Cancer cell *18*, 606-618.

Zhu, H., Guo, Z. K., Jiang, X. X., Li, H., Wang, X. Y., Yao, H. Y., Zhang, Y., and Mao, N. (2010). A protocol for isolation and culture of mesenchymal stem cells from mouse compact bone. Nature protocols *5*, 550-560.

4

LENALIDOMIDE INDUCES UBIQUITINATION AND DEGRADATION OF CK1A IN DEL(5Q) MDS

Jan Krönke[1,2,3]*, Emma C. Fink[1,3]*, Kyle MacBeth[4], Slater N. Hurst[1], Namrata D. Udeshi[3], Philip P. Chamberlain[4], Anita Gandhi[4], D.R. Mani[3], Tanya Svinkina[3], Rebekka K. Schneider[1], Marie McConkey[1], Elizabeth Griffiths[5], Martin Carroll[6], Lars Bullinger[2], Brian E. Cathers[4], Steven A. Carr[3], Rajesh Chopra[4], Benjamin L. Ebert[1,3*]

[1] Brigham and Women's Hospital, Division of Hematology, Boston, Massachusetts, USA.
[2] University Hospital of Ulm, Department of Internal Medicine III, Ulm, Germany.
3 Broad Institute of MIT and Harvard, Cambridge, Massachusetts, USA.
4 Celgene Corporation, San Diego, California, USA.
5 Roswell Park Cancer Center, Buffalo, New York, USA.
6 University of Pennsylvania, Division of Hematology and Oncology, Philadelphia, Pennsylvania, USA.
* These authors contributed equally to this work.

Correspondence:
Benjamin L. Ebert
Brigham and Women's Hospital
1 Blackfan Circle – Karp CHRB 5.210
Boston, MA 02115
E-mail: bebert@partners.org

Nature. 2015 Jul 9;523(7559):183-8.

ABSTRACT

Lenalidomide is a highly effective treatment for myelodysplastic syndrome (MDS) with deletion of chromosome 5q (del(5q)). Here, we demonstrate that lenalidomide induces the ubiquitination of casein kinase 1A1 (CK1α) by the E3 ubiquitin ligase CUL4–RBX1–DDB1–CRBN (known as $CRL4^{CRBN}$), resulting in CK1α degradation. CK1α is encoded by a gene within the common deleted region for del(5q) MDS and haploinsufficient expression sensitizes cells to lenalidomide therapy, providing a mechanistic basis for the therapeutic window of lenalidomide in del(5q) MDS. We found that mouse cells are resistant to lenalidomide but that changing a single amino acid in mouse Crbn to the corresponding human residue enables lenalidomide-dependent degradation of CK1α. We further demonstrate that minor side chain modifications in thalidomide and a novel analogue, CC-122, can modulate the spectrum of substrates targeted by $CRL4^{CRBN}$. These findings have implications for the clinical activity of lenalidomide and related compounds, and demonstrate the therapeutic potential of novel modulators of E3 ubiquitin ligases.

Main

The immunomodulatory agents (IMiDs) lenalidomide, thalidomide, and pomalidomide are the first drugs identified that promote the ubiquitination and degradation of specific substrates by an E3 ubiquitin ligase. These compounds bind CRBN, the substrate adaptor for the CRBN-CRL4 E3 ubiquitin ligase, and modulate the substrate specificity of the enzyme. In lymphoid cells, IMiDs induce degradation of two transcription factors-- IKZF1 and IKZF3- leading to the dramatic clinical efficacy of these molecules in multiple myeloma and increasing interleukin-2 release from T-cells. It has not yet been determined whether degradation of distinct substrates may mediate additional activities in other cell types and whether all IMiDs have the same substrate specificity.

Lenalidomide is a highly effective treatment for myelodysplastic syndrome (MDS) with deletion of chromosome 5q (del(5q), inducing cytogenetic remission in more than 50% of patients.[5] No biallelic deletions or loss of function mutations on the remaining allele have been detected in any of the genes in the del(5q) common deleted region, implying that MDS with del(5q) is a disease of haploinsufficiency.[6] We hypothesized that ubiquitination of a distinct CRBN substrate explains the efficacy of lenalidomide in del(5q) MDS.

Lenalidomide induces ubiquitination and degradation of casein kinase 1A1

In order to identify lenalidomide-regulated CRBN-CRL4 substrates in myeloid cells, we applied stable isotope labeling of amino acids in cell culture (SILAC)-based quantitative mass spectrometry to assess global changes in ubiquitination and protein levels in the myeloid cell line KG-1 (Fig. 1a-b). Lenalidomide altered the ubiquitination and protein levels of strikingly few proteins, demonstrating the highly specific effects of this drug on ubiquitin

ligase function. Consistent with previous studies, lenalidomide treatment decreased ubiquitination of CRBN (p=0.026) and increased ubiquitination of IKZF1 (p=7.23 x 10^{-6} and p=4.97 x 10^{-4} for two distinct sites), with a reciprocal decrease in IKZF1 protein abundance (p=0.006)[1-3]

In addition to IKZF1, we detected increased ubiquitination (p=0.04) and decreased protein abundance (p=0.006) of casein kinase 1A1 (CSNK1A1, p=0.006) following treatment with 1 µM lenalidomide. The *CSNK1A1* gene is located in the del(5q) common deleted region and is expressed at haploinsufficient levels in del(5q) MDS.[6] Furthermore, CSNK1A1 has been implicated in the biology of del(5q) MDS and has been shown to be a therapeutic target in myeloid malignancies, so it is an attractive candidate for mediating the effects of lenalidomide in del(5q) MDS.[7]

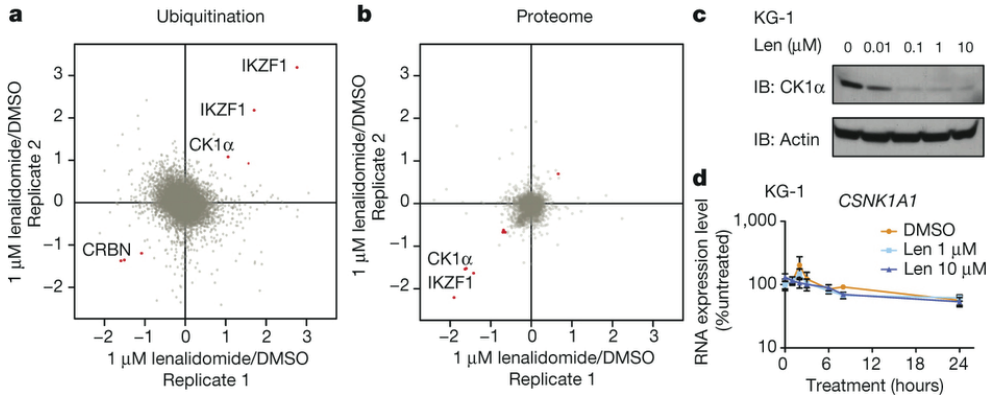

Figure 1: a, Log2 ratios for individual K-ε-GG sites of lenalidomide- (1 µM) versus DMSO-treated KG-1 cells for biological replicates 1 and 2. Each point represents a unique K-ε-GG site. Significantly regulated sites ($P < 0.05$) are red. **b**, Log2 ratios of protein abundance for lenalidomide- (1 µM) versus DMSO-treated KG-1 cells for biological replicates 1 and 2. Each point represents a unique protein group. Significantly regulated proteins ($P < 0.05$) are red. **c**, Effects of lenalidomide (Len) on endogenous CK1α protein levels in KG-1 cells after 24-h treatment. Data are representative of 5 independent experiments ($n = 5$). IB, immunoblot. **d**, *CSNK1A1* mRNA levels in KG-1 cells following lenalidomide treatment. Data are mean ± s.d., $n = 3$ biological replicates.

CSNK1A1 is a lenalidomide-dependent substrate of the CRBN-CRL4 E3 ubiquitin ligase

We next sought to determine whether CSNK1A1 is a lenalidomide-dependent substrate of the CRBN-CRL4 E3 ubiquitin ligase. We first confirmed that lenalidomide decreases CSNK1A1 protein levels in multiple human cell lines (Fig. 1c), as well as in primary AML cells obtained from the bone marrow of patients following a 6 day treatment with lenalidomide (Fig. 1d, Extended Data Fig 2). Lenalidomide decreased the half-life of the CSNK1A1 protein without altering *CSNK1A1* mRNA levels (Fig. 1e), consistent with a post-translational mechanism of regulation. The lenalidomide-dependent decrease in CSNK1A1 protein levels was abrogated by treatment with the proteasome inhibitor MG132 and the NEDD8-activating enzyme inhibitor MLN4924, which interferes with the activity of cullin-RING E3 ubiquitin ligases (Fig 2a). Homozygous genetic inactivation of the CRBN gene by CRISPR-Cas9 genome editing eliminated lenalidomide-dependent degradation of CSNK1A1 (Fig. 2B).

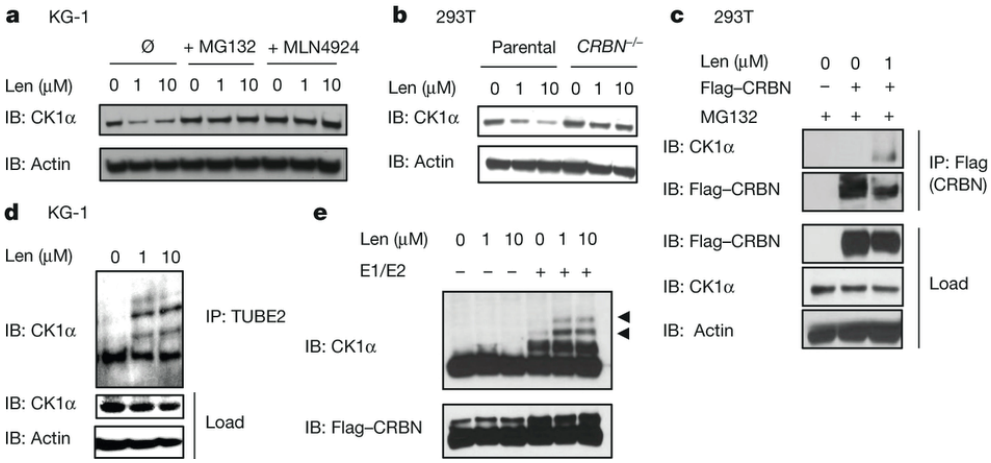

Figure 2: a, CK1α protein levels in KG-1 cells treated with DMSO or lenalidomide alone or in the presence of 10 μM MG132 or 1 μM MLN4924 for 6 hours. **b,** CK1α protein levels in CRBN knockout 293T cells treated with lenalidomide. **c,** Immunoprecipitation of FLAG-CRBN in 293T cells treated with DMSO or 1 μM lenalidomide in the presence of 1 μM MG132. **d,** Ubiquitination of endogenous CK1α in KG-1 cells treated with DMSO or lenalidomide analyzed by TUBE2 pull-down of ubiquitinated proteins followed by staining with a CK1α-specific antibody. Higher molecular weight bands represent ubiquitinated CK1α. **e,** Ubiquitination of CK1α by CRBN *in vitro* using lysine-free ubiquitin. Arrowheads indicate ubiquitinated CK1α. Results are representative of two (**a**, **b**, **d**, *n*=2) or three independent experiments (**c**, **e,** *n*=3).We next examined whether CSNK1A1 binds CRBN and is ubiquitinated by the CRBN-CRL4 E3 ubiquitin ligase. CSNK1A1 co-immunoprecipitated with FLAG-tagged CRBN (Fig. 2c) only in the presence of lenalidomide. Lenalidomide treatment increased the ubiquitination of FLAG-CSNK1A1 in 293T cells (Fig. 2d) and in the presence of CRBN *in vitro*, confirming that CSNK1A1 is a direct target of CRBN-CRL4 (Fig. 2e). Taken together, these experiments demonstrate that CSNK1A1 is a CRBN-CRL4 E3 ligase substrate that is ubiquitinated and degraded in the presence of lenalidomide.

We sought to identify a degron domain of CSNK1A1 that is required for lenalidomide-dependent degradation. Using a series of chimeric proteins of CSNK1A1 and a lenalidomide-insensitive homolog, CSNK1E, we identified a region in the N-terminus of CSNK1A1 that is essential for lenalidomide-induced degradation. Sequence alignment of this region with the previously delineated lenalidomide-responsive degron in IKZF1 and IKZF3[2] did not reveal any significant homology.

CSNK1A1 insufficiency sensitizes human cells to growth inhibition by lenalidomide

We next sought to explore the biological effects of CSNK1A1 depletion. CSNK1A1 is a serine/threonine kinase with multiple cellular activities, including negative regulation of the TP53 and β-catenin pathways.[8-10] In a conditional knockout of *Csnk1α1* in the murine hematopoietic system, homozygous inactivation induces apoptosis in normal and leukemic stem cells via tp53 activation,[7] while heterozygous loss of CSNK1A1 causes β-catenin accumulation and stem cell expansion.[7,11] Similarly, cells haploinsufficient for *Csnk1α1* preferentially undergo apoptosis in response to a nonselective casein kinase 1 inhibitor, D4476[12]. Based on these findings, and since del(5q) cells express about 50% of normal levels of *CSNK1A1* [6], we hypothesized that these cells would be more sensitive to further degradation of CSNK1A1 as compared to normal cells with two copies of the gene.

To evaluate whether decreased *CSNK1A1* expression sensitizes cells to lenalidomide, we transduced primary human $CD34^+$ hematopoietic stem and progenitor cells with GFP-tagged lentiviral vectors expressing *CSNK1A1* or control shRNAs. Cells expressing *CSNK1A1* shRNAs were depleted in the absence of treatment, demonstrating that low levels of CSNK1A1 inhibit the growth of hematopoietic cells (Fig. 3a). Treatment with lenalidomide enhanced the depletion of cells expressing *CSNK1A1* shRNAs relative to cells expressing control shRNAs, demonstrating that reduced CSNK1A1 levels sensitize hematopoietic cells to lenalidomide.

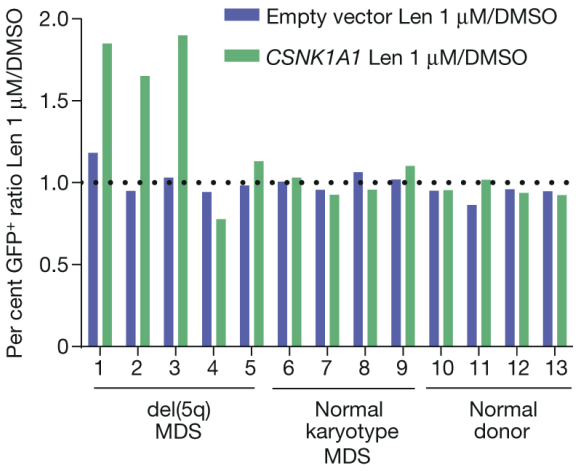

Figure 3: Ectopic *CSNK1A1* overexpression reduces lenalidomide sensitivity in primary MDS del(5q) cells
CD34+ cells derived from patient or control bone marrow were transduced with a lentiviral vector overexpressing *CSNK1A1* and *GFP* or an empty control vector and treated with DMSO or 1 μM lenalidomide. Results are reported as a ratio of the percentage of GFP+ cells in the lenalidomide condition to the percentage of GFP+ cells in the DMSO condition after 5 days of treatment. A ratio greater than 1 for the *CSNK1A1* vector but not for the empty vector indicates that *CSNK1A1* expression reduces lenalidomide sensitivity.
We next evaluated whether overexpression of *CSNK1A1* in del(5q) MDS could rescue sensitivity of these cells to lenalidomide treatment. We obtained samples from MDS patients with large heterozygous deletions of chromosome 5q, including heterozygous deletion of *CSNK1A1*, obtained prior to treatment with lenalidomide. We isolated CD34+ cells from the MDS patients and transduced the cells with a lentivirus expressing GFP and a *CSNK1A1* cDNA. Forced expression of *CSNK1A1* conferred resistance to lenalidomide in cells isolated from del(5q) MDS patients, but not in cells from MDS patients with a normal karyotype or normal adult CD34+ cells (Fig 3b, Extended Data Table 1). Therefore, although the del(5q) cells were haploinsufficient for a large number of genes, expression of *CSNK1A1* alone was sufficient to confer lenalidomide resistance.

Non-conserved amino acids in Crbn abolish lenalidomide activity in murine cells

We next sought to determine whether haploinsufficiency for *Csnk1a1* sensitizes cells to lenalidomide treatment using a *Csnk1a1* conditional knockout mouse model. In initial experiments, we found that lenalidomide did not decrease Csnk1a1 protein levels in murine Ba/F3 cells or primary murine leukemia cells. Consistent with this finding, mice do not develop the limb malformations observed in human embryos exposed to thalidomide[13] and primary murine multiple myeloma does not respond to lenalidomide[14], suggesting that murine cells are intrinsically resistant to IMiDs. Since CRBN is the direct protein target of lenalidomide, we examined whether expression of human CRBN could confer lenalidomide sensitivity to murine cells. Overexpression of human but not murine CRBN in murine Ba/F3 cells resulted in a lenalidomide-dependent decrease of CSNK1A1 protein levels, implying that amino acid differences between murine CRBN (mCRBN) and human CBRN (hCRBN) are responsible for the species-specific response to lenalidomide (Fig. 4a,b).

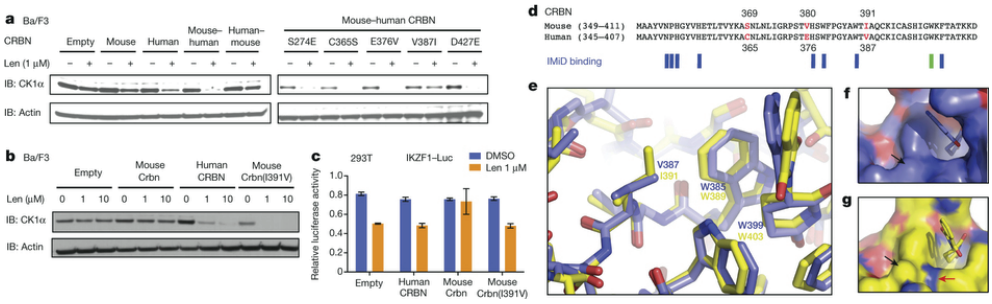

Figure 4: Amino acid changes in CRBN explain species-specific lenalidomide effects
a, Effect of the expression of human CRBN (h), mouse Crbn (m), chimeras of human and mouse CRBN (m-h and h-m, breakpoint at residue 221 (human) / 225 (mouse)) and variants of the m-h chimera where single amino-acids in the C-terminus were mutated to their corresponding mouse residue on lenalidomide-dependent CK1α degradation in mouse Ba/F3 cells. **b,** Expression of mouse *CrbnI391V* restores lenalidomide-dependent CK1α degradation in mouse Ba/F3 cells. **c,** Effect of hCRBN, mCrbn and mCrbnI391V on lenalidomide sensitivity of an IKZF1-luciferase fusion protein expressed in human 293T cells. Data are mean ± s.e.m. (*n*=3 biological replicates). **d,** Alignment of human and mouse CRBN IMiD binding region. Non-conserved amino acids are red. Amino acids involved in IMiD binding are indicated by blue bars. Mouse W403 is indicated with a green bar. **e,** Superposition of the IMiD binding domains of human CRBN (blue, PDB accession 4TZ4) and mouse Crbn (yellow, PDB accession 4TZC). Residues are labeled according to human isoform 2 (blue numbers) and mouse isoform 2 (yellow numbers). **f,** The V387 residue is indicated on the surface of human CRBN with a black arrow. **g,** The corresponding mouse residue, I391, is indicated on the surface of mouse Crbn with a black arrow. Mouse W403 is indicated by a red arrow. Results are representative of 3 (**a**, **b**, **c**) independent experiments.

In order to identify the amino acids responsible for this difference, we tested a series of human/mouse CRBN chimeric cDNAs for their ability to confer lenalidomide-induced CSNK1A1 degradation in murine Ba/F3 cells (Fig. 4a). We found that lenalidomide sensitivity was determined by the C-terminal half of CRBN, which contains only 5 non-conserved amino acids between human and mouse. Substitution of these positions in human CRBN with the corresponding amino acid in murine CRBN revealed only one substitution, V387I (human CRBN isoform 2), that disrupted the lenalidomide-responsiveness of human CRBN (Fig. 4a). Remarkably, substitution of the isoleucine at this position in murine CRBN for the human valine (mCRBN^{I391V}) was sufficient to confer lenalidomide-induced CSNK1A1 degradation in murine cells (Fig. 4b). Similar effects of these two point mutants were observed on lenalidomide-induced degradation of IKZF3 in human 293T cells (Fig. 4c), suggesting that a single amino acid change in CRBN determines lenalidomide-responsiveness for multiple substrates.

We modeled the effects of this murine-human amino acid substitution based on recently published crystal structures of the CRBN-DDB1-IMiD complex[15,16]. V387 of human CRBN (equivalent to I391 of murine CRBN) is located in the IMiD binding region of CRBN, but does not directly interact with lenalidomide (Fig. 4d). To investigate how the substitution of isoleucine for valine in murine CRBN confers lenalidomide-responsiveness, we superimposed

the structures for the murine and human IMiD-binding regions bound to lenalidomide as solved in Chamberlain et al. (2014). There are no backbone changes present at the site of the valine-isoleucine species differences (Fig. 4e), but the isoleucine residue is well-defined and oriented towards the indole NH moiety of W403 in the murine structure (Fig. 4g,h). The increase in steric bulk and rigid position of the isoleucine side-chain relative to the valine side-chain results in a bulge in the solvent accessible surface in the murine protein adjacent to both W403 and lenalidomide (Fig. 4f,). It has been proposed that IMiD binding produces a hotspot for local interactions by placement of the hydrophobic phthalimide or isoindolinone ring in an environment of potential hydrogen bond donors and acceptors from the surface of CRBN.[16] In this case, the larger side chain of the isoleucine residue found in rodents may sterically clash with substrate proteins such as IKZF1 and CSNK1A1 , blocking access to key hydrogen bonds from CRBN, such as from the indole NH from tryprophan 403 (human numbering). Steric clash with substrate proteins provides one potential explanation of why IMiDs bind murine CRBN[1] but do not promote degradation of IKZF1 and CSNK1A1.

Having determined the mechanism of lenalidomide resistance in mouse cells, we expressed the *mCrbnI391V* cDNA in hematopoietic cells from *Csnk1a1* conditional knockout mice to determine the effects of *Csnk1a1* haploinsufficiency on lenalidomide sensitivity. We isolated CD45.2+ c-Kit+ hematopoietic stem and progenitor cells from *Csnk1a1*+/−*Mx1Cre*+ and *Mx1Cre+* control littermates treated with poly (I:C) to induce gene excision in hematopoietic cells. We transduced these cells with a retroviral vector expressing *mCrbnI391V*, and cultured them in competition with similarly transduced isogenic CD45.1 c-Kit+ cells in the presence or absence of lenalidomide (Fig. 5a). Lenalidomide had no effect on control cells, but *Csnk1a1*+/−*Mx1Cre*+ cells were significantly depleted in the presence of lenalidomide (Fig. 5b). The enhanced sensitivity of *Csnk1a1*+/−*Mx1Cre*+ cells to lenalidomide was associated with induction of the p53 target gene *p21* (Fig. 5c) and increased levels of apoptosis (Fig. 5d), and was rescued by heterozygous deletion of *Trp53* (Fig. 5b), demonstrating a critical downstream role for the p53 pathway. These results are consistent with the clinical observation that *TP53* mutations confer lenalidomide resistance in MDS with del(5q).

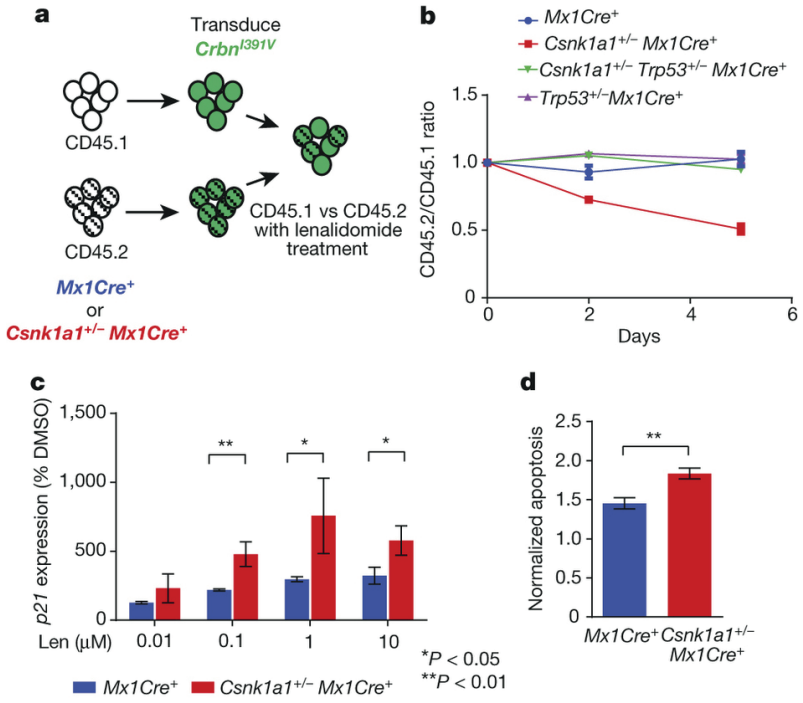

Figure 5: Effects of lenalidomide treatment on *Csnk1a1+/–* mouse hematopoietic cells

a, *Csnk1a1+/–Mx1Cre+* or *Mx1Cre+* c-Kit+ hematopoietic stem and progenitor cells (CD45.2) and competitor cells (CD45.1) were transduced with *mCrbnI391V*, mixed in equal ratios, and treated with lenalidomide or DMSO. The relative percentage of CD45.1+ and CD45.2+ cells was followed by flow cytometry over 5 days. **b,** Effects of 0.1 μM lenalidomide on the chimerism of *Csnk1a1+/– Mx1Cre+*, *Csnk1a1+/– Trp53+/– Mx1Cre+*, *Trp53+/– Mx1Cre+*, or *Mx1Cre+* cells (CD45.2) transduced with *mCrbnI391V* in comparison to CD45.1 competitor cells. Data are shown as mean ± s.e.m, *n*=3 biological replicates. **c,** Quantitative RT-PCR analysis of *p21* expression in *Csnk1a1+/–* or control cells transduced with *mCrbnI391V* and treated with DMSO or lenalidomide. Data are normalized to DMSO and shown as mean ± s.d, *n*=3 biological replicates. **d,** Ratio of CD45.2+ cells and CD45.1+ cells in late apoptosis (Annexin V+ DAPI+) after transduction with *mCrbnI391V* and four day treatment with 0.1 μM lenalidomide. CD45.2+ cells are either *Csnk1a1+/– Mx1Cre+* or *Mx1Cre+*. Data are normalized to DMSO treatment. Data are mean ± s.e.m, *n*=4 biological replicates. Results for **b**, **c**, and **d** are representative of three independent experiments with *hCRBN* or *mCrbnI391V*. *P*-values are from an unpaired two-sided *t*-test.

Differential degradation of CSNK1A1 by lenalidomide and other IMiDs

Thalidomide, lenalidomide, and pomalidomide target IKZF1 and IKZF3 for ubiquitination and degradation and are active in multiple myeloma, but only lenalidomide has been shown to be clinically effective in del(5q) MDS.[2] We therefore asked whether IMiDs induce degradation of the same substrates. We used tandem mass tag (TMT) quantitative proteomics in the MDS-L cell line to compare the activities of lenalidomide and CC-122, a third generation IMiD that also has a glutarimide ring and that has entered clinical trials (Fig. 6a). As expected, treatment with lenalidomide significantly decreased expression of both IKZF1 and CSNK1A1. In striking contrast, treatment with 1 μM CC-122 caused an even greater decrease in IKZF1 (log_2 fold change= -3.121, p=2.77 x 10^{-10}, 72 hours) than 10 μM lenalidomide (log_2 fold change= -2.406 p=2.10 x 10^{-8}, 72 hours), but had no effect on CSNK1A1 protein levels (log_2 fold change= -0.082, p>0.05)(Fig. 6b).

We confirmed the TMT mass spectrometry findings by western blot for IKZF1 and CSNK1A1 in KG-1 and MDS-L cells (Fig. 6c). While all IMiDs induced degradation of IKZF1 with a potency reflecting their clinical activity in multiple myeloma, thalidomide and CC-122 did not affect CSNK1A1 protein levels even at high concentrations. Although pomalidomide has a higher potency than lenalidomide in inducing the degradation of IKZF1 and IKZF3, it was less efficient in decreasing CSNK1A1 protein levels than lenalidomide, suggesting that the addition of single carbonyl group can affect substrate preference (Fig. 6a,c) Furthermore, treatment with excess CC-122 abrogated the lenalidomide-induced degradation of CSNK1A1, demonstrating that lenalidomide and CC-122 compete for the same binding site on CRBN (Fig. 6d) These experiments demonstrate that CSNK1A1 is specifically targeted by lenalidomide, indicating that lenalidomide may indeed be the best IMiD for the treatment of del(5q) MDS (Fig. 6e).

Intriguingly, lenalidomide, but not thalidomide and pomalidomide, was reported to induce the formation of two β-strands composed of CRBN residues 346-363.[16] Although conformational changes are difficult to interpret from structural data, the formation of these β-strands is expected to make significant changes in the surface of CRBN near the IMiD binding site[16] and thus it may contribute to the differential recruitment of IKZF1 and CSNK1A1. The interaction of specific IMiDs with particular substrates is therefore be governed by unique structural determinants, revealing the biological and clinical potential for members of this class of drugs to induce degradation of distinct sets of proteins.

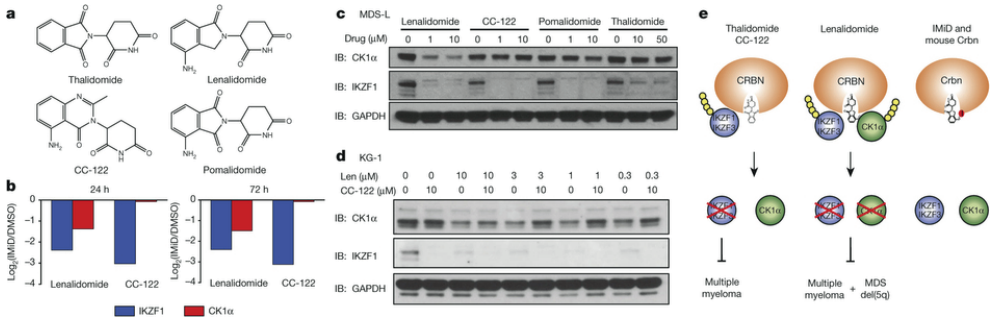

Figure 6: Substrate specificity of thalidomide analogues

a, Structures of thalidomide, lenalidomide, pomalidomide and CC-122. **b,** Protein levels of IKZF1 and CK1α assessed by tandem mass tag quantitative proteomics in MDS-L cells treated with DMSO, 10 μM lenalidomide, or 1 μM CC-122 for 24 hours (left panel) or 72 hours (right panel). *n*=3 (drug treatment) or *n*=4 (DMSO). **c,** Western blot analysis of CK1α and IKZF1 protein levels in MDS-L cells treated with DMSO or different concentrations of thalidomide, lenalidomide, pomalidomide, or CC-122. Results are representative of two independent experiments (*n*=2). **d,** KG-1 cells were treated with DMSO or lenalidomide in the absence or presence of different concentrations of CC-122. Results are representative of five independent experiments in various cell lines. **e,** Schematic presentation of the interaction of different thalidomide analogues with CRBN, substrates, and therapeutic indications.

DISCUSSION

We demonstrate that lenalidomide targets CSNK1A1 for degradation in myeloid cells, and that heterozygous deletion of *CSNK1A1* in del(5q) MDS provides a therapeutic window for selective targeting of the malignant cells by lenalidomide. The concept that genes within heterozygous deletions could cause vulnerabilities in cancer cells was first proposed 20 years ago[18] and has been more recently demonstrated as CYCLOPS genes (cancer vulnerabilities unveiled by genomic loss) in cell lines.[19] In del(5q) MDS, loss of *CSNK1A1* induces TP53 activity. Deletion of contiguous genes on chromosome 5q, such as *RPS14*, may further sensitize del(5q) cells to TP53 activation.[20,21] This mechanism of activity is consistent with the acquisition of TP53 mutations in del(5q) MDS patients who develop resistance to lenalidomide. Degradation of CSNK1A1 may also contribute to other clinical effects of lenalidomide such as myelosuppression and the activity of lenalidomide in the activated B-cell (ABC) subtype of diffuse large B-cell lymphoma[22].

Lenalidomide, like thalidomide and pomalidomide, binds CRBN and induces degradation of specific substrates. We found that a single amino acid difference between murine and human CRBN renders murine cells insensitive to IMiDs. This discovery enabled us to demonstrate, using a genetically engineered murine model, that *Csnk1a1* haploinsufficiency sensitizes cells to lenalidomide. This single amino acid change may also explain why thalidomide does not cause teratogenicity in mice and was approved for use in pregnant women, leading to the birth of more than 10,000 newborns with limb malformations and other disabilities.

Thalidomide, lenalidomide, and pomalidomide all induce CRBN-CRL4-mediated degradation of IKZF1 and IKZF3, but the subtle differences between these molecules cause dramatic changes in potency. We now find that thalidomide and a novel compound, CC-122, induce the degradation of IKZF1 and IKZF3 but not CSNK1A1. Since CSNK1A1 may also be involved in causing side effects like myelosuppression, CC-122 may be more specific in the treatment of multiple myeloma and other diseases that depend on IKZF1 and IKZF3, but would not be predicted to have activity in del(5q) MDS. CC-122, like the other IMiDs, has a glutarimide ring that anchors the molecule in CRBN, and structural variation in the remainder of the molecule is thought to determine substrate specificity.[15,16] These findings provide evidence that novel thalidomide-related molecules may have distinct biological activities, mediated by degradation of distinct sets of substrates, and that these IMiDs will be the first in a larger class of drugs with therapeutic utility through the targeting of specific proteins for degradation.

Author contributions:

J.K., E.C.F., and B.L.E. initiated the project. J.K., E.C.F., S.N.H., K.M. and A.G. designed and performed cell experiments and protein analysis. E.C.F., R.K.S., M.M. and M.C. performed mouse competition experiments. N.D.U., D.R.M., and T.S. performed KG-1 proteomics and analysis. E.G. and M.C. provided patient samples. P.P.C. performed the structural analysis. K.M. provided MDS-L proteomics. B.E.C., R.C., L.B., S.A.C., and B.L.E. supervised the work. J.K., E.C.F., and B.L.E. wrote the manuscript. All authors assisted in editing the manuscript.

Acknowledgments:

We thank Dirk Heckl for cloning of the EGI vector and technical advice and Ronald Mathieu and Mahnaz Paktinat for help with FACS sorting. E.C.F. was supported by award T32GM007753 from the National Institute of General Medical Sciences. The content is solely the responsibility of the authors and does not necessarily represent the official views of the National Institute of General Medical Sciences or the National Institutes of Health. J.K. was supported by the Deutsche Forschungsgemeinschaft (Kr3886/1-1 and 2-1, SFB1074) and the Else-Kröner Foundation.

REFERENCES:

1 Ito, T. *et al.* Identification of a primary target of thalidomide teratogenicity. *Science* **327**, 1345-1350, doi:327/5971/1345 [pii] 10.1126/science.1177319 (2010).

2 Krönke, J. *et al.* Lenalidomide causes selective degradation of IKZF1 and IKZF3 in multiple myeloma cells. *Science* **343**, 301-305, doi:10.1126/science.1244851 (2014).

3 Lu, G. *et al.* The myeloma drug lenalidomide promotes the cereblon-dependent destruction of Ikaros proteins. *Science* **343**, 305-309, doi:10.1126/science.1244917 (2014).

4 Gandhi, A. K. *et al.* Immunomodulatory agents lenalidomide and pomalidomide co-stimulate T cells by inducing degradation of T cell repressors Ikaros and Aiolos via modulation of the E3 ubiquitin ligase complex CRL4(CRBN.). *Br J Haematol* **164**, 811-821, doi:10.1111/bjh.12708 (2014).

5 List, A. *et al.* Efficacy of lenalidomide in myelodysplastic syndromes. *N Engl J Med* **352**, 549-557, doi:352/6/549 [pii] 10.1056/NEJMoa041668 (2005).

6 Boultwood, J. *et al.* Narrowing and genomic annotation of the commonly deleted region of the 5q- syndrome. *Blood* **99**, 4638-4641 (2002).

7 Jaras, M. *et al.* Csnk1a1 inhibition has p53-dependent therapeutic efficacy in acute myeloid leukemia. *J Exp Med* **211**, 605-612, doi:10.1084/jem.20131033 (2014).

8 Huart, A. S., MacLaine, N. J., Meek, D. W. & Hupp, T. R. CK1alpha plays a central role in mediating MDM2 control of p53 and E2F-1 protein stability. *J Biol Chem* **284**, 32384-32394, doi:10.1074/jbc.M109.052647 (2009).

9 Wu, S., Chen, L., Becker, A., Schonbrunn, E. & Chen, J. Casein kinase 1alpha regulates an MDMX intramolecular interaction to stimulate p53 binding. *Mol Cell Biol* **32**, 4821-4832, doi:10.1128/MCB.00851-12 (2012).

10 Price, M. A. CKI, there's more than one: casein kinase I family members in Wnt and Hedgehog signaling. *Genes Dev* **20**, 399-410, doi:10.1101/gad.1394306 (2006).

11 Schneider, R. K. *et al.* Role of casein kinase 1A1 in the biology and targeted therapy of del(5q) MDS. *Cancer Cell* (in press).

12 Järås, M. *et al.* Csnk1a1 inhibition has p53-dependent therapeutic efficacy in acute myeloid leukemia. *The Journal of experimental medicine* **211**, 605-612, doi:10.1084/jem.20131033 (2014).

13 Fratta, I. D., Sigg, E. B. & Maiorana, K. Teratogenic Effects of Thalidomide in Rabbits, Rats, Hamsters, and Mice. *Toxicology and applied pharmacology* **7**, 268-286 (1965).

14 Chesi, M. *et al.* Drug response in a genetically engineered mouse model of multiple myeloma is predictive of clinical efficacy. *Blood* **120**, 376-385, doi:10.1182/blood-2012-02-412783 (2012).

15 Fischer, E. S. *et al.* Structure of the DDB1-CRBN E3 ubiquitin ligase in complex with thalidomide. *Nature* **512**, 49-53, doi:10.1038/nature13527 (2014).

16 Chamberlain, P. P. *et al.* Structure of the human Cereblon-DDB1-lenalidomide complex reveals basis for responsiveness to thalidomide analogs. *Nature structural & molecular biology*, doi:10.1038/nsmb.2874 (2014).

17 Jädersten, M. *et al.* TP53 Mutations in Low-Risk Myelodysplastic Syndromes With del(5q) Predict Disease Progression. *Journal of Clinical Oncology* **29**, 1971-1979, doi:10.1200/jco.2010.31.8576 (2011).

18 Frei, E., 3rd. Gene deletion: a new target for cancer chemotherapy. *Lancet* **342**, 662-664 (1993).

19 Nijhawan, D. *et al.* Cancer vulnerabilities unveiled by genomic loss. *Cell* **150**, 842-854, doi:10.1016/j.cell.2012.07.023 (2012).

20 Ebert, B. L. *et al.* Identification of RPS14 as a 5q- syndrome gene by RNA interference screen. *Nature* **451**, 335-339, doi:nature06494 [pii] 10.1038/nature06494 (2008).

21 Narla, A. & Ebert, B. L. Ribosomopathies: human disorders of ribosome dysfunction. *Blood* **115**, 3196-3205, doi:blood-2009-10-178129 [pii] 10.1182/blood-2009-10-178129 (2010).

22 Yang, Y. *et al.* Exploiting synthetic lethality for the therapy of ABC diffuse large B cell lymphoma. *Cancer Cell* **21**, 723-737, doi:S1535-6108(12)00218-8 [pii] 10.1016/j.ccr.2012.05.024 (2012).

23 Hu, Y. *et al.* CSNK1alpha1 mediates malignant plasma cell survival. *Leukemia*, doi:10.1038/leu.2014.202(2014).

5

AN ENGINEERED MULTICOMPONENT BONE MARROW NICHE FOR THE RECAPITULATION OF HEMATOPOIESIS AT ECTOPIC TRANSPLANTATION SITES

Mónica S. Ventura Ferreira[1, 2], Christian Bergmann[3], Isabelle Bodensiek[2], Kristina Peukert[2], Jessica Abert[3], Rafael Kramann[4, 5], Paul Kachel[2], Björn Rath[6], Stephan Rütten[7], Ruth Knuchel[2], Benjamin L. Ebert[8, 9], Horst Fischer[3], Tim H. Brümmendorf[1], Rebekka K. Schneider[1, 2, 8]

[1] Department of Hematology, Oncology, Hemostaseology and Stem Cell Transplantation, University Hospital Aachen, RWTH Aachen University, Aachen, Germany
[2] Institute of Pathology, University Hospital Aachen, RWTH Aachen University, Aachen, Germany
[3] Department of Dental Materials and Biomaterials Research, University Hospital Aachen, RWTH Aachen University, Aachen, Germany
[4] Department of Clinical Immunology and Nephrology, University Hospital Aachen, RWTH Aachen University, Aachen, Germany
[5] Renal Division, Brigham and Women's Hospital, Department of Medicine, Harvard Medical School, Boston, USA
[6] Department of Orthopaedic Surgery, University Hospital Aachen, RWTH Aachen University, Aachen, Germany
[7] Electron Microscopy Facility, University Hospital Aachen, RWTH Aachen University, Aachen, Germany
[8] Division of Hematology, Department of Medicine, Brigham and Women's Hospital, Harvard Medical School, Boston, USA
[9] Broad Institute of Harvard University and Massachusetts Institute of Technology, Cambridge, USA

Corresponding author:
Rebekka K. Schneider, MD
Department of Hematology, Oncology, Hemostaseology and Stem Cell Transplantation, University Hospital Aachen, RWTH Aachen University, Aachen, Germany
Reschneider@ukaachen.de

J Hematol Oncol. 2016 Jan 25;9:4

BACKGROUND

Bone marrow (BM) niches are often inaccessible for controlled experimentation due to their difficult accessibility, biological complexity, and three-dimensional (3D) geometry.

METHODS

Here, we report the development and characterization of a BM model comprising of cellular and structural components with increased potential for hematopoietic recapitulation at ectopic transplantation sites. Cellular components included mesenchymal stromal cells (MSCs) and hematopoietic stem and progenitor cells (HSPCs). Structural components included 3D β-tricalcium phosphate (β-TCP) scaffolds complemented with Matrigel or collagen I/III gels for the recreation of the osteogenic/extracellular character of native BM.

RESULTS

In vitro, β-TCP/Matrigel combinations robustly maintained proliferation, osteogenic differentiation, and matrix remodeling capacities of MSCs and maintenance of HSPCs function over time. In vivo, scaffolds promoted strong and robust recruitment of hematopoietic cells to sites of ectopic transplantation, vascularization, and soft tissue formation.

CONCLUSIONS

Our tissue-engineered BM system is a powerful tool to explore the regulatory mechanisms of hematopoietic stem and progenitor cells for a better understanding of hematopoiesis in health and disease.

INTRODUCTION

The different components of the bone marrow (BM) microenvironment—consisting of (a) hematopoietic cells, (b) stromal cells and vasculature, (c) extracellular matrix, and (d) bone—are critical to explore for a better understanding of hematopoiesis during health and disease. These components are often inaccessible for controlled and rapid experimentation, thus limiting studies to the evaluation of conventional cell culture and transgenic animal models. The rationale to develop ectopic transplantable BM niches arises from the need to dissect regulatory mechanisms in the BM and the hematopoietic-stroma interaction. So far, no gold standard exists to specifically analyze the role of the BM stroma in vivo or to genetically modify stroma in its natural environment as stroma is not sufficiently transplantable in contrast to hematopoietic cells [1, 2].

Few approaches including in vivo imaging [3, 4], the design of three-dimensional (3D) environments using biomaterials [5, 6, 7, 8, 9, 10], and BM-on-a-chip [11] for the study of hematopoiesis have been introduced to date, but these system lack full BM recreation, as hematopoietic stem and progenitor cell (HSPC) interaction with the endosteal niche or with the supporting stroma is compromised or simply the geometry beneficial for a controlled manipulation is still missing.

Bioceramics such as β-tricalcium phosphate (β-TCP) are particularly interesting for bone tissue engineering as they provide characteristics for cellular interactions while ensuring superior biomechanical properties [12]. Matrigel is a basement membrane protein mixture typically used in vivo to stimulate tissue formation. [8]. Here, we combined 3D β-TCP scaffolds with defined and controlled geometry (bone component) with an extracellular matrix component composed of either collagen I/III or Matrigel (matrix component) to establish co-cultures of HSPCs and mesenchymal stromal cells (MSCs) (cellular component). The ultimate goal of the current study is to create artificial, transplantable BM niches that support hematopoiesis while allowing for the genetic modification of both hematopoietic and mesenchymal cells as to dissect their interaction.

METHODS

β-TCP scaffolds

β-TCP scaffolds were fabricated using slip casting into 3D-printed wax molds. First, two virtual models were constructed using computer-aided design (3-matic, Materialise, Leuven, Belgium). The models had a cylindrical shape with an inner diameter of 9.6 mm and a height of 4.9 mm. A rectangular lattice with 500-μm struts was incorporated into one of the models. The struts had a spacing of 2 mm and were connected to the cylinder. Into the second virtual model, a lattice with 800-μm struts (spacing 2.5 mm) was incorporated in the

same way. Finally, a sprue with a diameter of 9.6 mm and a height of 2.1 mm was added on one side of the cylinders. Both models were printed using a 3D wax printer (T76®PLUS, Solidscape, Idar-Oberstein, Germany) to generate the wax molds for the slip casting process. A suspension consisting of 68.7 wt% β-TCP, 29.3 wt% distilled water, and 2 wt% organic additives (0.2 wt% Contraspun, 1.4 wt% Optapix, 0.4 wt% Dolapix, Zschimmer und Schwarz, Lahnstein, Germany) was synthesized. The suspension was homogenized for 30 s using a SpeedMixerTM, (DAC 150.1 FVZ, Hauschild, Hamm, Germany) at a mixing rate of 3000 rpm. Afterwards, the suspension was filled with a pipette into the wax molds. The filled molds were devolatilized in a desiccator, and the suspension within was dried for 24 h at room temperature. The sprue was cut off with a scalpel until the ends of the vertical wax struts were exposed. The samples were heat treated for 30 min at 105 °C to melt out the wax (heating rate 2.5 K/min) and subsequently sintered for 3 h at 1200 °C (heating rate 3 K/min). The generated β-TCP scaffolds were cleaned in an ultrasound bath to remove particulate matter and dried at 80 °C for 24 h. Finally, the scaffolds were sterilized by autoclaving and dried at 80 °C for 24 h before they were used for cell culture.

Collagen I/III gels and Matrigel®

Collagen I/III were produced as previously described [13–16], and human mesenchymal stromal cells (hMSCs) or murine BM-derived mesenchymal stem cells (mBMSCs) were seeded at a density of 1 × 106 cells/mL. Matrigel® basement membrane matrix complex (BD Biosciences, 354234) was handled according to the manufacturer's instructions, and mBMSCs were seeded at a density of 1 × 106 cells/mL. Two hundred microliters of either collagen I/III gel or Matrigel® was combined with each one β-TCP scaffold. Gel polymerization was achieved by 1-h incubation at 37 °C in a 20 %-O2/5 %-CO2-humidified atmosphere.

Isolation and culture of hMSCs

MSCs from human femoral head spongiosa were collected after hip replacement surgeries and followed approved guidelines of the Ethics Committee of RWTH Aachen University. Cell isolation was performed according to previously described protocols [13–16]. For all experiments, hMSCs were passaged between 2–4 times before use. hMSCs were seeded on the β-TCP scaffolds at a density of ca. 1.5 × 105 cells/scaffold. Osteogenic differentiation was performed according to published protocols [8, 14].

Isolation and culture of human CD34+ progenitors

CD34+ progenitors were obtained by immunomagnetic bead selection (Miltenyi Biotec, Bergisch-Gladbach, Germany) from human umbilical cord blood units collected according to the guidelines of the Ethics Committee of RWTH Aachen University (EK187/08). CD34+ progenitors were cultured in StemSpan serum-free medium in the presence of SCF (50 ng), TPO (20 ng), Flt3-L (50 ng), and IL-6 (10 ng, all Peprotech, London, UK) as before [7, 8].

Isolation and culture of mBMSCs

mBMSCs were isolated from BM aspirates of 6–8-week-old C57BL/6 mice by mechanical crushing and collagenase treatment to liberate the stromal cells from the endosteal bone as described before [17]. Cells from six pooled mice were used for each experiment. mBMSCs were expanded in DMEM/F-12 with Glutamax™ (Life Technologies) supplemented with 1 nM dexamethasone (Sigma, Steinheim, Germany), 1 ng/mL fibroblast growth factor-2 (Peprotech, London, UK), 5 ng/mL epidermal growth factor (Peprotech), 2 % fetal calf serum (PAN Biotech), and 2 % penicillin/streptomycin (Life Technologies). mBMSCs were used between passages 2–4 for seeding.

Isolation and culture of murine c-kit+ cells

The hematopoietic cell fraction was collected by mechanical crushing/flushing of long bones and the pelvis, and c-kit+ cells were isolated by immunomagnetic bead selection using mouse CD117 (c-kit) microbeads (Miltenyi Biotec, Bergisch-Gladbach, Germany). Purity was confirmed by flow cytometry. Freshly isolated c-kit+ cells were used for co-cultures at ca. 1.5 × 105 cells/well and maintained in StemSpan serum-free expansion medium (SFEM) (Stem Cell Technologies Inc., Vancouver, Canada) containing 50 ng/mL stem cell factor (Peprotech), 50 ng/mL thrombopoietin (Peprotech), and 1 % penicillin/streptomycin (Life Technologies).

Culture conditions in β-TCP scaffolds

β-TCP scaffolds were transferred to 48-well tissue culture plates (Corning, Wiesbaden, Germany), and hMSCs embedded in the collagen I/III gels or directly seeded on the β-TCP scaffolds were kept in culture for 8 weeks. mBMSCs embedded in gels were pre-expanded for 1 week, and c-kit+ cells were seeded and co-cultures kept at 37 °C in a 20 %-O2/5 %-CO2-humidified atmosphere. Cells were recovered by vigorous pipetting and subsequent gel digestion using collagenase II (Life Technologies) for collagen I/III gels and dispase II (Life Technologies) for Matrigel® gels.

Flow cytometry

For analysis of maintenance of primitive phenotype in the human setting, 5-day cultured CD34+-isolated cells co-cultured with hMSCs for 5 days in β-TCP scaffolds with or without matrix component were assessed for the combined expression of CD34-FITC and CD38-PE (Miltenyi Biotec). For analysis of primitive phenotype and differentiation ability in the murine setting, c-kit+ cells from in vitro co-cultures were recovered at days 4, 7, 10, 14, and 18. In the in vivo setup, cells were recovered from explanted scaffolds 4 and 8 weeks after transplantation. Antibodies CD117-allophycocyanin, Sca1-phycoerythrin, lineages (CD3, CD5, B220, G1, CD11b, Ter119)-eFluor®450, Gr-1-allophycocyanin-cyanine7, CD11b-allophycocyanin, CD19-phycoerythrin-cyanine7, CD3-phycoerythrin, and Ter119-peridinin

chlorophyll-cyanine5.5 (all eBiosciences, Frankfurt, Germany) were used at 1:100, except for lineage antibodies used at 1:200 as recommended, in PBS/1 %-FCS for 30 min at 4 °C. A minimum of 100,000 events were acquired on a FACSCantoII flow cytometer (Becton Dickinson). Data were further analyzed using FlowJo (Tree Star Inc., Ashland, USA).

Methylcellulose colony assays

C-kit+ cells derived from 4-day or 14-day cultures were plated at 1 × 105 cells per 35-mm petri dish in duplicates of serum-free methylcellulose medium (MethoCult GF M3434, Stem Cell Technologies Inc., Vancouver, Canada). After 12 days of incubation at 37 °C and 5 % CO2 in a humidified atmosphere, colonies were scored using an inverted light microscope (Leica, Wetzlar, Germany). Colony-forming unit granulocyte-macrophages (CFU-GM) and colony-forming unit granulocyte-erythrocyte-macrophage-megakaryocyte (CFU-GEMM) were assayed according to morphological criteria.

SEM and FESEM in cryo-mode

β-TCP scaffolds from in vitro cultures and in vivo explantations were prepared for scanning electron microscopy (SEM) by fixation in 3 % glutaraldehyde for at least 24 h at 4 °C. A graded ethanol series of 30, 50, 70, 90, and 100 % followed for sample dehydration. Sample preservation was achieved by hexamethyldisilizane (HMDS) drying. Before gold sputtering and fixation on SEM stubs, scaffolds were sectioned one time longitudinal and orientated in the cross-sectional area for visualization. A field emission SEM microscope (ESEM XL 30 FEG, FEI, Philips, Eindhoven, The Netherlands) with a high-vacuum environment was used.

For a more detailed analysis of gel structure, field emission scanning electron microscopy (FESEM) in cryo-mode was performed for collagen I/III and Matrigel®. Gels were rapidly frozen in liquid nitrogen and transferred to the high-vacuum Balzers BF freeze-etching chamber of a FESEM instrument in cryo-mode (HITACHI S-4800, Hitachi, Tokyo, Japan) with secondary electron image resolution of 1.0–1.4 nm at voltages of 1–15 kV. Gels were sublimated for 1 h at 80 °C before image acquisition.

TEM

Freshly isolated, 4- and 14-day cultured c-kit+ cells were recovered from the scaffolds as already described, pelleted and fixed in 3 % glutaraldehyde, and processed for transmission electron microscopy (TEM) as described previously [13]. Cells were visualized using a transmission electron microscope at 60 kV (EM 400 T, Philips, Eindhoven, The Netherlands).

IHC

At the indicated time points, culture medium was removed and samples fixed in 10 % formalin for at least 24 h at 4 °C. Scaffolds were decalcified using EDTA for 48 h, sectioned, ethanol fixed and embedded in paraffin according to the standard protocols of the Institute

of Pathology, University Hospital Aachen. Paraffin sections of 3 µm were deparaffinized, hydrated using decreasing ethanol series and subject to heat-induced antigen retrieval using citrate buffer pH = 6.0. Immunohistochemistry stainings were performed using an Autostainer platform for immunohistochemistry (IHC) (Dako Cytomation). Primary antibodies used were specific for CD31 (1:100, rabbit polyclonal, Abcam), CD45(1:100, rabbit polyclonal, Abcam). Primary antibodies were diluted in Dako antibody diluent and incubated for 1 hour at room temperature. StreptABC complex/HRP followed by DAB for color development was used according to the Dako real detection system instructions (Dako Cytomation, K5001). Reticulin stain and hematoxilin-eosin stains were additionally performed according to routine histology protocols.

RT-qPCR

Isolation of total RNA from cultures was done with Tripure Isolation Reagent (Roche, Mannheim, Germany) [13, 14]. In brief, a high-capacity cDNA Reverse Transcriptase Kit (Applied Biosystems, Darmstadt, Germany) was used for RNA reverse transcription product amplification that was done using a 7300 Real-Time PCR System and SYBR green (Applied Biosystems, Darmstadt, Germany) running an amplification cycle consisting of 10-min denaturation at 95 °C, additional 40 cycles of denaturation at 95 °C for 15 s, and final extension of 1 min at 60 °C. The housekeeping gene GAPDH was used for normalization of data. Gene expression on collagen I/III gel controls was set to one using the $2^{-\Delta\Delta ct}$ method [8].

Calcium and phosphate assays

Calcium and phosphate content of culture supernatants was measured at weeks 1, 2, and 3 after cell seeding using a standard autoanalyzer. Alternatively, a commercially available colorimetric-based calcium assay kit (RANDOX, Crumlin, UK) was used to determine the amount of calcium released from the β-TCP scaffolds. The assay was carried out according to the manufacturer's instructions and absorbance measured at 578 nm using an Infinite® M200 microplate reader (Tecan, Männedorf, Switzerland).

Mouse transplantations

Six- to eight-week-old C57BL/6 mice were obtained from Jackson Laboratories (Maine, USA). Animals were kept at the Animal Research Facility Children's Hospital, Harvard Medical School, Boston, USA. Animals were handled according to institutional regulations and transplantations done according to standard protocols (mouse protocol number 13-04-2393R). mBMSCs were expanded in vitro for 1 week and then seeded on 500- and 800-µm β-TCP scaffolds in combination with collagen I/III or Matrigel®. Cell/matrix/scaffold hybrids were transplanted subcutaneously into the C57BL/6 mice.

Statistical analysis

Data presented was obtained from at least three independent donors. Results express mean ± SD, unless stated otherwise. Statistics as well as graphical representations were performed using GraphPad PrismTM 5.0 (GraphPad Software Inc., San Diego, USA). Statistical significance of data results from one-way ANOVA followed by Tukey's post hoc test (analysis of three or more groups). Significant differences were considered when $p < 0.05$.

RESULTS

β-TCP scaffold characterization

We first characterized the 3D porous β-TCP scaffolds, which were designed to mimic the spongious, structural part of the bone in terms of (i) osteoconductivity (porosity allowing for cell penetration and/or attachment and growth), (ii) osteogenicity (local osteoblastic mineral formation allowing for matrix calcification) [18], (iii) transplantability, (iv) inertness, and (v) hematopoiesis-supporting capacities. As pore size is known to affect cell attachment, proliferation, and migration [19], we tested the biological performance of β-TCP scaffolds with two different pore sizes—500 and 800 µm in diameter—similar to the geometry of the human bone and as used for replacement strategies [20, 21]. We applied scaffolds with 500- and 800-µm pore sizes in order to (a) simulate human bone properties, (b) maximize the surface area and volume available for stromal cell expansion, and (c) support bone ingrowth. As the literature reports strongly variable pore sizes ranging from 300 to 900 µm to be optimal, we analyzed if pore size matters for the recapitulation of extramedullary niches containing two cell types—adhering stromal cells and hematopoietic stem and progenitor cells [22].

β-TCP scaffolds were generated with interconnected macropore geometries for better cell growth, migration, and nutrient flow (Fig. 1a–g). The porosity of 500- and 800-µm scaffold was 14 and 17 vol.-%, respectively (Fig. 1e), comparable to the porosity of human cortical bone that is known to go from up to 8 % in young individuals to 24–28 % in elderly individuals [23, 24]. Maximized 500/800-µm scaffold magnitudes were provided for 3D culture including a surface area of 648/584 mm2 for stromal cell expansion and a volume of 51/60 mm3 for HSPC expansion.

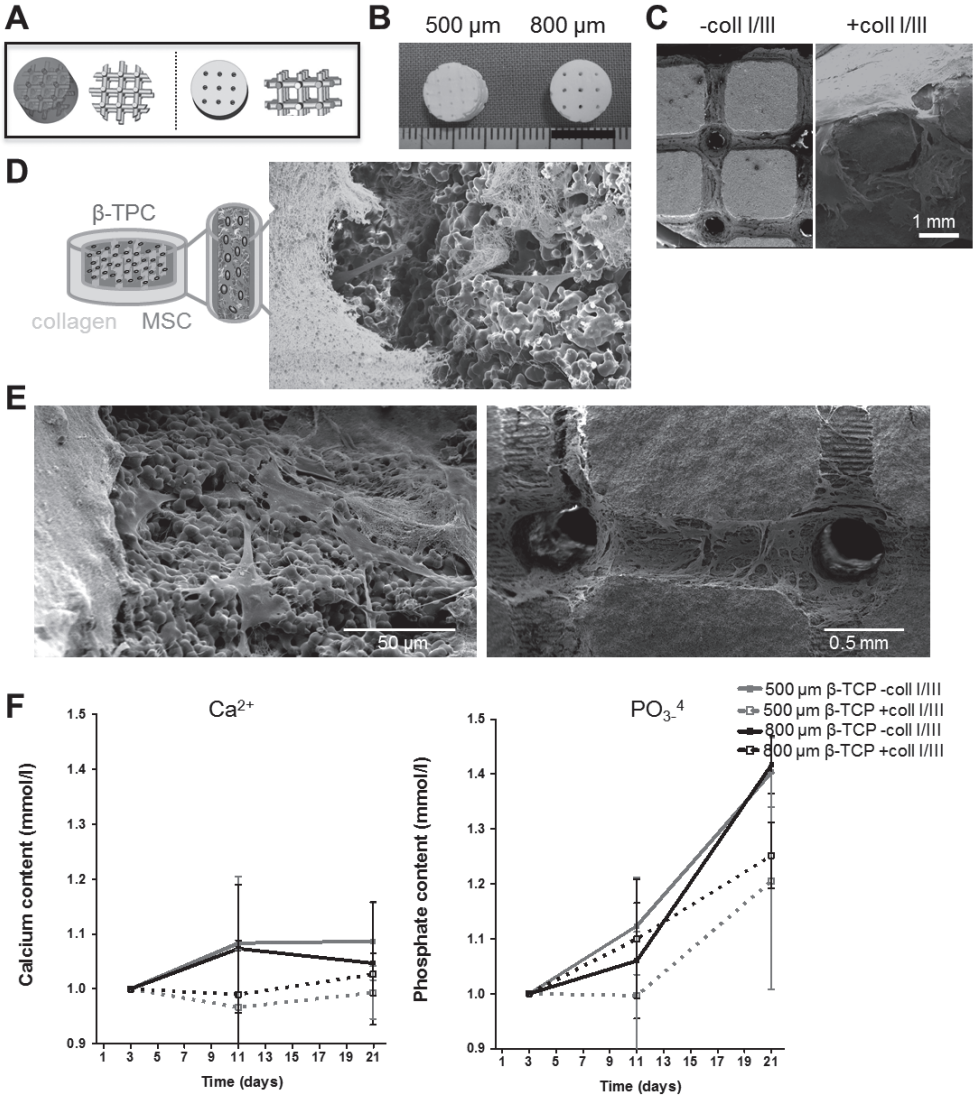

Figure 1: Characterization of β-TCP scaffolds. **a** Negative mold used for wax casting during production of the different β-TCP scaffold geometries. **b** Macroscopic view of the β-TCP scaffolds. **c** SEM view of the β-TCP scaffolds. **d** Schematic illustration of the long-term cultures consisting of three main components: mesenchymal stromal cells (MSCs; pink), β-TCP (blue), and collagen I/III (green). **e** Table of porosites. **f** Cell morphology and cell spreading on scaffolds analyzed by SEM. **g** Release of calcium (Ca2+) and phosphate (PO4 3−) to the culture supernatant. Concentrations were measured in the supernatants of β-TCP cultures at days 3, 11, and 21 after the beginning of the culture. Concentrations were normalized to 1 at day 3 and are presented in mmol/L. Results depict mean ± SD of three independent experiments

For scaffold characterization experiments, we seeded hMSCs onto 500- and 800-µm β-TCP in the presence or absence of collagen I/III (Fig. 1c, d, f). We first assessed the inertness of β-TCP scaffolds indicated by release of Ca2+ and PO43− in culture supernatants after 3, 11, and 21 days of culture (Fig. 1g). Analysis confirmed a minor increase in Ca2+ concentration in the culture medium of β-TCP-containing scaffolds, ca. 0.1 mmol/L for 500- or 800-µm β-TCP scaffolds. The PO43− concentration (Fig. 1g) increased over time in all β-TCP-containing supernatants (increase of 0.2–0.4 mmol/L) within ranges that are negligible and cannot be considered as indicators of spontaneous osteogenesis.

Assessment of the β-TCP scaffold potential for osteogenic differentiation

To determine if β-TCP induces a spontaneous osteogenic differentiation, we next analyzed the effect of β-TCP and collagen I/III on hMSC growth, osteogenic differentiation, and matrix production assessed by gene expression (Fig. 2). β-TCP scaffolds had good osteoconductivity as indicated by hMSC attachment, migration, and survival in the interconnected macropores of β-TCP scaffolds (Fig. 1f).

To analyze if the scaffold induced a spontaneous osteogenic differentiation of hMSCs, we seeded hMSCs in direct contact to 500/800-µm β-TCP scaffolds (Fig. 2). To dissect the additional effect of an extracellular matrix, we compared the spontaneous differentiation potential side-by-side to β-TCP/collagen I/III scaffolds and looked at hMSCs subjected to standard osteogenic differentiation protocols as a positive control (Fig. 2). BMP-2 and RUNX2 as early markers of osteogenic differentiation as well as the late marker osteopontin were not significantly up-regulated after 3 weeks of culture under nearly all β-TCP conditions, independent of the presence of collagen I/III gels (not shown). After 8 weeks of culture, the induction of early and late markers was maintained for cells cultured in β-TCP scaffolds in the absence of collagen I/III gels and decreased in the presence of collagen I/III gels (Fig. 2). This effect might be due to significant matrix remodeling that occurs in the presence of collagen I/III-containing scaffolds as indicated by the up-regulation of collagen I, fibronectin, laminin, and collagen IV in 8-week cultures (Fig. 2). Taken together, gene expression analysis provides no evidence for spontaneous osteogenesis upon in vitro culture or co-culture of hMSCs.

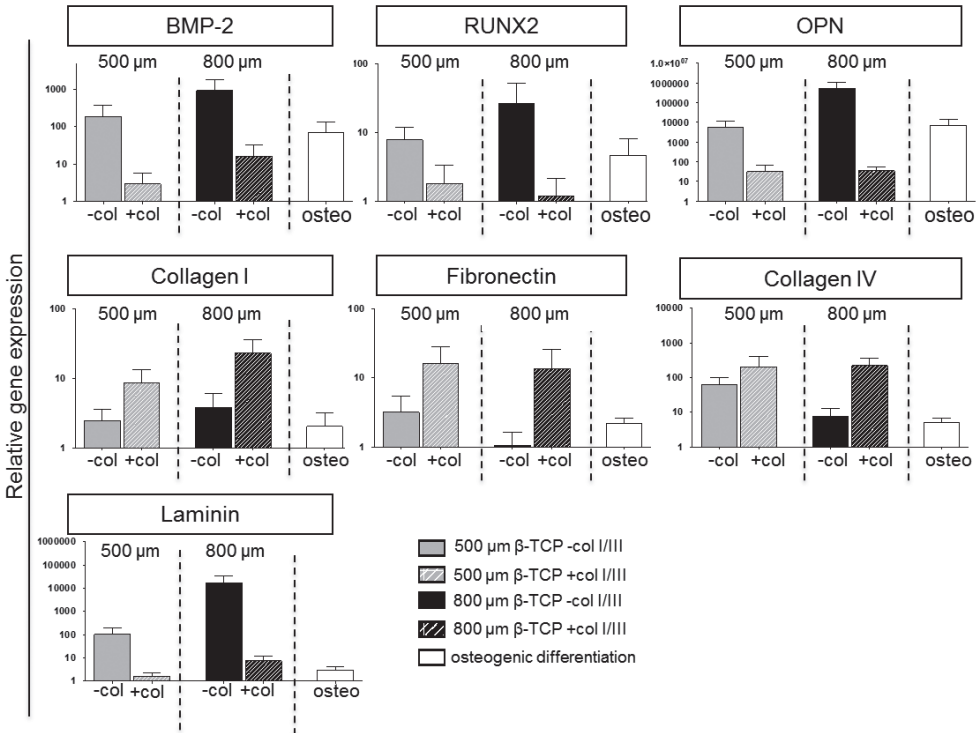

Figure 2: Osteogenic marker and extracellular matrix expression analysis of long-term MSC cultures on β-TCP scaffolds. The osteogenic markers BMP-2, RUNX2, and OPN as well as the extracellular matrix proteins collagen I, fibronectin, collagen IV, and laminin were analyzed after 8 weeks in culture. Data were calibrated relative to MSCs growing in collagen I/III gels, where gene expression was set to 1 for all genes. GAPDH was used as a housekeeping gene for normalization. Gene expression is presented as mean ± SD of three independent experiments and depicted on a logarithmic scale

Characterization of the β-TCP/matrix hybrids as extramedullary hematopoietic niches in vitro

We aimed to generate transplantable extramedullary hematopoietic niches and next analyzed the effect of β-TCP constructs on murine hematopoiesis in vitro. We combined 500- and 800-µm β-TCP scaffolds with either collagen I/III [8] or Matrigel® to improve cell engraftment and proliferation [25]. mBMSCs were cultured for 1 week on β-TCP scaffolds (with and without collagen I/III) before freshly isolated c-kit+ HSPCs from murine BM were added. In order to decide on the optimal combination of extracellular matrix and β-TCP pore size for future transplantation experiments, we assessed (i) viability, (ii) maintenance of a primitive HSPC phenotype and lineage differentiation, (iii) proliferation, and (iv) extracellular matrix remodeling.

Maintenance of the primitive hematopoietic stem and progenitor cell phenotype was monitored after 5 and 12 days for the human setting and 4, 7, and 14 days for the murine setting (Fig. 3a–c). Murine hematopoietic stem cells can be characterized in the bone marrow by being lineage-marker negative, c-kit+ and Sca1+ (LSK population; lin−Sca1+c-kit+), while hematopoietic progenitor cells are lineage-marker negative, Sca1− and c-kit+ (LK population; lin−Sca1−c-kit+). After 14 days, the viability in the β-TCP scaffolds alone or in combination with Matrigel® was independent of the pore size (Fig. 3a). The presence of a collagen matrix reduced the cell viability, probably due to significant matrix remodeling, as discussed before. The stromal cells in the collagen scaffolds can be characterized as lin−Sca1+c-kit−. We quantified the percentage of lin−Sca1+c-kit− stromal cells at day 4 and monitored their increase/decrease over time (Fig. 3b, c). In particular, 500-µm scaffolds had a positive effect on stromal cell expansion. We next assessed the maintenance of the LSK and LK phenotypes in vitro. Our results showed that β-TCP/extracellular matrix hybrids more robustly maintained a phenotypical LSK fraction over time compared to β-TCP alone. C-kit+ expression was shown to decrease over time in vitro independent of the hematopoietic stem and progenitor phenotype [26]. We thus quantified lineage-negative cells in the scaffolds over time as this population is enriched in hematopoietic stem and progenitor cells. The presence of 500-µm scaffolds showed a relative expansion of lineage-negative cells while this population maintained stable in the other conditions. We confirmed these results by using human HSPCs. In humans, the subset of CD34+CD38− HSPCs corresponds to a more primitive phenotype. Our data in short-term co-cultures showed that CD34+CD38− HSPCs were maintained most sufficiently in β-TCP scaffold containing collagen I/III, comparable to our results in the murine system

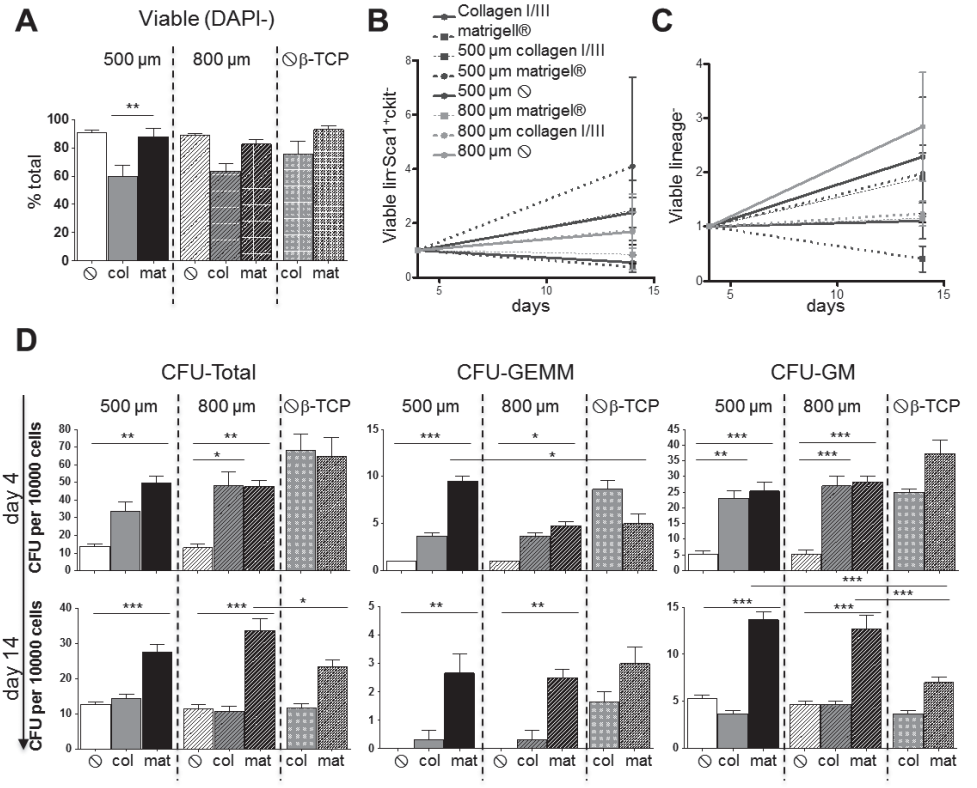

Figure 3: Hematopoietic stem cell characterization in β-TCP scaffolds in vitro. C-kit+ cells were subjected to the different β-TCP/matrix hybrids over 14 days in vitro. **a** Percentage of DAPI−-viable cells after 14 days of c-kit+ cell culture with and without collagen I/III/Matrigel® on β-TCP scaffolds in the presence of MSC support. **b** Expansion/decrease of lin−Sca1+c-kit− stromal cells normalized to day 4 of the culture. **c** Expansion/decrease of lin− normalized to day 4 of the culture. Mean ± SD of three independent experiments. **d** Colony-forming potential of cells isolated from 500- and 800-µm β-TCP scaffolds with and without collagen I/III/Matrigel® in the presence of MSC support at day 4 and day 14. Results are mean ± SD of three independent experiments. CFU colony-forming unit, GEMM granulocyte-erythrocyte-macrophage-megakaryocyte, GM granulocyte-monocyte. ⃠ without.

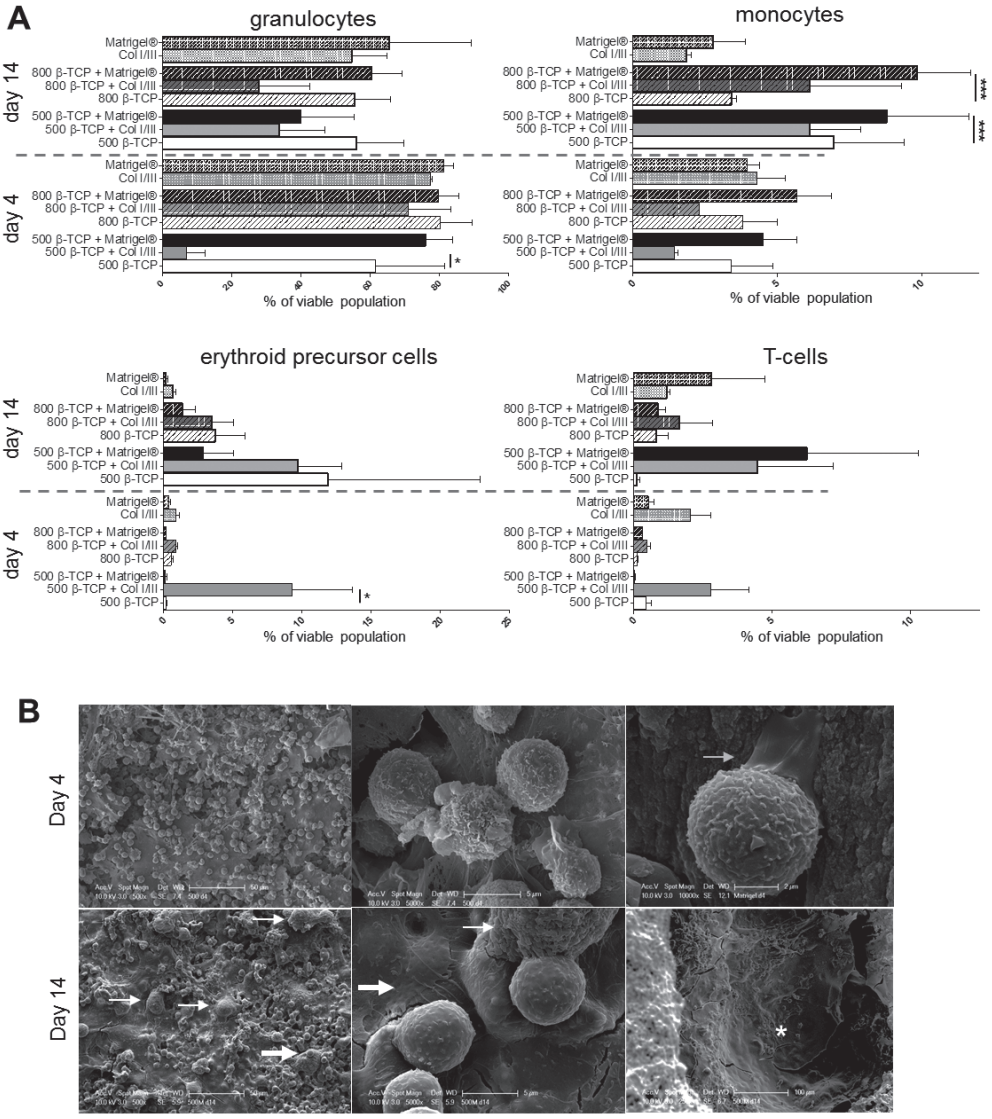

Figure 4: Analysis of trilineage differentiation of c-kit+ HSPCs on β-TCP scaffolds in vitro. **a** Differentiation potential of c-kit+ cells cultured for 4 and 14 days on β-TCP scaffolds with and without collagen I/III gel/Matrigel® in the presence of MSC support: granulocytes (Gr1+CD11b+), monocytes (Gr1−CD11b), erythroid precursor cells (Gr1−CD11b−CD3−CD19−), and T cells (Gr1−CD11b−CD3+). Percentage of viable cells is shown as mean ± SD of three independent experiments. **b** SEM of c-kit+ cells cultured on 500-µm β-TCP/Matrigel® scaffolds. Very left column highlights cell spreading and detailed cell morphology of day 4 and day 14 cultures. C-kit+-derived cells (red arrows) are in close contact to MSCs (white arrows). Cell extensions at day 4 in detail (green arrow). View from the interior of the β-TCP macropores at day 14 (asterisk)

In order to evaluate not only the HSPC phenotype but also their function among the different scaffold combinations as the ultimate readout for the maintenance of hematopoietic stem cell capacities, we performed colony-forming assays at day 4 and day 14 (Fig. 3d). Our data showed that murine cells cultured on β-TCP scaffolds alone for 4 days had significantly impaired CFU potential and HSPC function compared to all the other conditions. The presence of Matrigel® alone resulted in the significantly highest total number of colonies, and the combination of β-TCP/Matrigel® led to the highest number of CFU-GEMM colonies, representing multipotent myeloid progenitor cells. As expected, the CFU potential globally decreased after 14 days, but HSPCs cultured in the combination of β-TCP/Matrigel® scaffolds ($p < 0.001$ compared to 500-µm β-TCP and $p < 0.002$ compared to 800-µm β-TCP) gave rise to the significantly highest number of colonies, in particular to primitive CFU-GEMM colonies, indicating that the function of HSPCs was maintained under these conditions.

We next analyzed the lineage differentiation potential and asked whether or not scaffold combinations induce a lineage bias (Fig. 4a; Additional file 5: Figure S4). We analyzed granulocytes (Gr1+CD11b+), monocytes (Gr1−CD11b+), B-cells (Gr1−CD11b−CD19+), T cells (Gr1−CD11b−CD3+), and erythroid cells (Gr1−CD11b−CD3−CD19−) in the murine in vitro culture system at day 4 and day 14. All culture conditions induced myeloid differentiation into granulocytes and monocytes. The frequency of granulocytes decreased in tendency over the culture of 14 days, while the frequency of monocytes increased. After 14 days, the presence of Matrigel® in 500 and 800 µm significantly stimulated monocyte differentiation as compared to β-TCP scaffolds alone. We also detected both lymphoid (mainly T cells) and erythroid differentiation in all culture conditions, indicating that the scaffold-matrix hybrids support both trilineage differentiation as well as maintenance of primitive, functional HSPCs.

Next, we dissected the spatial distribution of human CD34+ HSPCs and murine c-kit+ cells in β-TCP/matrix hybrids combinations (Fig. 4b). HSPCs growing on β-TCP/Matrigel® were spread on top of the scaffolds as single cells or in close proximity to mBMSCs (Fig. 4b) or growing inside scaffold pores attached to the Matrigel® surface (Fig. 4b). After 14 days, the cell density was significantly increased but cells were predominantly positioned on top of the scaffolds/Matrigel, indicating that Matrigel does not support the migration of HSPCs due to high density and overall low porosity. This hypothesis was supported by imaging using SEM in cryo-mode. The Matrigel® porosity—as a result of the gelation process—was higher at the top part of the gel and lower at the bottom, a limitation which eventually led to the rare cell migration into the Matrigel®. Collagen I/III gels showed high cell densities on top as well as significant migration of hematopoietic cells inside the gel and cells growing in close proximity to mBMSCs and collagen fibers. Similarly, the addition of β-TCP to collagen I/III gels supported cell proliferation as well as migration both in the murine and human settings. In β-TCP scaffolds, the cell proliferation and density appeared significantly impaired despite the presence of a robust mBMSC layer covering the β-TCP surfaces. This leads to

the suggestion that β-TCP scaffolds are supportive of the growth of mBMSCs but that hematopoietic cells require an additional matrix structure.

Characterization of the β-TCP/matrix hybrids as extramedullary hematopoietic niches in vivo

To test the capacity of β-TCP scaffolds for supporting recruitment of hematopoietic cells and extramedullary hematopoiesis, 500- and 800-µm β-TCP scaffolds pre-seeded with mBMSCs were transplanted subcutaneously into C57BL/6 mice in the presence and absence of collagen I/III or Matrigel®. Hematopoiesis in the explanted scaffolds was evaluated 4 and 8 weeks after transplantation by flow cytometry, immunohistochemistry, and SEM (Figs. 5 and 6).

We performed H&E staining (Fig. 5a, b) in order to analyze the tissue and cell organization within the scaffolds. Histomorphological overviews in low magnification demonstrated that all scaffold pores—both in the periphery and in the central areas—were composed of a strongly vascularized extracellular matrix, partially adipose tissue, prominent histocyte-like cells aligning the β-TCP surface, and accumulations of hematopoietic cells in close proximity to vessels and the β-TCP surface (Fig. 5a). Higher magnification demonstrated dense clusters of hematopoietic cells in particular at the scaffold/matrix interface (Fig. 5b).

CD31 immunohistochemistry confirmed a dense vascular network in the scaffold, an important requisite for successful long-term engraft of scaffolds and recruitment of hematopoietic cells (Fig. 5c). CD31-positive cells were also seen at the β-TCP/tissue interface. CD45 staining highlighted the spatial organization of hematopoietic cells in dense clusters in proximity to both the vasculature and the scaffold interfaces (Fig. 5c). As observed in vitro, the β-TCP surface seeded with mBMSCs appears to provide appropriate conditions for the development of a bone-like niche, as we also noted the presence of multinucleated osteoclasts and osteoblasts. The presence of osteoclasts was confirmed by SEM showing spindle-shaped cells with brush-like microvilli (Fig. 5d).

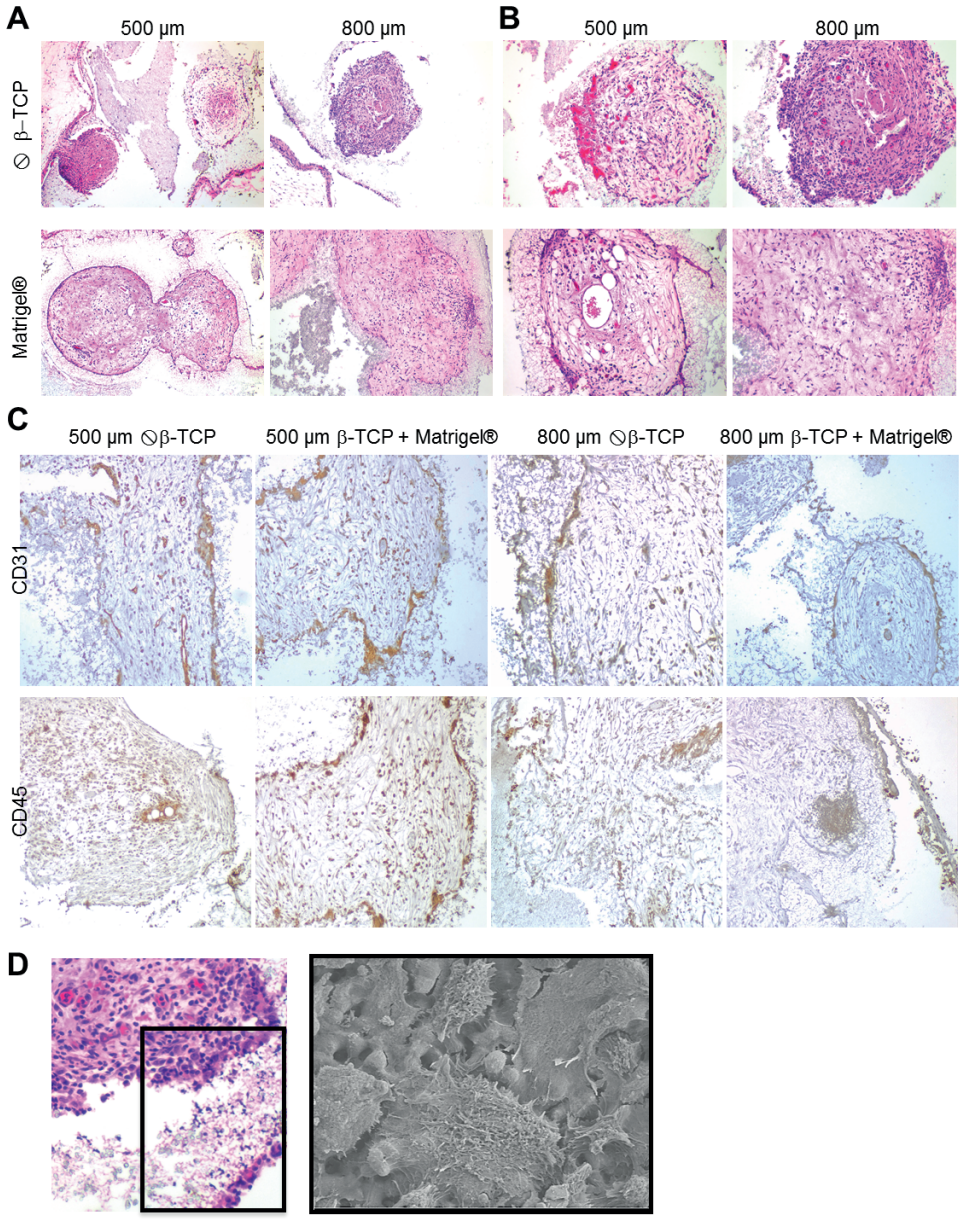

Figure 5: Histomorphology. 500µm or 800 µm β-TCP scaffolds were pre-seeded with mBMSC in the presence or absence of Matrigel®. Scaffolds were transplanted subcutaneously into C57B1/6 mice and analyzed for hematopoietic cell recruitment to sites of extramedullar hematopoiesis and hematopoietic tissue formation after 4 and 8 weeks. **a** Hematoxilin-eosin (HE) staining of the explanted scaffolds 8 weeks after transplantations. Magnification 100x. **b** Higher magnification of the explanted scaffolds after 8 weeks. Magnification 200x. **c** Immunohistochemistry for the endothelial surface marker CD31 and the pan-hematopoietic marker CD45 in explanted scaffolds 8 weeks after transplantation. **d** HE staining and by SEM for the identification of osteoclasts at the border of the β-TCP scaffold macropores in explants 4 weeks after transplantation.

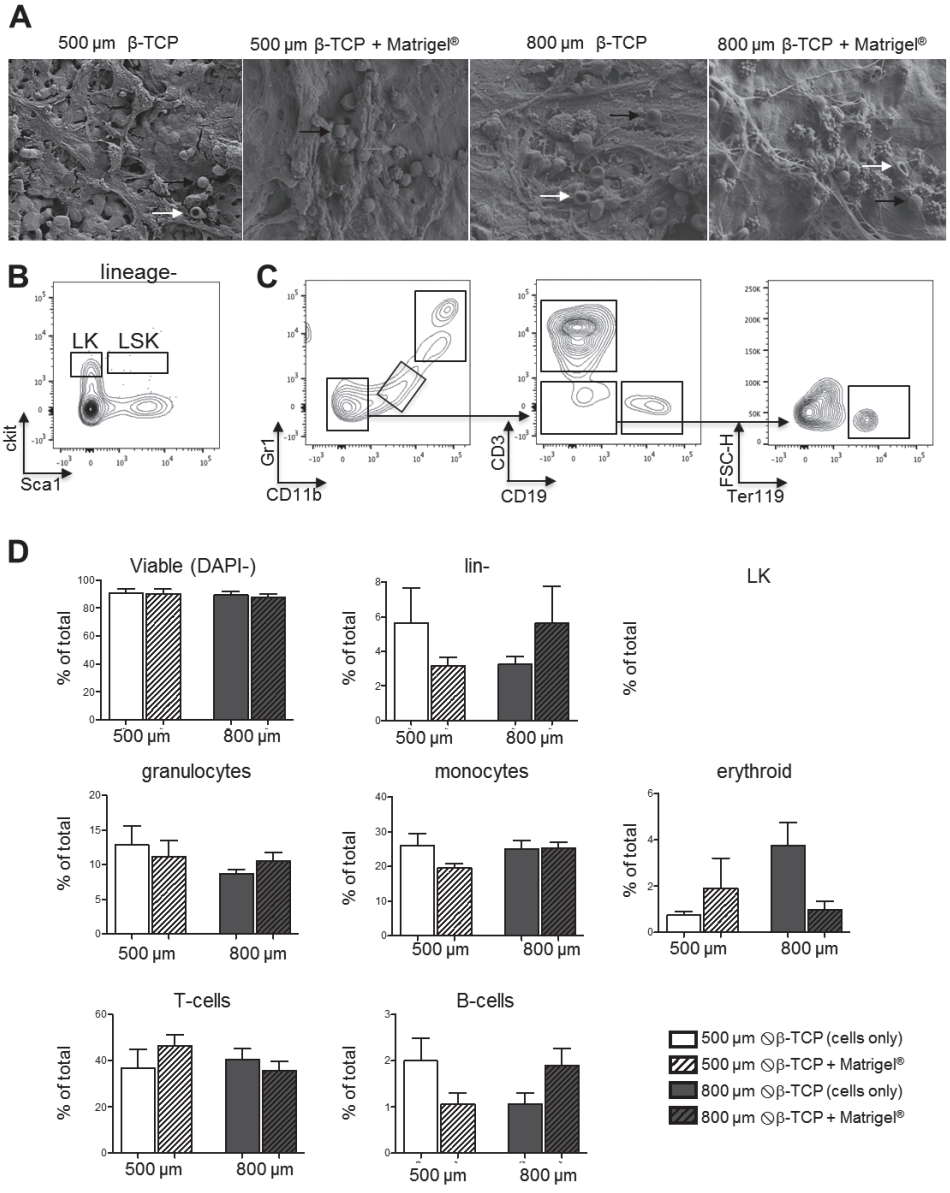

Figure 6: a SEM imaging ft he explanted scaffolds 4 weeks after transplantation. White arrows: erythrocytes; black arrows: T cells; red arrows: thrombocytes; gray arrow: neutrophils/granulocytes; asterisk: β-TCP. **b-c** Gating strategy ft he flow cytometry: Hematopoietic stem (LSK) and progenitor cells (LK) were identified by being negative for lineage markers and by the expression of Sca1 and c-kit. Lineages were identified by the following stainings: granulocytes (Gr1+CD11b+), monocytes (Gr1−CD11b−), erythroid precursor cells (Gr1−CD11b−CD3−CD19−), T cells (Gr1−CD11b−CD3+), B cells (Gr1−CD11b−CD19+). **d** Flow cytometry analysis ft he explanted scaffolds 4 weeks after transplantations. Surface marker expression is shown as a percentage ft he viable cell population; mean ± SD of three independent experiments.

We next sought to characterize the identity of hematopoietic cells (Fig. 6a–d). All β-TCP/matrix hybrid combinations were able to recruit hematopoietic cells to the site of transplantation as SEM confirmed hematopoietic cells inside the pores of the transplanted scaffolds (Fig. 6a).

Our first question was whether the implanted scaffolds promote extramedullary hematopoiesis including the presence of hematopoietic stem and progenitor cells. Flow cytometry confirmed the presence of cells of all hematopoietic lineages: myeloid (CD11b+Gr1+), lymphoid (Gr1−CD11b−CD19+ or CD3+), and erythroid (Gr1−CD11b−CD19−CD3− Ter119+) lineages (Fig. 6c, d). We did not detect an HSC-enriched LSK population but hematopoietic progenitor cells as indicated by the presence of lineage-negative and also myeloid progenitor cells (LK population). These data indicate that the majority of hematopoietic cells were recruited to the site of transplantation and do not represent in situ, extramedullary hematopoiesis. We did not observe significant differences in the recruitment of cell lineages in the different culture conditions, demonstrating that all conditions are suitable for ectopic transplantation independently of β-TCP pore size or presence of extracellular matrix. Discussion

DISCUSSION

The BM microenvironment is not transplantable making it challenging to dissect the regulatory mechanisms within the BM niche. We envisioned a widely available, easy reproducible, simple, and well-defined system for the creation of a transplantable human BM microenvironment. Establishing such a system would include not only a detailed characterization of the hematopoietic and mesenchymal fractions upon culture/transplantation but also the design of an appropriate scaffold material and structure. For the co-culture of HSPCs and mBMSCs/hMSCs, we applied β-TCP-printed scaffolds containing macro- and micropores similar to the bone—of inorganic (hydroxyapatite mineral) composition—in combination with an extracellular matrix gel—of organic (collagen type I matrix) composition.

As β-TCP materials are unstable when exposed to body fluids due to their small granule size, porosity, and higher dissolution rate compared to other types of bioceramics [27], we first set up to analyze the effects of β-TCP dissolution on the cultured cells. Typically high phosphate levels induce osteogenic differentiation, so we asked whether or not β-TCP scaffolds in our setting induced spontaneous osteogenic differentiation of MSCs by Ca/P release to the culture media. Our analysis revealed negligible Ca/P release and the exclusion of the possibility for spontaneous MSC-derived osteogenesis that could be detrimental for hematopoietic production. Importantly, we showed that our β-TCP scaffolds have the

ability to support MSC growth and extracellular matrix production in cultures up to 8 weeks without limiting effects.

Our in vitro data suggest that complete hematopoiesis is promoted by β-TCP scaffolds in combination with structural proteins and cytokines provided by Matrigel®. First, β-TCP/Matrigel® scaffolds more robustly maintained a primitive LSK fraction over time, with the Matrigel® component being responsible for maintenance of HSPCs within the scaffolds. Second, hematopoietic differentiation in both myeloid and lymphoid lineages was supported after 14 days in Matrigel®-containing conditions. Third, the CFU potential of β-TCP/Matrigel® scaffolds was significantly increased compared to other conditions implicating that Matrigel supports both the functional maintenance of HSPCs and their differentiation capacity. Fourth, β-TCP/Matrigel® scaffolds supported the remodeling of the ECM as an important requisite for cell differentiation and growth.

In vivo, β-TCP/Matrigel® scaffolds resulted in strong hematopoietic recruitment to the sites of the ectopic transplantations as confirmed by the detection of myeloid and lymphoid fractions 4 weeks after transplantations at levels comparable to the relative composition of the BM. Multinucleated osteoclasts and typically spindle-shaped osteoblasts were seen at the β-TCP scaffold/ECM interface. CD31-positive layers of recruited endothelial cells and adipose cells, typical for vascular niches, were both identified in explants showing the most efficient collagen matrix deposition. Adipose cells were regarded as simple as BM fillers but are now known to be negative regulators of the hematopoietic microenvironment [28]. BM tissue formation in our setting was mainly promoted by Matrigel®, a biodegradable basement membrane protein extracted from Engelbreth-Holm-Swarm sarcoma mouse cells, typically used to recreate 3D environments stimulating tissue formation. The main components of Matrigel® are known to be structural proteins laminin, collagen IV, and enactin, but numerous other intracellular proteins are present. Around 1300 proteins (either cytoplasmatic or nuclear) were identified in Matrigel® composition, and among those were collagen IV; actin; spectrin; tubulin; dynactin; filamin structural proteins like fibronectin, dynein, desmin, myosin, transferrin; and intracellular proteins such as adenylate kinase and heat shock family members [29]. Additionally, specific growth and transcription factors such as kruppel-like factor 6, kruppel-like factor 15, and connective tissue growth factor were identified. Future studies will be necessary to dissect which of these factors are most important to support both hematopoiesis and osteogenesis to generate more defined environments.

Our study demonstrates that varying pore sizes of the β-TCP scaffolds from 500 to 800 µm was irrelevant in terms of hematopoietic support function. This is an interesting finding as particle geometry, porosity, pore size distribution, and scaffold continuity are properties known to determine cell/scaffold interactions and thus cell fate [20, 30, 31]. Pore size, however, has been only considered crucial within three main pore size intervals. According to Petite et al., pore sizes smaller than 15–50 µm result in fibrovascular growth,

medium-sized pores of 50–150 µm encourage osteogenesis, while pores larger than 150 µm support the ingrowth of mineralized bone [20]. Contradicting studies even report that bone ingrowth is optimal for pore sizes varying from 300 to 900 µm [22].

The β-TCP scaffolds applied in our study had an interconnected net-like structure in the absence of dead-end pockets, macropores with mean pore size 500 or 800 µm, and micropores smaller than 15 µm. Our scaffolds were designed to maximize the surface area for stromal cell expansion, and we were able to demonstrate that these characteristics successfully promote vascular ingrowth as well as promotion of hematopoiesis.

Our engineered bone marrow has the potential to be applied for drug discovery studies and leukemia therapy as well as stem cell transplantation research [32, 33].

CONCLUSIONS

We introduce a multicomponent system that is optimal for the study of hematopoietic-mesenchymal interactions and the recapitulation of the native BM microenvironment in a transplantable mouse model. Macro- and microporous β-TCP scaffolds in combination with a Matrigel®-based component optimally supported hematopoiesis, including hematopoietic recruitment, proliferation, and differentiation as well as ECM remodeling. β-TCP/Matrigel® scaffolds further promoted vascularization and allowed for mature bone deposition and hematopoiesis—stroma interactions in subcutaneous ectopic transplantations of the BM niche in a murine model.

Acknowledgements

This work was supported by the intramural funding of RWTH Aachen to RKS (START grant and IZKF grant/O1-6). RKS was supported by the German Research Foundation (DFG1188/3-1), the Edward P. Evans Foundation, and the German Cancer Aid (Max-Eder). MSVF was supported by the Excellence Initiative of the RWTH Aachen University (Start Up; StUpPD_107_13). IB received support from DAAD.

REFERENCES

1 Plock JA, Schnider JT, Solari MG, Zheng XX, Gorantla VS. Perspectives on the use of mesenchymal stem cells in vascularized composite allotransplantation. Frontiers in immunology. 2013;4:175.

2 Schnider JT, Weinstock M, Plock JA, Solari MG, Venkataramanan R, Zheng XX, et al. Site-specific immunosuppression in vascularized composite allotransplantation: prospects and potential. Clinical & developmental immunology. 2013;2013:495212.

3 Lo Celso C, Lin CP, Scadden DT. In vivo imaging of transplanted hematopoietic stem and progenitor cells in mouse calvarium bone marrow. Nature protocols. 2011;6:1-14.

4 Nombela-Arrieta C, Pivarnik G, Winkel B, Canty KJ, Harley B, Mahoney JE, et al. Quantitative imaging of haematopoietic stem and progenitor cell localization and hypoxic status in the bone marrow microenvironment. Nature cell biology. 2013;15:533-43.

5 Mortera-Blanco T, Mantalaris A, Bismarck A, Aqel N, Panoskaltsis N. Long-term cytokine-free expansion of cord blood mononuclear cells in three-dimensional scaffolds. Biomaterials. 2011;32:9263-70.

6 Mortera-Blanco T, Rende M, Macedo H, Farah S, Bismarck A, Mantalaris A, et al. Ex vivo mimicry of normal and abnormal human hematopoiesis. Journal of visualized experiments : JoVE. 2012.

7 Ferreira MS, Jahnen-Dechent W, Labude N, Bovi M, Hieronymus T, Zenke M, et al. Cord blood-hematopoietic stem cell expansion in 3D fibrin scaffolds with stromal support. Biomaterials. 2012;33:6987-97.

8 Leisten I, Kramann R, Ventura Ferreira MS, Bovi M, Neuss S, Ziegler P, et al. 3D co-culture of hematopoietic stem and progenitor cells and mesenchymal stem cells in collagen scaffolds as a model of the hematopoietic niche. Biomaterials. 2012;33:1736-47.

9 Di Maggio N, Piccinini E, Jaworski M, Trumpp A, Wendt DJ, Martin I. Toward modeling the bone marrow niche using scaffold-based 3D culture systems. Biomaterials. 2011;32:321-9.

10 Chen Y, Jacamo R, Shi YX, Wang RY, Battula VL, Konoplev S, et al. Human extramedullary bone marrow in mice: a novel in vivo model of genetically controlled hematopoietic microenvironment. Blood. 2012;119:4971-80.

11 Torisawa YS, Spina CS, Mammoto T, Mammoto A, Weaver JC, Tat T, et al. Bone marrow-on-a-chip replicates hematopoietic niche physiology in vitro. Nature methods. 2014;11:663-9.

12 Walsh WR, Vizesi F, Michael D, Auld J, Langdown A, Oliver R, et al. Beta-TCP bone graft substitutes in a bilateral rabbit tibial defect model. Biomaterials. 2008;29:266-71.

13 Petite H, Viateau V, Bensaid W, Meunier A, de Pollak C, Bourguignon M, et al. Tissue-engineered bone regeneration. Nature biotechnology. 2000;18:959-63.

14 Demirkiran H. Bioceramics for osteogenesis, molecular and cellular advances. Advances in experimental medicine and biology. 2012;760:134-47.

15 Schneider RK, Anraths J, Kramann R, Bornemann J, Bovi M, Knuchel R, et al. The role of biomaterials in the direction of mesenchymal stem cell properties and extracellular matrix remodelling in dermal tissue engineering. Biomaterials. 2010;31:7948-59.

16 Schneider RK, Puellen A, Kramann R, Raupach K, Bornemann J, Knuechel R, et al. The osteogenic differentiation of adult bone marrow and perinatal umbilical mesenchymal stem cells and matrix remodelling in three-dimensional collagen scaffolds. Biomaterials. 2010;31:467-80.

17 Schneider RK, Neuss S, Stainforth R, Laddach N, Bovi M, Knuechel R, et al. Three-dimensional epidermis-like growth of human mesenchymal stem cells on dermal equivalents: contribution to tissue organization by adaptation of myofibroblastic phenotype and function. Differentiation. 2008;76:156-67.

18 Schneider RK, Pullen A, Kramann R, Bornemann J, Knuchel R, Neuss S, et al. Long-term survival and characterisation of human umbilical cord-derived mesenchymal stem cells on dermal equivalents. Differentiation. 2010;79:182-93.

19 Schneider RK, Adema V, Heckl D, Jaras M, Mallo M, Lord AM, et al. Role of casein kinase 1A1 in the biology and targeted therapy of del(5q) MDS. Cancer cell. 2014;26:509-20.

20 Gazdag AR, Lane JM, Glaser D, Forster RA. Alternatives to Autogenous Bone Graft: Efficacy and Indications. The Journal of the American Academy of Orthopaedic Surgeons. 1995;3:1-8.

21 Benton G, Kleinman HK, George J, Arnaoutova I. Multiple uses of basement membrane-like matrix (BME/Matrigel) in vitro and in vivo with cancer cells. International journal of cancer Journal international du cancer. 2011;128:1751-7.

22 Okada S, Nakauchi H, Nagayoshi K, Nishikawa S, Miura Y, Suda T. In vivo and in vitro stem cell function of c-kit- and Sca-1-positive murine hematopoietic cells. Blood. 1992;80:3044-50.

23 Harada S-i, Rodan GA. Control of osteoblast function and regulation of bone mass. Nature. 2003;423:349-55.

24 Demirkiran H. Bioceramics for osteogenesis, molecular and cellular advances. Adv Exp Med Biol. 2012;760:134-47.

25 Rezwan K, Chen QZ, Blaker JJ, Boccaccini AR. Biodegradable and bioactive porous polymer/inorganic composite scaffolds for bone tissue engineering. Biomaterials. 2006;27:3413-31.

26 Hannink G, Arts JJC. Bioresorbability, porosity and mechanical strength of bone substitutes: what is optimal for bone regeneration? Injury. 2011;42 Suppl 2:S22-5.

27 Eggli PS, Muller W, Schenk RK. Porous hydroxyapatite and tricalcium phosphate cylinders with two different pore size ranges implanted in the cancellous bone of rabbits. A comparative histomorphometric and histologic study of bony ingrowth and implant substitution. Clin Orthop Relat Res. 1988:127-38.

28 Buser D, Hoffmann B, Bernard JP, Lussi A, Mettler D, Schenk RK. Evaluation of filling materials in membrane--protected bone defects. A comparative histomorphometric study in the mandible of miniature pigs. Clinical oral implants research. 1998;9:137-50.

29 Gazdag A, Lane J, Glaser D, Forster R. Alternatives to Autogenous Bone Graft: Efficacy and Indications. J Am Acad Orthop Surg. 1995;3:1-8.

30 Fielding GA, Bandyopadhyay A, Bose S. Effects of silica and zinc oxide doping on mechanical and biological properties of 3D printed tricalcium phosphate tissue engineering scaffolds. Dent Mater. 2012;28:113-22.

31 Kishimoto M, Kanemaru S-i, Yamashita M, Nakamura T, Tamura Y, Tamaki H, et al. Cranial bone regeneration using a composite scaffold of Beta-tricalcium phosphate, collagen, and autologous bone fragments. Laryngoscope. 2006;116:212-6.

32 Naveiras O, Nardi V, Wenzel PL, Hauschka PV, Fahey F, Daley GQ. Bone-marrow adipocytes as negative regulators of the haematopoietic microenvironment. Nature. 2009;460:259-63.

33 Hughes CS, Postovit LM, Lajoie GA. Matrigel: a complex protein mixture required for optimal growth of cell culture. Proteomics. 2010;10:1886-90.

34 von Doernberg MC, von Rechenberg B, Bohner M, Grunenfelder S, van Lenthe GH, Muller R, et al. In vivo behavior of calcium phosphate scaffolds with four different pore sizes. Biomaterials. 2006;27:5186-98.

6

SUMMARY AND GENERAL DISCUSSION

1. SUMMARY

The studies presented in this thesis focused on the identification of genes that play a central role in the pathogenesis of myelodysplastic syndromes with a deletion of the short arm (q) of chromosome 5, the del(5q) MDS in **chapters 2-4**. The overall goal of the projects was to gain a better understanding of how gene haploinsufficiency in (del)5q MDS leads to a clonal advantage, ineffective hematopoiesis and how haploinsufficiency can be targeted (**chapter 2-4**).

Heterozygous deletion of *RPS14* occurs in del(5q) myelodysplastic syndrome (MDS) and has been linked to impaired erythropoiesis, characteristic of this disease subtype. So far, it was not well understood how ribosomal haploinsufficiency affects protein synthesis and if differentially translated proteins have a impact on the erythroid differentiation defect **(chapter 1)**. We generated a murine model with conditional inactivation of *Rps14* and demonstrated a p53-dependent erythroid differentiation defect with apoptosis at the transition from polychromatic to orthochromatic erythroblasts resulting in age- and erythroid stress dependent progressive anemia, megakaryocyte dysplasia, and loss of hematopoietic stem cell (HSC) quiescence **(chapter 2)**. Protein synthesis was significantly reduced in *Rps14* haploinsufficient hematopoietic stem cells and in particular in erythroid progenitor cells relative to wild-type cells. As assessed by quantitative proteomics, *Rps14* haploinsufficient erythroblasts expressed higher levels of proteins involved in innate immune signaling, notably the heterodimeric S100 calcium-binding proteins S100a8 and S100a9 (alarmins). S100a8 is functionally involved in the erythroid defect caused by the *Rps14* deletion, as addition of recombinant S100a8 was sufficient to induce a differentiation defect in wild-type erythroid cells (phenocopy), and genetic inactivation of *S100a8* expression rescued the erythroid differentiation defect of *Rps14*-haploinsufficient HSCs. Our data link *Rps14* haploinsufficiency in del(5q) MDS to activation of the innate immune system and induction of S100A8-S100A9 expression, leading to a p53-dependent erythroid differentiation defect. In future experiments I aim to focus on the role of chronic inflammation on myelodysplasia and on the role of monocytes and macrophages as disease-mediating, inflammatory bystander cells and ultimately, on how to therapeutically target this process.

A key question in the field is, which genes within the commonly deleted region (CDR) are necessary and sufficient for del(5q) HSC to achieve clonal dominance over normal HSC. *Csnk1a1* haploinsufficiency conferred increased intrinsic self-renewal of HSC and nuclear β-Catenin accumulation (**chapter 3**). In striking contrast, *Csnk1a1* homozygous inactivation is not tolerated in HSC due to activation of p53. The sensitivity of hematopoietic cells to *Csnk1a1*, β-catenin and p53 gene dosage provides a therapeutic window for targeting haploinsufficiency in del(5q) MDS cells.

The finding of targeting haploinsufficiency as a vulnerability of the hematopoietic stem cell in del(5q) MDS was a central concept in the study described in **chapter 4**. Here, we demonstrate that lenalidomide induces the ubiquitination of casein kinase 1A1 (CK1α) by the

E3 ubiquitin ligase CRL4(CRBN), resulting in CK1α degradation. Haploinsufficient expression sensitizes cells to lenalidomide therapy, providing a mechanistic basis for the therapeutic window of lenalidomide in del(5q) MDS. In future experiments I would like to test candidate molecules to specifically target the gene dosage effect in del(5q) HSC with limited effects on normal hematopoiesis, overcoming the problems of resistance to lenalidomide therapy and maintenance of the del(5q) MDS clone under therapy.

In the last part of the thesis (**chapter 5**) we aimed to create an artificial, transplantable BM niche that supports hematopoiesis while allowing for the genetic modification of both hematopoietic and mesenchymal cells as to dissect their interaction in steady state and under pathopyhsiological conditions (chapter 5). We established and characterized a multicomponent system that is optimal for the study of hematopoietic-mesenchymal interactions and the recapitulation of the native BM microenvironment in a transplantable mouse model. The combination of macro- and microporous β-TCP scaffolds and Matrigel optimally supports hematopoiesis, including hematopoietic recruitment, proliferation, and differentiation as well as ECM remodeling. In future experiments we intend to genetically modify stromal cells and study their impact on the HSC regulation in myeloproliferative neoplasms and their role in fibrotic transformation in myelofibrosis.

2. GENERAL DISCUSSION

In this final part, the different findings described in the thesis will be placed in perspective of the current knowledge and their implications for a better understanding of myelodysplastic syndromes and targeted therapy will be discussed.

Rps14 haploinsufficiency causes a block in erythroid differentiation mediated by S100A8 and S100A9

Summary of findings: *Heterozygous deletion of RPS14 occurs in del(5q) myelodysplastic syndrome (MDS) and has been linked to impaired erythropoiesis. We generated a murine model with conditional inactivation of Rps14 which recapitulates the erythroid phenotype of del(5q) MDS. Protein synthesis was significantly reduced in Rps14 haploinsufficient cells relative to wild-type cells, in particular in erythroid progenitor cells. Using quantitative proteomics and functional experiments in erythroblasts, we identified an unexpected link between Rps14 haploinsufficiency in del(5q) MDS, induction of S100A8-S100A9 expression and the p53-dependent erythroid differentiation defect.*

2.1.1 Innate immune system and inflammation in del(5q) MDS

Overexpression of immune-related genes is reported in MDS and hyperactivation of immune/toll-like receptor (TLR) signaling is a feature of MDS. We showed for the first time a functional link between activation of the innate immune system and ineffective hematopoiesis by induction of S100A8 and S100A9.

The heterodimeric protein complex S100A8/S100A9 is an endogenous TLR4 ligand upstream of TNFa leading to NF-kB activation and secretion of pro-inflammatory cytokines (Ehrchen et al. 2009). Our data demonstrate that S100a8 acts upstream of Tlr4 and Tnfα in the *Rps14* haploinsufficiency induced erythroid differentiation defect. Overactivation of TLRs has been implicated in HSC development, suggesting that changes in TLR expression and function could lead to dysregulated hematopoiesis (Maratheftis et al. 2007; Sioud and Floisand 2007; Boiko and Borghesi 2012). Further, overexpression or gain-of-function mutations in a subset of TLR4s has been described in MDS, but so far their direct functional effect on HSC remained elusive (Maratheftis, Andreakos et al. 2007).

MicroRNAs (miRNAs) further play a role in MDS as negative regulators of innate immune signaling in MDS (Starczynowski et al. 2010). miR-146a lies within chromosome 5q33.3 and its deletion occurs in 80% of all del(5q) MDS patients. Consistent with deletion of a single miR-147a allele, expression in HSC from del(5q) MDS patients is reduced by greater than 50%. miR-146a is also down-regulated in non-del(5q) MDS patients, suggesting that other mechanisms may contribute to its reduced expression in MDS. Concomitant knockdown of miR-145 and -146a using a miRNA decoy approach in mouse HSC resulted in elevated platelets, neutropenia, megakaryocytic dysplasia and myeloid leukemia (Starczynowski and

Karsan 2010; Starczynowski, Kuchenbauer et al. 2010). MiR-146a deficient HSCs produce higher levels of pro-inflammatory cytokines, such a IL-6, TNFα, granulocyte-macrophage colony-stimulating factor (GM-CSF) and IL-1ß, in response to TLR activation.

Of note, RPS14 and miR-145/miR-146a are universally co-deleted in the 5q- syndrome, and converge on TLR4 signaling (Starczynowski and Karsan 2010; Starczynowski, Kuchenbauer et al. 2010; Reynaud et al. 2011; Starczynowski et al. 2011; Rhyasen et al. 2013; Chang et al. 2014), highlighting the cooperating effects of genes on 5q (Figure 1). In future experiments, we will transduce *Rps14* and Csnk1a1 haploinsufficient mice with the miR decoy leading to haploinsufficient expression of miR-145/146a. We hypothesize that combination of these lesions will recapitulate the complete del(5q) MDS phenotype by activating TLR4 signaling and and a downstream inflammatory environment, including an increase of Tnfα.

Specific cytokines are elevated in the serum of MDS patients (Kordasti et al. 2009) and these inflammatory signals can alter proliferation and apoptosis of MDS HSPCs (Kristinsson et al. 2011; Takizawa et al. 2012). Indeed, chronic immune stimulation, coupled with senescence-dependent changes (Verschoor et al. 2013) in both HSPCs and the BM microenvironment (Raaijmakers et al. 2010) may be central to disease pathogenesis. Our analysis of *Rps14* haploinsufficient HSCs suggests that inflammatory cues induced by *Rps14* haploinsufficiency impact HSC aging and quiescence (Rossi et al. 2007; Pang et al. 2011; Reynaud, Pietras et al. 2011; Du et al. 2013). In patients with chronic inflammation, cytokines in bone marrow have been associated with inhibition of erythropoiesis (Means 1995). In particular, TNFα expression has been implicated in erythroid defects observed in patients with DBA (Bibikova et al. 2014) and is up-regulated in the bone marrow serum of MDS patients (Jacobs-Helber et al. 2003; Sawanobori et al. 2003). TNFα was shown to increase TLR4-expression in a dose-dependent manner, whereas depletion of TNFa with anti-TNFα treatment of MDS bone marrow cells resulted in decreased TLR4 expression, suggesting that the TLR4 expression is TNFα dependent. Furthermore, Maratheftis et al. found a significant correlation between TLR4 expression and apoptosis in CD34+ MDS BM cells, providing evidence for increased TLR4 expression and cell-intrinsic defects associated with MDS HSCs (Maratheftis, Andreakos et al. 2007).

Taken together, these studies and our study provide evidence for the role of HSC-expressed TLRs in the pathogenesis of MDS. Inhibition of TLRs or the inflammatory environment may represent an attractive therapeutic strategy in the treatment of MDS. Our data suggest that inhibiting TLRs, Nfkb signaling or S100A8/S100A9 might be the best strategy as inhibition of Tnfα alone was not sufficient to rescue the erythroid differentiation defect.

S100 proteins participate in an autoregulatory feedback loop with p53, serving both as upstream drivers of p53 transcription and as direct downstream p53 transcriptional targets (Tan et al. 1999; Mueller et al. 2005; Li et al. 2009; Bresnick et al. 2015). Consistent with these reports, our data demonstrate that p53 is required for induction of S100a8 expression

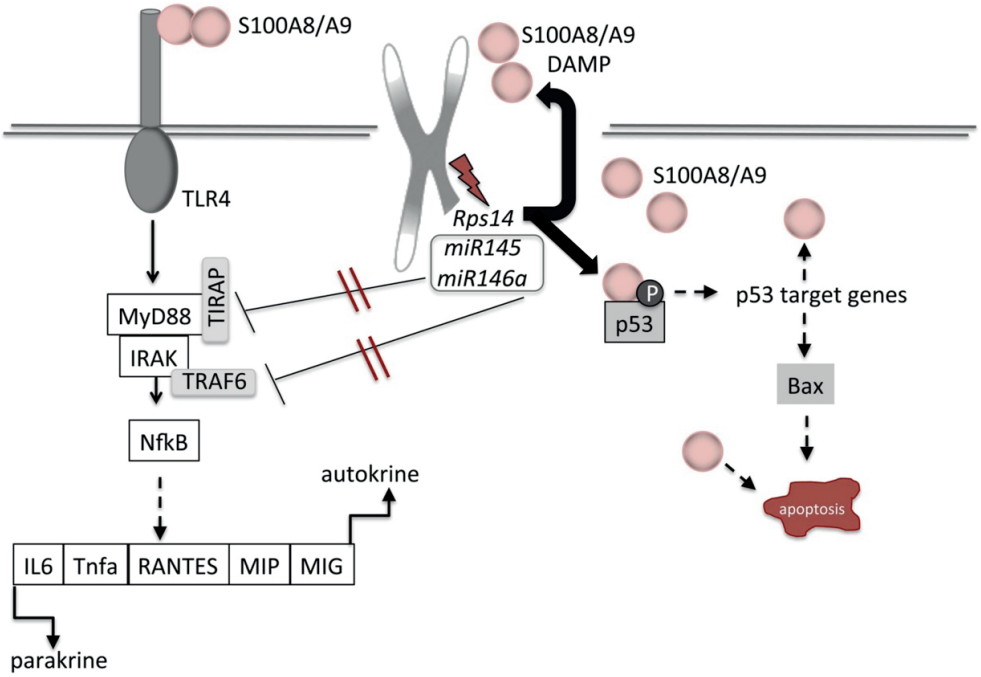

Supplementary figure 7

Figure 1: Proposed mechanism how compound haploinsufficiency of Rps14 (chapter 2), Csnk1a1 (chapter 3 and 4) and miRNA145/146a (Starczynowski, Kuchenbauer et al. 2010) converge on TLR4 signaling and induction of p53.

in *Rps14* haploinsufficient cells, and that recombinant S100a8 is sufficient to induce p53 activity in erythroid progenitor cells, leading to a block in terminal erythroid differentiation (Figure 1). It was shown in recent reports that S100 proteins can be intracellularly located and regulate cell growth, cell-cycle progression and apoptosis by interacting with the relevant intracellular signal-regulation pathways. S100 proteins can interact with p53 and affect p53 transcriptional activity, resulting in expression changes of p53 target genes (Ehrchen, Sunderkotter et al. 2009).

In summary, chronic innate immune signaling and activation is widely reported in MDS. Our studies in non-del(5q) MDS (normal karyotype) indicate that induction of S100A8 occurs as a stress response upon genetic abnormalities in MDS. The consequences of increased TLR signaling in MDS can result in systemic effects on hematopoiesis, such as those due to inflammation and abnormal adaptive and innate immunity in HSCs. In addition to these non-cell-autonomous consequences of chronic innate immune activation, increased TLR signaling within HSC from MDS patients was also reported and thought to contribute to cell-intrinsic defects in HSCs. We also demonstrated that S100A8/S100A9 exerts both extrinsic and intrinsic effects on hematopoiesis.

Open questions yet need to be answered in future studies:
1) How is chronic innate immune signaling and activation in MDS best measured?
2) How exactly is the innate immune pathway activated in MDS and in which hematopoietic lineage?
3) Which MDS subtypes (which mutations) exhibit activation of the innate immune system?

2.1.2 The erythroblastic island in MDS

In addition to granuloyctes and macrophages, which produce these proteins under steady-state conditions, other cell types induce S100A8/S100A9 expression in response to stress (Hiratsuka et al. 2006). We found significant induction of S100A8 in both $CD11b^+$ monocytes and $F4/80^+$ macrophages and concomitant increased expression of S100A8 in late-stage erythroblast, which was associated with p53 induction. Spatially, erythroid progenitor cells interact with a central macrophage in the erythroblastic island. Our data indicate that disruption of the regulatory mechanisms in the erythroblastic island contribute to the erythroid differentiation defects in *Rps14* haploinsufficient bone marrows.

S100A9 activation has been described in MDS patient samples and myeloid-derived suppressor cells (MDSC) driven by the S100A9/CD33 pathway perturb hematopoiesis (Chen et al. 2013). Elevated levels of circulating cytokines, chemokines, and interleukins, including interleukin 6 (IL6), transforming growth factor (TGF-ß), tumor necrosis factor-α (TNF-a), and interferon (INF-y), characterize chronic inflammation and malignancy and are commonly found to be up-regulated in MDS (Flores-Figueroa et al. 2002). It is also likely that local concentrations may be even higher within erythroid niches because of direct secretion by central macrophages (Chasis and Mohandas 2008). In patients with chronic inflammation, cytokines in bone marrow have been associated with inhibition of erythropoiesis. This suppression is mechanistically complex and multifactorial, not only because it is induced by multiple cytokines, chemokines and interleukins but also because each of these proteins by itself may have more than one effect upon erythroid development.

TNF-α inhibits erythropoiesis either by caspase-mediated cleavage of the major erythroid transcription factor GATA-1 resulting in apoptosis and/or by retarding proliferation; the precise mechanism(s) remains controversial (Dai et al. 2003). In MDS, macrophages have been shown to produce high levels of TNF-α (Flores-Figueroa, Gutierrez-Espindola et al. 2002). Elevated levels of INF-y induce both macrophages and erythroblasts to secrete soluble TRAIL (TNF-related apoptosis inducing ligand), which inhibits erythroblast differentiation (Zamai et al. 2000). IL-6 up-regulates hepcidin expression, which inhibits iron export by binding to the iron exporter ferroportin and inducing its internalization and degradation, thereby blocking availiability of iron for erythropoiesis (Nemeth and Ganz 2006; Nemeth and Ganz 2006).

In summary, there are myriad means by which elevated cytokines, chemokines and interleukins in MDS lead to disordered erythropoiesis. It remains an open question how MDS

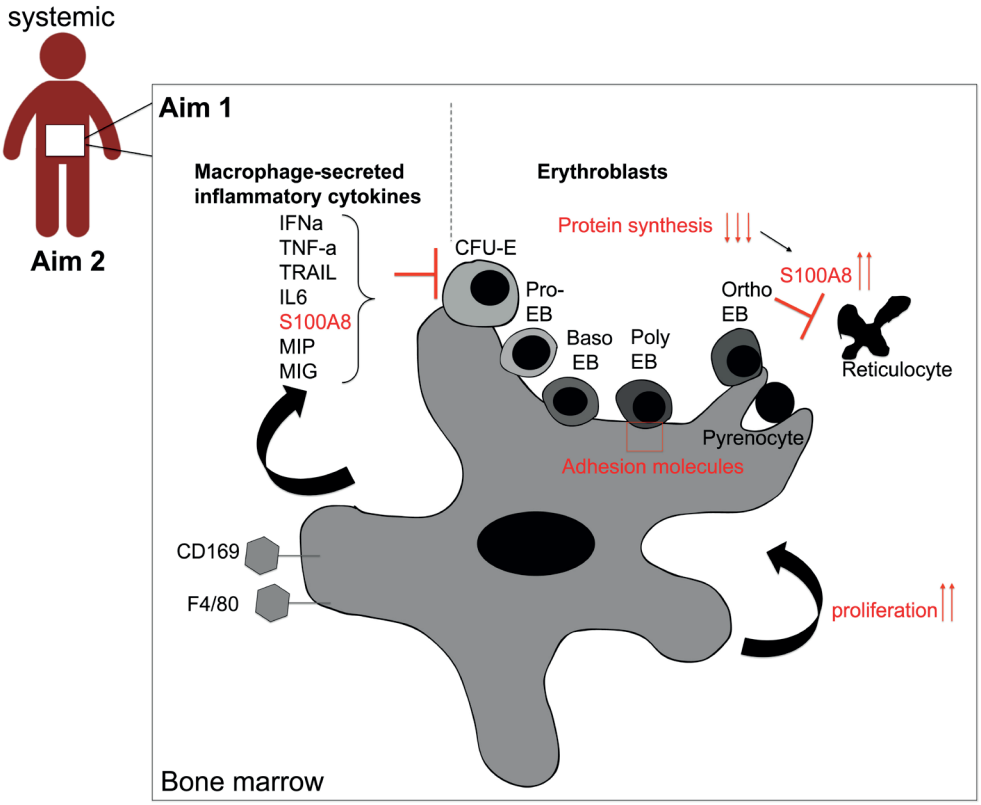

Figure 2: The erythroblastic island is the regulatory unit of erythropoiesis. From the CFU-E stage to the formation of the reticulocyte, developing erythroblasts attach to the macrophage. The underlying mechanisms of ineffective erythropoiesis and dysregulation in the erythroblastic island in del(5q) MDS and in ribosomopathies are not well understood. Our data revealed that Rps14 haploinsufficiency leads to induction of S100A8/S100A9 expression in macrophages and erythroblasts and leads to the terminal erythroid differentiation block.

contributes to elevated cytokines and how cytokines contribute to the disturbed regulation in the erythroblastic island. We demonstrated that an increase of S100A8 in macrophages and in erythroblasts causes a block in erythroid differentiation.

Future studies will dissect 1) how S100A8 in macrophages affects the erythroid differentiation and 2) if dysfunction in macrophages is sufficient to induce a block in erythroid differentiation (Figure 2).

2.1.3 Reduced protein synthesis in ribosomopathies

Ribosome biogenesis is a highly regulated, complex process (Fatica and Tollervey 2002). Eukaryotic ribosomes are comprised of 2 subunits: the small 40S subunit and the large 60S subunit. These subunits join together to form the active 80S ribosome. Ribosomes contain 4 structural ribosomal RNAs (rRNAs). The 40S subunit contains the 18S rRNA, and

the large 60S subunit contains the 28S, 5.8S, and 5S rRNAs. These rRNAs are complexed with approximately 79 ribosomal proteins in eukaryotic ribosomes. Ribosome assembly is a complex and highly regulated process using a significant investment of cellular biosynthetic energy. More than 200 assembly factors and small nucleolar RNAs (snoRNAs) are required to synthesize ribosomes.

The relative functional significance of rRNAs and the ribosomal proteins has been a matter of interest for many years. In the 1970s it was believed that ribosomal proteins were the functionally active part of the ribosome, whereas rRNA was essentially a scaffold to keep proteins in the optimal position. Since the 1980s this hypothesis was completely turned around and it was shown that ribosomal proteins are the scaffold for rRNAs. The crystal structure of the ribosome confirmed the predominance of rRNA sites, but also revealed that a number of ribosomal proteins were located in positions of functional importance, e.g. RPS12 at the decoding center, RPL11 and RPL10 as components involved in translation factor binding (Wool 1996). Over the years specific functions of many individual ribosomal proteins were identified and it is accepted that both proteins and RNA are essential for the optimal functioning of the ribosome.

Several ribosomal proteins have been found to have extraribosomal functions including DNA repair, autoregulation of ribosomal protein synthesis and translation and regulation of development of malignant transformation on mainly through interaction with p53 (Warner and McIntosh 2009). Ribosomopathies are disorders resulting from impaired ribosome biogenesis and function. Diamond-Blackfan-Anemia (DBA) and 5q- syndrome are the two clinical syndromes for which there is abundant genetic and experimental evidence that the impairment in erythropoiesis is due to mutations in ribosomal genes (Shimamura 2006; Ganapathi and Shimamura 2008). The mechanism by which translation control is perturbed in ribosomopathies still remains an outstanding question.

We demonstrated in our studies that *Rps14* haploinsufficiency leads to significantly decreased protein synthesis in bone marrow cells, in particular in erythroid cells. So far, it remains elusive which proteins were less translated in *Rps14* haploinsufficient erythroblasts and how they contribute to the erythroid differentiation defect and to induction of S100A8 in steady state hematopoiesis and under cellular stress conditions. It is reasonable to believe that the anemia in DBA is due to similar mechanisms. Future studies will clarify which proteins are less translated in *Rps14* haploinsufficiency and how they additionally contribute to the block in erythroid differentiation.

2.1.4 Functional relevance of ribosomal proteins in malignancies

Both tumor suppressor genes and oncogenes have been shown to modulate the ribosome protein biosynthesis as well as ribosome translation. The interaction of p53 with ribosomal proteins seems to be involved in the association between ribosomal proteins and cancer (Ruggero and Pandolfi 2003; Deisenroth and Zhang 2010).

We demonstrated a p53-dependent erythroid differentiation defect in *Rps14* haploinsufficiency and we were able to rescue the block in erythroid differentiation in a p53 null background. These findings indicate that p53 induction is critical for the anemia caused by ribosomal dysfunction. It was shown in cell lines that the combination of a defective ribosome biogenesis pathway and p53 activation results in strong antiproliferative responses (Lindstrom and Nister 2010). So far, it remains elusive if loss of p53 does not only rescue the erythroid differentiation defect but contributes to malignant transformation.

Ribosomopathies in general are characterized by hypoproliferative phenotypes such as bone marrow failure and anemia early in life, followed by elevated cancer risks later in life. This transition from hypo- to hyperproliferation presents an intriguing paradox in the field of hematology known as the "Dameshek's riddle" (Dameshek 1967). Recent cancer sequencing studies also revealed somatically acquired mutations and deletions in ribosomal proteins in T-cell acute lymphoblastic leukemia and solid tumors, further extending the list of ribosomopathies and strengthening the association between ribosomal defects and oncogenesis (De Keersmaecker et al. 2013). Future experiments will need to determine if Rps14 haploinsufficiency leads to malignant transformation in long-term studies by itself or with additional loss of p53.

2.2 Role of casein kinase 1A1 in the biology and targeted therapy of del(5q) MDS and as a target of lenalidomide

Summary of findings: *The casein kinase 1A1 gene (CSNK1A1) is a putative tumor suppressor gene located in the common deleted region for del(5q) myelodysplastic syndrome (MDS). We demonstrated in a murine model with conditional inactivation of Csnk1a1 that haploinsufficiency induces hematopoietic stem cell expansion and a competitive repopulation advantage, whereas homozygous deletion induces hematopoietic stem cell failure. Based on this finding, we found that heterozygous inactivation of Csnk1a1 sensitizes cells to a CSNK1 inhibitor relative to cells with two intact alleles. We further demonstrated that lenalidomide induces the ubiquitination of casein kinase 1A1 by the E3 ubiquitin ligase CUL4-RBX1-DDB1-CRBN, resulting in CK1α degradation. In addition, we identified recurrent somatic mutations in CSNK1A1 on the non-deleted allele of patients with del(5q) MDS. These studies demonstrate that CSNK1A1 plays a central role in the biology of del(5q) MDS and is a promising therapeutic target.*

β-catenin is a major driver of stem cell self-renewal and neoplasia in multiple cellular lineages (Willert et al. 2003; Baba et al. 2005; Yeung et al. 2010; Elyada et al. 2011). Hematopoietic stem cells have a graded response to b-catenin, with modest levels leading to increased stem cell self-renewal (Baba, Garrett et al. 2005), and more marked induction leading to stem cell exhaustion (Albuquerque et al. 2002; Kirstetter et al. 2006; Lane et al. 2010; Luis et al. 2011). Forced expression of β-catenin, in combination with HOXA9 and MEIS1, induces leukemia in progenitor cells (Wang et al. 2010), and β-catenin is essential for leukemia cells driven by the MLL-AF9 oncogene (Miller et al. 2013).

CK1a is a member of the β-catenin destruction complex and is therefore a known, central regulator of β-catenin activity (Cheong and Virshup 2011). In our studies, *Csnk1a1* haploinsufficiency conferred to increased intrinsic self-renewal of HSC, with associated nuclear β-catenin accumulation, cyclin D1 induction, and exit from quiescence in LT-HSCs. Increased LT-HSC proliferation and expansion was a cell-intrinsic effect in our study. Inactivation of *Csnk1a1* in stromal cells in our model caused stromal b-catenin levels to increase, with consequent effects on hematopoiesis, including pancytopenia and hematopoietic stem and progenitor cell depletion. This observation is consistent with recent studies demonstrating that b-catenin accumulation in the stroma negatively regulates HSC maintenance and might also contribute to leukaemogenesis (Lane, Sykes et al. 2010; Kode et al. 2014).

APC, another member of the β-catenin destruction complex, is also deleted in the vast majority of del(5q) MDS cases. Hematopoietic cells with *Apc* haploinsufficiency have been shown to have enhanced repopulation potential, indicating a cell intrinsic gain of function in the LT-HSC population. However, in contrast to *Csnk1a1* haploinsufficiency, *Apc* haploinsufficient bone marrow was unable to repopulate secondary recipients due to loss of the quiescent HSC population (Lane, Sykes et al. 2010; Wang et al. 2010). Different levels of Wnt activation may explain these findings. Similarly, deletions of *Csnk1a1* and of *Apc* in the gut have significantly different effects. While *Csnk1a1* deletion led to robust activation of Wnt target genes and proliferation without invasion, *Apc* deletion induced immediate dysplastic transformation and rapid death (Elyada, Pribluda et al. 2011). CK1a has many phosphorylation targets that could alter stem cell function (Bidere et al. 2009; Elyada, Pribluda et al. 2011; Wu et al. 2012). As has been postulated previously, it is possible that CK1a inactivation restrains hyperactive Wnt signaling through mechanisms yet to be defined. We aim to elucidate further mechanisms and targets of *Csnk1a1* in future studies which might explain the discrepany on the stem cell phenotype caused by *Csnk1a*1 and *Apc* haploinsufficiency.

Our sequencing studies revealed recurrent mutations in a gene located in an MDS common deleted region on chromosome 5q. SNP array studies have not identified any genes on 5q that undergo homozygous deletion in del(5q) MDS (Gondek et al. 2008; Graubert et al. 2009; Heinrichs et al. 2009). Indeed, our studies would indicate that homozygous inactivation of *CSNK1A1* would be highly deleterious to a hematopoietic cell. In functional studies, expression of the identified *CSNK1A1* E98V allele, in the setting of inactivation of both wild-type alleles to mimic the genetic context of the mutations observed in patients, caused an induction of nuclear β-catenin and a significant HSC cell cycle progression compared to expression of the wild-type *CSNK1A1*.

These specific mutations were confirmed in three independent studies. Heuser et al. found CSNK1A1 mutations in 17 of 237 patients with MDS or sAML and del(5q) (7.2%), comparable to our study (Heuser et al. 2015). Thirteen of the patients had missense mutations affecting glutamic acid E98 in exon 3 (76%) and four patients (24%) had missense

mutations affecting aspartic acid (D140), confirming these mutational hotspots. Bello et al. confirmed these mutations a few months later in 5 out of 104 del(5q) MDS patients (approximately 5%) and demonstrated concomitant up-regulation of ß-Catenin in those patients by gene expression analysis, similar to our results in the functional characterization of the mutation (Bello et al. 2015). In the most recent publication Alexander Smith and colleagues investigated the frequency and clinical associations of mutations of the *CSNK1A1* gene. Using whole exome sequencing and targeted next-generation re-sequencing, they detected mutations in seven (18%) out of 39 patients with isolated del(5q) at the time of diagnosis. Interestingly, they found that the mutation was higher in patients that progressed to AML (four out of 10; 40%) than it was in those who did not (three out of 29; 10%). Further they demonstrated that six out of seven patients (85%) with a CSNK1A1 with del(5q) MDS did not achieve a complete cytogenetic response to lenalidomide and that the median progression free survival for patients with the mutation was significantly lower than in those without the mutation (Smith et al. 2015). Larger studies are clearly needed to establish the effect of CSNK1A1 mutations on patient survival and response to treatment. Strikingly, the mutation in the CSNK1A1 gene was only found in patients with del(5q) not in MDS with normal karyotype. Future experiments using a conditional knock-in mouse strain will be helpful to study the long-term hematopoietic effects of the mutant allele expressed at physiological levels.

Targeting haploinsufficiency as a vulnerability in del(5q) MDS

The concept that genes within heterozygous deletions could cause vulnerabilities in cancer cells was first proposed 20 years ago (Frei 1993) and has been more recently demonstrated as CYCLOPS genes (cancer vulnerabilities unveiled by genomic loss) in cell lines (Nijhawan et al. 2012). We found that heterozygous inactivation of *Csnk1a1* causes hematopoietic stem cell expansion and β-catenin activation. In addition, we found that *Csnk1a1* haploinsufficiency sensitizes cells to casein kinase inhibition, demonstrating an approach for the targeting of heterozygous deletions in cancer.

Thus, it was of particular interest for us that lenalidomide targets CSNK1A1. We demonstrate that lenalidomide targets CSNK1A1 for degradation in myeloid cells, and that heterozygous deletion of *CSNK1A1* in del(5q) MDS provides a therapeutic window for selective targeting of the malignant cells not only by CSNK1 inhibitors but also by lenalidomide, explaining the good response in del(5q) MDS. Deletion of contiguous genes on chromosome 5q, such as *RPS14*, may further sensitize del(5q) cells to lenalidomide therapy by TP53 activation (Ebert et al. 2008; Narla and Ebert 2010). This mechanism of activity is consistent with the acquisition of TP53 mutations in del(5q) MDS patients who develop resistance to lenalidomide. In the future, we will combine *Rps14* and *Csnk1a1* haploinsufficiency and analyze if the compound haploinsufficiency sensitizes *Rps14/Csnk1a1* compound haploinsufficient cells even more for the treatment.

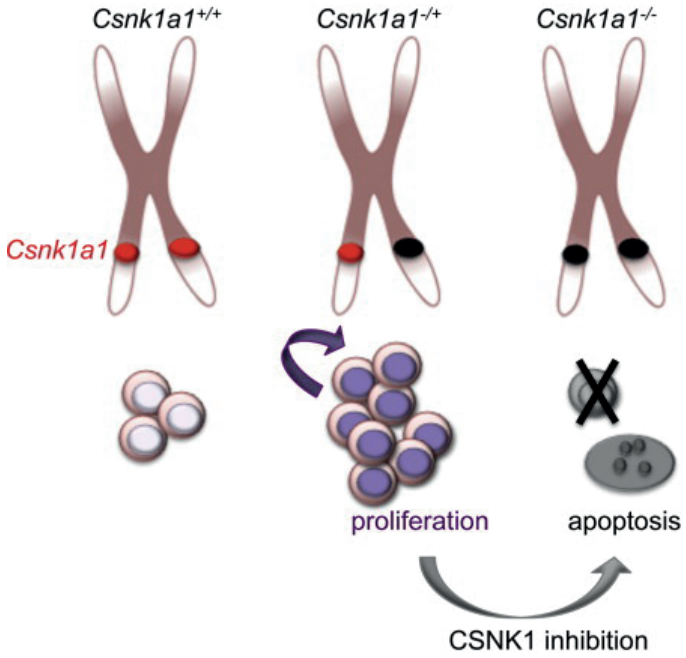

Figure 3: Csnk1a1 haploinsufficient cells are sensitized for treatment with a CSNK1 inhibitor and additional Csnk1a1 inhibition induces p53 and apoptosis while wild-type cells are not affected.

2.3 Dissecting hematopoietic-stromal interactions in a transplantable bone marrow niche at extramedullary sites

Summary of findings: *We characterized a multicomponent system that is optimal for the study of hematopoietic-mesenchymal interactions and the recapitulation of the native BM microenvironment in extramedullary sites. Macro- and microporous β-TCP scaffolds in combination with Matrigel optimally supported hematopoiesis, including hematopoietic recruitment, proliferation, and differentiation as well as ECM remodeling. β-TCP scaffolds in combination with Matrigel further promoted vascularization and allowed for mature bone deposition and hematopoiesis—stroma interactions in subcutaneous ectopic transplantations of the BM niche in a murine model.*

The rationale of our approach was inspired by extramedullary hematopoiesis in which the body develops hematopoietic-inductive spaces for the ectopic growth of HSPCs during states of bone marrow failure. This compensatory process is a well-recognized clinical observation that occurs in a variety of non-osseous tissues including the spleen, liver, and skin (Koch et al. 2003). Although extramedullary sites do not have the same microenvironment as the endogenous bone marrow, they are assumed to retain the essential elements involved in

HSPC migration and engraftment. We used a bioengineering approach to recapitulate this functional microenvironment to study hematopoietic biology. For the co-culture of HSPCs and mBMSCs/hMSCs, we applied β-TCP-printed scaffolds containing macro- and micropores similar to the bone—of inorganic (hydroxyapatite mineral) composition—in combination with an extracellular matrix gel—of organic (collagen type I matrix) composition.

Subdermally implanted scaffolds induced the development of two important tissue structures found in the bone marrow niche: a sinusoidal-like vasculature and interstitial space for the housing of a large number of hematopoietic cells. Previous studies of similar scaffold designs have shown that the pores 30–40 μm in diameter efficiently promote vascularization upon implantation (Fukano et al. 2006). These designs, although promoting vasculature, do not create a separate organized hematopoietic cavity for the influx and efflux of cells. Our study demonstrates that varying pore sizes of the β-TCP scaffolds from 500 to 800 μm was irrelevant in terms of hematopoietic support function. This is an interesting finding as particle geometry, porosity, pore size distribution, and scaffold continuity are properties known to determine cell/scaffold interactions and thus cell fate (Dazzi et al. 2006; Prockop 2009; Prockop et al. 2010). Pore size, however, has been only considered crucial within three main pore size intervals. According to Petite et al., pore sizes smaller than 15–50 μm result in fibrovascular growth, medium-sized pores of 50–150 μm encourage osteogenesis, while pores larger than 150 μm support the ingrowth of mineralized bone (Sacchetti et al. 2007). Contradicting studies even report that bone ingrowth is optimal for pore sizes varying from 300 to 900 μm (Tsigkou et al. 2010). The β-TCP scaffolds applied in our study had an interconnected net-like structure in the absence of dead-end pockets, macropores with mean pore size 500 or 800 μm, and micropores smaller than 15 μm. Our scaffolds were designed to maximize the surface area for stromal cell expansion, and we were able to demonstrate that these characteristics successfully promote vascular ingrowth as well as promotion of hematopoiesis. In the future, it will be sufficient to use larger pores which will make the production of the scaffolds easier. Our data so far show that the combination of a matrix component with b-TCP is more important than the geometry of a scaffold.

Our *in vitro* data suggest that complete hematopoiesis is promoted by β-TCP scaffolds in combination with structural proteins and cytokines provided by Matrigel as an extracellular matrix. First, β-TCP/Matrige scaffolds more robustly maintained a primitive LSK fraction over time. Second, hematopoietic differentiation in both myeloid and lymphoid lineages was supported after 14 days in Matrigel-containing conditions. Third, the CFU potential of β-TCP/Matrigel scaffolds was significantly increased compared to other conditions implicating that Matrigel supports both the functional maintenance of HSPCs and their differentiation capacity. Fourth, β-TCP/Matrigel scaffolds supported the remodeling of the ECM as an important requisite for cell differentiation and growth.

In vivo, β-TCP/Matrigel scaffolds resulted in strong hematopoietic recruitment to the sites of the ectopic transplantations as confirmed by the detection of myeloid and lymphoid

fractions 4 weeks after transplantations at levels comparable to the relative composition of the BM. Multinucleated osteoclasts and typically spindle-shaped osteoblasts were seen at the β-TCP scaffold/ECM interface. CD31-positive layers of recruited endothelial cells and adipose cells, typical for vascular niches, were both identified in explants showing the most efficient collagen matrix deposition. These data show that we generated sites of extramedullary hematopoiesis. One important question is which cytokines/growth factors/extracellular matrix components in matrigel lead to the significant support of hematopoiesis.

It will be important to define these important factors better in order to standardize the scaffolds and use them as a „screening tool“ for drug discovery studies and for dissecting the regulatory mechanisms of stromal cells and hematopoeitic cells in health and disease.

REFERENCES

Albuquerque, C., C. Breukel, et al. (2002). "The 'just-right' signaling model: APC somatic mutations are selected based on a specific level of activation of the beta-catenin signaling cascade." Hum Mol Genet **11**(13): 1549-1560.

Baba, Y., K. P. Garrett, et al. (2005). "Constitutively active beta-catenin confers multilineage differentiation potential on lymphoid and myeloid progenitors." Immunity **23**(6): 599-609.

Bello, E., A. Pellagatti, et al. (2015). "CSNK1A1 mutations and gene expression analysis in myelodysplastic syndromes with del(5q)." Br J Haematol.

Bibikova, E., M. Y. Youn, et al. (2014). "TNF-mediated inflammation represses GATA1 and activates p38 MAP kinase in RPS19-deficient hematopoietic progenitors." Blood **124**(25): 3791-3798.

Bidere, N., V. N. Ngo, et al. (2009). "Casein kinase 1alpha governs antigen-receptor-induced NF-kappaB activation and human lymphoma cell survival." Nature **458**(7234): 92-96.

Boiko, J. R. and L. Borghesi (2012). "Hematopoiesis sculpted by pathogens: Toll-like receptors and inflammatory mediators directly activate stem cells." Cytokine **57**(1): 1-8.

Bresnick, A. R., D. J. Weber, et al. (2015). "S100 proteins in cancer." Nat Rev Cancer **15**(2): 96-109.

Chang, K. H., A. Sengupta, et al. (2014). "p62 is required for stem cell/progenitor retention through inhibition of IKK/NF-kappaB/Ccl4 signaling at the bone marrow macrophage-osteoblast niche." Cell Rep **9**(6): 2084-2097.

Chasis, J. A. and N. Mohandas (2008). "Erythroblastic islands: niches for erythropoiesis." Blood **112**(3): 470-478.

Chen, X., E. A. Eksioglu, et al. (2013). "Induction of myelodysplasia by myeloid-derived suppressor cells." J Clin Invest **123**(11): 4595-4611.

Cheong, J. K. and D. M. Virshup (2011). "Casein kinase 1: Complexity in the family." Int J Biochem Cell Biol **43**(4): 465-469.

Dai, C., I. J. Chung, et al. (2003). "Reduction of cell cycle progression in human erythroid progenitor cells treated with tumour necrosis factor alpha occurs with reduced CDK6 and is partially reversed by CDK6 transduction." Br J Haematol **121**(6): 919-927.

Dameshek, W. (1967). "Riddle: what do aplastic anemia, paroxysmal nocturnal hemoglobinuria (PNH) and "hypoplastic" leukemia have in common?" Blood **30**(2): 251-254.

Dazzi, F., R. Ramasamy, et al. (2006). "The role of mesenchymal stem cells in haemopoiesis." Blood Rev **20**(3): 161-171.

De Keersmaecker, K., Z. K. Atak, et al. (2013). "Exome sequencing identifies mutation in CNOT3 and ribosomal genes RPL5 and RPL10 in T-cell acute lymphoblastic leukemia." Nat Genet **45**(2): 186-190.

Deisenroth, C. and Y. Zhang (2010). "Ribosome biogenesis surveillance: probing the ribosomal protein-Mdm2-p53 pathway." Oncogene **29**(30): 4253-4260.

Du, W., S. Amarachintha, et al. (2013). "Inflammation-mediated notch signaling skews fanconi anemia hematopoietic stem cell differentiation." J Immunol **191**(5): 2806-2817.

Ebert, B. L., J. Pretz, et al. (2008). "Identification of RPS14 as a 5q- syndrome gene by RNA interference screen." Nature **451**(7176): 335-339.

Ehrchen, J. M., C. Sunderkotter, et al. (2009). "The endogenous Toll-like receptor 4 agonist S100A8/S100A9 (calprotectin) as innate amplifier of infection, autoimmunity, and cancer." J Leukoc Biol **86**(3): 557-566.

Elyada, E., A. Pribluda, et al. (2011). "CKIalpha ablation highlights a critical role for p53 in invasiveness control." Nature **470**(7334): 409-413.

Fatica, A. and D. Tollervey (2002). "Making ribosomes." Curr Opin Cell Biol **14**(3): 313-318.

Flores-Figueroa, E., G. Gutierrez-Espindola, et al. (2002). "In vitro characterization of hematopoietic microenvironment cells from patients with myelodysplastic syndrome." Leuk Res **26**(7): 677-686.

Frei, E., 3rd (1993). "Gene deletion: a new target for cancer chemotherapy." Lancet **342**(8872): 662-664.

Fukano, Y., N. G. Knowles, et al. (2006). "Characterization of an in vitro model for evaluating the interface between skin and percutaneous biomaterials." Wound Repair Regen **14**(4): 484-491.

Ganapathi, K. A. and A. Shimamura (2008). "Ribosomal dysfunction and inherited marrow failure." Br J Haematol **141**(3): 376-387.

Gondek, L. P., R. Tiu, et al. (2008). "Chromosomal lesions and uniparental disomy detected by SNP arrays in MDS, MDS/MPD, and MDS-derived AML." Blood **111**(3): 1534-1542.

Graubert, T. A., M. A. Payton, et al. (2009). "Integrated genomic analysis implicates haploinsufficiency of multiple chromosome 5q31.2 genes in de novo myelodysplastic syndromes pathogenesis." PLoS One **4**(2): e4583.

Heinrichs, S., R. V. Kulkarni, et al. (2009). "Accurate detection of uniparental disomy and microdeletions by SNP array analysis in myelodysplastic syndromes with normal cytogenetics." Leukemia **23**(9): 1605-1613.

Heuser, M., M. Meggendorfer, et al. (2015). "Frequency and prognostic impact of casein kinase 1A1 mutations in MDS patients with deletion of chromosome 5q." Leukemia **29**(9): 1942-1945.

Hiratsuka, S., A. Watanabe, et al. (2006). "Tumour-mediated upregulation of chemoattractants and recruitment of myeloid cells predetermines lung metastasis." Nat Cell Biol **8**(12): 1369-1375.

Jacobs-Helber, S. M., K. H. Roh, et al. (2003). "Tumor necrosis factor-alpha expressed constitutively in erythroid cells or induced by erythropoietin has negative and stimulatory roles in normal erythropoiesis and erythroleukemia." Blood **101**(2): 524-531.

Kirstetter, P., K. Anderson, et al. (2006). "Activation of the canonical Wnt pathway leads to loss of hematopoietic stem cell repopulation and multilineage differentiation block." Nat Immunol **7**(10): 1048-1056.

Koch, C. A., C. Y. Li, et al. (2003). "Nonhepatosplenic extramedullary hematopoiesis: associated diseases, pathology, clinical course, and treatment." Mayo Clin Proc **78**(10): 1223-1233.

Kode, A., J. S. Manavalan, et al. (2014). "Leukaemogenesis induced by an activating beta-catenin mutation in osteoblasts." Nature **506**(7487): 240-244.

Kordasti, S. Y., B. Afzali, et al. (2009). "IL-17-producing CD4(+) T cells, pro-inflammatory cytokines and apoptosis are increased in low risk myelodysplastic syndrome." Br J Haematol **145**(1): 64-72.

Kristinsson, S. Y., M. Bjorkholm, et al. (2011). "Chronic immune stimulation might act as a trigger for the development of acute myeloid leukemia or myelodysplastic syndromes." J Clin Oncol **29**(21): 2897-2903.

Lane, S. W., S. M. Sykes, et al. (2010). "The Apc(min) mouse has altered hematopoietic stem cell function and provides a model for MPD/MDS." Blood **115**(17): 3489-3497.

Li, C., H. Chen, et al. (2009). "A novel p53 target gene, S100A9, induces p53-dependent cellular apoptosis and mediates the p53 apoptosis pathway." Biochem J **422**(2): 363-372.

Lindstrom, M. S. and M. Nister (2010). "Silencing of ribosomal protein S9 elicits a multitude of cellular responses inhibiting the growth of cancer cells subsequent to p53 activation." PLoS One **5**(3): e9578.

Luis, T. C., B. A. Naber, et al. (2011). "Canonical wnt signaling regulates hematopoiesis in a dosage-dependent fashion." Cell Stem Cell **9**(4): 345-356.

Maratheftis, C. I., E. Andreakos, et al. (2007). "Toll-like receptor-4 is up-regulated in hematopoietic progenitor cells and contributes to increased apoptosis in myelodysplastic syndromes." Clin Cancer Res **13**(4): 1154-1160.

Means, R. T., Jr. (1995). "Pathogenesis of the anemia of chronic disease: a cytokine-mediated anemia." Stem Cells **13**(1): 32-37.

Miller, P. G., F. Al-Shahrour, et al. (2013). "In Vivo RNAi screening identifies a leukemia-specific dependence on integrin beta 3 signaling." Cancer Cell **24**(1): 45-58.

Mueller, A., B. W. Schafer, et al. (2005). "The calcium-binding protein S100A2 interacts with p53 and modulates its transcriptional activity." J Biol Chem **280**(32): 29186-29193.

Narla, A. and B. L. Ebert (2010). "Ribosomopathies: human disorders of ribosome dysfunction." Blood **115**(16): 3196-3205.

Nemeth, E. and T. Ganz (2006). "Hepcidin and iron-loading anemias." Haematologica **91**(6): 727-732.

Nemeth, E. and T. Ganz (2006). "Regulation of iron metabolism by hepcidin." Annu Rev Nutr **26**: 323-342.

Nijhawan, D., T. I. Zack, et al. (2012). "Cancer vulnerabilities unveiled by genomic loss." Cell **150**(4): 842-854.

Pang, W. W., E. A. Price, et al. (2011). "Human bone marrow hematopoietic stem cells are increased in frequency and myeloid-biased with age." Proc Natl Acad Sci U S A **108**(50): 20012-20017.

Prockop, D. J. (2009). "Repair of tissues by adult stem/progenitor cells (MSCs): controversies, myths, and changing paradigms." Mol Ther **17**(6): 939-946.

Prockop, D. J., D. J. Kota, et al. (2010). "Evolving paradigms for repair of tissues by adult stem/progenitor cells (MSCs)." J Cell Mol Med **14**(9): 2190-2199.

Raaijmakers, M. H., S. Mukherjee, et al. (2010). "Bone progenitor dysfunction induces myelodysplasia and secondary leukaemia." Nature **464**(7290): 852-857.

Reynaud, D., E. Pietras, et al. (2011). "IL-6 controls leukemic multipotent progenitor cell fate and contributes to chronic myelogenous leukemia development." Cancer Cell **20**(5): 661-673.

Rhyasen, G. W., L. Bolanos, et al. (2013). "Targeting IRAK1 as a therapeutic approach for myelodysplastic syndrome." Cancer Cell **24**(1): 90-104.

Rossi, D. J., D. Bryder, et al. (2007). "Deficiencies in DNA damage repair limit the function of haematopoietic stem cells with age." Nature **447**(7145): 725-729.

Ruggero, D. and P. P. Pandolfi (2003). "Does the ribosome translate cancer?" Nat Rev Cancer **3**(3): 179-192.

Sacchetti, B., A. Funari, et al. (2007). "Self-renewing osteoprogenitors in bone marrow sinusoids can organize a hematopoietic microenvironment." Cell **131**(2): 324-336.

Sawanobori, M., S. Yamaguchi, et al. (2003). "Expression of TNF receptors and related signaling molecules in the bone marrow from patients with myelodysplastic syndromes." Leuk Res **27**(7): 583-591.

Shimamura, A. (2006). "Inherited bone marrow failure syndromes: molecular features." Hematology Am Soc Hematol Educ Program: 63-71.

Sioud, M. and Y. Floisand (2007). "TLR agonists induce the differentiation of human bone marrow CD34+ progenitors into CD11c+ CD80/86+ DC capable of inducing a Th1-type response." Eur J Immunol **37**(10): 2834-2846.

Smith, A. E., A. G. Kulasekararaj, et al. (2015). "CSNK1A1 mutations and isolated del(5q) abnormality in myelodysplastic syndrome: a retrospective mutational analysis." Lancet Haematol **2**(5): e212-221.

Starczynowski, D. T. and A. Karsan (2010). "Deregulation of innate immune signaling in myelodysplastic syndromes is associated with deletion of chromosome arm 5q." Cell Cycle **9**(5): 855-856.

Starczynowski, D. T., F. Kuchenbauer, et al. (2010). "Identification of miR-145 and miR-146a as mediators of the 5q- syndrome phenotype." Nat Med **16**(1): 49-58.

Starczynowski, D. T., W. W. Lockwood, et al. (2011). "TRAF6 is an amplified oncogene bridging the RAS and NF-kappaB pathways in human lung cancer." J Clin Invest **121**(10): 4095-4105.

Takizawa, H., S. Boettcher, et al. (2012). "Demand-adapted regulation of early hematopoiesis in infection and inflammation." Blood **119**(13): 2991-3002.

Tan, M., C. W. Heizmann, et al. (1999). "Transcriptional activation of the human S100A2 promoter by wild-type p53." FEBS Lett **445**(2-3): 265-268.

Tsigkou, O., I. Pomerantseva, et al. (2010). "Engineered vascularized bone grafts." Proc Natl Acad Sci U S A **107**(8): 3311-3316.

Verschoor, C. P., J. Johnstone, et al. (2013). "Blood CD33(+)HLA-DR(-) myeloid-derived suppressor cells are increased with age and a history of cancer." J Leukoc Biol **93**(4): 633-637.

Wang, J., A. A. Fernald, et al. (2010). "Haploinsufficiency of Apc leads to ineffective hematopoiesis." Blood **115**(17): 3481-3488.

Wang, Y., A. V. Krivtsov, et al. (2010). "The Wnt/beta-catenin pathway is required for the development of leukemia stem cells in AML." Science **327**(5973): 1650-1653.

Warner, J. R. and K. B. McIntosh (2009). "How common are extraribosomal functions of ribosomal proteins?" Mol Cell **34**(1): 3-11.

Willert, K., J. D. Brown, et al. (2003). "Wnt proteins are lipid-modified and can act as stem cell growth factors." Nature **423**(6938): 448-452.

Wool, I. G. (1996). "Extraribosomal functions of ribosomal proteins." Trends Biochem Sci **21**(5): 164-165.

Wu, S., L. Chen, et al. (2012). "Casein kinase 1alpha regulates an MDMX intramolecular interaction to stimulate p53 binding." Mol Cell Biol **32**(23): 4821-4832.

Yeung, J., M. T. Esposito, et al. (2010). "beta-Catenin mediates the establishment and drug resistance of MLL leukemic stem cells." Cancer Cell **18**(6): 606-618.

Zamai, L., P. Secchiero, et al. (2000). "TNF-related apoptosis-inducing ligand (TRAIL) as a negative regulator of normal human erythropoiesis." Blood **95**(12): 3716-3724.

A

ADDENDUM

ENGLISH SUMMARY

The studies presented in this thesis focused on the identification of genes that play a central role in the pathogenesis of myelodysplastic syndromes with a deletion of the short arm (q) of chromosome 5, the del(5q) MDS in **chapters 2-4**. The overall goal of the projects was to gain a better understanding of how gene haploinsufficiency in (del)5q MDS leads to a clonal advantage, ineffective hematopoiesis and how haploinsufficiency can be targeted (**chapter 2-4**).

Heterozygous deletion of *RPS14* occurs in del(5q) myelodysplastic syndrome (MDS) and has been linked to impaired erythropoiesis, characteristic of this disease subtype. So far, it was not well understood how ribosomal haploinsufficiency affects protein synthesis and if differentially translated proteins have a impact on the erythroid differentiation defect **(chapter 1)**. We generated a murine model with conditional inactivation of *Rps14* and demonstrated a p53-dependent erythroid differentiation defect with apoptosis at the transition from polychromatic to orthochromatic erythroblasts resulting in age- and erythroid stress dependent progressive anemia, megakaryocyte dysplasia, and loss of hematopoietic stem cell (HSC) quiescence **(chapter 2)**. Protein synthesis was significantly reduced in *Rps14* haploinsufficient hematopoietic stem cells and in particular in erythroid progenitor cells relative to wild-type cells. As assessed by quantitative proteomics, *Rps14* haploinsufficient erythroblasts expressed higher levels of proteins involved in innate immune signaling, notably the heterodimeric S100 calcium-binding proteins S100a8 and S100a9 (alarmins). S100a8 is functionally involved in the erythroid defect caused by the *Rps14* deletion, as addition of recombinant S100a8 was sufficient to induce an erythroid differentiation defect in wild-type erythroid cells (phenocopy), and genetic inactivation of *S100a8* expression rescued the erythroid differentiation defect of *Rps14*-haploinsufficient HSCs. Our data link *Rps14* haploinsufficiency in del(5q) MDS to activation of the innate immune system and induction of S100A8-S100A9 expression, leading to a p53-dependent erythroid differentiation defect. In future experiments I aim to focus on the role of chronic inflammation on myelodysplasia and on the role of monocytes and macrophages as disease-mediating, inflammatory bystander cells and ultimately, on how to therapeutically target this process.

A key question in the field is, which genes within the commonly deleted region (CDR) are necessary and sufficient for del(5q) HSC to achieve clonal dominance over normal HSC. *Csnk1a1* haploinsufficiency conferred increased intrinsic self-renewal of HSC and nuclear ß-Catenin accumulation (**chapter 3**). In striking contrast, *Csnk1a1* homozygous inactivation is not tolerated in HSC due to activation of p53. The sensitivity of hematopoietic cells to *Csnk1a1*, β-catenin and p53 gene dosage provides a therapeutic window for targeting haploinsufficiency in del(5q) MDS cells.

The finding of targeting haploinsufficiency as a vulnerability of the hematopoietic stem cell in del(5q) MDS was a central concept in the study described in **chapter 4**. Here, we demonstrate that lenalidomide induces the ubiquitination of casein kinase 1A1 (CK1α) by the E3 ubiquitin ligase CRL4(CRBN), resulting in CK1α degradation. Haploinsufficient expression sensitizes cells to lenalidomide therapy, providing a mechanistic basis for the therapeutic window of lenalidomide in del(5q) MDS. In future experiments I would like to test candidate molecules to specifically target the gene dosage effect in del(5q) HSC with limited effects on normal hematopoiesis, overcoming the problems of resistance to lenalidomide therapy and maintenance of the del(5q) MDS clone under therapy.

In the last part of the thesis (**chapter 5**) we aimed to create an artificial, transplantable BM niche that supports hematopoiesis while allowing for the genetic modification of both hematopoietic and mesenchymal cells as to dissect their interaction in steady state and under pathopyhsiological conditions (chapter 5). We established and characterized a multicomponent system that is optimal for studying hematopoietic-mesenchymal interactions and for the recapitulation of the native BM microenvironment in a transplantable extramedullary niche (mouse model). The combination of macro- and microporous β-TCP scaffolds and Matrigel optimally supports hematopoiesis, including hematopoietic recruitment, proliferation, and differentiation as well as ECM remodeling. In future experiments we intend to genetically modify stromal cells and study their impact on the HSC regulation in myeloproliferative neoplasms and their role in fibrotic transformation in myelofibrosis.

DUTCH SUMMARY (NEDERLANDSE SAMENVATTING)

De studies besproken in dit proefschrift richtten zich op de identificatie van genen die een belangrijke rol spelen in de pathogenese van het myelodysplastisch syndroom (MDS) met een deletie van de korte arm (q) van chromosoom 5, de del(5q). Het doel van deze studies was om beter te begrijpen hoe haploinsufficiëntie in (del)5q MDS kan leiden tot klonale uitgroei en ineffectieve hematopoiese, en hoe deze haploinsufficiëntie kan worden behandeld.

Heterozygote deletie van RPS14 komt voor in del(5q) MDS en is geassocieerd met een dysfunctionele erythropoiese, karakteristiek voor dit subtype van MDS. Het is echter niet goed bekend op welke manier deze ribosomale haploinsufficiëntie invloed uitoefent op de eiwit synthese, en of differentieel getransleerde eiwitten een rol spelen bij het erythroïde differentiatie defect dat wordt gezien in dit subtype van MDS (**hoofdstuk 1**). Om deze vraag te kunnen beantwoorden hebben wij een muismodel gemaakt waarin sprake is van conditionele inactivatie van Rps14. In dit muismodel vonden wij een p53-afhankelijk erythroïde differentiatie defect, waarbij apoptose optreedt in de transitie van polychromatische naar orthochromatische erytroblasten. Dit leidde tot een leeftijd- en erythroïde stress-afhankelijke progressieve anemie, dysplasie van megakaryocyten en een verlies van hematopoietische stamcel (HSC) “quiescence” (**hoofdstuk 2**).

De eiwitsynthese is significant verminderd in Rps14 haploinsufficiënte HSCs in vergelijking met wild type cellen, met name in erythroïde voorloper cellen. Middels kwantitatieve proteoom studies konden we aantonen dat Rps14 haploinsufficiënte erytroblasten een hogere expressie hebben van eiwitten die betrokken zijn bij de aangeboren immuun respons, in het bijzonder de heterodimerische S100 calcium bindende eiwitten S100a8 en S100a9 (alarmins) (Hoofdstuk..). Wij hebben laten zien dat S100a8 functioneel betrokken is bij het erythroïde defect ten gevolge van Rps14 haploinsufficientie: Toevoeging van recombinant S100a8 bleek voldoende om een differentiatie defect te induceren in wild type erythroïde cellen (phenocopy), en omgekeerd bleek dat genetische inactivatie van S100a8 het erythroïde differentiatie defect van Rps14-haploinsufficiënte HSCs opheft.. Deze data verbindt Rps14 haploinsufficiëntie in del(5q) MDS met inactivatie van het aangeboren immuun systeem en de inductie van S100A8-S100A9 expressie, wat leidt tot een p53 afhankelijk differentiatie defect. In vervolg experimenten ben ik van plan mij te richten op de rol van chronische ontsteking in myelodysplasie en op de functie van monocyten en macrofagen als bij deze ziekte betrokken zijnde ontstekingscellen. Tot slot zal ik mij richten op de vraag hoe dit proces het beste therapeutisch behandeld kan worden.

Een belangrijke vraag in dit vakgebied is welke genen in de “common deleted region” (CDR) noodzakelijk en voldoende zijn voor de klonale uitgroei van HSCs die wordt gezien bij del(5q) MDS. Csnk1a1 haploinsufficiëntie leidt tot een verhoogde, intrinsieke zelfvernieuwing van HSCs en tot opstapeling van nucleair β-catenine (**hoofdstuk 3**).

Daarentegen wordt homozygote inactivatie van Csnk1a1 niet getolereerd in HSC, vanwege de activatie van p53. Deze genuanceerde gevoeligheid van HSCs voor de hoeveelheid Csnk1a1, e en p53 activiteitbiedt aangrijpingspunten voor therapeutische manipulatie van de haploinsufficiëntie in del(5q) MDS.

Deze mogelijkheid om de haploinsufficiënte status van HSCs in del(5q) MDS als doelwit te gebruiken staat centraal in de studie die beschreven wordt in **hoofdstuk 4.** In dit hoofdstuk tonen wij dat lenalidomide de ubiquitinatie van casein kinase 1A1 (CK1α) induceert middels de E3 ubitiquitin ligase CRL4 (CRBN), wat resulteert in de degradatie van CK1α. Aangezien haploinsufficiëntie cellen gevoelig maakt voor behandeling met lenalidomide, geeft deze bevinding een mechanistische basis voor het therapeutische gebruik van lenalidomide in del(5q) MDS. In vervolg experimenten zou ik graag kandidaat moleculen testen die aangrijpen op het gen-doserings effect in del(5q) HSCs en minimale effecten hebben op de normale hematopoiese, om zo het probleem van therapie resistentie voor lenalidomide, en de persistente aanwezigheid van de del(5q) MDS kloon tijdens behandeling te voorkomen.

In het laatste deel van dit proefschrift **(hoofdstuk 5)** hebben we gepoogd een transplanteerbaar beenmerg niche model te maken waarinde normale hematopoiese wordt ondersteund, en de mogelijkheid biedt voor genetische modificatie van zowel de hematopoietische als de mesenchymale cellen, zodat de interacties in normale en pathofysiologische condities onderzocht kunnen worden (hoofdstuk 5). We hebben hiervoor een multi-componenten systeem gemaakt en gekarakteriseerd, dat optimaal is voor onderzoek naar de hematopoietische-mesenchymale interacties en voor het nabootsen van het micromilieu in het beenmerg in een transplanteerbaar model. De combinatie van macro- en microporeuze β-TCP “scaffolds” en Matrigel ondersteunt optimale hematopoiese, inclusief hematopoietische recruitering , proliferatie en differentiatie van hematopoietische stam en progenitor cellen, en extracellulaire matrix (ECM) re-modellering. In toekomstige studies streven wij ernaar stromale cellen genetisch te modificeren en hun rol in HSC regulatie in myeloproliferatieve maligniteiten, en fibrotische transformatie in myelofibrose te onderzoeken.

CURRICULUM VITAE

Rebekka K.M. Schneider was born in Bonn, Germany, on November 18th, 1981. After receiving her high school diploma in Aachen, she went to Medical School in Aachen and graduated in 2007. She performed her MD thesis in the Institute of Pathology in Aachen (Supervisor Prof. R. Knuechel-Clarke) on the role of mesenchymal stromal cells in wound healing of the skin. She defended her MD thesis in June 2008 with *summa cum laude*. She started her clinical training (residency and fellowship) in Pathology in 2008 and in parallel collaborated with the Department of Hematology in Aachen to dissect the role of mesenchymal stromal cells in myeloproliferative neoplasms. In this time period, she further supervised MD students, master students and PhD students and was awarded multiple research grants to conduct her research in parallel to her clinical training. She performed her PhD training mainly in Benjamin L. Ebert's lab at the Brigham and Women's Hospital in Boston, MA, USA from 2012-2015. She dissected the role of haploinsufficiency of genes on 5q on the clonal advantage and erythroid differentiation defect on del(5q) MDS. She was awarded with the Artur-Pappenheim Award of the German Society of Hematology (DGHO), the Tito-Bastianello Award of the International MDS Society and the Innovation Award of Academic Medicine in Germany for her PhD work.

FELLOWSHIPS

01/2014-04/2015 Research Fellowship Award, Edward P. Evans MDS Foundation
01/2012-12/2013 Research Fellowship, German Research Foundation (DFG)

PRIZES, AWARDS AND HONORS

2016 Innovationspreis Deutsche Hochschulmedizin (Award for Innovation in Medicine, Consortium of Academic Medicine Germany) (10 000€)
2016 Arthur Pappenheim Award, German Society of Hematology and Oncology (DGHO) (7 500€)
2015 Tito Bastianello Young Investigator Award, MDS Foundation ($4 000)
2015 Abstract Achievement Award, American Society of Hematology. (500€)
2015 Best Abstract Award, FASEB meeting Hematological Malignancies (500€)
2014 Year's Best in Hematology, Schneider et al. Role of casein kinase 1A1 in the biology and targeted therapy of del(5q) MDS", selected by the American Society of Hematology
2013 Abstract Achievement Award, American Society of Hematology (500€)
2010 Best Abstract Award, German Society of Pathology (500€)
2009 Best Abstract and Presentation Award, German Society of Stem Cell Research (500€)
2009 Borchers Award of the RWTH Aachen University for excellent doctoral thesis, June 2009

SUPERVISION OF GRADUATE STUDENTS AND POSTDOCTORAL FELLOWS

2008-2012	6 graduate students (Andrea Püllen, Julia Anraths, Simone Couson, Kristina Peuckert, Julia van de Kamp, Isabelle Leisten); RWTH Aachen
06/2013-08/2013	Lisa P. Chu, HONORS award American Society of Hematology
06/2013-08/2013	Can Aztekin, Istanbul (Turkey), Summer Student Harvard Stem Cell Institute
09/2013-12/2015	Emma Fink, MD/PhD Student, Harvard Medical School, Boston, USA

TEACHING ACTIVITIES

	RWTH Aachen University Hospital
2008- 2012	Lectures and Practical Course Cardiovascular Pathology
2008- 2012	Lectures and Practical Course Aging
2008- 2012	Lectures and Practical Course Hematology and Immunology
2008- 2012	Practical Course Developmental Pathology
2009-2012	Lectures and Practical Course Oncology
2010-2012	Lectures and Practical Course Pulmonology
2009-2011	Discussion and interpretation of critical cases in cardiothoracic Surgery
2008-2011	Demonstration and discussion of clinical autopsies
2015-2016	Lectures and Practical Course Hematology and Immunology

INSTITUTIONAL RESPONSIBILITIES

2014-2015	Instructor and Graduate Student Advisor, Brigham and Women's Hospital, Hematology Division, Boston, MA

ORGANISATION OF SCIENTIFIC MEETINGS

2014-2015	Work in Progress Meeting, Department of Hematology, Brigham and Women's Hospital, Harvard Medical School, Boston, MA, USA

MEMBERSHIPS OF SCIENTIFIC SOCIETIES

International Academy of Pathology (IAP); Harvard Stem Cell Institute (HSCI); Harvard Postdoctoral Association; Stem Cell Network Northrhine Westphalia, Germany; German Society for Stem Cell Research (GSZ); American Society of Hematology (ASH); European Hematology Association (EHA); German Society of Pathology (DGP)

LIST OF PUBLICATIONS

Research articles (peer-reviewed)

Published articles: 43
H-Index (ISI): 21
citation (ISI): 1493
first and last authorship: 14

1. Kramann R, Goettsch C, Wongboonsin J, Iwata H, **Schneider RK**, Kuppe C, Kaesler N, Chang-Panesso M, Machado FG, Gratwohl S, Madhurima K, Hutcheson JD, Jain S, Aikawa E, Humphreys BD. Adventitial MSC-like Cells Are Progenitors of Vascular Smooth Muscle Cells and Drive Vascular Calcification in Chronic Kidney Disease. **Cell Stem Cell**. 2016 Nov 3;19(5):628-642.

2. Obeng EA, Chappell RJ, Seiler M, Chen MC, Campagna D, Schmidt PJ, **Schneider RK**, Yu L, Lord AM, McConkey ME, Ali AM, Raza A, Buonamici S, Smith PG, Mullally A, Wu CJ, Fleming MD and Ebert BL. Physiologic expression of *Sfb1*K700E causes impaired erythropoiesis, aberrant splicing, and sensitivity to a spliceosome inhibitor. **Cancer Cell**. 2016 Sep 12;30(3):404-17.

3. **Schneider RK**, Schenone M, Ventura Ferreira M, Kramann R, Joyce CE, Hartigan C Beier F, Brümmendorf TH, Germing U, Platzbecker U, Büsche G, Knüchel R, Chen MC, Waters CS, Chen E, Chu LP, Novina CD, Lindsley RC, Carr SA, Ebert BL. Rps14 haploinsufficiency causes a block in erythroid differentiation mediated by S100A8/S100A9. **Nature Medicine** 2016 Mar;22(3):288-97.

4. Elf S, Abdelfattah N, Chen E, Perales-Patón J, Rosen E, Ko A, Peisker F, Florescu N, Giannini S, Wolach O, Morgan E, Losman JA, **Schneider RK**, Al-Shahrour F, Mullally A. Mutant calreticulin requires both its mutant C-terminus and the thrombopoietin receptor for oncogenic transformation. **Cancer Discovery**, 2016 Apr;6(4):368-81.

5. Puram RV, Kowalczyk MS, de Boer CG, **Schneider RK**, Miller PG, McConkey M, Tothova Z, Tejero H, Heckl D, Järås M, Chen M, Li H, Tamayo A, Cowley GS, Rozenblatt-Rosen O, Al-Shahrour F, Regev A, Ebert BL. Core circadian clock genes regulate leukemia stem cells in AML. **Cell.** 2016 Apr 7;165(2):303-16.

6. Ventura Ferreira MS, Bergmann C, Bodensik I, Peukert K, Abert J, Kramann, R, Kachel, P, Rath B, Rütten S, Knuchel R, Ebert BL, Fischer H, Brümmendorf T, **Schneider RK**. An engineered multicomponent bone marrow niche for the recapitulation of hematopoiesis at ectopic transplantation sites. **Journal of Hematology and Oncology,** 2016 Jan 25;9:4.

7. Kowalczyk MS, Tirosh I, Heckl D, Nageswara Rao T, Dixit A, Haas BJ, **Schneider RK**, Wagers AJ, Ebert BL, Regev A. Single cell RNA-seq reveals changes in cell cycle and differentiation programs upon aging of hematopoietic stem cells. **Genome Res.** 2015 Dec;25(12):1860-72.

8. Wen JQ, Yang Q, Goldenson B, Malinge S, Lasho T, **Schneider RK**, Breyfogle LJ, Schultz R, Gilles L, Koppikar P, Abdel-Wahab O, Pardanani A, Stein B, Gurbuxani S, Mullally A, Levine RL, Tefferi A, Crispino JD. Targeting megakaryocytic-induced fibrosis in myeloproliferative neoplasms by AURKA inhibition. **Nature Medicine**. 2015 Dec;21(12):1473-80.

9. Krönke J*, Fink EC*, Hollenbach PW, MacBeth KJ, Hurst SN, Udeshi ND, Chamberlain PP, Mani DR, Wah Man H, Gandhi AK, Svinkina T, **Schneider RK,** McConkey M, Järås M, Griffiths E, Wetzler M, Bullinger L, Cathers BE, Carr SA, Chopra R, and Ebert BL. Lenalidomide induces ubiquitination and degradation of CK1α in del(5q) MDS**. Nature**. 2015 July 9;523(7559):183-8.

10. Ugrankar R, Berglund E, Akdemir F, Tran C, Soo Kim M, Noh J, **Schneider RK**, Ebert B, Graff JM. Drosophila glucome screening identifies Ck1alpha as a regulator of mammalian glucose metabolism. **Nature Communications**. 2015 May 21;6:7102.

11. Kramann R, Fleig SV, **Schneider RK**, Fabian SL, DiRocco DP, Maarouf M, Wongboonsin J, Ikeda Y, Heckl D, Chang SL, Rennke HG, Waikar SS, Humphreys BD Pharmacological Gli2 Inhibition prevents myofibroblast cell-cycle progression and reduces kidney fibrosis. **Journal of Clinical Investigation** 2015 Aug 3;125(8):2935-51.

12. **Schneider RK**, Ademà V, Heckl D, Järås M, Mallo M, Lord AM, Chu LP, McConkey ME, Kramann R, Mullally A, Bejar R, Solé F, Ebert BL. Role of casein kinase 1A1 in the biology and targeted therapy of del(5q) MDS. **Cancer Cell**. 2014 Oct 13;26(4):509-20.

13. Kramann R, **Schneider RK**, DiRocco DP, Machado F, Fleig S, Bondzie PA, Henderson JM, Ebert BL and Humphreys BD. Perivascular Gli1+ Progenitors Are Key Contributors to Injury-Induced Organ Fibrosis. **Cell Stem Cell**. November 2014.

14. **Schneider RK**, Ziegler S, Leisten I, Ferreira MSV, Schumacher A, Rath B, Fahrenkamp D, Muller-Newen G, Crysandt M, Wilop S, Jost E, Koschmieder S, Knuchel R, Brummendorf TH, Ziegler P. Activated fibronectin-secretory phenotype of mesenchymal stromal cells in pre-fibrotic myeloproliferative neoplasms. **Journal of Hematology and Oncology.** 2014 Dec 14;7:92.

15. Chen E, **Schneider RK**, Breyfogle LJ, Rosen EA, Poveromo L, Elf S, Ko A, Brumme K, Levine R, Ebert BL, Mullally A. Distinct effects of concomitant Jak2V617F expression and Tet2 loss in mice combine to promote disease progression in myeloproliferative neoplasms. **Blood.** 2014 Jan 8;125(2):327-35.

16. Järås M, Miller PG, Chu LP, Puram RV, Fink EC, **Schneider RK**, Al-Shahrour F, Peña P, Breyfogle LJ, Hartwell KA, McConkey ME, Cowley GS, Root DE, Kharas MG, Mullally A, Ebert BL. Csnk1a1 inhibition has p53-dependent therapeutic efficacy in acute myeloid leukemia. **Journal of Experimental Medicine**. 2014 Apr 7;211(4):605-12.

17. Losman JA, Looper R, Koivunen P, Lee S, **Schneider RK**, McMahon C, Cowley G, Root D, Ebert BL, Kaelin WG Jr. (R)-2-Hydroxyglutarate Is Sufficient to Promote Leukemogenesis and Its Effects Are Reversible. **Science**. 2013, March 29;339(6127):1621-5.

18. Mullally A, Poveromo L, **Schneider RK**, Al-Shahrour F, Lane SW, Ebert BL. Distinct roles for long-term hematopoietic stem cells and erythroid precursor cells in a murine model of Jak2V617F polycythemia vera. **Blood.** 2012 Jul 5;120(1):166-72.

19. De Vita S, **Schneider RK**, Garcia M, Wood J, Gavillet M, Ebert BL, Gerbaulet A, Roers A, Levine RL, Mullally A, Williams DA. Loss of Function of TET2 Cooperates with Constitutively Active KIT in Murine and Human Models of Mastocytosis. **PLoS One**. 2014 May 2;9(5).

20. Kramann R, Erpenbeck J, **Schneider RK**, Röhl AB, Hein M, Brandenburg VM, van Diepen M, Marx N, Floege J, Schlieper G. Speckle Tracking Echocardiography Detects Uremic Cardiomyopathy Early and Predicts Cardiovascular Mortality in ESRD. **Journal of the American Society of Nephrology**. 2014 Apr 3.

21. Qin J, Sontag S, Lin Q, Mitzka S, Leisten I, **Schneider RK**, Wang X, Jauch A, Peitz M, Brüstle O, Wagner W, Zhao RC, Zenke M. Cell Fusion Enhances Mesendodermal Differentiation of Human Induced Pluripotent Stem Cells. **Stem Cells and Development**. 2014 Aug 11.

22. Kramann R, Kunter U, Brandenburg VM, Leisten I, Ehling J, Klinkhammer B, Knüchel R, Floege J and **Schneider RK.** Osteogenesis of heterotopically transplanted mesenchymal stromal cells in rat models of chronic kidney disease. **Journal of Bone and Mineral Research**. 2013 December;28(12):2523-34.

23. Ventura Ferreira MS, **Schneider RK**, Wagner W, Jahnen-Dechent W, Labude N, Bovi M, Piroth DM, Knüchel R, Hieronymus T, Müller AM, Zenke M, Neuss S. 2D Polymer-based Cultures expand Cord Blood-derived Hematopoietic Stem Cells and Support Engraftment of NSG mice. **Tissue Engineering Part C (Methods).** 2013 Jan;19(1):25-38.

24. Leisten I, Kramann R, Ventura Ferreira MS, Ziegler P, Wagner W, Neuss S, Knüchel R and **Schneider RK**. 3D co-culture of hematopoietic stem and progenitor cells and mesenchymal stem cells in collagen scaffolds as a model of the hematopoietic niche. **Biomaterials.** 2012 Feb;33(6):1736-47.

25. Koos R, Brandenburg V, Mahnken AH, Schneider RK, Dohmen G, Marx N, Kramann R. Sclerostin as potential novel biomarker for aortic valve calcification: an in vivo and ex vivo study. The Journal of Heart Valve Disease 2013, The Journal of Heart Valve Disease. 2013 May;22(3):317-25.

26. Kramann R, Brandenburg VM, Schurgers LJ, Ketteler M, Westphal S, Leisten I, Bovi M, Jahnen-Dechent W, Knüchel R, Floege J and Schneider RK. Novel insights into osteogenesis and matrix remodelling associated with calcific uraemic arteriolopathy. Nephrology Dialysis Transplantation. 2013 March; 28(4): 856-868.

27. Kramann R, Couson S, Neuss S, Floege J, Knuechel R and Schneider RK. Exposure to uremic serum disrupts the vascular niche in a three-dimensional co-culture system of human mesenchymal stem cells and human umbilical cord endothelial cells. Nephrology Dialysis Transplantation. 2012 Jul;27(7):2693-702.

28. Ventura Ferreira MS, Schneider RK, Jahnen-Dechent W, Labude N, Bovi M, Hieronymus T, Zenke M and Neuss S. Highly efficient Cord Blood-Hematopoietic Stem Cell Expansion in 3D Fibrin Scaffolds with Stromal Support. Biomaterials. 2012 Oct;33(29):6987-97.

29. Walenda G, Hemeda H, Schneider RK, Merkel R, Hoffmann B, Wagner W. Human Platelet Lysate Gel Provides a Novel 3D-Matrix for Enhanced Culture Expansion of Mesenchymal Stromal Cells. Tissue Engineering Part C Methods. 2012 Dec;18(12):924-34.

30. van de Kamp J, Kramann R, Anraths J, Schöler HR, Ko K, Knüchel R, Zenke M, Neuss S and Schneider RK. Epithelial morphogenesis of germline-derived pluripotent stem cells on organotypic skin equivalents in vitro. Differentiation. 2012 Mar; 83(3):138-47.

31. Schneider RK, Puellen A, Kramann R, Raupach K, Bornemann J, Knuechel R, Pérez-Bouza A, Neuss S. The osteogenic differentiation of adult bone marrow and perinatal umbilical mesenchymal stem cells and matrix remodelling in three-dimensional collagen scaffolds. Biomaterials. 2010 Jan;31(3):467-80.

32. Neuss S, Schneider RK, Tietze L, Knüchel R, Jahnen-Dechent W. Secretion of fibrinolytic enzymes facilitates human mesenchymal stem cell invasion into fibrin clots. Cells Tissues Organs. 2010;191(1):36-46.

33. Kramann R, Couson SK, Neuss S, Kunter U, Bovi M, Bornemann J, Knüchel R, Jahnen-Dechent W, Floege J and Schneider RK. Exposure to uremic serum induces a procalcific phenotype in human mesenchymal stem cells. Arteriosclerosis Thrombosis Vascular Biology. 2011 Sep;31(9):e45-54.

34. Schuh A, Liehn EA, Sasse A, Schneider R, Neuss S, Weber C, Kelm M, Merx MW. Improved left ventricular function after transplantation of microspheres and fibroblasts in a rat model of myocardial infarction. Basic Research in Cardiology. 2009 Jul;104(4):403-11.

35. Ko K, Reinhardt P, Tapia N, Schneider RK, Araúzo-Bravo MJ, Han DW, Greber B, Kim J, Kliesch S, Zenke M, Schöler HR. Brief report: evaluating the potential of putative pluripotent cells derived from human testis. Stem Cells. 2011. Aug;29(8):1304-9.

36. Ko K, Araúzo-Bravo MJ, Tapia N, Kim J, Lin Q, Bernemann C, Han DW, Gentile L, Reinhardt P, Greber B, Schneider RK, Kliesch S, Zenke M, Schöler HR. Human adult germline stem cells in question. Nature. 2010 June 24;465(7301).

37. Schneider RK, Anraths J, Kramann R, Bornemann J, Bovi M, Knüchel R, Neuss S. The role of biomaterials in the direction of mesenchymal stem cell properties and extracellular matrix remodelling in dermal tissue engineering. Biomaterials. 2010. Nov;31(31):7948-59.

38. Schneider RK, Püllen A, Kramann R, Bornemann J, Knüchel R, Neuss S, Perez-Bouza A. Long-term survival and characterisation of human umbilical cord-derived mesenchymal stem cells on dermal equivalents. Differentiation. 2010. Mar;79(3):182-93.

39. Schneider RK, Neuss S, Stainforth R, Laddach N, Bovi M, Knuechel R, Perez-Bouza A. Three-dimensional epidermis-like growth of human mesenchymal stem cells on dermal equivalents: contribution to tissue organization by adaptation of myofibroblastic phenotype and function. Differentiation. 2008 Feb;76(2):156-67.

BIBLIOGRAPHIE – REVIEW ARTICLES AND EDITORIALS (PEER-REVIEWED)

1. Kramann R and **Schneider RK**. Parathyroid hormone-regulated protein and regulation of cell survival in the kidney. **Kidney International**. 2013; 83(5):777-9.

2. Buta C, David R, Dressel R, Emgård M, Fuchs C, Gross U, Healy L, Hescheler J, Kolar R, Martin U, Mikkers H, Müller FJ, **Schneider RK**, Seiler AEM, Spielmann H, Weitzer G. Reconsidering Pluripotency Tests: Do we still need Teratoma Assays? Stem Cell Research 2013. **Stem Cell Research**. 2013; 11(1):552-562.

3. **Schneider RK**, Knüchel R, Neuss S. [Mesenchymal stem cells and their interaction with biomaterials: Potential applications in tissue engineering.]. **Der Pathologe**. 2011 Nov; 32 Suppl. 2:296-303.

4. **Schneider RK**, Neuss S, Knüchel R, Perez-Bouza A. [Mesenchymal stem cells for bone tissue engineering]. **Der Pathologe**. 2010 Oct;31 Suppl 2:138-46. Aachen, 20. Juli 2016

Name PhD student:	Rebekka K. Schneider-Kramann
Promotors:	Prof. Dr. H.R. Delwel, Prof. Dr. I.P. Touw
Supervisors:	Prof. Dr. H.R. Delwel, Prof. Dr. B.L. Ebert
Erasmus MC Department:	Hematology
Research school:	Molecular medicine (Mol Med)
PhD period:	January 2012- July 2015

1. PhD training

	Year	Workload (Hours/ECTS)
General academic skills/Research skills		
• Biomedical English Writing and Communication	2012	1
• Research Management for PhDs and Postdocs	2012	1
• Laboratory animal science	2012	3
• Basic introduction course SPSS	2012	0.6
• Photoshop and Illustrator CS5 workshop	2012	0.3
• Flow cytometry introduction/FlowJo	2015	1
In-depth courses and workshops		
• Hematopathology clinical conference	2012-2015	4
• Analysis of microarray and RNA seq data	2013	1
• Genome engineering course Broad Institute, Cambridge,	2015	1
• Molecular Cancer work discussion Broad Institute, Cambridge, USA (weekly, Tuesdays)	2012-2015	3
• Work in progress meeting Department of Hematology, Brigham and Women's hospital, Boston, USA	2012-2015	2
• Hematology lunch meeting, Dana Farber cancer Institute, Boston, USA	2012-2015	2
• Journal Club	2012-2015	2

SUMMARY OF PHD TRAINING AND TEACHING ACTIVITIES

	Year	Workload (Hours/ECTS)
Presentations		
• 55th Annual Meeting American Society of Hematology (oral)	2013	
• 56th Annual Meeting American Society of Hematology (oral)	2014	
• 57th Annual Meeting American Society of Hematology (oral)	2015	
• 13th International Symposium on Myelodysplastic Syndromes Washington DC, USA (oral)	2015	
• Grand Rounds Hematology, Department of Hematology, Brigham and Women's Hospital, Harvard Medical School, Boston (oral)	2015	
• SFB Dresden invited talk (oral)	2015	
• D-A-CH MDS meeting 2013, Düsseldorf (oral)	2013	
• Myeloid Malignancies Meeting, Department of Hematology, Brigham and Women's Hospital, Harvard Medical School, Boston (oral)	2014	
• Cancer Biology Meeting, Department of Hematology, Brigham and Women's Hospital, Harvard Medical School, Boston (oral)	2014	
• D-A-CH MDS meeting 2014, Düsseldorf (oral)	2014	
• Deutsche Krebskonferenz, Berlin 2014 (oral)	2014	
• Ribosome Function and Ribosomopathies Expert meeting, Stowers Institute, Kansas City, MO, USA (oral)	2013	
• FASEB Hematological Malignancies Meeting 2015 (oral)	2015	
• Work discussion meeting (9x)	2012-2015	
• Journal club (4x)	2012-2015	
International conferences		
• 54th Annual Meeting American Society of Hematology	2012	1
• 55th Annual Meeting American Society of Hematology	2013	1
• 56th Annual Meeting American Society of Hematology	2014	1
• 57th Annual Meeting American Society of Hematology	2015	1
• 13th International Symposium on Myelodysplastic Syndromes.	2015	1
• FASEB Hematological Malignancies Meeting 2015	2015	1
2. Teaching activities		
Lecturing		
• Bone marrow histopathology (weekly)	2012-2015	2
Teaching activities		
• Supervising master students	2012-2015	3
• Supervising international summer students	2012-2015	2
• Supervising ASH honors students	2012-2015	2
total		56.4

ACKNOWLEDGEMENTS

I owe a great amount of gratitude to many people who have accompanied, guided, supported, motivated, entertained and inspired me through the tumultuous roads of science and lab life over the last years.

Most importantly Professor Ebert, Ben: I still remember how nervous I was before interviewing with you in May 2011 in Boston. From the first minutes talking to you, I knew that being in your lab and being mentored by you would be the best thing that could happen in my scientific career. Your mentorship throughout the 3.5 years in your lab and now being back in Europe, has been and is phenomenal. I am deeply grateful for all our scientific discussions and your guidance in my scientific career. You gave me so much strength in science and confidence in designing experiments and testing hypotheses. I feel more confident about what I want and how I get there. Your lab is perfectly balanced – scientifically as well as with various personalities; everyone collaborates, there is no back stabbing, there is constant laughter, a little bit of drama and wonderful extracurricular activities – at your place, the Yard house or of course at Bertucci's. I thank you from the bottom of my heart for having offered me the opportunity to work in your lab and for guiding me to where I am today.

Dear Professor Delwel, dear Ruud, since the first time we have talked, you have been an incredible and thoughtful mentor for me. Thank you for all the amazing conversations about science and career choices and for creating a scientific home for me in Rotterdam. I am so incredibly grateful for your support to make this possible and for thinking through all the details. Thank you also for getting the ball rolling on my thesis and the defense. I am very happy to work at Erasmus MC and to interact with you. You are an exceptional scientific mentor and I am looking forward to many collaborations, discussions and conversations about science, life and the world.

Dear Professor Touw, dear Ivo, I still remember our first conversation in spring 2015. Within just a few minutes, we were in the middle of an inspiring and thought-provoking discussion about bone marrow failure and myelodysplastic syndromes. I am very grateful for all the conversations about politics, life and science we had since then. Thank you also for very insightful comments on grants and for reading version after version, I learn so much. Your fascination for science is inspiring. Thank you for being my mentor!

Dear Professor Löwenberg, dear Bob, you are the embodiment of a mentor. Thank you for taking time to think through the different aspects of a scientific and clinical career, for discussing options, for listening and also for supporting not only me but also Rafael. Thank you also for asking the right questions – everything seems more clear after talking to you.

You said in one of your interviews with ASH „...once you make a choice, don't look back. Just go for it". This has been a very important statement for me over the last year. Thank you for providing perspectives, guidance and motivation.

Dear Professor Sonnelveld, dear Pieter, thank you very much for your incredible support in getting me started in the Department of Hematology at Erasmus MC. I felt warmly welcome from the very first second. I am very happy to be part of the team.

Dear Dr. Raaijmakers, dear Marc – my research grant for joining Ben's lab was on dissecting the role of the stroma in AML by performing an shRNA screen. Your Nature paper was my central reference showing that the stroma, indeed, can contribute to the malignant transformation of hematopoietic stem cells. I was and am very excited about this beautiful work. It was such a pleasure to talk to you last year during my interview – how amazing that our completely independent work converged on the role of S100A8/S100A9 in myeloid neoplasm. I am very much looking forward to starting collaborative projects with you and to many more exciting discussions and findings.

Dear Dr. Cupedo, dear Tom – thank you very much for making me feel so welcome in Rotterdam. Your comments on my ERC proposal were extremely helpful and significantly improved the proposal. I am looking forward to exploring Leiden with you and your family, the latest in the summer.

Thank you, Annelies, Eudia and Egied, for providing me with technical and administrative support. I would have been lost multiple times without you. Egied, thank you for making "the science look so beautiful" in this thesis. This book will always be a wonderful memory for me.

Marie and Damien, you are the heart of Ben's lab. Marie, I still don't know how you did it – answering my questions before I even asked them. You two have been so wonderful over the years in Ben's lab, always supportive, always a shoulder to lean on. We had such an amazing time, full of laughter, drama, some tears here and there, so much joy – I could have never been so productive without you. You have made every day in Ben's lab an amazing day.

My dear lab family, Esther, Michelle, Allegra, Edwin and Rishi – you were always there: early in the morning, late in the night, even days without sleep did not seem so bad with you around or after "a good breakfast" at ABP, Pat's Place or McDonald's or a nice dinner at Bertucci's, take away from Rod Dee, or Mac'n Cheese from ABP. No matter how stressed out I was – I always felt better after talking to you. I never left you guys without a smile on my face. Also, what would I have been in the lab without our "candy drawer". You made the

time in the lab so incredibly memorable for me. I can't wait for our next reunion.

Dear Professor Brümmendorf, my dearest thank you for your support over the last years and for the hours we spent talking and discussing. Thank you in particular for listening, understanding and figuring out what I want and need in my career as a scientist and also as a pathologist. It was a special and memorable event to celebrate the Artur-Pappenheim award in Leipzig with you in 2016. Thank you for guiding me there, I am very grateful for continuous support, thoughts about my future as a scientist and especially for being in my committee for the thesis defense.

Dear Professor Mullally, dear Ann. Simply said – you are my role model. You were the first person I talked to in Ben's lab, I directly thought you were amazing and it was such a pleasure to start in the lab next to you. I love your positive attitude, your energy, your love and passion for science, your humor and your generosity for sharing protocols and also thoughts on projects. I have learned so much from you. Thank you for coming to Berlin last year and for being in the PhD defense committee! It means a lot to me. I am looking forward to establishing the Boston-Rotterdam axis for collaborations and celebrations.

Dear Professor Losman, dear Julie, thank you for being both an amazing scientist and a wonderful friend, simply you rock! You had me crash your apartment last year when I came back to Boston for revision experiments and we had such a good time. I have so many special memories from sharing rooms with you at ASH – thank you for even fixing my "zipper" problems. Thank you also for introducing me to Oysters and to "really good cocktails".

Dear Dr. de Pater, dear Emma, thank you so much for helping me to get started in the department, for answering my "mouse house questions" and for introducing me to everyone. I am looking forward to discussing experiments with you, learning from your CRISPR expertise and working together with you. 1981 rocks!

Dear Leonie, Onno, Paulette, Patricia and Marije- what would I be without your continuous support. Thank you for answering all my questions, for establishing the lunch "What's app group" (really important), for coffee breaks and for the very good mood in the lab. You were so instrumental in getting me settled in the lab and in Rotterdam – my dearest thank you!

Dear Josephine, first of all thank you for translating the summary of my thesis in Dutch (and also thanks to your dad) – this was so incredibly helpful! Thank you also for the wonderful time in Boston, for nice lunches, for fun in the lab, for providing Dutch candy and for "keeping the boys in bay" in the lab. Cheers to many more ASH runs and to the Boston-Netherland axis!

To my little sister, Hannah – you are not only my sister, you are my best friend. Thank you for always having an open ear for me and for visiting me in Boston and the USA on a regular basis. It was so great to have you around for ASH 2013 in New Orleans – your support before my first talk at ASH was incredible (and the pancakes that morning so delicious). Thank you for always cheering me up, for "running, pumping and jumping" together and for supporting me on every path in life!

To my parents: Johann Wolfgang von Goethe once said: "*There are two things children should get from their parents: roots and wings*." I could not phrase better how you support me. You always have an open door and open ear for me. No matter where we go – you are there! Thank you for visiting us in Boston and exploring our life abroad and for supporting my decision to go to Rotterdam. You drove me to Rotterdam, explored the city with me and I could not have asked for a better start, thank you for making this day so special for me and thank you for always having my back!

To Rafael, my smart, funny, loving, supportive, creative and dedicated husband: What would I do without you? We are a team since medical school and I love exploring the world and life with you. We had couple of exceptional years in Boston. Thank you for always finding a path with me – nothing ever seems too hard when you are around. I am looking forward to every step on the way and wherever life will take us. We don't have a home, you are my home.